

JOHANNES HÖPFNER

a new method of **seawater desalination**  
**via acrylic acid based hydrogels**

synthesis, characterisation, and experimental realisation



Scientific  
Publishing



Johannes Höpfner

**A new method of seawater desalination via  
acrylic acid based hydrogels**

Synthesis, characterisation, and experimental realisation



# **A new method of seawater desalination via acrylic acid based hydrogels**

Synthesis, characterisation, and experimental realisation

by

Johannes Höpfner



Dissertation, Karlsruher Institut für Technologie (KIT)  
Fakultät für Chemie- und Biowissenschaften, 2013  
Referenten: Prof. Dr. Manfred Wilhelm,  
Prof. Dr. Christopher Barner-Kowollik

#### Impressum



Karlsruher Institut für Technologie (KIT)  
KIT Scientific Publishing  
Straße am Forum 2  
D-76131 Karlsruhe

KIT Scientific Publishing is a registered trademark of Karlsruhe Institute of Technology. Reprint using the book cover is not allowed.

[www.ksp.kit.edu](http://www.ksp.kit.edu)



*This document – excluding the cover – is licensed under the Creative Commons Attribution-Share Alike 3.0 DE License (CC BY-SA 3.0 DE): <http://creativecommons.org/licenses/by-sa/3.0/de/>*



*The cover page is licensed under the Creative Commons Attribution-No Derivatives 3.0 DE License (CC BY-ND 3.0 DE): <http://creativecommons.org/licenses/by-nd/3.0/de/>*

Print on Demand 2013

ISBN 978-3-7315-0143-5





A new method of seawater  
desalination via acrylic acid based hydrogels  
Synthesis, characterisation, and experimental realisation

---

Zur Erlangung des akademischen Grades eines  
DOKTORS DER NATURWISSENSCHAFTEN  
(Dr. rer. nat.)

Fakultät für Chemie und Biowissenschaften  
Karlsruher Institut für Technologie (KIT) –  
Universitätsbereich

genehmigte  
DISSERTATION

von  
Johannes Höpfner  
aus München

---

Dekan: Prof. Dr. M. Bastmeyer  
Referent: Prof. Dr. M. Wilhelm  
Korreferent: Prof. Dr. C. Barner-Kowollik  
Tag der mündlichen Prüfung: 08.02.2013



## Kurzfassung

Die Versorgung mit Trinkwasser stellt in vielen Region der Welt ein zunehmendes Problem dar. Eine mögliche Lösung ist die Gewinnung von Frisch- aus Meerwasser durch Entfernung des enthaltenen Salzes. Heute sind verschiedene Methoden der Meerwasserentsalzung bekannt (z.B. die Umkehrosmose). In der vorliegenden Arbeit wird dagegen ein vollständig neues Verfahren zur Meerwasserentsalzung entwickelt. Es basiert auf polymeren Hydrogelen als Separationsmaterial.

Hydrogele sind eine Klasse der polymeren Netzwerke, die hydrophile Eigenschaften aufweisen. In Kontakt mit Wasser nehmen sie dieses auf und quellen. Häufig tragen sie Ladungen auf den Polymersträngen und erreichen so besonders hohe Wasserkapazitäten. Die Wasseraufnahme kann bis zum 1000-fachen des Gewichts an Polymer betragen, weshalb diese Materialien als Superabsorber bezeichnet werden.

In Salzlösungen wie Meerwasser quellen diese Polymere jedoch weniger stark (bis zu einem Faktor 100). Bei einem Überschuss zugesetzter Salzlösung, erhält man zwei Phasen: eine Gelphase sowie die überstehende Lösungssphase. Jedoch verteilen sich die mobilen Ionen der Salzlösung zwischen diesen beiden Phasen nicht gleichmäßig. Vom Gel werden relativ weniger dieser Ionen als Wasser aufgenommen. Der Grund sind die mit dem Gel verbundenen Ladungsträger. Diese können das Gel nicht verlassen und schirmen die mobilen Ionen durch einen elektrostatischen Effekt ab. Die Abstoßung der Ionen kann durch die Donnan-Membran-Theorie beschrieben werden und der Umfang der Abstoßung konnte qualitativ vorhergesagt werden. Der erzeugte Konzentrationsunterschied bildet die Grundlage für die Separation von mobilen Ionen und Wasser.

In der vorliegenden Arbeit wird ein Prozess entwickelt, der diesen Separationseffekt zur Meerwasserentsalzung nutzt. Dieser Prozess wird in drei Stufen umgesetzt: Zunächst wird das Polymernetzwerk in einem Überschuss Salzwasser gequollen. Dann wird der an mobilen Ionen angereicherte Überstand entfernt und verworfen. Das abgereicherte Wasser wird zuletzt aus dem Hydrogel unter Druck ausgepresst und entsalztes Wasser erhalten. Für die Umsetzung des letzten Schritts wurde eine Filterpresse und Energie benötigt. Im Rahmen dieser Arbeit wurde ein entsprechender Teststand für das Abquellen des Gels konstruiert. Der Teststand fasst 0,5 L und erlaubt es, Drücke bis 100 bar aufzubringen. Zusätzlich ist er mit drei Sensoren ausgestattet, die den Pressprozess beobachten. Die Sensoren zeichnen online mit hoher Genauigkeit den Volumenstrom des ausgepressten Wassers, den Druck in der Presse und den Salzgehalt des Wassers auf. Damit erlaubt der Teststand die genaue Beschreibung des Abquellungsprozesses und den Vergleich verschiedener Entsalzungsexperimente.

In Experimenten wurde der Entsalzungsprozess mit verschiedenen Hydrogelen sowie unterschiedlichen technischen Parametern untersucht. Die verwendeten Hydrogele wurden auf der Basis von Polyacrylsäure hergestellt. Dabei wurden die synthetischen Parameter Vernetzungsgrad, Ionisierungsgrad und Wassergehalt bei der Vernetzung variiert und die Auswirkungen untersucht. Außerdem wurde eine Reihe von statistischen Copolymeren mit anderen Monomeren hergestellt und untersucht sowie kommerzielle Referenzmaterialien verwendet. Als technische Parameter wurden die Geschwindigkeit der Quellung sowie des Auspressen des Hydrogels untersucht. Das Verhältnis von Lösung zu Polymer in der Probe und der Salzgehalt der Lösung wurden als Parameter untersucht. Es konnte gezeigt werden, dass Gele basierend auf Acrylsäure mit hohen Vernetzungsgraden (5 mol-%) und geringem Wassergehalt bei der Synthese (< 2 g Wasser pro g Monomer) die beste Separationsleistung aufweisen. Der Ionisierungsgrad der Monomere sollte über 20 mol-% liegen, spielt aber nur eine geringe Rolle. Insgesamt erlauben die getesteten Prozessparameter eine Umsetzung

in einem Prozess in großen Maßstab. Ein Entsalzungzyklus kann über kurze Quell- und Auspresszeiten in 30 min oder weniger umgesetzt werden. Die Meerwassерentsalzung kann für alle relevanten Salzkonzentrationen ( $c(NaCl) = 0,1 - 35 \text{ g/L } NaCl$ ) durch geführt werden, jedoch werden mehrere Zyklen benötigt. Aus den gewonnenen Daten kann der Energieaufwand für einen vollständigen Entsalzungsprozess abgeschätzt werden. Dieser liegt bei 20 bis 80 kWh/m<sup>3</sup> bezogen auf erzeugtes Frischwasser im Vergleich zu 2 bis 10 kWh/m<sup>3</sup> für die etablierten Technologien im großtechnischen Maßstab.

Die für diese Untersuchung eingesetzten Hydrogele wurden zum größten Teil selbst hergestellt, wofür die freie radikalische Polymerisation verwendet wurde. Damit konnten die Syntheseparameter auf die gewünschten Werte eingestellt werden. Die Proben wurden durch die Standardmethoden der Gleichgewichtsquellung, mechanische Deformation und Solextraktion charakterisiert. Diese Methoden liefern für den Entsalzungsprozess wichtige Kenngrößen. Darüber hinaus kann die statistische Maschenweite der Netzwerke berechnet und damit die Vernetzungseffizienz abgeschätzt werden. Diese liegt in der Regel deutlich unter den erwarteten Werten und sinkt mit zunehmendem Vernetzungsgrad.

Die topologische und dynamische Heterogenität der hergestellten Netzwerkstrukturen wurden mit verschiedenen weitergehenden Methoden untersucht. Dies ist zu einen die Methode des Ausschlusses eines gelösten, linearen Referenzpolymers. Dadurch kann die Porengrößenverteilung in dem Gel abgeschätzt werden. Diese Methode wurde zum ersten Mal auf acrylsäurebasierte Gele angewendet. Darüber hinaus wurden NMR-Spektroskopie und NMR-Relaxometrie genutzt. Die Spektroskopie erwies sich als wenig geeignet, da die untersuchten Proben nicht-behebbar verbreiterte Linien zeigten und damit die spektrale Auflösung ungenügend war. Dagegen erlaubte es die NMR-Relaxometrie die dynamischen Unterschiede verschiedener Polymerketten in der Probe aufzulösen. Besonders das transversale Relaxationsverhalten ( $T_2$ ) ist sensitiv auf Änderungen der Synthe-

separameter und zeigt Unterschiede in der Dynamik der Polymerketten klar auf. Zusätzlich kann die Verteilungsfunktion der dynamischen Komponenten durch die inverse Laplace Transformation berechnet werden. Dagegen war das longitudinale Relaxationsverhalten ( $T_1$ ) kaum sensitiv auf chemische Änderungen. Zum ersten Mal wurde die, von Saalwächter et al. entwickelte, Methode des Doppelquantenkohärenzaufbaus im Niederfeld auf Acrylsäure basierte Hydrogele angewendet. Damit konnten die Ergebnisse der transversalen Relaxation bestätigt werden und die deutliche dynamische Heterogenität der Proben direkt abgebildet werden. Im Besonderen war es möglich das unterschiedliche Relaxationsverhalten der Domänen in Hydrogelpartikeln mit Kern-Schale-Morphologie aufzulösen.

In der vorliegenden Arbeit wurde die Methode der Meerwasserentsalzung mit Hydrogelen entwickelt und erstmals umgesetzt. Der Effekt konnte nachgewiesen werden und der Einfluss der Geleigenschaften und Prozessparameter sowie der Energiebedarf bestimmt werden. Damit ist der Einsatz der vorgeschlagenen Methode für die Meerwasserentsalzung möglich.

## Acknowledgement

Even though I wrote this oeuvre dutifully on my own, the work on which it is based could not have been possible without the help and contribution of others. I would like to thank these several people:

- **Prof. Manfred Wilhelm**

As my supervisor this whole research is based on his idea and would, as a matter of fact, not been possible without him. I'm grateful for encouragement, support in many endeavours (my trips to Israel and Chile, the HBS application to name just a few), and for him listening and commenting my ideas but also giving me space to try them out.

- **The Heinrich Böll Society, the Deutsche Forschungsgemeinschaft, and the state of Baden-Württemberg**

These agencies funded my research and various other expenses. Especially, I would like to highlight the contribution of the HBS which also sponsored my trip to Israel and many very nice seminars.

- **PD Dr. Gisela Guthausen**

She provided me with patient counsel on many NMR related problems, and made the topic well understandable for a non-physicist. I could discuss my results with her and she gave many helpful comments on the draft of this thesis.

- **Prof. Kay Saalwächter**

He provided the minispec application and fit function for the DQ coherence measurements and gave helpful comments on their acquisition and evaluation.

- **Prof. Moshe Gottlieb**

He made my stay in his group in Be'er Scheva possible and offered me insights in rheology, politics, and bird bevs.

- **Prof. Bernabe Rivas Quiroz**

He invited me to Chile, would have been my host, and helped when an act of nature struck.

- **Dimitri Merger, Karin Schlag, Julius, and Stefan Horn**

As students or interns they worked under my supervision on various parts of this thesis project. Without them I would not have been able to generate this wealth of results I was able to select for drafting my thesis.

- **Prof. Burkhard Luy and Martin Koos**

For performing the NMR-spectroscopy measurements on their machines and helping me understand the results.

- **Prof. Christian Holm, Dr. Peter Košovan, and Tobias Richter**

Together we are conducting the fruitful collaboration on simulating the desalination with hydrogels by ESPRESSO.

- **Dr. Nico Dingenuots**

We had heated discussion on the nature on entropy elasticity and he commented on the draft of my thesis.

- **Dr. Christopher “Kiki” Klein**

As the local soft matter rheology expert he helped with the measurements on the ARES and commented on the rheology part of my thesis.

- **Ingo Naue and Daniel Zimmermann**

Ingo helped me getting started with CAD and answered patiently my many questions. Daniel helped me out with some technical drawings for the press setup.

- **The workshop team**

For building the press setup in a way that actually works, being very helpful and discussing the design of many important details.

- **Dr. Vitor “Jack” Barroso**

He introduced me to the Gabo.

- **Everyone who made PDL**

Analysing my data without this fine open-source tool-kit was actually quite fun. It would have much harder without.

- **Manuela Belzik and Joav Diaz**

They represent all the very nice people who cared for me in Israel, showed me the country, and who’s company I was lucky enough to enjoy. I liked it really very much.

- **The whole group**

Thank you for discussions on my work, commenting on my thesis, and helping always out where necessary. Besides, all of you made work-life-balance real hard the last few years ;-) I’ll remember many coffee breaks, BBQs, parties, and trips. I would like to highlight Karl Ratzsch who went out of his way to support me on the minispec and Timo Beskers for helping out with inverse SEC idea.

- **Thomas, Claudia, and Hans**

We came a long way, without you I wouldn’t have made it. Thank you.

- **My parents and Gusti**

For perpetual, unconditional encouragement, support, and interest. Gusti I wish you could have lived to see this day.

- **Franziska**

There is probably non of the above points which you didn’t shared

with me, helped me with, or discussed with me. Yet, I can't begin to put your contribution into words ...

Karlsruhe, January 2013

*Johannes Höpfner*

## Nomenclature

AAc .....	Acrylic acid
AAm .....	Acrylamide
ADC .....	Analogue-to-digital converter
ANSI 304 .....	Typical stainless steel variety (also identified by UNS S30400 or V2A)
AUL .....	Absorbency under load
B1110 .....	A commercial superabsorbent polymer from the BASF with additional surface cross-linking
BPP .....	(Theory of) Bloembergen, Purcell and Pound (see also [Bloembergen48])
CO .....	Amount of co-monomer in mol-% that is co-polymerised with AAc in a gel
CPMG .....	Carr-Purcell-Meiboom-Gill (pulse sequence, see as well [Carr54, Meiboom58])
CYCLOPS ....	Cyclically ordered phase sequence (or cycle)
DC .....	Degree of cross-linking (given by the mole-fraction of the tetra-functional monomer in respect to the other monomers)
de .....	dummy echoes (echoes in a CPMG-pulse train for which no data is acquired)
DI .....	Deionised water
DMTA .....	Dynamic mechanical thermal analysis
DN .....	Degree of neutralisation (given by the mole-fraction of acidic monomer in its charged form)
DQ .....	Double quantum (effects in NMR)
DRI .....	Differential refractive index (measurement)

ds	dummy scans/shots
FID	Free induction decay
FO	Forward osmosis (desalination technique)
FOF	Field offset steps
FS	Frequency sweep (rheological test)
FT	Fourier transform
FWHM	Full width half maximum (a measure for the broadness of a peak)
HEMA	(Hydroxyethyl)methacrylate
HF-NMR	High-field NMR (spectroscopy)
HMBC	Heteronuclear multiple bond correlation (a 2D-NMR experiment)
HSQC	Heteronuclear single quantum coherence (a 2D-NMR experiment)
ILT	Inverse Laplace transform ( $\mathcal{L}^{-1}\{F(t)\}$ )
IR	Inversion recovery pulse sequence
KWW	Kohlrausch-Williams-Watts (function; also called stretched exponential function)
LF-NMR	Low-field NMR (spectroscopy)
$M_N$	Number averaged molecular weight (of a polymer)
$M_W$	Weight averaged molecular weight (of a polymer)
MAAc	Methacrylic acid
MAS	Magic angle spinning (in NMR, rotation of the sample at about $54.7^\circ$ towards the B-field)
MBA	<i>N,N'</i> -Methylenebisacrylamide (tetra-functional cross-linking monomer)
MQ	Multiple quantum (effects in NMR)
MSE	Magic sandwich echo (pulse sequence)
ne	number of echoes
NF	Normal force
NiPAM	N-isopropylacrylamide

NMR .....	Nuclear magnetic resonance (spectroscopy)
ns .....	number of scans/shots
OS .....	Oversampling (averaging reduction of data)
OSS .....	Oscillatory strain sweep (rheological test)
pAAc .....	poly(Acrylic acid)
PDI .....	Polydispersity index (defined as the ratio of $M_W$ to $M_N$ )
pMMAc .....	poly(Methacrylic acid)
PSD .....	Pore size distribution (function)
PTFE .....	poly(tetrafluoroethylene) also called Teflon™
$Q_{eq}$ .....	Equilibrium degree of swelling of an individual polymer; this gives maximum amount of water taken up into the gel in g solution by g polymer
$Q_{rel}$ .....	Relative degree of swelling of an individual polymer; gives the water in the system with respect to $Q_{eq}$ (if greater than 1 more water is available than can be taken up)
$Q_{syn}$ .....	Composition of the synthesis mixture of a sample (given as swelling degree in g of water by g of all monomers)
QM .....	Quantum mechanics
rd .....	recycle delay
RDC .....	Residual dipolar coupling
RF .....	Radio frequency (used in NMR measurements)
RO .....	Reverse osmosis (desalination technique)
RT .....	Room temperature
SAP .....	Superabsorbent polymer
SE .....	Solute exclusion (for pore size measurement)
SEC .....	Size exclusion chromatography
SMA .....	Simple moving average (also called box-car average)
SPS .....	Sodium persulfate (radical initiator)
SR .....	Saturation recovery pulse sequence
$T_{1\rho}$ .....	Spin-lattice relaxation time in the rotating frame
$T_1$ .....	Longitudinal relaxation time in NMR

$T_2$	Transverse relaxation time in NMR
TEMED	<i>N,N,N',N'</i> -tetramethylethylenediamine (accelerator for SPS)
TOCSY	Total correlated spectroscopy (a 2D-NMR experiment)
TRIS	Tris(hydroxymethyl)aminomethane (typically used as a buffer in the weak basic range)
XX4	Special phase cycle for CPMG pulse sequence using 4 combinations of pulse phases in the x-direction only
XY16	Special phase cycle for CPMG pulse sequence using 16 combinations of pulse phases in x-y-plane

# Contents

<b>Kurzfassung</b>	<b>i</b>
<b>Acknowledgement</b>	<b>v</b>
<b>Nomenclature</b>	<b>ix</b>
<b>1 A seawater desalination process based on hydrogels</b>	<b>1</b>
<b>2 Description and theory of polymeric networks</b>	<b>9</b>
2.1 Statistical concepts for the description of networks . . . . .	9
2.2 Discussion of characterisation methods and parameters . . . . .	22
<b>3 Synthesis of gel samples and characterisation by standard methods</b>	<b>33</b>
3.1 Procedure and parameters of synthesis . . . . .	34
3.2 Swelling properties . . . . .	38
3.3 Mechanical behaviour . . . . .	46
3.3.1 Experiments under shear . . . . .	47
3.3.2 Experiments under compression . . . . .	53
3.3.3 Discussion of results and calculation of the network parameters . . . . .	61
3.4 Sol content . . . . .	68
<b>4 Investigation of the network heterogeneity</b>	<b>73</b>
4.1 Mesh size distribution by partition of linear probe polymers	74
4.2 NMR-spectroscopy . . . . .	79

4.3 NMR-relaxometry . . . . .	85
4.3.1 Relaxation phenomena in Gels . . . . .	85
4.3.2 Longitudinal relaxation measurements . . . . .	95
4.3.3 Transverse relaxation measurements . . . . .	98
4.3.4 Residual dipolar coupling measured by double quantum coherences . . . . .	118
<b>5 Construction of a test setup for the desalination process</b>	<b>129</b>
5.1 Design and construction of the test setup . . . . .	129
5.2 Experimental procedure and data analysis . . . . .	136
5.2.1 Experimental procedure . . . . .	136
5.2.2 Volume and flux data . . . . .	138
5.2.3 Pressure data . . . . .	143
5.2.4 Brine concentration data . . . . .	145
5.2.5 Combination of the channels . . . . .	146
5.3 Error estimation and repeatability . . . . .	146
<b>6 Salt rejection and desalination capacity of hydrogels as a function of the chemical composition</b>	<b>157</b>
6.1 Influence of the degree of cross-linking, neutralisation, and reference state of poly(acrylic acid) networks . . . . .	158
6.2 Copolymer networks . . . . .	170
6.3 Commercial superabsorbent polymers . . . . .	172
<b>7 Technical aspects of seawater desalination</b>	<b>181</b>
7.1 Relevant process parameters . . . . .	182
7.2 Discussion of the separation process by a hydrogel under pressure . . . . .	196
7.3 Estimation of energy consumption . . . . .	201
<b>8 State of research and perspective</b>	<b>209</b>
<b>A Appendix</b>	<b>219</b>

A.1	Polymer samples and materials . . . . .	219
A.2	Experimental characterisation procedures . . . . .	224
A.3	Low field NMR equipment and measuring schemes . . . .	231
A.4	Parts and assembly of the press setup . . . . .	245
<b>B</b>	<b>Lists and tables</b>	<b>259</b>
<b>C</b>	<b>Curriculum vitae</b>	<b>287</b>



## **1. A seawater desalination process based on hydrogels**

Hydrogels are often referred to as “superabsorbers” due to their huge uptake of water or aqueous solutions [Buchholz98]. It is not uncommon for the solvent capacity of hydrogels to exceed several 100 times their own weight. It is this feature in particular which has generated so much scientific interest across a wide range of fields for this class of materials. The structures of hydrogels are cross-linked polymeric chains which usually carry charges attached to their backbones [Flory53]. The affinity to water has offered hydrogels on one side a range of large volume applications and on the other they are also used for specialised high-tech products. Into the former category fall typically personal hygiene products. They are used for the fast absorption of high quantities of bodily fluids [Masuda94]. The production of absorbent material for this sector alone exceeded  $8 \cdot 10^6$  t in 2011 [Wiertz11]. Other examples in the same category are the use as underwater-cable insulations, the addition to agricultural soil to retain water close to the plants or as a separating agent for water-oil slurries e.g. in down the hole applications [Hogari94, Kazanskii92, Osada01]. Into the category of specialised applications fall high-tech applications that need only minor amounts of the material but high level of sophistication in its design. On the forefront of this field are the stimuli responsive gels that switch their swelling state due to an external stimulus such as salt [Ohmine82], temperature [de las Heras Alarcon05, Schmaljohann06, Ganta08], light[Zhao09], pH [de las Heras Alarcon05, Schmaljohann06, Ganta08], electrical current [Osada92], or the presence of certain small molecules [Ulijn07]. Among the numerous practical applications of stimuli responsive hydrogels are

the controlled release of drugs [Schmaljohann06, Ganta08], the use as actuators in fluidics [Gerlach10, Kwon10], and artificial muscles [Kuhn49, Katchalsky49, Kuhn50].

Yet, all of the large scale applications are limited in the breadth of their purpose. Only the ability of gels to absorb large quantities of water is utilised. In the present thesis, however, a new usage for this class of materials is proposed, that depends on their strong swelling in water but goes beyond. Here, the charges attached to the polymer chains, that enable the extensive osmotic potential and drive the solvent uptake, are also used to screen off added salt from the gel. When swelling a gel in an aqueous electrolyte solution, the water enters the absorbent but the charges remain mainly in the supernatant solution [Katchalsky55, Victorov06a, Victorov06b]. As a consequence, there is a difference in concentration between the two phases. This enables a broad range of separation or enrichment processes due to differences in the content of the two phases.

The separation process can be understood in a simple gedankenexperiment. In a dry charged polymer network (polyelectrolyte) the volume is filled only with partially charged repeating units and, therefore, the charge density is very high. When the polymer phase is placed in contact with a brine phase, water starts to enter the polymer, swelling it. Due to the high charge density inside the network, the mobile ions of the brine are shielded from the network by electrostatic interactions. The high concentration of immobilised charges prevents the entry of surrounding charges. This process is depicted in **fig. 1.1**. When the swelling progresses, the polymer is diluted by the entering water and the charges within move further apart reducing the charge density. Then, the salt can enter as well, but is still subjected to the electrostatic potential in the gel and the amount that enters is still smaller with respect to the concentration outside. Thus, even at high degrees of swelling the amount of added ions is always smaller in the gel than outside [Flory53]. This effect can be described in terms of a Donnan membrane equilibrium, an approach described by Katchalsky *et al.* [Donnan32, Katchalsky55].

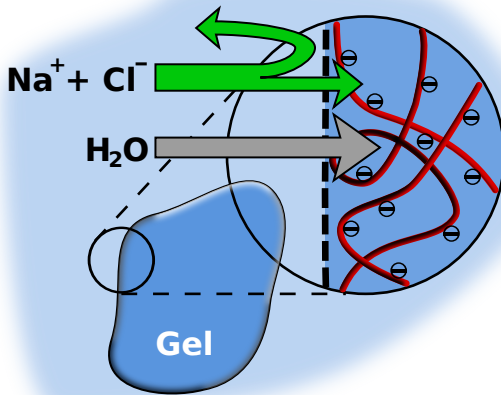


**Figure 1.1.:** Schematic of the separation mechanism of water and dissolved ions by the use of a charged polymer network (gel). When placed in a salt solution, here composed from sodium chloride, the gel takes up the brine but with a lower concentration of mobile ions than found outside. This is achieved by the high charge density inside the gel.

The described process can be reversed, when the gel is removed from the solution. By subjecting the gel to a pressure, that is larger than its osmotic pressure, water is forced from the gel. Similar to the above presented arguments, the charge density is increasing again. This forces first the mobile ions out of the gel with part of the water. The salt concentration of the draining solution is continuously decreasing as the gel shrinks and in the very end, at extremely high charge densities in the polymer, theoretically, pure water is received.

This effect permits a large number of applications in separation and enrichment processes, that are not based on volume exclusion such as membrane based separations. In principle all separation problems which are concerned with charged moieties could be treated. In this work the author decided to focus the research on one particularly interesting example: the desalination of seawater to produce fresh water.

Seawater desalination is in the focus of interest today due to a shortage of fresh water resources in many parts of the world [Khawaji08]. A number of drivers are currently straining the natural freshwater resources, such as population growth, increasing standard of living, climate change, and depletion of the fossil aquifers [WWAP12, JMP10]. One of the possible solutions is producing fresh water from the oceans by the removal of the contained salt (about 3.5 wt.-%). Seawater contains a large number of different ions but mostly sodium chloride (87 wt.-% of the ionic content) and a number of divalent ions [Gerlach94]. Seawater desalination is already undertaken on a large scale by a number of countries such as Saudi Arabia, the United Arab Emirates, the USA, and Spain [Khawaji08]. The global installed capacity is expected to reach  $62 \times 10^6 \text{ m}^3$  of freshwater production per day by 2015 [Fritzmann07]. All methods which separate salt from water require energy to overcome the osmotic pressure seawater (about 27 bar). Several technologies are in use for the production of freshwater, the highest market shares are held by reverse osmosis and a number of distillation processes [Fritzmann07].

The process envisioned for seawater desalination with hydrogels follows three steps and is depicted in **fig. 1.2** [Höpfner10]. First the dry polymer beads and an excess of brine solution of concentration  $c_0$  are mixed (step 1). When the gel is swollen, as much as possible of the supernatant phase is removed (step 2). This phase now contains a larger concentration of ionic content. The polymer is subjected to an external stimulus, in this case hydrostatic pressure, to free the solution from it (step 3). The water received in the end has a lower salt concentration than initially used ( $c < c_0$ ), thus constituting a successful desalination.

With this principle in mind several fundamental questions remain. How large is this effect and can it be used over the whole concentration range of ionic species of interest for seawater desalination (0.1 – 3.5 wt.-%)? How can the squeezing of the gel be successfully implemented? The pro-

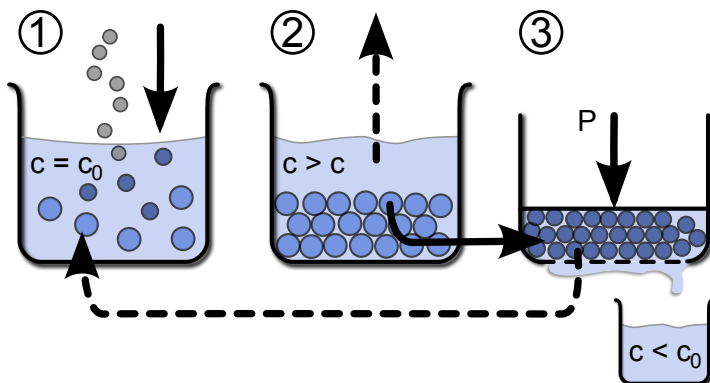


**Figure 1.2.:** Schematic of a three step process proposed here for seawater desalination using hydrogels. The dry polymer is placed in an excess of brine of concentration  $c_0$  and swells (1). The salt is partly rejected and remains in the supernatant phase that is later discarded (2). The gel is subjected to pressure and water with a lower salt concentration is gained (3).

cess needs to be characterized and evaluated: What are drivers and limiting effects in terms of material and process parameters and how can the desalination performance be improved? Is more than one step necessary to gain almost salt-free water? At last, the most important question for a real application: what are the energy demands in comparison to established desalination processes?

Several steps were undertaken to answer these questions. First, a working material of suitable properties had to be found. The material itself was chosen from a pool of samples which are obtained from two sources: self-synthesised samples and industrially produced reference samples. The self-synthesised samples were produced by free radical polymerisation of acrylic monomers in the presence of a tetra-functional cross-linker as shown in **fig. 1.3**. These samples are further described in section 3.1. The properties of the hydrogels are of interest for the process itself but are also a tool to acquire an understanding of the underlying structure. These

## 1. A seawater desalination process based on hydrogels

---

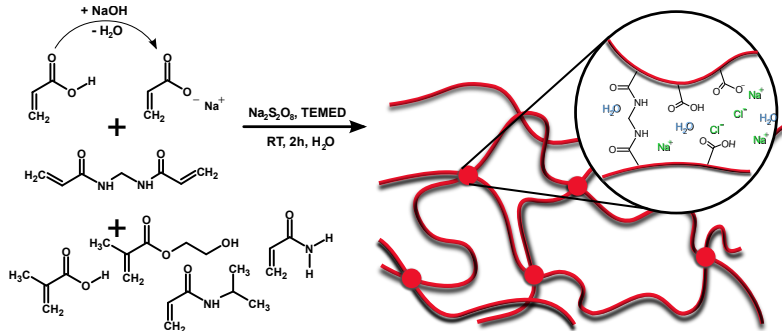


**Figure 1.3.:** The self-synthesised hydrogels are produced by free radical (co-)polymerisation of acrylic monomers with the tetra-functional cross-linker *N,N'*-methylenebisacrylamide. Four other possible monomers are given, which were used to produce copolymers in this work. The reaction proceeds in water at room temperature due to a redox initiator system composed from sodium persulfate and *N,N,N',N'*-tetramethylethylenediamine (TEMED, ((*H*<sub>3</sub>*C*)<sub>2</sub>*N*)<sub>2</sub>(*CH*<sub>2</sub>)<sub>2</sub>).

structure-property relationships are established in chapter 2 based on the elements of a statistical network description. The properties are measured by various molecular and macroscopic characterisation techniques for absorbent materials. The standard techniques such as swelling capacity, section 3.2, and mechanical response, section 3.3, only measure macroscopic properties of gels as a result of their averaging structure. The heterogeneity of the molecular structure is only accounted for by specialised techniques. The pore size distribution inside the gel is approximated by using linear probe polymers in the solute exclusion technique (sec. 4.1) [Kuga81]. NMR-spectroscopy is employed to gather information on the connectivity of the monomers (sec. 4.2). NMR-relaxometry is used in section 4.3 to probe local topological constraints of the system. In this context also the newly developed NMR low-field double quantum coherence method is employed for the first time to investigate acrylic based hydrogels [Lange11]. With well characterised samples at hand a test setup is necessary to conduct the desalination experiments. In particular the step 3 in fig. 1.2 needs a

press setup to separate polymer beads from the solution. The design and construction of such a test setup are described in chapter 5. It is equipped with three sensors (volume flux, pressure, and salt concentration) to track the processes taking place inside the gel. The acquisition of the data, their treatment, and an error estimation are given.

The effect of the material composition and the process parameters on the desalination effect are studied. In chapter 6 the influence of different types of working material is investigated in terms of the structure of poly(acrylic acid) gels and the influence of co-monomers and the use of industrially produced samples. In chapter 7 the influence of the process parameters is investigated, an energy consumption estimate is made, and the desalination process is discussed in detail. In the concluding chapter 8, the achieved progress in this work is evaluated and further possible developments are outlined. As an example, the ion distribution between a gel and a solution phase can be predicted by coarse-grained computer simulations [Höpfner13, Limbach06]. These experiments were performed in cooperation with the group of Prof. Holm (University of Stuttgart).



## **2. Description and theory of polymeric networks**

The ultimate test of any theory is its predictiveness of experimental results. Under optimal conditions it fosters the prediction of macroscopic observable quantities from a small set of microscopic parameters and a comprehensive model. These structure-property relations are useful in understanding experimental results as well as tailoring real materials for a specific purpose.

In the case of hydrogels, the properties of equilibrium solvent capacity, mechanical strength and ion uptake or rejection can be understood and predicted to some extent by a statistical theory. Treating the gel as a collection of polymeric chains and summing up over their properties yields an equation of state for the system. It is found, that this expression is compromised of three parts that deal with individual effects. From the equation of state, some special cases can be derived that serve as basis for some of the characterisation methods in chapter 3.

### **2.1. Statistical concepts for the description of networks**

The classical way of deriving an equation of state for polymeric networks or hydrogels is using a micro-scale model of its structure. By a statistical treatment the macroscopic properties are derived by averaging over the system as a whole and considering that all possible realisations are present in the ensemble with their respective statistical weights. This is a so-called mean field approach as no explicit correlations between moieties are considered.

## 2. Description and characterisation possibilities

---

A gel is a network of polymer chains linked together that has incorporated a large amount of solvent. The junctions between the single chains introduce constraints into the system of polymers which hinder their motion. Due to the cross-links, the network can not be dissolved but only dilated. Hydrogels are a special class of gels based on polyelectrolytes, which exhibit charged groups on the polymer chains. They can take up very large amounts of water (10 – 1 000 times their own weight) into the pores that are formed between the polymer strands.

Besides the gel part, some polymeric material is present within the gel that is not linked to the primary network. This mobile fraction of polymer is usually called sol.

### Elements of a polymeric network

The microscopic picture to describe polymeric networks is relatively compact and uses only a few concepts and descriptive quantities which are introduced here. The microscopic picture is given with all relevant features for the later development of a theoretical description and the basic quantities describing the network [Mark88].

The network is considered to consist of an ensemble of flexible primary polymer chains, their number customary designed  $N_2$ , which are coiled randomly. These polymeric chains are linked to each other to form a continuous network. Thus,  $\mu$  junction points or nodes divide the primary chains up into  $v$  meshes — the building blocks of the network. A node has the functionality  $\phi$ , that is the number of meshes which meet there (or  $\phi/2$  polymer chains). Additionally, the number of closed rings found in the structure is used, it is typically called the cycle rank  $\xi$ . It is dependent on the previously introduced quantities. All these numbers are explained in terms of two sample networks in **fig. 2.1** and calculated by the relationships given below.

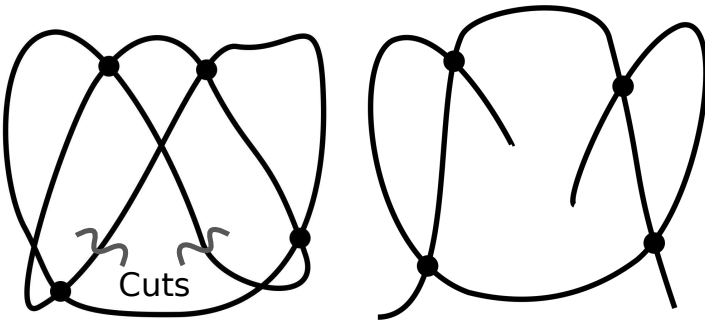


**Figure 2.1.:** Schemata of networks with ideal (left) and a regular (right) topology are shown. Both networks have  $\mu = 4$  junctions with  $\phi = 4$  functionality of the nodes. In the ideal network, made from one primary chain ( $N_2 = 1$ ), this amounts to  $v = 8$  meshes or  $\xi = 5$  cycles. For the regular network two strands were cut (see marks) to form  $N_2 = 2$  primary chains with  $v = 10$  meshes of which are  $v_e = 6$  are elastic.  $\xi = 3$  closed loops remain. Adapted from [Queslel85].

In the literature, mostly networks of ideal topology are discussed [Flory53, Dušek69, Treloar75, Mark88]. These are compromised of only one primary chain, with no loose ends present. In this case each mesh is linked to exactly two nodes and consequently the number of junction points is

$$\mu = \frac{2v}{\phi} . \quad (2.1)$$

Additionally all meshes are part of closed loops, thus

$$\xi = v - \mu + 1 \approx v - \mu = \left(1 + \frac{2}{\phi}\right)v . \quad (2.2)$$

For the description of a network often the (average) length of a mesh instead of their number is used. The length is then given by the mesh molecular weight  $M_c$ . It can be calculated from the number of meshes by (2.3) or in dependence of the cycle rank by introducing relation (2.2). Additionally,

the Avogadro number  $N_A$ , the density of the gel in the state of cross-linking  $\rho$ , and the corresponding gel volume  $V_0$  are used.

$$M_c = \frac{\rho N_A V_0}{v} = \frac{\rho N_A V_0}{\xi} \cdot \left(1 + \frac{2}{\phi}\right) \quad (2.3)$$

In a network of regular topology defects in terms of loose chain ends are allowed. Such chains are only connected to a junction on one side as seen on the right of [fig. 2.1](#) [Queslel85]. Here  $N_2$  is larger than unity and the number of effective meshes connected to two junctions is given by

$$v_e = v - 2N_2 \quad . \quad (2.4)$$

In the case of a regular topology, no strict relationship between  $v_e$  and  $\mu$  is available, while the relationship for  $\xi$ , eq. 2.2, still holds if the number of effective meshes is used instead. Different treatments for the problems arising from chain ends are found in the literature [Flory53, Dušek69]. Other types of defects such as rings or entanglements cannot be described within this framework.

## Equation of state and free energy

The response of a gel to an external stimulus is the result of the changes on the molecular level. These are related over an equation of state, being defined in terms of a suitable thermodynamic quantity. This quantity is usually taken to be the Gibbs free energy  $G$  or the Helmholtz free energy  $A$  depending on the changes impeding on the gel. The system under consideration is composed of two phases  $x$ , the gel (Phase II) and a surrounding solution (Phase I). The phase is denoted by the superscript index. The equilibrium condition is a zero free energy difference between the two phases as given by (2.5) [Flory53]. Mostly, it is convenient to use the intensive quantity of the chemical potential  $\mu_j$  instead, as defined by (2.6) in the case

of constant volume and temperature. The subscript  $j$  index denotes the component.

$$\Delta A = A^I + A^{II} = 0 \quad (2.5)$$

$$\Delta\mu_j = N_A \left( \frac{\partial \Delta A}{\partial n_j} \right)_{V,T} \quad (2.6)$$

A complete equation of state is calculated by separating  $\Delta A$  into independent contributions, arising from different interactions. This approach, introduced by Frenkel, Flory, and Rehner [Flory43], has been much disputed but is so far the only possibility to tackle this problem [Hooper90]. It treats each mesh as individual that does not feel the presence of others. Usually, the total change of energy is separated into contributions from the elasticity of the network  $A_{\text{el}}$ , the mixing of solvent and network  $\text{solvent}A_{\text{mix}}$ , and the mixing of charges and solvent  $\text{solvent}A_{\text{ion}}$  (2.7).

$$\Delta A = \Delta A_{\text{mix}} + \Delta A_{\text{el}} + \Delta A_{\text{ion}} \quad (2.7)$$

It is customary to formulate the equation of state in terms of the solvent component (subscript 1) in the gel phase, thus

$$\Delta\mu_1 = \Delta\mu_{1,\text{mix}} + \Delta\mu_{1,\text{el}} + \Delta\mu_{1,\text{ion}} \quad . \quad (2.8)$$

The effect of the single contributions to the free energy are easiest visualised when considering the case of swelling of a network. The mixing and ionic contributions usually force water into the gel for maximum dilution of the polymeric entities, however, the elastic restoring forces drive the sample towards its unstrained state. An equilibrium swelling is found, when these effects are in balance. The individual terms are discussed successively while for each a theoretical approach is given, that can be used for calculation from microscopic quantities.

## The mixing term

The free energy of mixing of polymer and solvent has two contributions. First, due to the increase of the number of possible configuration of molecular entities the entropy  $S$  rises. Secondly, the enthalpic interactions between solvent and polymer have to be considered as well. The entropic term can be approximated by the ideal mixing law (Raoult's law) which, however, neglects the polymeric nature of the solute. Therefore the Flory-Huggins theory for polymer solutions is used in this case [Huggins41, Flory41]. This theory was developed for noncross-linked systems, but it is also routinely employed for the description of gels and networks [Flory53, Mark88, Joanny96]. The approach is based on the random distribution of solvent molecules and polymer segments on a lattice. The entropy is defined by the number of possible configurations. The enthalpy of the interaction is given by the number of contact sites between polymer and solvent molecules. Only one type of interactions between neighbouring sites without orientation dependence is usually considered. The interaction parameter  $\chi$  describes the strength of this interaction normalised to  $k_B T$  and is in the order of 0.5. Values above 0.5 describe a bad solvent that enthalpically favours demixing and values below 0.5 a good solvent with additional benefit from contact sites. Additionally, polymer segments and solvent molecules are assumed to be of equal size and the interactions at all polymer-solvent contact sites to be equal. A detailed statistical treatment gives (2.9) for the free energy of mixing [Flory53].

$$\Delta G_{\text{mix}} = \Delta H_{\text{mix}} - T \Delta S_{\text{mix}} = k_B T (N_1 \ln v_1 + N_2 \ln v_2 + \chi N_1 v_2) \quad (2.9)$$

Here,  $v_j$  denotes the volume fraction and  $N_j$  the number of molecules with  $j = 1$  for the solvent and 2 for polymer components. The conversion to the chemical potential results in [Flory53]

$$\Delta \mu_{\text{mix}} = RT (\ln(1 - v_2) + \chi v_2^2 + v_2) \quad . \quad (2.10)$$

This theory is especially successful in non-polar environments, while in polar, protic systems strong, orientation dependent interactions such as hydrogen bonds are present, which are not accounted for by this approach. Remedy can only be archived in models with a higher number of interaction parameters. Several improvements have been formulated such as a virial expansion of  $\chi$  or the approach of Prange *et al.*, which includes three interaction parameters [Horkay07, Prange89, Hooper90]. The latter approach includes an additional parameter to account especially for hydrogen bonding and has been successfully employed. An entirely different approach is given by scaling theory, which has the advantage of a more empiric treatment of the problem [de Gennes79]. However, the mixing contribution is usually the least difficult to compute when ionic gels are considered.

### The elastic term

The elastic contribution to the change of the free energy is described by the change of this function with the deformation of an ensemble of polymer chains. The elastic behaviour of the network has an entropic and an enthalpic component. For the free energy of a single chain (2.11) is obtained. For this derivation the enthalpy  $C$  is considered to be the same for all conformations. It does not depend on the end-to-end distance vector  $\mathbf{r}$  and is eliminated when computing the difference of two states. In real systems this is a good approximation for small deformations only. The larger the applied deformations are, the higher is the influence of the enthalpic contribution to  $A_{el}$ .

$$A_{el} = H_{el} - TS_{el} = C(T) - k_B T \ln W(\mathbf{r}) . \quad (2.11)$$

The first step in treating the entropic contribution is to obtain a suitable chain length distribution function  $W(\mathbf{r})$ . A simple approach is given by a random walk chain statistic, it gives the Gaussian type probability function (2.12) of finding an end-to-end vector of the length  $\mathbf{r}$  [Mark88, Flory43].

## 2. Description and characterisation possibilities

---

This approach assumes an infinite number of junctions between the two ends; usually it can be safely applied for chain length between two junction points of more than 100 bonds.

$$W(\mathbf{r})dV = \left( \frac{3}{2\pi \langle \mathbf{r}^2 \rangle_0} \right)^{\frac{3}{2}} \cdot \exp \left( -\frac{3\mathbf{r}^2}{2\langle \mathbf{r}^2 \rangle_0} \right) dV \quad (2.12)$$

The quantity  $\langle \mathbf{r}^2 \rangle_0$  gives the mean value of the end-to-end distance vector in the undeformed state. The generalisation of this approach for a single chain to a polymeric network and macroscopic deformations requires a model to relate the macroscopic deformation to the deformation on the scale of a chain [Bastide96]. An extensive discussion has been documented in the literature to the nature of this relation. For details the reader is referred to the literature [Bastide96, Dušek69]. However, most treatments arrive at a result that can be written in general as

$$A_{el} = A \left( \frac{v_e k_B T}{2} \right) (\lambda_x^2 + \lambda_y^2 + \lambda_z^2) + B v_e k_B T \ln (\lambda_x^2 \lambda_y^2 \lambda_z^2) + C \quad , \quad (2.13)$$

where especially the values of the constants  $A$  and  $B$  are under discussion. In the school of Flory the so-called affine network assumption was developed [Flory53, Treloar44]. The individual chains are assumed to be each deformed in same manner as the macroscopic body. This yields  $B = 2/\phi$  and  $A = 1$ . In contrast, the phantom network assumption, originally developed by James and Guth [James43, James47], yields  $A = 1 - 2/\phi$  and  $B = 0$ .<sup>1</sup> It has to be noted, that in a perfect tetra-functional network  $A$  is exactly two times larger for the phantom model than for the affine deformation approach.

In reality, the part of formula (2.13) depending on  $B$  does seldom matter. It would generate considerable contributions only at very high deformations where the other assumptions underlying the theory also fail [Bastide96]. In

---

<sup>1</sup>In many texts  $v_e$  and  $\phi$  are replaced by  $\xi$  through relation (2.2)

real rubbers, often an intermediate behaviour in between the phantom and the affine limiting cases is found for the parameter  $A$  [Mark88]. Therefore, the so-called constrained junction theory was developed, that incorporates both views and describes the intermediate regime. This theory accounts for the change of  $A$  with the deformation of the material [Erman82, Flory82]. A parameter  $\kappa$  is introduced to account for the "confinedness" of the system. Unfortunately,  $\kappa$  is difficult to compute from microscopic quantities and is rather used as a fit parameter. Thus, the predictive capabilities of this whole approach are restricted [Horkay07]. This is probably the reason why this theory has not found wide-spread adoption so far. Here the simple phantom approach is adopted for further considerations. In reality this has proven to be valid for most systems swollen at an intermediate degree [Mark88], thus it can be written

$$\Delta A_{\text{el}} = \left(1 - \frac{2}{\phi}\right) \left(\frac{v_e k_T}{2}\right) (\lambda_x^2 + \lambda_y^2 + \lambda_z^2 - 3) \quad . \quad (2.14)$$

The conversion of this result to an expression of chemical potential usually requires a specific case of deformation and is therefore discussed in section 2.2.

For applications in which very large deformations are reached, the description by the Gaussian type chain statistics fails and leads to qualitatively wrong predictions (e.g. no strain hardening). It assumes an infinite chain length and can therefore not account for the finite extensibility of the real polymeric chain [Andrade80]. Deformation of chains up or close to the contour length is met with a very strong opposition.

Using the model of the freely jointed chain, a chain statistic can be derived that incorporates the finite extensibility [Treloar75, Cohen91]. However, real chains do have constraints in terms of bond angles as well and, therefore, the number of bonds along a chain is not used. Rather, the smaller number  $n$  of the statistical segments is used which behave as if they were freely jointed. The statistical segments are analogous to the number Kuhn

segments but different values are obtained. The solution of the problem was adapted for the use of Hydrogels in the case of isotropic dilation (swelling) by Oppermann [Oppermann92, Schröder96, Brendel99]. In the notation of Flory<sup>2</sup> the formula reads

$$\Delta\mu_{\text{el}} = \frac{\xi RT V_1}{3N_A V_0} \cdot \left( \frac{v_{2c}}{v_{2m}} \right)^{-2/3} v_{2c} n^{1/2} \mathfrak{L}^{-1} \left( n^{-1/2} \left( \frac{v_{2c}}{v_{2m}} \right)^{1/3} \right) \quad (2.15)$$

The solution includes the inverse of the Langevin function  $\mathfrak{L}$  and  $V_1$  the molar volume of the solvent. This description has been successfully used to describe the behaviour in the case of large deformations (e.g. elongation by several 100 % of the initial chain end-to-end distance) and can be used to describe the elasticity of much shorter chains, of 20 bonds and up, sufficiently. This approach is only used when necessary. Due to the need of the additional parameter  $n$  that is not straightforward to compute and need to solve  $\mathfrak{L}^{-1}$  numerically.

### The ionic term

The ionic term deals specifically with the contribution to the free energy of species which are charged and can “exchange” between the phases. The solvent and the gel phase have to obey the principle of electro-neutrality [Flory53, Oppermann92]. This means, that the same amount of positive and negative charges has to be present in each phase, to prevent it from being not macroscopically charged. Thus, the ionic term is similar to the mixing contribution but with a electro-neutrality side condition. Only mobile species are considered a priori as these are free to distribute in the two phases, charges bound to the polymer are considered a posteriori by the electro-neutrality principle. When formulating the chemical potential of the solvent in one phase, one obtains (2.16). Assuming a dilute solutions

---

<sup>2</sup>The entity  $v^*$  of Oppermann corresponds to  $v_c/V_0 N_A$  in the Flory notation and the swelling degrees  $q$  are just the inverse of the polymer volume fraction  $v_2$ .

$\gamma_k = 1$  holds and the mole fraction  $x_k$  of the solvent can be replaced by the approximation on the right hand side of the equation [Flory53, p. 590].

$$\mu_k = \mu_k^0 + RT \ln a_k = \mu_k^0 + RT \ln \gamma_k x_k \approx \mu_k^0 - V_1 RT \sum_k c_k^j \quad (2.16)$$

The activities of ionic species in solution and especially in (ionic) gels can be obtained by theory or through measurements only with great difficulty. Therefore, it is customary to replace them by concentrations in the approximation of diluted solutions [Flory53, Oppermann92, Hooper90]. As gels are semi-dilute systems at best, this introduces serious complications and the results obtained from this approximation are usually qualitative only. However, no general improvement has been found so far. When writing the chemical potential difference of the two phases for all mobile ionic species in the line of the Donnan approach one obtains [Donnan32]

$$\Delta\mu_{\text{ion}} = -RTV_1 \sum_k c_k^H - c_k^I \quad . \quad (2.17)$$

Here, the illustrative case of a system of a ionic gel with an added simple 1:1 electrolyte (co-ions) of concentration  $c_s$  in an infinitely large bath is considered. In an additional assumption, the counterions of the gel are taken to be the same as in the added electrolyte. Therefore, the four charged species reduce to only two different ones which have to be considered. The bound charges of the gel have to stay in the gel and hold an equal amount of counterions of opposite charges due to electro-neutrality. Their concentration is  $i\rho v_2/M_M$  where  $v_2$  is the polymer volume fraction,  $i$  is the ionisation degree of the monomers and  $M_M$  their molecular weight. However, a number of the co-ions with the same sign as the bound charges can move into the gel due to entropic reasons; their concentration inside the gel is  $c'$ . Again due to electro-neutrality they draw their counterions with them. Thereby for the two considered charged species in the solution phase the same concentration  $c_s$  is found while in the gel phase, the concentration of one species is

## 2. Description and characterisation possibilities

---

higher due to the present gel counterions.<sup>3</sup> With the assumption of the gel being in an infinite solution bath ( $c_s$  is constant) one obtains [Schröder96, p. 23]

$$c_s^2 = c' \cdot \left( c' + \frac{i\rho v_2}{M_M} \right) \quad (2.18)$$

and by solving for  $c'$  and substituting  $c'$  and  $c_s$  into (2.17) the chemical potential (2.19) can be calculated.

$$\Delta\mu_{\text{ion}} = 2RTV_1 \left[ c_s - \sqrt{c_s^2 + \left( \frac{i\rho v_2}{2M_M} \right)^2} \right] \quad (2.19)$$

In this result the number of charges on the polymer is given as degree of ionisation  $i$  per monomer unit, while in the terminology of Oppermann  $M_2$  is used as the molecular weight of the backbone per one free charge [Schröder96].

This result enables the calculation of not only the influence of charges in the system on the chemical potential but also the ion distribution between gel and solution phases. By solving the quadratic equation (2.18) one obtains for the distribution ratio [Victorov06a, Victorov06b]

$$\frac{c'}{c_s} = \frac{-\frac{i\rho v_2}{2M_M} + \sqrt{c_s^2 + \left( \frac{i\rho v_2}{2M_M} \right)^2}}{c_s} \quad . \quad (2.20)$$

As mentioned above the overall concentration of charges is always larger inside the gel than outside but only including bound charges. The concentration of diffusible ions is smaller inside. The concentration ratio of diffusible ions inside and outside the gel ( $c'/c_s$ ) is a function of the amount of added salt and the polymer volume fraction and is depicted for some examples in **fig. 2.2**. This approximate approach shows directly, that the

---

<sup>3</sup>Thus, no matter what actual concentrations used, the amount of charges in the gel is always larger than outside [Flory53, p. 586].

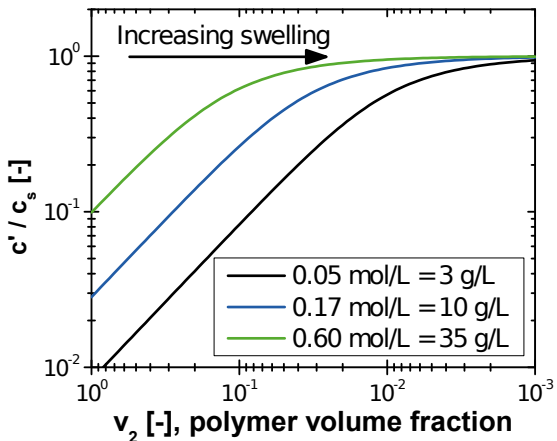


**Figure 2.2.:** The relative concentration of mobile ions  $c'/c_s$  in the gel and the solution phases is shown as calculated by the Donnan approach by (2.20). With increasing swelling of the gel (lower polymer volume fraction  $v_2$ ) the difference between the phases is decreasing. The three curves describe different salt concentrations in the external solution  $c_s$ . The values in g/L are computed for  $\text{NaCl}$  as the dissolved electrolyte.

concentration difference between the phases is largest for small swelling degrees and low concentrations of added salt solution.

No definitive theory has so far been worked out for the treatment of the activities in highly concentrated ionic solutions. Theoretical calculations on model geometries prove, however, that when increasing the concentration the charges on the polymer backbone they start to form localized pairs with their counterions (so called Mannig condensation) [Skolnick77]. Their effective concentration for the overall phase is decreased. Thus, an increase of charging of the polymer does not result in more effective charges when a certain threshold is reached.

## 2.2. Discussion of characterisation methods and parameters

The formulation of an equation of state for the system hydrogel and the surrounding solution offers the possibility to probe the network for its structure and properties by suitable experiments. As a result, the network parameters described in the previous section can be obtained. The most important parameter is the number of meshes per unit volume or in another way the mesh length. Additionally, the true degree of ionisation, the number of statistical segments per chain, or the Flory-Huggins interaction parameter can be obtained from experiments. When the Gaussian chain statistics is used, only a single parameter is used to describe the network which can be calculated from a single experiment. For the statistic of the freely jointed chain two parameters describe the network. In this case a series of experiments conducted e.g. at different salt concentrations is necessary [Schröder96, p. 26].

In this work, the evaluation of equilibrium swelling and modulus data of hydrogels in terms of the equation of state is discussed. Both approaches probe the equation of state in equilibrium type experiments. This means, the results are taken when a steady state has been reached and the dynamic processes within the phases have ceased to play a role. Both types of experiments use the equation of state under different boundary conditions. Thereby, the equation of state has to be evaluated for each case. This equation of state is worked out in turns for swelling and mechanical data.

### Equilibrium swelling experiments

The swelling of a polymeric network is a process, that increases the body's volume by taking up a solvent or solution. The solvent and solutes mix with the units of the network and the network is deformed in the course. The deformation is an isotropic dilation: an equal extension along the three principal axes  $t = x, y$  and  $z$  (**fig. 2.3**). This deformation is measured by the deformation ratio  $\lambda_t = L_t / L_{0,t}$  and given for this isotropic case as  $\lambda_t = (1/v_2)^{1/3}$

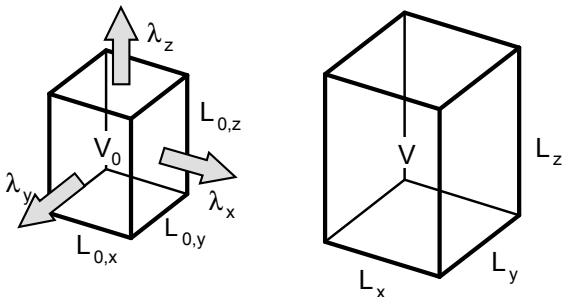


**Figure 2.3.:** Schematic drawing of the dilation of a body during swelling from  $V_0$  to  $V$  by extending all principal axes  $x$ ,  $y$ , and  $z$  from  $L_{0,t}$  to  $L_t$ . The extension ratio is defined as  $\lambda_t = L_t / L_{0,t}$ .

where  $v_2$  is the polymer volume fraction in the gel [Mark88, p. 50]. The swelling equilibrium is reached when the chemical potential for the solvent  $\mu_1$  is the same inside the network and in the surrounding solution. If no additional pressure is exerted on the system, the so-called case of free swelling, the equilibrium condition is fulfilled when setting equation (2.8) to zero [Flory53, p. 587].

$$\Delta\mu_1 = \Delta\mu_{1,\text{el}} + \Delta\mu_{1,\text{mix}} + \Delta\mu_{1,\text{ion}} = 0 \quad (2.21)$$

In this equation, the single contributions to the chemical potential are substituted by the equations discussed in the previous section. Here, the case of swelling in pure water without any added salt is considered. This will lead to very large degrees of swelling and therefore a strong extension of the polymeric chains. Thus, the Langevin type chain statistic for the elastic contribution (2.15) has to be used to describe the finite extensibility of the chains. Additionally, equations (2.10) and (2.19) are used for the mixing and ionic contribution, respectively, to yield (2.22).

$$\begin{aligned}\Delta\mu_1 = & RT \left( \ln(1 - v_2) + \chi v_2^2 + v_2 \right) \quad (2.22) \\ & + \frac{\xi RTV_1}{3N_A V_0} \left( 1 - \frac{2}{\phi} \right) \left( \frac{1}{v_2} \right)^{-2/3} v_{2c} n^{1/2} \mathfrak{L}^{-1} \left( n^{-1/2} \left( \frac{1}{v_2} \right)^{1/3} \right) \\ & + 2RTV_1 \left[ c_s - \sqrt{c_s^2 + \left( \frac{i\rho v_2}{2M_M} \right)^2} \right]\end{aligned}$$

This general expression has to be adjusted for the specific experiments conducted in the present work: no co-ions were present thus  $c_s = 0$ . The cross-linking process that defines the equilibrium state of the gel was performed in solution with a polymer volume fraction of  $v_{2c}$ . Therefore,  $v_2$  of the considered state has to be replaced by the weight fraction  $v_{2m} = v_2/v_{2c}$  with respect to the reference state. At last,  $\xi$  is replaced by  $M_c$  using relation (2.3). Thereby, one obtains (2.23) which can easily be solved for  $M_c$  and computed from known quantities. This done in section 3.3.

$$\begin{aligned}\Delta\mu_1 = & RT \left( \ln(1 - v_{2m}) + \chi v_{2m}^2 + v_{2m} \right) \quad (2.23) \\ & + \frac{\rho RTV_1}{3M_c} \left( 1 - \frac{2}{\phi} \right) \left( \frac{v_{2c}}{v_{2m}} \right)^{-2/3} v_{2c} n^{1/2} \mathfrak{L}^{-1} \left( n^{-1/2} \left( \frac{v_{2c}}{v_{2m}} \right)^{1/3} \right) \\ & - \frac{RTV_1 i\rho v_{2m}}{M_M}\end{aligned}$$

In the case of the Gaussian chain statistics, the elastic term would read [Oppermann92, Schröder96]

$$\Delta\mu_{1,el} = \frac{\rho RTV_1}{M_c} \left( 1 - \frac{2}{\phi} \right) v_{2c}^{2/3} v_{2m}^{1/3} . \quad (2.24)$$

The equilibrium degree of swelling can be predicted from a set of parameters and depends strongly on the chosen model. An example for such a model calculation is shown in **fig. 2.4**. The single contributions to the chemical potential are calculated for a hydrogel of typical composition (DC = 1 mol-%,  $Q_{syn} = 4$  g/g, DN = 75 mol-%, see appendix A.1) as a function

of the solvent content of the network. The experimental value is 105 g/g. The intersections of the lines, indicated by arrows, show an equilibrium given by the equivalence of the chemical potential contributions. At these points, the theoretical swelling degrees  $Q_{\text{eq}}$  for different models can be extracted. In a non-ionic hydrogel only the mixing contribution is compared to the elastic term and the  $Q_{\text{eq}}$  is given by the intersection of the black and red lines at  $Q_{\text{eq}} = 10.5$ . It is easily seen, that the type of chain statistic does not have a considerable effect in this case. For ionic hydrogels, the combination of the employed ionic and mixing term is needed (green line), which is much greater and enables higher swelling. The type of chain statistic plays a very important role here: the simple Gaussian approach overestimates the equilibrium swelling by one decade (intersection with the grey line,  $Q_{\text{eq}} = 2300$ ) while the Langevin approach gives a good approximation of the experimental result (intersection with the red line, ( $Q_{\text{eq}} = 133$ )). This approach can also be used to obtain network parameters for other important cases of swelling not considered in this work. First, this would be the swelling in the presence of added salt where  $c_s \neq 0$ . However, a meaningful calculation is only possible if diluted solutions are used, otherwise very large deviations from the experiments are seen, as activities would be needed to account for the true salt concentration [Schröder96, p. 22]. Another case is the swelling under load where an external pressure  $p_{\text{ext}}$  is applied to the gel. The chemical potential needs another term to calculate the equilibrium condition. A formulation of the previously developed formulas in terms of osmotic pressure  $\Pi_j$  (2.25) is more useful [Buchholz98, p. 201].

$$\Pi_1 = \frac{\Delta\mu_1}{V_1} \quad (2.25)$$

The recalculation of above quantities is straight forward and the new equilibrium condition now reads including the external hydrostatic pressure

$$p_{\text{ext}} = \Pi_{1,\text{el}} + \Pi_{1,\text{mix}} + \Pi_{1,\text{ion}} \quad . \quad (2.26)$$

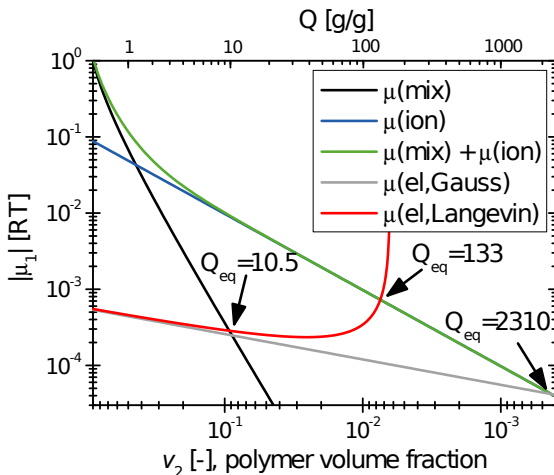


**Figure 2.4.:** The absolutes of different contributions to the chemical potential of the solvent  $|\mu_1|$  in a swollen hydrogel are shown as a function of solvent content in the gel ( $v_2 \approx 1/Q$ ). The equilibrium swelling based on the different contributions is given by the intersections (arrows). The bottom x-axis scales with the polymer volume fraction  $v_{2m}$  and the top with the swelling degree  $Q$ . The functions were calculated for a model gel with  $\chi = 0.5$ ,  $c_s = 0$ ,  $i = 0.3$ ,  $M_M = 72$  g/mol,  $\rho = 1.3$  g/cm<sup>3</sup>,  $V_1 = 18$  cm<sup>3</sup>/mol,  $n = 10$ ,  $v_{2c} = 0.2$ ,  $\phi = 4$ , and  $M_c = 7200$  g/mol which corresponds to a degree of cross-linking of 1 mol-% for acrylic acid. The elastic contribution was calculated for Gaussian and Langevin based chain statistics. The experimental value for the closest matching gel in this work is  $Q_{\text{eq}} = 105$  g/g.

## Deformation experiments

In a deformation experiment the response of a polymeric network to an applied stress is used to calculate the characteristic network parameters. The basic relation is given by the change of the free energy with deformation  $\lambda_t$  of the specimen along the coordinates  $t$  and the strain  $\sigma_t$ .

$$\sigma_t = \frac{\lambda_t}{V} \left( \frac{\partial \Delta A}{\partial \lambda_t} \right)_{T,V} = \frac{\lambda_t}{V} \left( \frac{\partial \Delta A_{el}}{\partial \lambda_t} \right)_{T,V} \quad t = x, y, z \quad (2.27)$$

For the evaluation of  $\Delta A$  it is assumed, that the deformation is fast in comparison with the exchange of solvent or solutes with the surrounding bath. This means the degree of swelling does not change due to the deformation, thereby the mixing and the ionic contribution are not dependent on  $\lambda_t$  and the right hand side of (2.27) is true.

If the deformation is not too large and carried out on samples that are moderately swollen and have long meshes the Gaussian chain statistic is usually suitable for treatment of the problem at hand. For the discussion of cases where this assumption is not valid, the reader is referred to the work of Treloar and Oppermann [Treloar75, Schröder96]. The further evaluation of (2.27) depends on the type of deformation that is applied to the sample. A very large number of experiments is discussed in the literature: beside the classic compression and shear experiments also indentation, wave propagation, scattering experiments, and many others are used to probe the elastic response of the material [Geissler88, Horkay00, Hu10, Lionetto05, Geissler82]. Here, only the first two examples are discussed further.

In the case of uni-axial compression or equally tension of a body along the arbitrary  $x$  direction, it is expanding (or shrinking) in the other two dimensions (**fig. 2.5**). Assuming a constant volume the three stretch ratios are defined in terms of  $\alpha$  as follows.

$$\lambda_x = \alpha v_{2m}^{1/3} \quad (2.28)$$

$$\lambda_z = \lambda_y = \alpha^{-1/2} v_{2m}^{1/3} \quad (2.29)$$

Using (2.28) and (2.14) in (2.27) yields the constitutive equation for the compression of swollen networks (2.30). The first part of the equation relating to the network characteristics is a constant with respect to the defor-

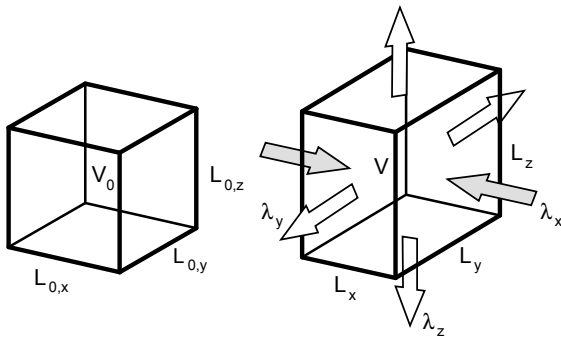


**Figure 2.5.:** Schematic drawing of the deformation of a body by compressing one axis ( $x$ ) and extending the others ( $y$ ,  $z$ ). The undeformed and deformed lengths of the axes  $t$  are  $L_{0,t}$  and  $L_t$ , respectively. The extension ratio is defined as  $\lambda_t = L_t / L_{0,t}$ .

mation while the second part is a function of this. The type of deformation dependence is called Neo-Hookean behaviour due to its resemblance to the classical Hooke's law for a very small deformation  $\alpha$ . Comparison with the Hooke's law<sup>4</sup> yields that the leading constant is the Young's modulus divided by three [Treloar75].

$$\sigma_x = \underbrace{\left(1 - \frac{2}{\phi}\right) \left(\frac{v_e k_T}{2V}\right) v_{2m}^{2/3}}_{E/3} \left(\alpha - \frac{1}{\alpha^2}\right) \quad (2.30)$$

It is customary for rubber-like materials to express the measured data by the means of the reduced stress  $f^*$ , that is normalised to the unstrained, dry cross-section of the sample  $A_d$ .

$$f^* = \frac{f v_2^{1/3}}{A_d \left(\alpha - \frac{1}{\alpha^2}\right)} \quad (2.31)$$

<sup>4</sup>The Hooke's law reads  $\sigma = E \cdot \varepsilon$  and the Neo-Hookean law  $\sigma = C(\lambda - \lambda^{-2})$  with  $\lambda = 1 + \varepsilon$ . If the latter is expanded into a Taylor series one obtains  $C(\lambda - \lambda^{-2}) \approx C(1 + \varepsilon - 1 + 2\varepsilon) = 3C \cdot \varepsilon$ . Comparing this result with classical Hooke's law one finds  $C = E/3$ .

By multiplying both sides of (2.30) with the deformed area  $A$  to obtain the force  $f$  and substituting it into (2.31), the reduced stress is obtained (2.32). For a material obeying the Neo-Hookean law,  $f^*$  is independent of the deformation. It is a constant equal to the modulus of rigidity  $G$  [Mark88, Baselga87].

$$f^* = \left(1 - \frac{2}{\phi}\right) \cdot \frac{v_e k_B T v_{2c}^{2/3}}{V_0} \quad (2.32)$$

Experimental data of cross-linked system can be described by this prediction only at very small deformations ( $\alpha < 1.2$ ). At higher deformations, it overestimates the stress and the reduced stress is not independent of the deformation. This failure is a result of the assumptions underlying the statistical network theory. Especially, the assumption of equal sized meshes and a behaviour at the phantom limit is problematic.

To overcome this problem Mooney and Rivlin developed a simple approach introducing a deformation dependent term into the constitutive equation of  $f^*$  [Mooney40, Rivlin48, Gumbrell53]. Their result (2.33) is based on continuum mechanic considerations and does not have an underlying microscopic model. They use two material constants  $C_1$  and  $C_2$ , usually referred to as Mooney-Rivlin coefficients.

$$f^* = \left(2C_1 + \frac{2C_2}{\alpha}\right) \quad (2.33)$$

This equation can account for strong deviations from the Neo-Hookean behaviour in strain-stress data as well.  $C_1$  is proportional to the constant found in the Neo-Hookean model and one can use the same microscopic interpretation. The microscopic interpretation of  $C_2$  has been the subject of intensive discussion; it is often attributed with the change of "affine-ness" of the meshes during the deformation [Horkay07, Dušek69]. The Mooney-Rivlin approach is nevertheless surprisingly successful in incorporating the deviations from simple entropy elasticity especially in the tension of rubber.

When plotted, this equation corresponds to a horizontal line in the plot of reduced stress against  $\alpha^{-1}$ .

The second case of deformation to be discussed is shear. In the case of simple shear the material is strained by fixing one face, arbitrarily in the x-y-plane, of the sample and moving the opposite face parallel. In contrast, the case of pure shear can be depicted for a cubic sample in the following way: the material is held at two opposed edges and those drawn in opposing directions along edges axes from each other, distorting the body to a rhombus. In both cases, the sample dimension in the perpendicular z direction is held constant. For the case of pure shear the stretching ratios are formulated to (2.34) when a constant volume is assumed [Wall42, Mark88].

$$\lambda_z = 1 \times v_{2m}^{1/3} \quad \lambda_x = \alpha v_{2m}^{1/3} \quad \lambda_y = \frac{1}{\alpha} v_{2m}^{1/3} \quad (2.34)$$

Substituting equations (2.34) and (2.14) in (2.27) yields the constitutive law.

$$\sigma_x = \left(1 - \frac{2}{\phi}\right) \left(\frac{v_e k_B T}{2V}\right) v_{2m}^{2/3} \left(\alpha^2 - \frac{1}{\alpha^2} - 2\right) \quad (2.35)$$

Using the shear strain defined as  $\gamma = \alpha - 1/\alpha$  [Wall42, Flory53], one obtains (2.36) for the case of pure shear, which is, except of the dilation term, equal to the classical Hooke's law and the statistical interpretation of the modulus of rigidity  $G$  is readily identified.

$$\sigma_x = \underbrace{\left(1 - \frac{2}{\phi}\right) \left(\frac{v_e k_B T}{2V}\right) v_{2m}^{2/3}}_G \gamma^2 \quad (2.36)$$

For the case of simple shear the material law is given by [Flory53]

$$\sigma_x = \underbrace{\left(1 - \frac{2}{\phi}\right) \left(\frac{v_e k_B T}{2V}\right) v_{2m}^{2/3}}_G \gamma \quad . \quad (2.37)$$

When comparing the experiments carried out under compression and shear deformation the same results are obtained. In shear experiments, the modulus of rigidity  $G$  is measured and in compression and tension the Young's modulus  $E$  which is three times larger than the constant obtained for the Neo-Hookean solid. Yet, these material constants are independent but are connected by the Poisson's ratio  $\nu_P$  as given in (2.38) [Geissler80, Graessley08]. The Poisson's ratio gives the ratio of relative length  $L$  change to relative width  $D$  change of a body (2.39) under deformation. This is equal to the volume change of the material. For a perfectly incompressible, elastic material a value of  $\nu_P = 0.5$  is obtained. In this case  $E/3 = G$  which is exactly the constant obtained from the Neo-Hookean law.

$$2(1 + \nu_P) = \frac{E}{G} \quad (2.38)$$

$$\nu_P = \frac{\Delta D/D}{\Delta L/L} \quad (2.39)$$

## Conclusion

Typical characterisation methods for polymeric networks like swelling and mechanical measurements only show part of the reality. They are only capable of giving one value for the mesh length or number of meshes and junctions. However, in any real gel a distribution of mesh sizes and pore diameters is found. The methods based on evaluating the equilibrium equation of state can only recover a mean value of this distribution. Yet, for understanding the properties and also the behaviour in the experiments, this is not sufficient. The evaluations presented in this chapter, derived from the equilibrium thermodynamics of the gel and solution phase, are a good tool for understanding the general behaviour of the network and also some semi-quantitative investigations. However, for a deeper insight in the structure and the properties a knowledge of the complete mesh size dis-

## 2. Description and characterisation possibilities

tribution function would be most helpful. Both approaches, the standard experiments and more advanced techniques which explore the distribution, are presented in the next two chapters based on experimental data gathered from gel samples.

### **3. Synthesis of gel samples and characterisation by standard methods**

The optimisation of the desalination process introduced in chapter 1 depends completely on the knowledge of the properties of its working material — the hydrogel. The polymer is in the centre and controls the capabilities of the process. The basic features of the gel have to be well known, such as the amount and speed of solvent uptake, the mechanical strength or the content of extractable polymeric material. These features do not only control the solvent uptake but also the uptake or rejection of ions, which is the driving force of the desalination process discussed in the later chapters. If only a small part of the ions in the surrounding solution can penetrate the gel, after a desalination experiment, water with a low salt concentration will be obtained.

The gel samples and their basic properties are investigated in this chapter. Samples were of commercial origin and self-synthesised by free radical polymerisation. The structure of the latter networks could be altered as needed by varying several synthetic parameters and introducing comonomers. The known information on the commercial superabsorbers is given as well. The optimisation of the desalination process can only succeed with a knowledge of the basic properties of the gels. The swelling behaviour is investigated first: the amount and dynamics of the solution uptake define the gel as an absorber and the mesh size can be calculated from the data. The swelling capacity defines the amount of polymer that is needed in the desalination process as will be shown later (section 7.1). The swelling speed has to be known to define the equilibrium conditions and is important for the potential technical throughput of the desalination process.



**Figure 3.1.:** Photograph of swollen hydrogel beads.

By investigating the mechanical behaviour the resistance to deformation of the gels is measured. An important information for the pressure that is theoretically needed in the desalination process. The mean mesh size values obtained by equilibrium swelling and deformation experiments are evaluated in terms of the theory given in the previous chapter. The sol content is a measure for the efficiency of the synthesis and also critical, if water with a certain quality is to be produced. A large content of polymer in the desalinated water would be unfavourable for some applications. In contrast to these techniques focused on macroscopic properties, in the next chapter the microscopic structure and pore size distribution are investigated.

### **3.1. Procedure and parameters of synthesis**

The polymer samples used in the scope of this work can be divided into two categories: industrially produced samples and self-synthesised hydrogels. First the general considerations on the preparation procedure of hydrogels on the basis of acrylic acid and other monomers are described. The synthetic parameters are introduced as well as a number of possible comonomers. Finally, the industrial superabsorbent polymers obtained from the BASF are described.

The hydrogels in this work were produced by free radical polymerisation of acrylic monomers in water [Buchholz98, Umendra99]. An example of the product is shown in fig. 3.1. Here, the approach of *in situ* cross-linking is chosen instead of cross-linking of the final chains due to simplicity. The bi-functional monomer acrylic acid (AAc) is polymerised together with a oligo-functional cross-linking monomer at the time of synthesis. For the latter, the tetra-functional *N,N'*-methylenebisacrylamide (MBA) is used in this study, a standard cross-linker used in commercial applications as well [Buchholz98]. Through the cross-linker, junction points are formed which connect the individual polymeric chains made from poly(acrylic acid) (pAAc) to form a continuous network which reaches the sample dimensions. Only a single, large molecule is produced. The reaction schema if given in **fig. 3.2**. Instead of acrylic acid other monomers can be used or copolymerised by the same reaction. In this work the monomers of (hydroxyethyl)methacrylate (HEMA) [Yarimkaya07a, Yarimkaya07b], methacrylic acid (MAAc), N-isopropylacrylamide (NiPAM) [Snowden96, Jones00], and acrylamide (AAm) [Rangaraj97, Mudiyanselage08] were used which are shown in **fig. 3.3**.

Part of the carboxylic acid function of acrylic acid can be transferred to its carboxylate form by the addition of a strong base (e.g. *NaOH*). Here, it was chosen to do this prior to synthesis, instead of a post-synthesis modification due to practical reasons.<sup>1</sup>

The polymerisation reaction proceeds via a radical chain reaction [Umendra99]. The double bonds of the acrylic monomers are transformed into two single C-C-bonds connecting the monomers in a chain. By this reaction a very large enthalpic gain is freed. The chain carrier is a radical generated by a suitable initiator. The initiator should be water soluble and work at ambient temperatures. The latter requirement is due to the heat dissip-

---

<sup>1</sup>Partly ionised acrylic acid polymerises slower and can therefore be better handled and the post synthesis modification of uncharged pAAc was found to be slow due to diffusion and solubility issues.

### 3. Synthesis of gel samples and characterisation by standard methods

---

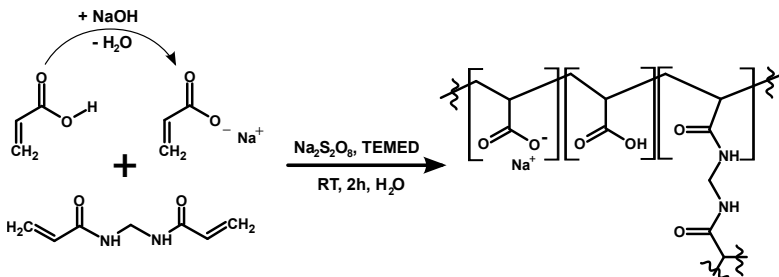


**Figure 3.2.:** Schema of the free radical polymerisation reaction of acrylic acid and sodium acrylate to form a polymeric network. The tetra-functional monomer  $\text{MBA}$  forms the junction points. More information is given in the text.

tion and the generation of regular gel slaps for rheological tests (see fig. 3.8). In the present work, sodium persulfate (SPS) together with the accelerator  $N,N,N',N'$ -tetramethylethylenediamine (TEMED) is used. SPS decomposes readily at room temperature and is known to work well with a number of acrylic monomers. However, the absence of oxygen is necessary as it inhibits the reaction and leads to undefined samples and an increased sol content. The kinetics of radical chain reactions is well studied and the general theory [Odian04, Lechner03, Tieke05] as well as its application to the synthesis of poly(acrylic acid) is found in the literature and not discussed here further [Oppermann92, Umendra99, Vervoort05].

Water is conveniently used as a solvent and the reaction is carried out in bulk. The product is usually used for water based applications and water is non-toxic and allows an effective transfer of the heat produced during the polymerisation reaction. The routes via emulsion or dispersion polymerisation were not used due to problems with the desired sample amount and particle sizes (0.1 – 1 mm).

The synthesis procedure is adapted from similar procedures in recent literature [Oppermann92, Umendra99, Vervoort05]. It is discussed in appendix A.1 with the exact quantities involved and a list of produced sam-

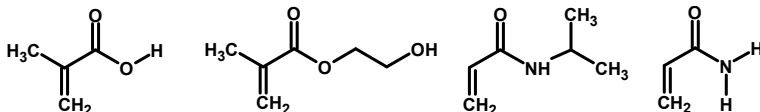


**Figure 3.3.:** Comonomers used in the polymerisation with acrylic acid. From left to right are drawn: methacrylic acid (MAAc), (hydroxymethyl)methacrylate (HEMA), N-isopropylacrylamide (NiPAM), and acrylamide (AAm).

ples. A part of the synthesis mixture was transferred into molds prior to polymerisation in order to acquire specimen of regular shape for mechanical test (see **fig. 3.8**).

The reaction procedure outlined above offers several parameters that can be adjusted to alter the obtained gel. All parameters can be given with respect to the amount of acrylic monomer in the mixture. First, the statistical mesh length of the network is given by the amount of cross-linker added. The degree of cross-linking (DC) is defined as ratio of moles of all bifunctional monomers to the moles of polyfunctional monomer:

$$DC = \frac{n(MBA)}{n(AAc) + n(\text{comonomer})} \times 100\% \quad [DC] = \text{mol-\%} \quad . \quad (3.1)$$

The amount of charges on the polymer backbone is given by the percentage of acidic monomer that is converted to its ionic form by addition of a base (or acid if a polycationic monomer is used). Therefore, the degree of neutralisation (DN) is given as

$$DN = \frac{n(NaOH)}{n(AAc)} \times 100\% \quad [DN] = \text{mol-\%} \quad . \quad (3.2)$$

The reference state of the gel is defined at the time of synthesis by the amount of solvent present in the network structure. It defines the relaxed state of the meshes with respect to all other connected meshes. Beside this, kinetic points have to be considered. At a higher monomer dilution, longer primary chains are produced but also the proportion of inelastic defect in-

### 3. Synthesis of gel samples and characterisation by standard methods

---

creases. Here, the reference state is defined by a swelling ratio by mass ( $Q_{\text{syn}}$ ), as the ration of all polymer components with respect to water.

$$Q_{\text{syn}} = \frac{m(H_2O)}{m(\text{AAc}) + m(\text{MBA}) + m(\text{comonomer})} \quad [Q_{\text{syn}}] = \text{g/g} \quad (3.3)$$

At last, when a copolymer is produced by adding a second monomer, its incorporation in the polymer strand is assumed to be statistical with the weight of its respective mole fraction in the mixture (CO).

$$\text{CO} = \frac{n(\text{comonomer})}{n(\text{AAc}) + n(\text{comonomer})} \times 100\% \quad [\text{CO}] = \text{mol-\%} \quad (3.4)$$

A variation of all of this parameters was undertaken within this thesis. A list of the produced samples is found in the appendix in tab. A.1. The specific batch is described in this work by a shorthand incorporating these synthetic parameters. First, the main monomer is given (e.g. AAc), next the DC in mol-%, then the DN in mol-% and at the end  $Q_{\text{syn}}$  (in g/g) is written. If a comonomer is added its type and amount (in mol-%) is written after the first monomer. Following this schema, shorts such as pAAc-DC1-DN75-Q4 and p(AAc-HEMA50)-DC1-DN78-Q4 are obtained.

Industrially produced samples of superabsorbent polymers (SAP) were obtained from the BASF. The exact composition is unknown and only a few specifics were released, which are summarized in **tab. 3.1**.

## 3.2. Swelling properties

Swelling is a typical process of polymeric networks and one of the most important features used in applications [Brannon-Peppas90]. By swelling, the network structure is extended as a suitable solvent is taken up into it and the previously liquid phase is solidified and immobilised. Swelling is used extensively for the characterisation of gels as the equilibrium swelling

**Table 3.1.:** Details of the commercial hydrogel samples obtained from the BASF. The Luquasorb 1280 samples were produced with  $K^+$  counter-ions to the acrylate groups instead of the  $Na^+$  ions normally used.

Sample name	Monomer	Particle size μm	Structure
Luquasorb 1030	AAc	300	regular
Luquasorb B1110	AAc	160	core-shell
Luquasorb 1280 RL	AAc (contains $K^+$ )	< 500	regular
Luquasorb 1280 RS	AAc (contains $K^+$ )	1000 – 4000	regular
Hysorb	AAc	(unknown)	(unknown)
VP 300	MAAc	150 – 800	regular

capacity is closely connected to the topology of the gel as shown in the previous chapter.

The degree of swelling of a network is quantified by the ratio of solvent to polymeric material. In the swollen gel this ratio can either be volume or mass based — in the present work the latter option is used and the ratio  $Q(t)$  is defined as (3.5). The value of  $Q(t)$  obtained when all exchange process have ceased is the equilibrium swelling degree  $Q_{eq}$ , if the sample is free from other constraints. It is a thermodynamic property of a gel, depending on solvent quality, temperature, pressure and additional solutes. Further,  $Q_{eq}$  is a characteristic feature of a gel that is not controlled by one but several synthetic parameters.

$$Q(t) = \frac{m(\text{H}_2\text{O})(t)}{m(\text{polymer})} \quad (3.5)$$

When placing dry polymer in contact with a solvent reservoir, it will take up solvent and swell. This is a time dependent process and therefore the swelling degree  $Q(t)$  is time dependent [Tanaka79, Buchholz98]. When dry polymer is in contact with a solution, in the beginning  $Q(0) = 0$  holds as no solvent is present in the polymer and  $Q(t)$  increases upon solvent

uptake. For many samples the maximum degree of swelling is equal to the long time limit  $Q_{\text{eq}}$  giving a monotonic increase in  $Q(z)$ . The analysis of this time dependence yields time constants that are mainly controlled by external and macroscopic parameters of the gel particles. The solvent uptake process is diffusion controlled and therefore the main factors for its rate are particle form and size as well as the bulk modulus [Tanaka79].

The equilibrium values  $Q_{\text{eq}}$  and the kinetic constants controlling the build up were measured for a variety of samples of neat pAAc gels, their copolymers and commercial samples. The investigated ionic hydrogels typically show high solvent capacities with a strong dependence on the sample composition (e.g. the degree of cross-linking). The degree of swelling can be obtained by a procedure described in appendix A.2. The equilibrium values of  $Q_{\text{eq}}$  were usually taken after  $t = 24$  h in salt solutions of 10 g/L  $\text{NaCl}$  (brine) and in deionised water (DI). They are given as the mass ratio (3.5) because the knowledge of the densities is not necessary this way. The accuracy of these measurements is typically high with a standard error below 1 %. This error is given by the standard deviation of three independent experiments on the same batch.

For neat pAAc networks, three synthetic parameters were investigated which all showed a considerable effect on  $Q_{\text{eq}}$ . These are the degree of cross-linking (DC), the degree of neutralisation (DN), and the water content of the monomer solution  $Q_{\text{syn}}$ . These quantities and the polymer structure are further explained in the previous section. A number of different DC values was investigated in two series of  $Q_{\text{syn}}$  values of 2 and 4 g/g and in brine and DI. In all cases, a strong decrease of solvent capacity with higher DC values was found as seen in **fig. 3.4**. For the measurements in brine a function of  $Q_{\text{eq}} = A \log(\text{DC}) + B$  was found to represent the data well. Slopes values  $A$  of  $-30.6$  and  $-12.2$  were obtained for  $Q_{\text{rel}} = 4$  and 2 g/g, respectively. This is to be expected because at lower DC values a looser network is formed that can incorporate more solution by dilution. This dependence is well known from the literature [Schröder96, Yin92, Flory53]

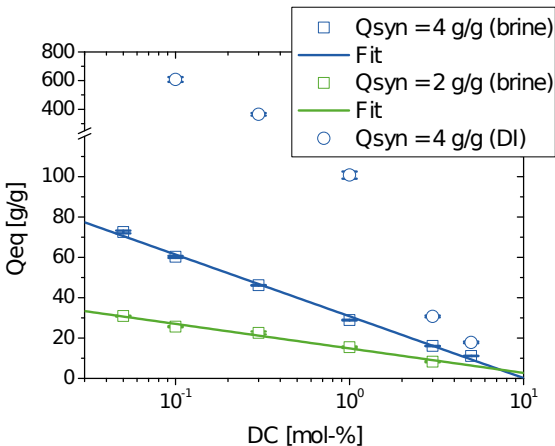


**Figure 3.4.:** The equilibrium swelling degree  $Q_{\text{eq}}$  of pAAC gels in salt solution (10 g/L  $\text{NaCl}$ ) and deionised water (DI) is shown as a function of the cross-linking degree (DC).  $Q_{\text{syn}}$  and DN were fixed at 4 g/g and 75 mol-%, respectively. The symbols denote the data with errors bars obtained from the standard deviation of three repeated measurements and the lines are representations of the best fit of the function  $Q_{\text{eq}} = A \log(\text{DC}) + B$  to the data. See the text for the fit parameters.

and obtained results are close to the ones recorded there [Yin92, p. 103]. A closer examination of the values in terms of the statistical theory will be presented in section 3.3.3.

The solvent capacity is directly proportional to the parameter  $Q_{\text{syn}}$  for measurements in brine as seen in **fig. 3.5**, on top. The increase of absorption capacity is drastic with a slope of 5.5 of  $Q_{\text{syn}}$  against  $Q_{\text{eq}}$  for the brine case. This effect can be understood in terms of three effects. First, more solvent can be absorbed at a higher  $Q_{\text{syn}}$ , as this is the reference state from which no force is necessary to extend the network chains. Further, when more water is present in the synthesis mixture the amount of elastically inactive defects such as dangling chain ends and rings is increasing while, at last, the amount of extra-elastic effects such as entanglements is decreasing. In the literature, the influence of  $Q_{\text{syn}}$  is much less studied, e.g. Brendel does

not observe a dependence at low values of this parameter [Brendel99]. The dependence of  $Q_{\text{eq}}$  on the parameter DN is more complicated than the previously discussed examples. In **fig. 3.5**, lower part, an increase at low DN is observed but above 25 mol-% a broad plateau in the solvent capacity is reached and at a high DN the capacity is even decreasing. On the first thought, it is expected to find a steady increase with DN as more charges in the network increase linearly the osmotic potential of the gel (see section 2.1). However, at high charge concentrations the effect of screening and reduced activity the amount of effective free charges. Above DN = 30 mol-%, the activity of ions is reduced in a way that the osmotic potential is levelled off [Skolnick77, Schröder96]. The decrease at high DN is known in the literature but lacks a good explanation as of today; the efficiency of synthesis might be an issue.

The introduction of comonomers into the neat pAAc network does not alter the swelling capacity to a large extend. In **fig. 3.6**, top, the results for copolymers of 50 mol-% AAc (DC = 0.3 mol-% DN = 75,  $Q_{\text{syn}} = 4 \text{ g/g}$ ) and the same amount of comonomers are shown.<sup>2</sup> The differences in  $Q_{\text{eq}}$  caused by the comonomers are small, within 15 % for all monomers except HEMA. Here, a considerable reduction of 50 % in  $Q_{\text{eq}}$  is seen. The reason for the deviation is not known. The values for industrially produced samples from the BASF were also recorded and are shown in **fig. 3.6** on the bottom. The sample B1110 with additional surface cross-linking shows the lowest capacity as is to be expected.

The kinetics of the swelling process can be determined by measuring the solvent absorption at different times before the equilibrium value is reached. The speed of the solvent uptake is controlled by the diffusion of the solvent within the particle and has been theoretically analysed by Tanaka *et al.* [Tanaka79]. The uptake is known to vary with the type of the gel (modulus and solvent interaction), particle form and most notably the

---

<sup>2</sup>The copolymer samples were produced and investigated by Mr. Dimitri Merger under the supervision of the author.

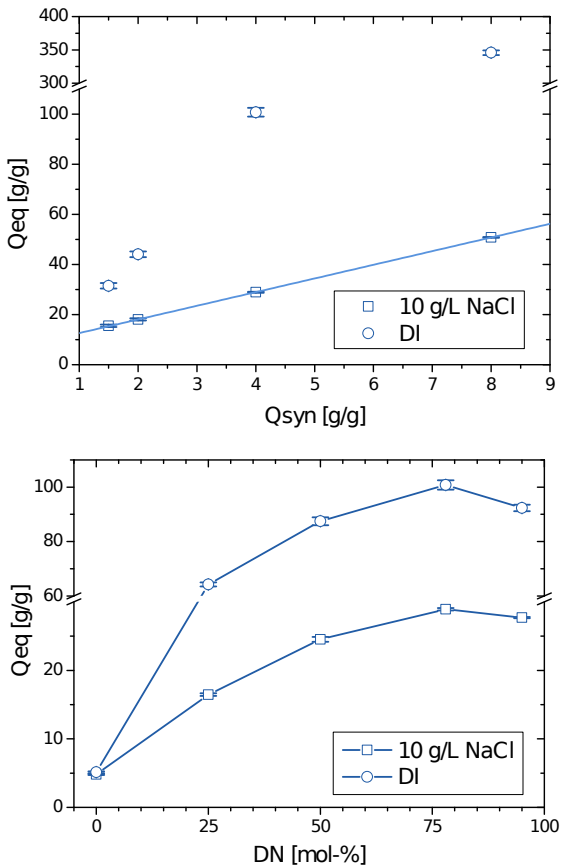


**Figure 3.5.:** The equilibrium swelling degree ( $Q_{eq}$ ) of pAAc gels as a function of  $Q_{\text{syn}}$  and DN is shown. The degree of cross-linking is constant for all samples (DC = 1 mol-%). The samples are either swollen in deionised water (DI) or brine (10 g/L  $\text{NaCl}$ ). The symbols denote the data with errors bars obtained from the standard deviation of three repeated measurements. On top, the line indicates a linear fit to the data and below they only serve as a guide to the eye.

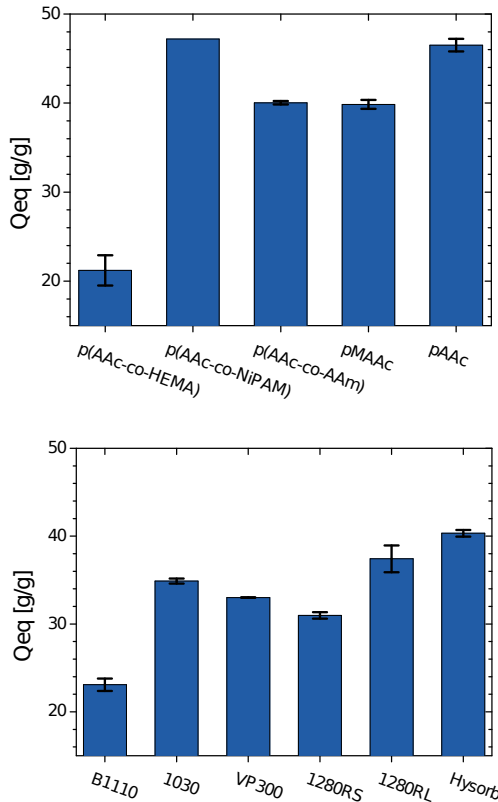


**Figure 3.6:** The equilibrium swelling degree ( $Q_{eq}$ ) in several self-synthesised copolymers of acrylic acid (top) and commercial samples (below) in brine (10 g/L  $NaCl$ ) is depicted. The self-synthesised gels contain 50 mol-% AAc (DC = 0.3 mol-% DN = 75 mol-%,  $Q_{syn} = 4$  g/g) and the same amount of the indicated comonomer. Further information on the commercial samples is found in tab. 3.1. The bars denote the data with errors bars obtained from the standard deviation of three repeated measurements.

particle size and is in principle well investigated [Tanaka79, Buchholz98]. Here, only a few samples were tested to justify the swelling times used in the other experiments.

The method employed here is described in appendix A.2; it suffers somewhat from inaccuracy as the removal of excess solvent takes some time during which the swelling continues. One sample of the commercial hydrogel B1110 and the self-synthesised pAAc-DC5-DN75-Q4 were investigated for swelling in brine. In the case of the former gel also an experiment was conducted, where 13.6 wt.-% of the sodium chloride were exchanged for  $CaCl_2$ . This mimics the amount of divalent cations in sea water that are known to reduce the swelling of hydrogels. The results are shown in **fig. 3.7** and the kinetics are found to be quite fast and the maximum absorption is reached for all samples within few minutes. A single exponential model (3.6) is adopted from the literature and fitted to the data [Tanaka79]. All points were used, except for the B1110 sample with  $CaCl_2$  content, for which the last three points were omitted as they clearly deviated from the model behaviour as explained below. The obtained fit values are given in **tab. 3.2**. The time constants  $\tau$  can not be directly compared as the particle sizes are different for the two polymers: the pAAc sample consists of beads in the range 300 – 650  $\mu m$  and B1110 of beads around 180  $\mu m$ . When the latter sample is treated with a mixture of  $NaCl$  and  $CaCl_2$  a similar swelling capacity is reached at first and starts to decline after 30 min. Probably this is an effect of the enrichment of  $Ca^{2+}$  ions in the gel as they are captured from the large excess solution present in the swelling setup. They act as additional cross-linking points connecting two negative charges on the backbone. Thereby, the degree of cross-linking is effectively increased and  $Q_{eq}$  consequently reduced, however, the maximum value and time constant in the early behaviour are practically unaffected.

$$Q(t) = Q_{\max} \cdot \left[ 1 - \exp \left( \frac{-t}{\tau} \right) \right] \quad (3.6)$$

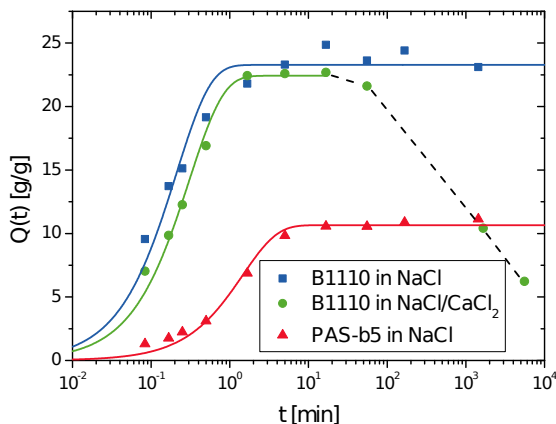


**Figure 3.7.:** The time dependent swelling degree of industrially produced sample B1110 and the self-synthesised polymer pAAc (DC = 5 mol-%) is shown. In the case of a salt solution containing only sodium chloride brine ( $c(NaCl) = 10 \text{ g/L}$ ) the increase is monotonic to the maximum, if 13.6 wt.-% of sodium chloride is replaced by calcium chloride a reduction after some time is observed. The straight lines are fits of eq. (3.6) to extract time constants given in tab. 3.2, the dashed line is a mere guide to the eye.

**Table 3.2.:** Fit parameters obtained by adjusting (3.6) to the time dependent swelling data of hydrogels in various electrolyte solutions shown in fig. 3.7.

Polymer	Solution	$Q_{\max}$ [g/g]	$\tau$ [s]
B1110	10 g/L NaCl	23.3	13
B1110	10 g/L NaCl/CaCl <sub>2</sub>	22.4	18
pAAc-DC-DN75-Q4	10 g/L NaCl	10.7	88

### 3.3. Mechanical behaviour

The entropy elastic nature of the network can most easily be probed by recording its response to deformation. As seen in section 2.2, the network

structure or more specifically the effective number of meshes gives rise to the observed moduli. Applying this theory allows to calculate the average length of these meshes from the mechanical moduli. The modulus can in principle be probed by any mechanical method that yields a solution for the elastic equation of state. For rubbers, mostly tension is employed [Treloar75]. However, in the case of hydrogels only the methods of shear and compression are routinely employed on macroscopic samples<sup>3</sup> due to the characteristics of the material [Clark87]. The samples are brittle at high DC and complex formed standard specimen such as dumbbells for tension are difficult to obtain. A specimen of regular shape is required for accurate measurements (see fig. 3.8) which can be a simple cylinder in the case of compression and shear. Here, both shear and compression were investigated in several variants to determine the best course to obtain stable results. An experimental procedure is developed that includes the optimisation of the test parameters. First, the shear experiments are discussed, then those in compressional mode. The two methods probe different moduli that have to be compared via the Poisson's ratio and are interpreted in terms of the rubber-elasticity theory.

### 3.3.1. Experiments under shear

The mechanical response under shear is probed by oscillatory mechanical measurements. The sample is excited by a sinusoidal shear strain with the amplitude  $\gamma_0$  and the frequency  $\omega_1/2\pi$ . The resulting stress  $\sigma$  and the phase angle  $\delta$  are measured. From these quantities the complex modulus  $G^*$  is obtained. Details on the theory and evaluation of shear rheological experiments are available in the literature [Ferry80, Macosko94, Larson99]. The two parameters used to describe the gel in the linear regime are the absolute of the complex modulus  $|G^*|$  as the gel strength and the tangent of the loss angle  $\tan \delta$  as a measure of the viscous contribution. These are

---

<sup>3</sup>Also indentation measurements and tension have been reported but were not found useful for the samples at hand.

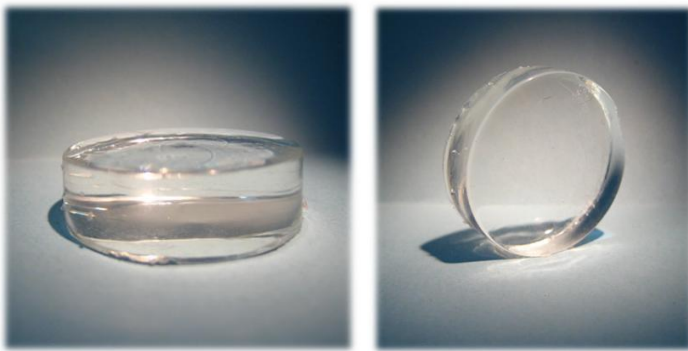


**Figure 3.8.:** Examples of specimen used for rheological investigations. They were produced by polymerisation in a cylindrical mold. Clear, bubble free and well shaped specimen are thereby obtained.

both dependent on a number of factors such as frequency, strain, and the applied normal force. The influence of these parameters is assessed and results from hydrogels of different composition compared.

The measurements were carried out with an ARES G2 strain controlled rotational rheometer that has previously been described in the literature [Franck08, Reinheimer11]. In general, the values in the linear rheological regime will be used for the interpretation [Hyun11]. This region is typically found by varying the dynamic strain exerted on a sample in a so called oscillatory strain sweep (OSS) experiment; the experimental parameters are listed in appendix A.2. An example recorded for the sample pAAc-DC1-DN75-Q2 is shown in **fig. 3.9** on top. The viscous contribution is found to be below  $\tan \delta = 0.1$  for all investigated samples as expected for cross-linked materials [Clark87, p. 85]. The modulus and the loss tangent are found to be almost constant over a wide strain range, starting at the lowest values and ending usually around  $\gamma_0 = 1 - 10\%$  (here 2%). A significant decrease in  $|G^*|$  and an increase of viscous response are observed thereafter. A rise in modulus would be expected due to finite chain extensibility in the network [Breedveld04, Baker10]. The actually observed softening

in gels is probably due to loss of contact with the geometry or mechanical failure of the sample [Baker10]. The value at  $\gamma_0 = 0.1\%$  is taken as representative for the linear regime; it is indicated in fig. 3.9 by arrows.

The loss of contact with the geometry by slipping can be prevented to some extend by holding the sample tightly between the two plates of the geometry. This is achieved by exerting a normal force (NF) on the sample. It also makes sure, that the small surface crudities are pressed flat and the whole sample surface is in contact with the geometry. An example of an OSS with the effect of different NF applied to the sample pAAc-DC0.3-DN83-Q4 is shown in the lower part of **fig. 3.9**. With increasing normal force,  $|G^*|$  and  $\tan \delta$  are both rising considerably. For an isotropic sample the responses to two deformations are considered independent of each other. Yet, for rubbers and hydrogels it was found, that an superimposed strain increases the apparent modulus recorded by oscillatory deformation [Oppermann85, Gent70]. Therefore, the normal force should not be too high, otherwise, the results are obscured. It was found that for a small deformation of 5 % of the specimen the deviations are in a reasonable range. The effect of the measurement frequency was considered as well. It is measured by changing the oscillatory frequency in a so called frequency sweep (FS) experiment. The typical results are shown in **fig. 3.10**, on top, for a sample with DC = 3 mol-%. The modulus and the viscous contribution (high  $\tan \delta$ ) are found to rise steadily, but to a small extend within 5 % of the value. This behaviour has been reported in the literature [Oppermann85, Yin92, Breedveld04]. A considerable increase is found for frequencies higher than 10 Hz, which has, to the knowledge of the author, so far not been reported. In theory no dependence on  $\omega_1/2\pi$  is expected at all, as the sample is trapped in the rubber elastic regime and no flow can occur [Clark87, p.86]. The observed small dependence is probably an artefact of loose ends and sol in the sample, that is not (tightly) linked to the network. The upturn at high frequencies can be an effect of probing the glassy state of the material. The temperature and DN dependence were not investigated in the course of this work.

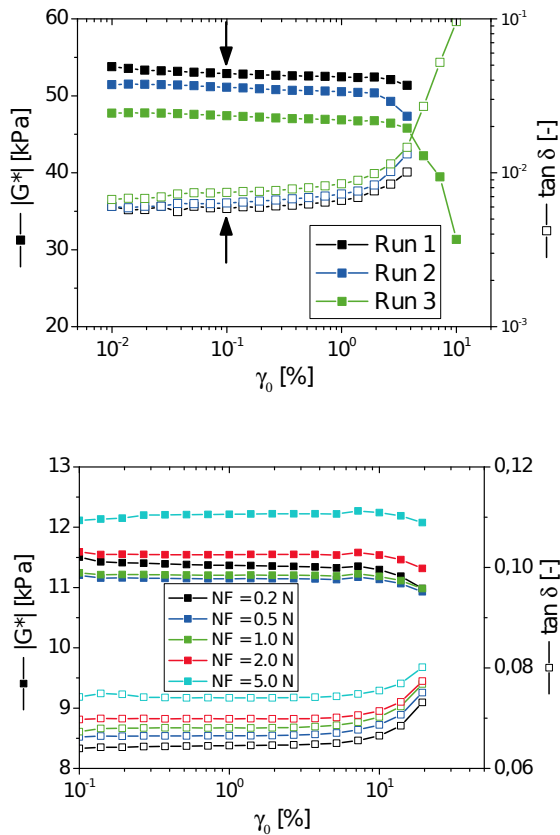


**Figure 3.9.:** Examples of mechanical properties of hydrogels under shear: on top a variation of the oscillatory strain is shown. Three consecutive runs on the same sample pAAc-DC1-DN75-Q2 were performed, the arrows denote the point where the data for the linear regime was extracted. Below, the influence of the normal force was investigated on the sample pAAc-DC0.3-DN83-Q4. The measurements were performed with a frequency of  $\omega_1/2\pi = 1$  Hz at room temperature. For an explanation of the sample names see sec. 3.1.

The influence of the water content of the sample is investigated via the synthetic parameter  $Q_{\text{syn}}$ . The samples were used "as prepared" and their water content is directly given by the water content in the reaction mixture (see sec. 3.1). Four samples with  $Q_{\text{syn}}$  values between 1.5 to 8 g/g were compared as shown in **fig. 3.10**, below. The dependence on the water content is strong:  $|G^*|$  is decreasing exponentially and an overall increase in the viscous part with increasing  $Q_{\text{syn}}$  is observed, with the exception of  $Q_{\text{syn}} = 2 \text{ g/g}$ . When more water per unit volume is present, the effective concentration of elastic meshes is reduced — the sample is softer for small and medium degrees of swelling [Schröder96, p. 28]. An influence on the structure by the changed synthesis conditions should be present as well, but does not play a major role.

A second series of hydrogel samples with variation of the degree of cross-linking (DC) but constant  $Q_{\text{syn}}$  is investigated as well. Here, a strong dependence of the mechanical characteristics on DC is seen as well. Six samples with a DC between 0.05 and 5 mol-% were investigated as shown in **fig. 3.11**.  $|G^*|$  is increasing with increasing number of cross-links. The dependence is not strictly linear but a stronger increase at higher DC is found. More cross-links introduce more but shorter meshes which exert a higher elastic force as predicted by theory. This general dependence is supported by many studies [Baselga87, Yin92, Schröder96, Brendel99]. For example Stanley *et al.* investigated similar samples of lightly cross-linked pAAc gels and found a linear increase of  $G'$  with DC and a value of 7 kPa at 0.1 mol-% cross-linker which is close to the result found in this study [Yin92, p. 109]. The obtained values will be discussed in quantitative terms of and with respect to the molecular structure in section 3.3.3. The viscous contribution is decreasing with DC but levels off over 1 mol-%, which has also been reported by Yin et al.

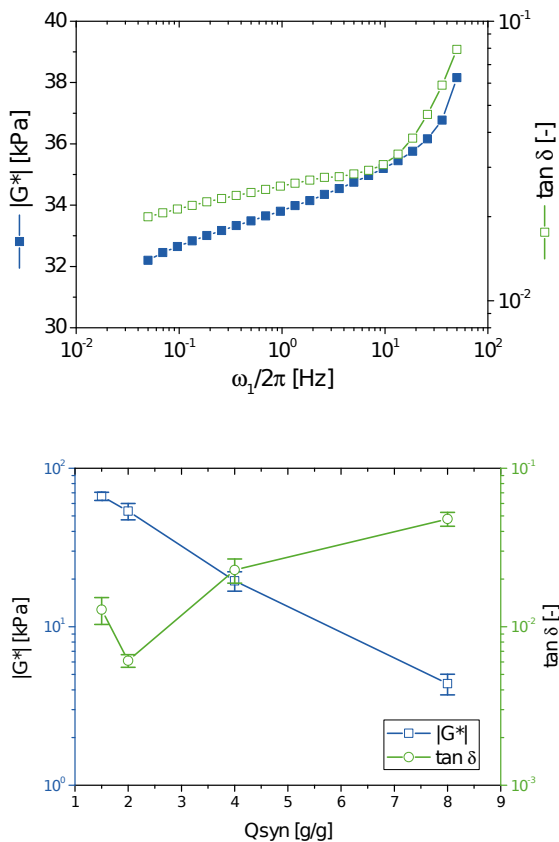


**Figure 3.10.:** The influence of the oscillation frequency  $\omega_1/2\pi$  and water content of the sample on the mechanical characteristics loss tangent and complex modulus are investigated. On top, the frequency dependence is shown for a sample. Below samples prepared with a variation of the water content of the synthesis mixture ( $Q_{\text{syn}}$ ) are investigated at a fixed DC and DN. The values were measured at  $\gamma_0 = 0.1\%$  with a frequency of  $\omega_1/2\pi = 1$  Hz at room temperature.

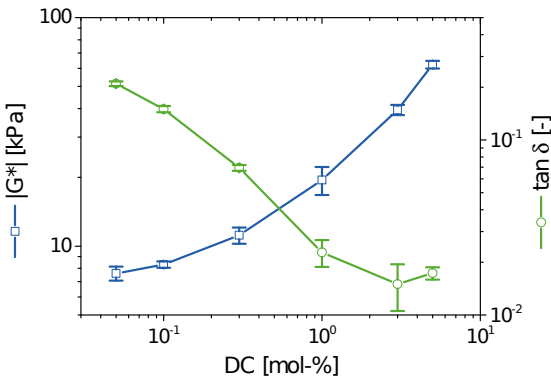


**Figure 3.11.:** The mechanical characteristics of pAAc gel samples of varying degree of cross-linking (DC) are investigated. The parameter  $Q_{\text{syn}} = 4 \text{ g/g}$  was constant for all samples. The values of complex modulus  $|G^*$ | and loss tangent  $\tan \delta$  were taken at a stain of  $\gamma_0 = 0.1\%$  in the linear regime at a frequency of  $\omega_1/2\pi = 1 \text{ Hz}$  at room temperature.

### 3.3.2. Experiments under compression

The second method routinely employed for the investigation of the mechanical characteristics of hydrogels is compressional deformation. However, a different set of advantages and disadvantages is found for this method. The description of compressional rheology can be found in the literature [Treloar75, Mark88]. The compressional deformation can be applied to the samples in continuous or oscillatory deformation mode. In the latter case, a small sinusoidal deformation is superimposed on a larger, static pre-strain. The resulting stress  $\sigma$  is recorded from the applied force. As the result the Young's modulus is obtained in the case of continuous deformation the modulus  $E$  and in the case of oscillatory deformation the complex modulus  $|E^*$ . In the latter case the sample is described by the absolute of the modulus  $|E^*$  and the loss tangent  $\tan \delta$ . The results depend on a set of experimental parameters such as the deformation speed or frequency and the pre-strain that is applied. Additionally, the influence of the contact between sample and geometry plays an important role and is investigated here. The experi-

ments were carried out with an Eplexor 150N that provides both discussed measurement options and has been described elsewhere [Ghaddum91]. The experimental details are given in appendix A.2.

The experiments with continuous deformation are easier to carry out and depend on less parameters. They are thus discussed first. The sample is continuously compressed by a strain given as  $\lambda_t = L_t / L_{0,t}$  where  $L_{0,t}$  is the unreformed sample height and  $t$  the axis of compression. The result is obtained in form of a typical strain-stress curve. An example is given in **fig. 3.12**, which was recorded for sample pAAc-DC0.3-DN83-Q4 and the contact was lubricated with silicone oil (AK 5 000,  $\eta \approx 5000$  Pas). The sample shows a linear dependence if the stress  $\sigma$  is plotted against  $\lambda - \lambda^{-2}$  (a higher deformation gives smaller values). For a Neo-Hookean material, the modulus is given by the slope in this diagram, which is constant. When plotting the same data in a Mooney-Rivlin-plot, on the bottom in the same figure, almost horizontal lines are found for the lubricated case. Only below a deformation of  $\lambda - \lambda^{-2} = -0.1$  a deviation occurs. The early behaviour is attributed to the uneven surface of the sample. The Mooney-Rivlin constants are given as the intercept ( $C_1$ ) and the slope ( $C_2$ ), which is almost zero for  $\lambda^{-1} > 1.05$ . Thus the Neo-Hookean modulus is used.

The interface between the sample and the geometry defines how the sample is deformed upon compression. When the sample is compressed, its size is decreasing in direction of the force. Consequently, the size in the other two dimensions increases to keep the sample volume approximately constant.<sup>4</sup> The lateral expansion can occur in two distinct ways as shown in **fig. 3.13**. If the interface is sticky, the sample cannot move and a barrel distortion on the contour is observed (top). If the sample can slip the contour is maintained and a regular deformation is observed (below). The latter can usually only be achieved by sufficient lubrication of the interface. Unfortunately, the two cases yield different mechanical characteristics as fig. 3.12 shows: in

---

<sup>4</sup>The ratio of these deformations is actually controlled by the Poisson's ratio of the sample and only true for value of 1/2.

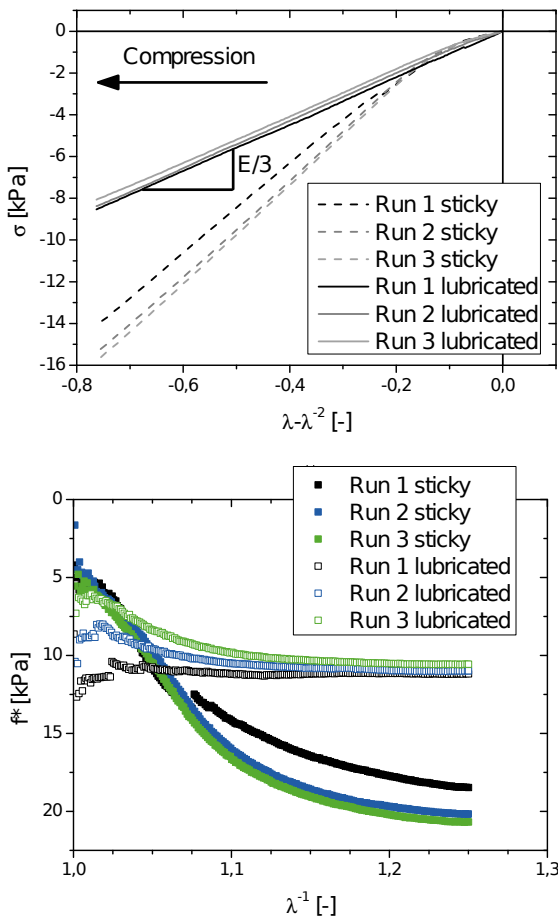


**Figure 3.12.:** Strain-stress curves obtained for continuous compression of the hydrogel pAAc-DC0.3-DN83-Q4 are shown. Three consecutive runs were recorded for either the contact between sample and geometry being sticky or lubricated by silicone oil (AK 5 000,  $\eta \approx 5\,000$  mPas). On top, the data is plotted according to the Neo-Hookean law (see eq. 2.30) and the modulus  $E$  is determined from the slope to 33.9 kPa. Below, the same measurements are displayed in the so called Mooney-Rivlin-plot (see eq. 2.33), where a horizontal line describes Neo-Hookean materials.

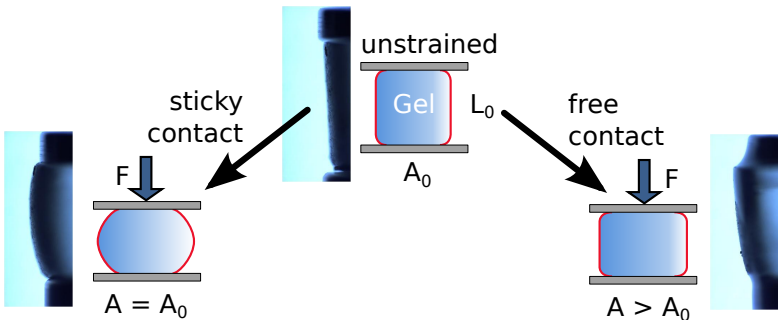


**Figure 3.13.:** When a gel sample is compressed, its contour depends on the contact to the geometry. If it is sticky the sample does not move and a barrelling out is observed (top). In the case of a sideways sliding, usually achieved by lubrication, the contour is maintained (below). The pictures were taken from a sample with DC = 0.3 mol-% at a compression of  $\lambda = 0.87$ .

the barrel distortion case the results are neither linear in the Neo-Hookean or Mooney-Rivlin-plot. Over most of the investigated range a steeper slope of the stress-strain curve is found, the sample appears harder. This suggests a strong energy elastic contribution for this deformation mode. However, at deformations smaller than  $\lambda - \lambda^{-2} = -0.1$  the sample appears softer, which is usually a result of sample crudity. When lubricant is present the uneven surface is compensated by the oil and sooner in contact with the geometry.

The effect of the higher apparent modulus in the case of a sticky contact is known to be a problem in the literature. Some authors note that the absence of a barrel distortion must be carefully checked [Geissler88, Horkay10, Brown06]. The higher Young's modulus probably arises from additional shear forces that are necessary for this deformation. In both cases, however, the Neo-Hookean fit to the data is used to obtain a modulus value for later comparison.

The influence of the synthetic parameter DC on the moduli is investigated for continuous compression at a lubricated and a sticky contact. A series

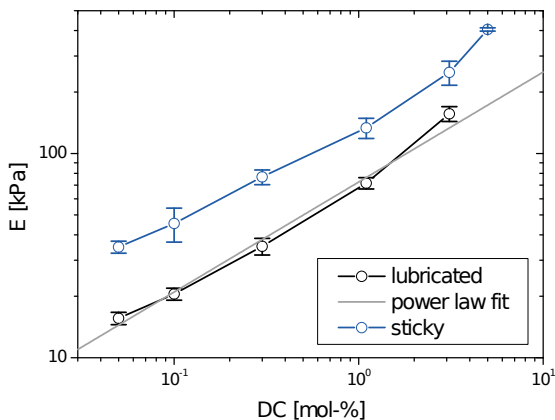


**Figure 3.14.:** The Young's modulus increases with the cross-linking degree (DC) in the pAAc hydrogel samples. The parameter  $Q_{\text{syn}} = 4 \text{ g/g}$  was constant for all samples.  $E$  is here recorded by continuous compression of 0.3 mm/min at RT for a lubricated and a sticky contact between sample and geometry. For the case of lubrication silicone oils of various viscosity were used. A power law was adjusted to the data giving an exponent of 0.54, for which the representation is drawn.

of samples with DC ranging from 0.05 to 3 mol-% is considered. The results are given in **fig. 3.14** for the sticky and the lubricated contact. A suitable lubricant was chosen for each sample by using oils of increasing viscosity for higher DC values (from AK 2 000 to AK 50 000 with  $\eta = 2 000 - 50 000 \text{ mPas}$ ). The recorded moduli increase linearly with DC for both contacts. As in the previous section for shear, this is in agreement with theory and findings in the literature [Baselga87, Yin92, Schröder96, Brendel99]. Yet, the moduli obtained for the sticky contact are always by about a factor of two larger than for a lubricated contact. The difference decreases slightly with increasing DC, which could be an indication, that the lubrication of very hard samples is difficult. A power law fit to the data with lubrication yields a scaling exponent of 0.54 and a prefactor of 73 (shown in **fig. 3.14**). A quantitative comparison with theory and literature will be given in the next section.

The investigation of hydrogel samples by oscillatory compression can be conducted when several additional parameters are taken into account. For the frequency dependence in compression a similar dependence as for shear experiments is found (not shown). Thus, the frequency  $f = 1$  Hz is used for this measurements as well. The deformation of the sample in such an experiment is two fold. First the sample has to be subjected to a constant initial load on which the oscillatory deformation amplitude is superimposed.<sup>5</sup> The deformation imposed by the initial load has to be larger than the deformation amplitude, otherwise, the contact to the sample is lost during the oscillation, rendering the results void. The static load is given by the static strain  $\lambda_s = L_{\text{pre}}/L_0$  and the amplitude is conveniently denoted as the dynamic strain  $\varepsilon = \lambda_{\text{dyn}} - 1$ .

An example of the dependence of mechanic behaviour on the static and dynamic strain is given in **fig. 3.15** for the sample pAAc-DC1-DN75-Q4 without the use of a lubricant. Within the results two trends can be observed: first, a plateau in the modulus is found for a range of dynamic strains at a given static strain. At large dynamic strains, a decrease is observed and the loss tangent also shows a plateau but then increases. This probably marks the departure from the linear regime as also seen for the shear experiments above. Secondly, when the static strain is increased,  $|E^*|$  is increasing considerably. For the oscillatory deformation an apparent modulus  $|E_{\text{app}}^*|$  is measured that needs to be corrected for the Neo-Hookean behaviour of the material by (3.7). This correction is an effect of probing the local slope of the strain-stress curve by the oscillation [Oppermann85]. An example of this correction is illustrated in fig. 3.15, where the effect is considerable. A correction factor of about 4 is found for  $\lambda_s = 0.8$ . After application of the correction, the measured curves coincide at a much lower value. For the smallest dynamic strain the value is a little lower, which can be explained by the sample roughness. If not all of the sample is in contact with the geometry, only a part is strained, requiring a lower force. The sample

---

<sup>5</sup>The deformation speed of the sample is defined by the amplitude and the frequency.

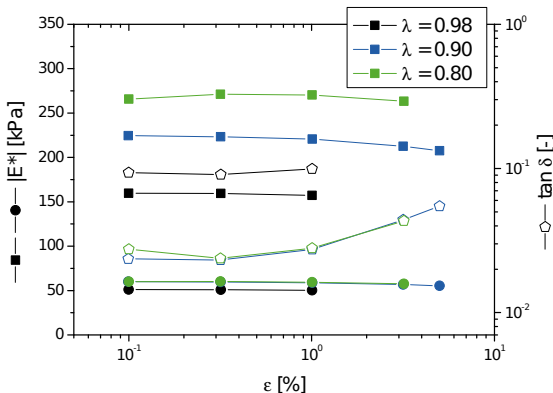


**Figure 3.15.**: Mechanical behaviour of the hydrogel pAAc-DC1-DN75-Q4 under oscillatory compression is given as an example. Results for three different pre-strain values  $\lambda_s$  were recorded for  $f = 1$  Hz at room temperature. The squares and circles denote  $|\mathcal{E}^*|$  before and after correction by (3.7), respectively. The open symbols give  $\tan \delta$ .

would appear softer and "harden" at higher static strains (below  $\lambda_s = 0.95$ ). Therefore, the values at  $\lambda_s = 0.9$  and  $\varepsilon = 0.3\%$  are taken to compare the samples.

$$|\mathcal{E}^*| = \frac{|\mathcal{E}_{app}^*|}{1 + 2\lambda_s^{-3}} \quad (3.7)$$

The dependence on pre-strain of the modulus and loss tangent just presented are also found for samples with other degrees of cross-linking. The results for  $|\mathcal{E}^*$  and  $\tan \delta$  for three pre-strains are displayed in **fig. 3.16** as a function of DC. The offset between the three data series can be nicely explained by the correction (3.7), that is applied here to the results at  $\lambda_s = 0.90$  as discussed above. Interestingly, the modulus dependence on DC is much smaller for samples below a DC of 0.3 mol-%. The values of the loss tangent are decreasing with DC and are very similar for  $\lambda_s$  values of 10 and 20 %. The values at 2 % are much higher and are also much more uncertain. As explained before this is a result of only a part of the sample being in contact with the geometry and, therefore, appearing softer.

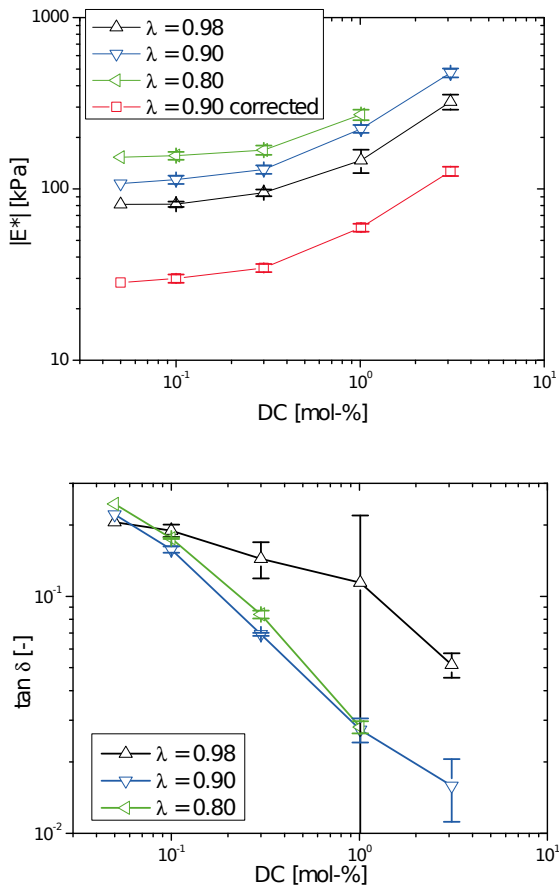


**Figure 3.16.:** pAAc hydrogel samples with varying degree of cross-linking were investigated under oscillatory compression. The parameter  $Q_{\text{syn}} = 4 \text{ g/g}$  was constant for all samples. On top, the complex Young's modulus and below the loss tangent are shown. Curves for three different static strain values  $\lambda_s$  were recorded for  $f = 1 \text{ Hz}$  at room temperature. In the case of  $\lambda_s = 0.90$  the results were corrected for the influence of pre-strain by (3.7).

### 3.3.3. Discussion of results and calculation of the network parameters

The mechanical properties of hydrogel samples were probed with four different methods: oscillatory shear, continuous compression with sticky and lubricated contact, and oscillatory shear. Here, the results are compared and interpreted and the best method is chosen. From the results the statistical mesh length and the cross-link efficiency are calculated.

The same series of samples with a variation of the parameter DC is measured with the four different mechanical methods. The results are given in **fig. 3.17**. The  $|G^*|$  values were multiplied by 3 to compare them with the Young's modulus as discussed in section 2.2. The modulus values obtained for continuous compression with a sticky contact are the highest for all samples. They are mostly by a factor of 2 higher than the results of all other methods. These all show quite similar results with minor differences. Though, the oscillatory methods report higher moduli at low DC and lower ones at higher DC, than found for lubricated continuous compression. The reason for this effect might be the experimental procedure. The lubrication necessary for continuous compression works well for low DC samples and is difficult for a high DC. In contrast, the normal force used in shear experiments is difficult to control for low DC samples and works well for a high DC.

In theory, the modulus of rigidity should always be by a factor of 3 smaller than the Young's modulus if the volume is constant (sec. 2.2). Deviations from this rule (up to 40 %) are observed here, but they are probably not caused by a change in volume during the deformation. The differences are rather an effect of measurement difficulties discussed in the previous section.

In light of these findings the lowest values of the moduli are most probably the ones closest to the true moduli as all described effects result in an apparent hardening of the samples. The method of continuous compression

with a sticky surface should not be used for quantitative interpretation due to energy elastic effects in the results. The other methods are in principle equivalent, giving a scaling exponent ( $\log E = A \log(DC)^B$ ) similar to the one obtained for continuous compression. From the experimental point of view, the oscillatory methods are the easiest to carry out.

In the investigated samples the theory of rubber elasticity describes the results well. For continuous compression (lubricated contact) a constant slope is found if the Neo-Hookean strain ( $\lambda - \lambda^{-2}$ ) is used for representation (see fig. 3.12). Additionally, the reduced stress does not show a deformation dependence. Therefore, it can be concluded that the Neo-Hookean model fits the data well and the Mooney-Rivlin approach is unnecessary ( $C_2 = 0$ ). This is found as well for similar swollen or very low cross-linked networks in the literature [Baselga87, Belkebir-Mrani77, Mark88]. The validity of the Neo-Hookean model is also supported by the well behaved correction of oscillatory compression that is derived from the Neo-Hookean law. Due to this reasoning the network parameters are calculated directly from the obtained moduli.

The theoretical average length of a mesh in the a polymeric network can be easily calculated from the composition of the synthesis mixture assuming ideal, statistical incorporation. The mesh size is calculated as the average molecular weight of the polymer chain between two junctions  $M_c^{\text{th}}$  by (3.8) which was adapted from the literature [Baselga87]. The parameter DC in the formula is the mole-fraction of cross-linking monomer with respect to all monomers given in mol-%. The chain length is inverse proportional to DC as shown in **fig. 3.18**.

$$M_c^{\text{th}} = \frac{(100 - DC) \cdot M(\text{AAc})}{2DC} \quad (3.8)$$

The mesh length between two junctions can be obtained from the moduli by employing the theoretical framework given in section 2.2. The effective number of meshes can be calculated from eq. (2.32) in the case of com-

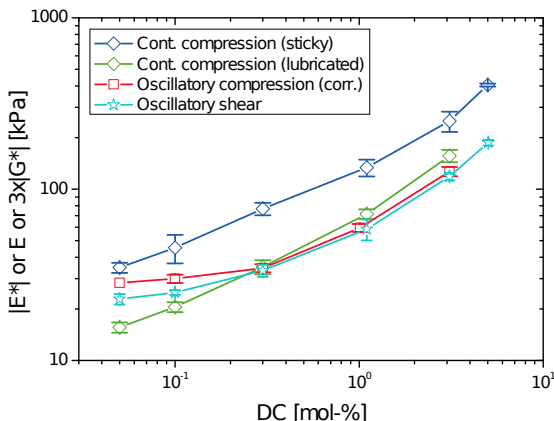


**Figure 3.17.:** Mechanical moduli of pAAc hydrogels with varying degree of cross-linking (DC) obtained by different methods are compared. The parameter  $Q_{\text{syn}} = 4 \text{ g/g}$  was constant for all samples which were used as prepared. This graph summarises the results of the previous section for oscillatory and continuous compression and shear experiments. For the experimental conditions see the respective sections. For the shear experiments  $3 \times |G^*|$  was plotted as given by the theory (sec. 2.2).

pression or eq. (2.36) for pure shear under the assumption of validity of Gaussian chain statistic is valid and the network is close to the phantom limit due to swelling. Here, however, the shear modulus is expressed in terms of the molecular weight  $M_c^{\text{mech}}$  of the chain between two junctions. This is obtained by using eq. (2.3) and assuming the dilation factor is unity as the samples were measured in the as prepared state to obtain (3.9).  $M_c^{\text{mech}}$  is an effective quantity in the sense, that all deviations from theory such as network defects are not accounted for separately but are incorporated. For an explanation of the symbols used see sec. 2.2.

$$G = \left(1 - \frac{2}{\phi}\right) \frac{\rho R T v_{2c}^{2/3}}{M_c^{\text{mech}}} \quad (3.9)$$

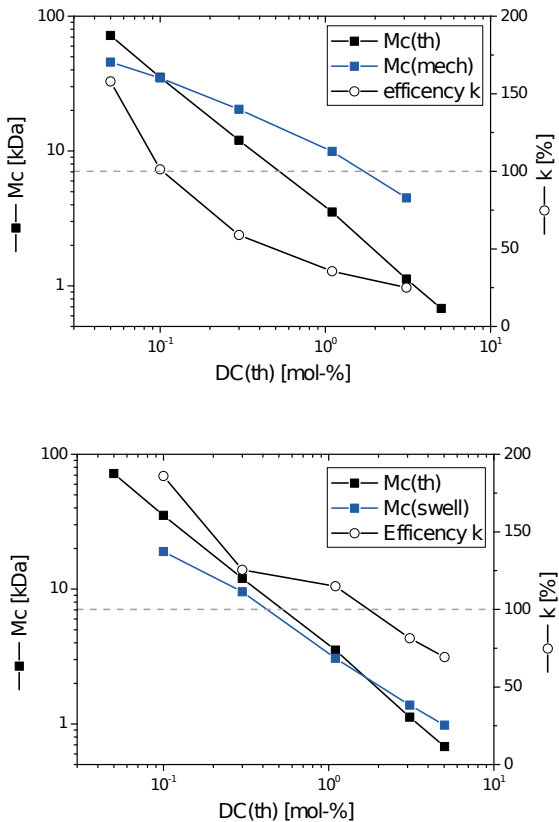


**Figure 3.18.:** The mesh size and cross-link efficiency of hydrogel networks are shown. The values calculated from the synthesis mixture ( $M_c^{\text{th}}$ ) are compared with values from compression experiments (on top) and equilibrium swelling (below). The experimental results were analysed by means of the statistical theory as described in the text.  $k$  is the ratio of synthesis and experimentally determined values and a the dashed line marks 100 %.

The values shown in **fig. 3.18** are calculated from the moduli obtained by continuous compression (lubricated) presented in the previous section. The cross-linker functionality  $\phi$  of MBA is 4, the temperature 298 K and the density  $\rho$  of dry pAAc is 1 500 mg/m<sup>3</sup> [Hiraoka82].  $v_{2c}$  is approximated by  $Q_{\text{syn}}$  the mass fraction taken from the synthesis mixture because as prepared gels were investigated. From the ratio of the theoretical and the experimental moduli the cross-linker efficiency  $k$  is calculated by (3.10) and shown in the same figure.

$$k = \frac{M_c^{\text{mech}}}{M_c^{\text{th}}} \times 100\% \quad (3.10)$$

When comparing the dependence on DC of  $M_c^{\text{mech}}$  and  $M_c^{\text{th}}$  in fig. 3.18, the latter is much stronger. The power exponents are  $-0.56$  and  $-1$ , respectively. This deviation from the theory is explained by the continually decreasing cross-linker efficiency with increasing cross-linker concentration. This trend is typically found in such samples [Baselga87, Schröder96]. The values below the threshold of 100 % can be explained by the formation of inelastic network defects such as small rings or the direct connection of cross-linker units in close proximity to form highly linked domains [Weiss79, Weiss81, Geissler82, Gupta83]. The values above 100 % are caused when meshes are not connected to the next spacial node but to one further away. Thereby, non-recoverable entanglements are formed between meshes that act as elastic junctions as well. For the calculations presented here few assumptions have to be made and those are well justified, therefore, the results are well founded.

The same approach can in principle also be used to calculate the mesh length from the equilibrium swelling results. Swelling is an expansion of the network by incorporation of solvent molecules, driven by the osmotic potential of the network and the ions and is constrained by the rubber elasticity. Using this equilibrium condition for the chemical potential expression, eq. (2.23), was derived in section 2.2 for the case of no added salt and cross-linking in the solution. This can be solved for the mesh molecular weight from swelling experiments  $M_c^{\text{swell}}$ .

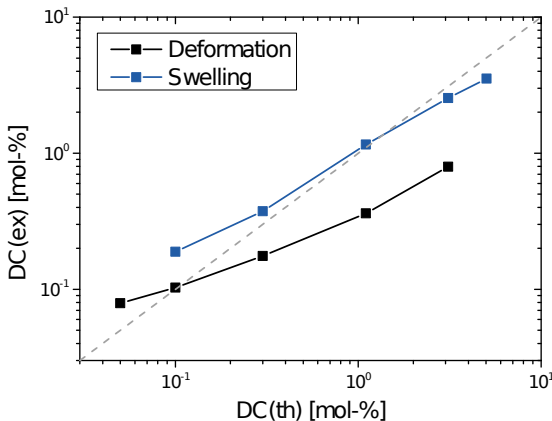


**Figure 3.19.:** Relationship between cross-linking degree from synthesis DC and as determined from deformation and swelling experiments DC(ex). Both were determined for pAAc gels with  $Q_{\text{syn}} = 4 \text{ g/g}$  and DN = 75 mol-% at room temperature. The swelling was performed in deionised water and results of continuous compression with a lubricated contact were used. The dashed line indicates the equality of the two quantities.

$$M_c^{\text{swell}} = - \frac{\frac{1}{3} \rho V_1 \left(1 - \frac{2}{\phi}\right) \left(\frac{v_{2c}}{v_{2m}}\right)^{-2/3} v_{2c} n^{1/2} \mathfrak{L}^{-1} \left(n^{-1/2} \left(\frac{v_{2c}}{v_{2m}}\right)^{1/3}\right)}{\ln(1 - v_{2m}) + \chi v_{2m}^2 + v_{2m} - \frac{V_1 i \rho v_{2m}}{M_M}} \quad (3.11)$$

The calculation can be done with the following quantities: for  $T$ ,  $\phi$ ,  $\rho$  and  $v_{2c}$  the same values as above are used. The volume fraction of polymer at the equilibrium swelling  $v_{2m}$  (relative to the state of reference) is approximated from  $Q_{\text{eq}}$  by assuming a density in this state of unity. The molar volume of water  $V_1$  is taken to be  $18 \text{ cm}^3/\text{mol}$  [Oppermann92] and the interaction parameter is calculated from  $\chi = 0.44 + 0.06 v_{2m}$ . Due to the mathematical complexity of the inverse Langevin function a Padé approxi-

mation is used as described in the literature [Cohen91]. Thus, remains the problem of the determination of the degree of ionisation  $i$  and the number of statistical segments per chain  $n$ . For an accurate calculation those have to be determined from independent experiments as proposed by Oppermann [Schröder96]. The complete set of the necessary tests was not performed for the samples at hand, due to the high number of necessary tests. Here, an approximation is used instead with  $i = 0.3$ , which is the maximum effective value that can be achieved due to counter-ion condensation. The parameter  $n$ , introduced in sec. 2.2 is usually found to be in the order of 10 for acrylic acid as monomer. Here, the data from Brendel for the same system is used to approximate the parameter  $n$  [Brendel99]. The results are given in **fig. 3.18** on top. The values of the averaged molecular weight of the meshes obtained here, follow the same trend that was found in the data obtained from the moduli. The dependence on DC is yet stronger with a power law exponent of  $-0.77$ . However, the  $M_c^{\text{swell}}$  values are lower by a factor of 3 and consequently the cross-linking efficiency is higher over the whole range of DC. A comparison of the theoretical DC from the synthesis mixture and the results from measurements is given in **fig. 3.19**. In conclusion, the common theory can even be applied at such high degrees of swelling if the right concepts for the change in chemical potential are used. However, due to the large number of approximations which are not always well justified, the values from swelling experiments are much more uncertain than those based on deformation experiments.

The use of mechanical deformation experiments yields clear differences in the properties of hydrogels with different composition in terms of DC or  $Q_{\text{syn}}$ . With increasing number of cross-links the samples become harder. By benchmarking four different types of mechanical tests it was found that oscillatory shear and continuous compression yield the best results. The results can be used to calculate the effective mesh length and from there the cross-linking efficiency, which is usually lower than 100 % especially for highly cross-linked samples. The calculations can also be performed

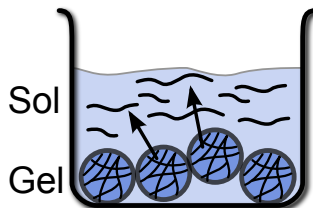


**Figure 3.20.:** Schematic of the technique to determine the sol content of a gel sample: the non-cross-linked content of the gel beads can diffuse into the surrounding water. By separating the solution phase thereafter, the polymeric content can be determined gravimetrically.

on the basis of swelling data but more approximations are needed and this approach is less favourable.

### 3.4. Sol content

During the cross-linking reaction which forms a hydrogel not all polymer chains are connected to the network [Buchholz98, p. 130]. They are left within the gel sample but not directly interacting with the primary network. This fraction of polymeric material is called sol and is mostly an unwanted side product. It adds to the samples weight but with only small effect on  $Q_{\text{eq}}$  or the moduli and may be leaking from the gel. This can affect the water quality and the surrounding. No theory is available to calculate the sol content as a function of reaction mixture. The dependence on the reaction parameters is complicated but is thought to increase with low DC, high  $Q_{\text{syn}}$  and the presence of oxygen during cross-linking.

The sol content can be determined by extracting the sample with a suitable solvent as **fig. 3.20** depicts. In this solution the polymeric content can be determined by titration, spectroscopy, or gravimetry [Buchholz98, p. 130]. In the present work, the gravimetric approach was chosen because of its simplicity. It is explained in appendix A.2 as known from the literature [Brendel99, p. 35]. The results for the sol content of samples are shown

in **fig. 3.21** for the synthetic parameters DC and  $Q_{\text{syn}}$ . As expected the sol content rises when looser networks are formed (higher  $Q_{\text{syn}}$ , lower DC). For a smaller density of cross-linking points, the chances of a growing chain to miss all cross-linking points increases. The values of sol content found are typical but higher than found in optimized commercial samples. Values of  $14.2 \pm 0.2$  and  $4.4 \pm 0.7$  wt.-% were measured for the BASF samples 1030 and B1110, respectively.

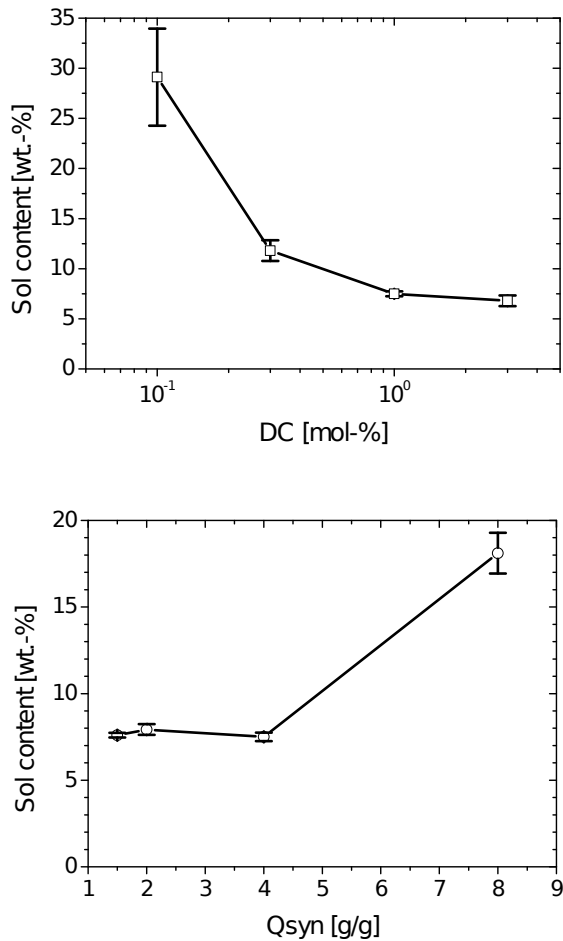


**Figure 3.21.:** The sol content for a series of neat pAAc gel samples is shown. On top, it is given as a function of DC at fixed  $Q_{\text{syn}}$  and DN and below as a function of  $Q_{\text{syn}}$  at fixed DC and DN.

## Conclusion

The bulk properties of the synthesised gels were measured and trends could be established by the employed characterisation techniques. The standard techniques of equilibrium swelling and mechanical measurements asses the basic properties of the hydrogels used for the desalination experiments later on (chapters 5 to 7). Using the statistical theory of polymeric networks their averaged mesh size can be calculated.

Four different types of mechanical measurements were investigated but the techniques of oscillatory shear and continuous compression with a well lubricated contact yielded the best results. When using the obtained data to calculate the dependence of the mesh length (in molecular weight) on the cross-link density a qualitative agreement with theory is found. However, the real scaling exponent is with  $-0.56$  considerably lower than expected from the theory ( $-1$ ). This is most probably a result of the decreasing cross-link efficiency, which is considerably lower than  $100\%$  for DC values above  $0.1\text{ mol-}\%$ . The viscous contribution to the modulus is small ( $\tan \delta = 0.2 - 0.02$ ) and decreasing with lower DC values. The incorporation of more water during the synthesis softens the samples and increases the viscous part.

The dependence on DC was also recovered by the second standard technique the determination of the equilibrium swelling degree. Networks with a lower DC or higher  $Q_{\text{syn}}$  value exhibit a higher swelling capacity. In the case of  $Q_{\text{syn}}$ , this is an effect of the reference state but also of the increasing number of network defects. Here, a stronger decrease of mesh length with increasing DC is found. The scaling exponent  $-0.77$  is closer to the theoretical prediction. Kinetic experiments showed, that the uptake process is very fast for small beads and that divalent cations such as Calcium only influence the swelling properties at longer times.

The sol content is considerable for all investigated samples and starts at  $8\text{ wt.-}\%$  and increases drastically for lower DC and higher  $Q_{\text{syn}}$  samples.

### 3. Synthesis of gel samples and characterisation by standard methods

This has to be expected as in looser packed networks the probability is larger of a growing chain not to be connected to the network. The structure on the scale of a single mesh can't be elucidated by the standard methods as they use a mean field approach. Therefore, specialised techniques focusing on the smaller scale are discussed next.

## 4. Investigation of the network heterogeneity

The understanding of the microscopic structure of hydrogels is a challenge still to be tackled. While it is clear, that the gel is a network formed from meshes and junction points, the exact structure remains unknown. The meshes have different lengths and can be connected to form several types of topological defects when compared to an ideal network which include rings, entanglements, or dangling ends. Both effects lead to a distribution in mesh and pore size (PSD) in the gel. The quantification of mesh size distribution and defects from the synthesis conditions alone is not possible. However, many properties of gels seem to be influenced by this distribution. These deviations from the ideal network topology cannot be tackled with the standard methods described in the previous chapter. These methods are based on a mean field theory and are oblivious to deviations in the structure. In this chapter methods are introduced and tested which have the capability to give information about the pore size and mesh length distribution in a gel beyond the mean value.

The methods chosen are the solute exclusion method, NMR-spectroscopy, and NMR-relaxometry. The solute exclusion method probes the PSD of the gel with linear reference polymers [Kuga81]. In an approach which corresponds to an inversion of the SEC-experiment the volume available in the gel to probes of a certain sizes is measured. The use of the NMR effect is one of the most powerful tools at disposal to the chemist today [Bovey88]. By NMR-spectroscopy the connectivity and local structure of a molecule can be probed by investigation of the chemical shift and coupling especially in two-dimensional methods. By NMR-relaxometry the magnetic relaxation behaviour of a material is recorded. This behaviour can be

translated into the dynamics in the sample on the basis of the BPP theory [Bloembergen48]. These motions are by nature constrained in gels, as they are cross-linked systems. Therefore, the dynamic heterogeneity is also a measure for the topological heterogeneity of the hydrogels.

#### **4.1. Mesh size distribution by partition of linear probe polymers**

The complete pore size distribution (PSD) of a porous material can be evaluated when the structure is probed with well characterised linear polymers. This method, known as solute exclusion (SE), was first reported by Aggebrandt [Aggebrandt64]. In general, linear probe polymers of well known constitution are dissolved and introduced to the porous material filled with the same solvent. The degree of penetration depending on the probe size is used to characterise the PSD. The standard methods of equilibrium swelling and mechanical measurements presented in the previous chapter can probe only a mean value of the PSD, while the SE method can investigate the distribution function at several different points [Aggebrandt64, Stone69]. This method can be applied to hydrogels as a form of porous material. However, this has, to the best of the authors knowledge, only once been attempted for acrylic based hydrogels [Walther94]. This method offers potentially a great gain of information on the gel structure and is therefore pursued further. Here, the following approach is adopted: solutions of narrow size distributed linear polymers are mixed with gel samples and the migration of the probe polymers into the gel is evaluated by measuring their concentration in the supernatant solution (**fig. 4.1**). Depending on the size of the probe only part of the gel volume is accessible. By using several sizes of probe polymers the complete rejection curve can be approximated. This rejection curve could be transformed back to the pore size distribution by known methods (e.g. Inverse Laplace transform). Here, only some prelimi-

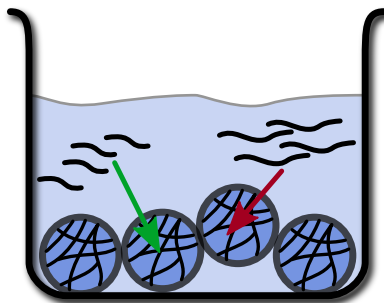


**Figure 4.1.:** Schematic of the solute exclusion technique to explore the pore size distribution of a hydrogel with linear probe polymers. The probe polymers in the solution phase can diffuse into the gel. Their distribution between the two phases is dependent on their size with respect to the pores in the gel large enough to accommodate them.

nary work is shown that gives a proof of principle for the method and some experimental considerations are discussed.

In a first approach, mixtures of poly(methacrylic acid) (pMMAc) polymers were used as probes in the so called mixed solute exclusion method and their concentration evaluated on-flow after separation by size exclusion chromatography (SEC) [Kuga81, Walther94]. However, several problems hampered this effort so a second experiment was devised. Dextrans were used and their concentration evaluated separately by refractive index measurement in a static experiment. At last, some perspective is given of what is possible with this method.

For the first approach, the procedure of Prausnitz *et al.* was adapted for the use with poly(acrylic acid) (pAAc) gels and the equipment at hand [Walther94].<sup>1</sup> The pAAc gels were swollen to equilibrium in neat deionized water (DI) and mixed with several pMMAc probe solutions each of which contained a mixture of two to three individual linear polymers. From the supernatant phase of the mixtures, samples were taken over the course

<sup>1</sup>The experiments with pMMAc probes were conducted by Mrs. Karin Schlag and the ones with Dextrans by Mr. Stefan Horn, both under the supervision of the author.

of two weeks. The samples were analysed by aqueous SEC with differential refractive index (DRI) detection. The peak heights in the elograms were evaluated to determine the concentration. Further details on the experimental procedure and exact composition of the samples can be found in appendix A.2. The evaluation, however, was difficult due to several reasons which become evident for example in the elograms of Mix 2 in **fig. 4.3** on top. First, the individual components of the mixture were not well separated: the broad peak at 7.1 mL contains the signals of two polymers with weights of 326 and 34.9 kDa and even for the sample with the lowest molecular weight (1.2 kDa) no baseline separation is seen. Thus, it was impossible to gain accurate concentrations for all components. The problems are two-fold: the upper limit of the separation range of the column in use was 100 kDa. Therefore, the signals of the higher  $M_w$  components were shifted towards higher elution volumes and smeared out. Additionally, the column was overloaded due to the combination of three standards in one measurement thus broadening the peaks further. An exclusion from the gel was recorded for all samples but no trend over time could be observed, which is demonstrated for Mix 2 in **fig. 4.2** in the lower part. Already after 24 h the intensity has decayed to within the error margin of the equilibrium value and no further trend is seen in the data. This leads to the conclusion that most of the process was already finished when the first sample was taken after one day.

In a related problem the solvent used for the experiments was not the same as the eluent of the SEC setup (TRIS buffer solution, see appendix A.2) thus ghost peaks (not shown) from changes in the eluent during one SEC run were recorded at the end of elogram. This partly obscured the peaks of the low molecular weight probe polymers. The samples could not be filtered before injection to the SEC, as their volume was too small, which might play a role in the above mentioned problems.

In a second approach several changes were made to overcome the previously encountered problems. Dextrans were used as probe polymers with

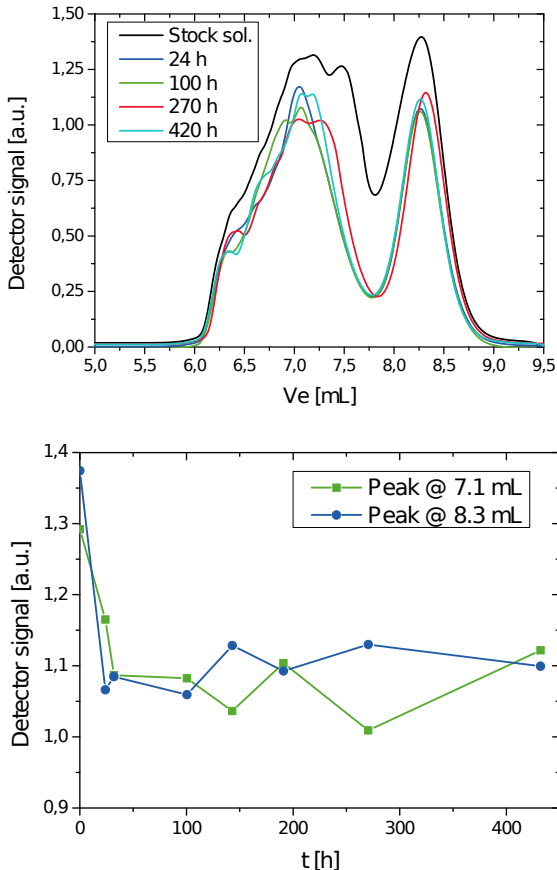


**Figure 4.2.:** The time dependent solute exclusion of linear pMAAc probes from a pAAc hydrogel (DC = 1 mol-%,  $Q_{\text{syn}} = 4 \text{ g/g}$ ) are recorded by DRI for selected SEC elugrams (top) and the change of the peak heights over time (bottom) is shown. Here, as an example Mix 2 is shown that contained probes of  $M_W$  values of 326, 34.9, and 1.2 kDa.

$M_w$  values of 1.3, 24, and 273 kDa which are non-charged and should, therefore, interact less with the gel. In this case, the dry polymer instead of the swollen one is mixed with the probe solutions. Thereby, water has to flow into the polymer and takes the probes with it. Thereby the process is speed up in contrast to the already swollen gel where the diffusion is responsible for the partition of the probes. The concentration was determined by static DRI measurements on single probe polymer solutions, thus eliminating the need for SEC experiments and their problems all together. The samples were taken at shorter times. Hereby, considerable improvement of the data was achieved. The results are shown in **fig. 4.3** for two pAAc gels with DC of 0.1 and 1.0 mol-% mixed with the Dextrans and blind samples for each of the probes. Two theoretical border values can be determined for the concentration of probe polymers in the supernatant phase. At complete permeation of the gel, the concentration of probes would stay the same at 0.5 mg/mL as the available volume is constant. At complete rejection from the gel the available volume would be 3/4 of the original, giving a limiting upper concentration of 0.67 mg/mL. It should be noted that the concentration of the blind samples (samples without any gel) was up to 0.01 mg/mL above the expected value and the gel blind tests (gels in water without any probe polymers) showed a leaking of sol of up to 0.03 mg/mL. Therefore, the error of these measurements is at least 0.04 mg/mL probably in the way to high concentrations. In addition,  $Q_{eq}$  is subjected to some error of about 5 % (see sec. 3.2).

For the gel with DC = 0.1 mol-% a small rejection of the two smaller probes was found, while it was considerably stronger for the largest of the Dextrans. This suggests, that the average pore size is in the range of the medium sized probe. In the higher cross-linked gel, only the smallest polymer showed a good penetration, the middle one was almost completely excluded and the largest was even excluded to above the theoretical limit, but within the experimental error. The typical pores are thus considerably smaller than the 24 kDa Dextran. The results are in accordance with the

theory predicting pores that are considerably smaller at higher DC. The experiments show, a size-dependent rejection of reference polymers can be investigated well with the second proposed method. However, more experiments and improvements are necessary in future: More probes should be used to generate a complete rejection curve which can afterwards be inverted to give the pore size distribution. The measurements should be carried out for a longer time to check whether equilibrium conditions were already met. The results seem to suffer from a systematic error that needs to be reduced by removing the sol fraction completely and better knowledge of the equilibrium swelling degree ( $Q_{eq}$ ). The method seems viable on pAAC hydrogels and worth further investigation.

## 4.2. NMR-spectroscopy

The investigation of chemical compounds including polymers by high-field NMR-spectroscopy (HF-NMR) is a routine procedure [Hatada04, Mirau05, Schmidt-Rohr94]. In this section only measurements are presented and evaluated, that were carried out at  $^1\text{H}$ -resonance frequencies of 250 MHz and above. They exhibit full spectral resolution and the aim of their use is the analysis of the incorporation of the cross-linking monomer and the structures on a small length scale using scalar coupling effects. In contrast, relaxation experiments carried out at low magnetic field are discussed in the next chapter. Here, typical aspects of HF-NMR spectra of hydrogels are discussed and the possible reasons for line broadening are investigated. At last, the possibility of 2D-NMR analysis of hydrogels is discussed.

A NMR spectrum of hydrogel beads in  $\text{D}_2\text{O}$  recorded under standard high-field conditions yields few information.<sup>2</sup> The resonance lines are broad and few features are found (**fig. 4.4**). The assignment of  $^1\text{H}$ -NMR (250 MHz,  $\text{D}_2\text{O}$ ) is as follows  $\delta = 1.58 \text{ ppm (bs, } 2\text{H, } -\text{CH}_2-$ ,  $2.19 \text{ ppm (bs, } 1\text{H, } -\text{CH}-)$ .

---

<sup>2</sup>Standard conditions are a  $^1\text{H}$ -NMR resonance frequency of 250 MHz and 32 scans. The sample contained about 5 wt.% of polymer in  $\text{D}_2\text{O}$ , which is below the gel capacity and individual particles are present.

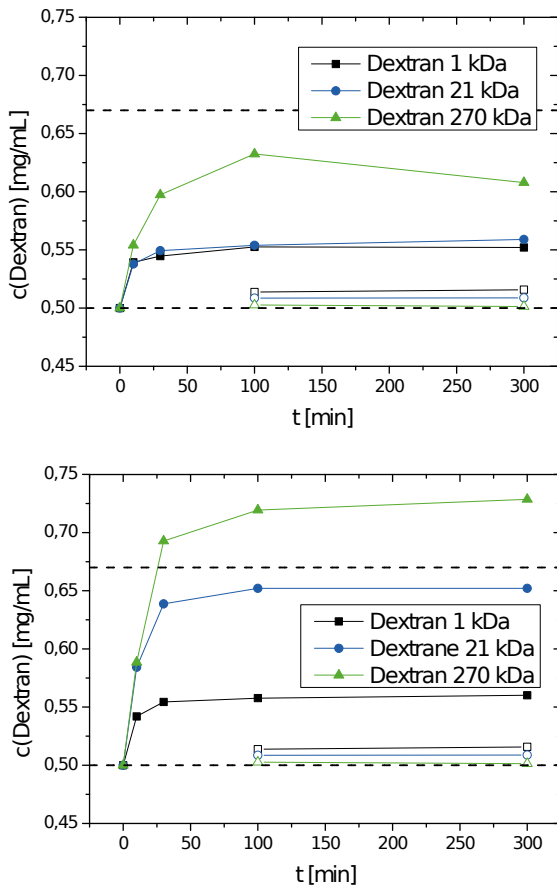


**Figure 4.3.: Time evolution of the concentration of Dextrans is shown for different molecular weights in the supernatant phase over pAAc hydrogels with DC = 0.1 mol-% (top) and DC = 1.0 mol-% (both  $Q_{\text{syn}} = 4 \text{ g/g}$ ). The closed symbols give the mixtures with gel while the open ones are for blind samples. The lines are just a guide to eye and the dashed lines give the theoretical borders calculated from complete rejection (upper) and complete permeation (lower) of the Dextrans.**

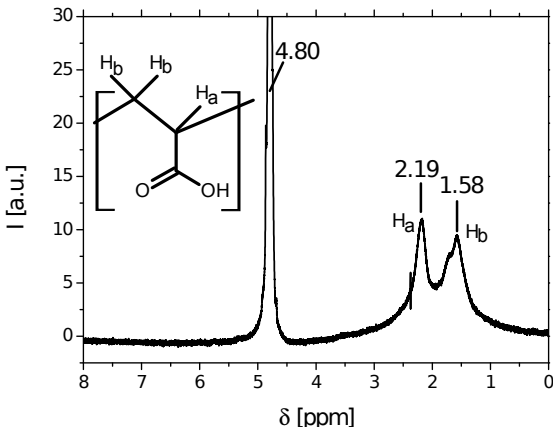


**Figure 4.4.:** Standard HF-NMR spectrum of a pAAc hydrogel with DC = 1 mol-%,  $Q_{\text{syn}} = 2 \text{ g/g}$ . The sample was recorded in  $D_2O$  with a  $^1\text{H}$  resonance frequency of 250 MHz. The signal of residual  $HDO$  is seen at 4.80 ppm.

Additionally, residual  $HDO$  is found at 4.80 ppm that probably stems from proton exchange with the carboxylic acid groups on the polymer which is not seen.

A considerable broadening of the resonance lines is observed. In the case of the single line at 2.2 ppm it amounts to about 130 Hz FWHM. This can be caused by three effects: first the residual dipolar coupling of the protons due to restricted motions, secondly a wide distribution of chemical shifts of non-equivalent spins (chemical shift distribution) and at last the inhomogeneities of the local B-field. The latter might be caused by the grain to air interfaces in the sample and possibly by the ions present. The effect of dipolar coupling has already been investigated by experiments under magic angle spinning (MAS) conditions in the authors diploma thesis [Höpfner09]. The result is given in **fig. 4.5** for a sample prepared with a DC = 5 mol-%. The spectra of two rotor rotation frequencies were stacked to identify spinning side bands which were marked with asterisks. Again,  $HDO$  is found at 4.8 ppm. For the same peak at 2.2 ppm a width of 70 Hz

(FWHM) is observed. This shows, that dipolar coupling is present in the sample but not the only cause of line broadening. The influence of the grain-air interfaces can be reduced, when using a single block sample. This was archived by polymerising the monomer mixture directly in the NMR tube. A sample of pAAc with DC = 1 mol-% and  $Q_{\text{syn}} = 4 \text{ g/g}$  was produced and the spectrum recorded.<sup>3</sup> The same resonance lines as above are seen. Additional peaks stem from *HDO* and around 3 ppm probably from the accelerator TEMED still present in the "as prepared" sample. In this case as well, no considerable decrease in line width is seen (around 100 Hz (FWHM) for the line at 2.2 ppm). From these facts it is concluded, that all three effect play a role including the unresolvable chemical shift distribution. This means that baseline separated signals and a finer structure and, with them, information on microstructure cannot be recovered in proton NMR. The investigation of other NMR-active nuclei, especially  $^{13}\text{C}$ , is a feasible way to overcome this, but was not investigated further due to the low sensitivity.

The second interesting information that could be drawn from HF-NMR experiments is the connectivity of the single nuclei by two-dimensional methods [Castignolles09]. Hereby, the connection between neighbouring atoms or those a few bonds away can be investigated. Especially for the case of the cross-linker the immediate environment is of high interest. By investigation of their environment the formation small rings or direct connection to another linker molecule might be quantified. Both effects should be visible by correlation methods. However, several methods were tried, namely  $^1\text{H}$ -TOCSY, edited  $^1\text{H}, ^{13}\text{C}$ -HSQC, and  $^1\text{H}, ^{13}\text{C}$ -HMBC but all failed to yield information on a pAAc sample. Only signals from *HDO* and the accelerator TEMED were recovered (not shown). This is due to the fast spin-spin relaxation process with a time constant of about 1 ms (see below). Therefore, all information on the polymer part of the sample is already lost

---

<sup>3</sup>This measurement and the 2D experiments were carried out by Dipl.-Chem. Martin Koos at the Institute of Organic Chemistry (KIT).

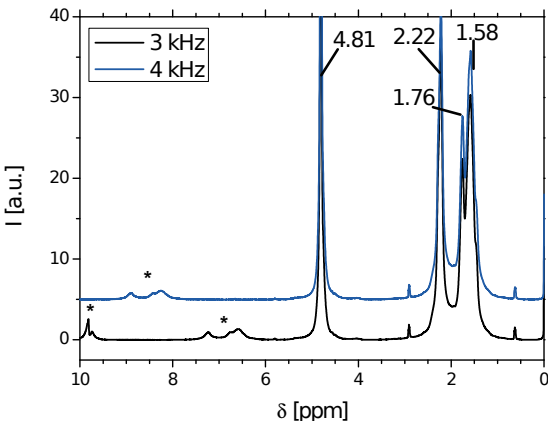


**Figure 4.5.:** Two high field NMR spectra of a pAAc hydrogel ( $DC = 5 \text{ mol-}\%$ ,  $Q_{\text{syn}} = 2 \text{ g/g}$ ) are shown, which were recorded under MAS conditions with rotor spinning frequencies of 3 and 4 kHz. Thereby the spinning side-bands are identified and marked with asterisks.

during the mixing and delay times necessary in the 2D experiments (up to 100 ms). The  $T_2$  relaxation time was estimated from the three spectra given in **fig. 4.6**. They were taken after different Hahn echo delay times ( $2\tau$ ) at a  $^1\text{H}$ -resonance frequency of 600 MHz. The principle of the Hahn echo experiment is described in detail in the next section (sec. 4.3.3). The  $T_2$  time obtained here is in agreement with the value (about 1 ms) found in low-field NMR-experiments discussed in the next section.

In total, the HF-NMR methods fail to yield specific information on the hydrogel samples. The high spectral resolution of HF-NMR is not sufficient to resolve the microstructure of the peaks that stem from the polymer. This is caused by a number of problems inherent to the used samples. Especially, the homo-nuclear dipolar coupling and its distribution over parts of the polymeric material with different mobility cannot be eliminated. Standard 2D-experiments are not possible due to the fast spin-spin relaxation in the polymer. The incorporation and surrounding of the cross-linker can thus not be elucidated by  $^1\text{H}$ -NMR methods tested here.

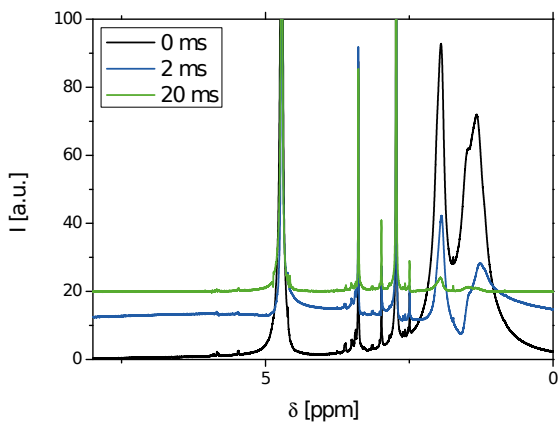


**Figure 4.6.:** Three spectra of a pAAC hydrogel with a DC of 1 mol-% ( $Q_{\text{syn}} = 4 \text{ g/g}$ ) are shown that were recorded after different Hahn echo delays. The time given in the legend corresponds to the total delay of  $2\tau$  in the pulse sequence.

## 4.3. NMR-relaxometry

Relaxometry is a simple yet powerful tool to investigate the dynamics in materials. The dynamics in hydrogels is strongly correlated to the topology, as the junction points impose permanent constraints on the polymeric chains. This leads to a heterogeneity in dynamics which also reflects the differences of the size of meshes. This method does not depend on spectral resolution as needed for the NMR-spectroscopy used in the previous section. Therefore, without loss in the possible results, the high magnetic field instruments for which measurement time is limited can be replaced by simpler low-field instruments (e.g. 20 MHz  $^1\text{H}$ -resonance frequency) which are inexpensive and offer easier access. Due to the use of robust well chosen methods the same informations on molecular dynamics can be gained with this approach [Saalwächter07]. These type of instrument and methods have proven themselves useful in the investigation of similar materials before.

The information is obtained by measuring longitudinal and transverse relaxation processes as well as the residual dipolar coupling in the network. These results are presented in turn after some general remarks on pulse NMR methods and a short theoretical introduction. A theory is needed, that is able to correlate measurement data to local mobility at a semi-quantitative level at least. Here the approach first developed by Bloembergen, Purcell and Pound (BPP) will be used [Bloembergen48].

### 4.3.1. Relaxation phenomena in Gels

#### Basics of pulse NMR

A short introduction into the method of pulse NMR and its concepts of description will be given, before any specific relaxation processes are discussed. For a more detailed review of the matter of nuclear magnetism, the

reader is trustfully referred to the extensive literature [Bovey88, Slichter78, Abragam61, Fukushima81].

The nuclear angular momentum or spin  $I$  is a quantity inherent to all nuclei and governed by the principles of quantum dynamics (QM). The nucleus also posses a magnetic moment  $\mu$  as an effect of its charge, that is collinear with the spin. Here we will consider a nucleus with a non-vanishing but small spin of  $I = 1/2$ , for which hydrogen would be a good example. The spin is quantized into  $2I + 1 = 2$  discrete states with the expectation values of  $m_I = +1/2$  and  $-1/2$ .

In an external magnet field  $B_0$  along the axis (z), the two spin niveaus are no longer degenerated. The two states correspond to different energy levels. An ensemble of similar spins will distribute between the two states randomly, with the population numbers  $N_{m_I}$ . However, the overall distribution will be governed by the energy difference  $\Delta E$  of the two states and is given by the Boltzmann relationship (4.1). It can, with good accuracy in the high temperature approximation, expanded into a Taylor series. It should be noted that the energy difference  $\Delta E$  is small when compared to the thermal energy and therefore the population difference is quite small as well (around 100 ppm).

$$\frac{N_{+1/2}}{N_{-1/2}} = \exp\left(-\frac{\Delta E}{k_B T}\right) \approx 1 - \frac{\hbar\omega}{k_B T} \quad (4.1)$$

Here a complete ensemble of identical spins in a volume element of a sample will considered, which adopt the Boltzmann partition in thermal equilibrium. The macroscopic net magnetisation  $M$  of the sample is the result of the ensemble of spins in a magnetic field.  $M$  can be described by the picture of a classical gyroscope. The macroscopic magnetisation can be seen as precessing around the axis z on an cylinder cone. All possible orientations towards the magnetic field lie on the cylinder surface (**fig. 4.7**, left). This precession is usually described by a so-called Larmor frequency  $\omega_L$ , eq. (4.2), and depends on the field strength  $B_0$  and the type of the nucleus,

described by its gyromagnetic ratio  $\gamma$ .

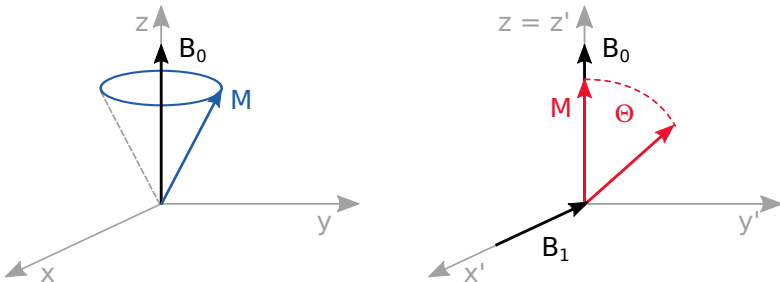


**Figure 4.7.:** Schema of the laboratory frame with a magnetisation precessing around  $z$  (left) and the rotating frame with net-magnetisation subjected to a pulse  $B_1$  (right).

$$\omega_L = \gamma B_0 \quad (4.2)$$

A spin can only pass to another state with an energy exchange in form of an energy quantum. This is exchanged with a second, non-stationary magnetic field, that is, in the case of a field emitting from the probe coil, designated with  $B_1$ . The effective part of this field is perpendicular to  $B_0$ , that is in the  $x$ - $y$ -plane, and rotates at the same frequency as the magnetisation (4.3).

$$\Delta E = h\nu = \hbar\omega_L \quad (4.3)$$

It is cumbersome to visualize this energy exchange in the fixed coordinate system of the laboratory frame ( $x$ ,  $y$ ,  $z$ ) even for the picture of the net-magnetisation. More conveniently a rotating frame with  $x'$  and  $y'$  is adopted, that precesses with  $\omega_L$  around the field's axis  $z' = z$ , as shown in **fig. 4.7**, right side. In this frame of reference the magnetisation is fixed along  $z$  without a field  $B_1$  present. When present,  $B_1$  is a static field on, for example, the  $x'$ -axis. If the second field with a frequency  $\omega_L$  is switched on for a time  $\tau_p$ , it will transfer energy into the system and causes spins

to pass from one state to the other. This is described by a rotation of the magnetisation vector around  $x'$ , given by the pulse angle  $\Theta$  in eq. (4.4).

$$\Theta = \gamma B_1 \tau_P \quad (4.4)$$

This angle describes the state of the resulting magnetisation after the pulse: at  $90^\circ$  or  $\pi/2$  it will be zero in  $z$ -direction and completely along  $y'$ . Further rotation to  $180^\circ$  or  $\pi$  turns  $M$  to be collinear to  $-z'$  and the component in the  $x'-y'$ -plane is zero. The pulse introduces a non-equilibrium state where the direction of  $M$  is different from  $z$ .

### **Motion of nuclei and spectral density**

The sample containing spins can be transferred to a non-equilibrium excited state by a broad-band radio-pulse. The magnetisation is then no more collinear with  $z$  and can be separated into a component  $M_z$  along  $z$  and one  $M_y$  along the  $y'$ -axis. Both components will individually return to their equilibrium state, which gives rise to two different relaxation phenomena which are discussed in the following sections. First the basic mechanism that permits these processes is explained.

In any sample the nuclei are not fixed, but in constant movement with respect to each other, either by translational or rotational dynamics. This motion can be, in first approximation, thought of as being random. Since the nuclei possess magnetic moments, they give rise to fluctuating, local magnetic fields with a broad range of frequencies and directions. Only matching fluctuations allow the transfer of energy or alignment between the nuclei and the surrounding, as will be discussed in the next sections.

The autocorrelation function  $C(t)$  gives the decay of self-similarity in the system over time due to motion of the molecules. The correlation time  $\tau_c$  is the characteristic decay time of this function. The Fourier transformation (FT) of  $C(t)$  is the spectral density function  $J(\omega)$  which gives the respective power of the fluctuations in the frequency domain. In general neither the

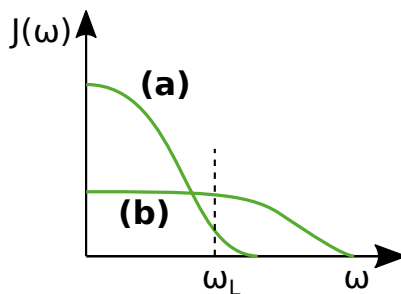


**Figure 4.8.:** Model examples of the spectral density function  $J$  at long (a) and short (b) correlation times  $\tau_c$ . It is decaying monotonically towards higher frequencies.

autocorrelation function nor the spectral density can be computed analytically.  $C(t)$  can be thought as a monotonic decreasing function, as shown in **fig. 4.8**. However, for the simple case of truly random motion an analytical solution is possible. In this case the local autocorrelation function is exponential decaying. After FT for  $J$  a Lorentz-function (4.5) depending on the parameter  $\tau_c$  is obtained.

$$J(\omega) = \frac{2\tau_c}{1 + \omega^2\tau_c^2} \quad (4.5)$$

The function  $J$  is a tool to visualize how relaxation processes in samples can differ. Predominantly slow motions in a sample, caused by high viscosity, low temperature and often characteristic for large molecules, give long correlation times and a steep drop of the  $J$ -function with a small spectral power density at high frequencies. In contrast fast motions in a sample give a broad distribution with a broad range of frequencies but low amplitude for each, as shown in the cases (a) and (b) in fig. 4.8 respectively.

### Longitudinal Relaxation

First, the relaxation process of the part of the magnetisation along the z-axis  $M_z$  is discussed. This process is also called longitudinal relaxation. The

magnetisation returns to its full equilibrium value  $M_0$  along z. A dissipation of energy is here required as the Boltzmann equilibrium population of spin states has to be reestablished. This is done by exchange with other degrees of freedom in the sample summed up under the term "lattice", the process is also known as spin-lattice relaxation [Bloembergen48, Bovey88].

For a change of the spin state a stimulated emission (or absorption) is necessary, which in turn needs a local magnetic field with the appropriate direction and frequency, that is here the Larmor frequency  $\omega_L$ . These fields are generated by other nuclei's motions, as described above, and therefore its power corresponds to the value  $J(\omega_L)$ . This is usually small and therefore the exchange is slow, with the spins being only weakly coupled to the lattice.

The equation of motion of the magnetisation is a set of differential equations first introduced by Bloch [Bloch46]. For the longitudinal part of the magnetisation it reads

$$\frac{dM_z}{dt} = -\frac{M_z - M_0}{T_1} \quad . \quad (4.6)$$

The solution to this equation is a function of the type  $M(T) \propto M_0 \exp(-t/T_1)$ , depending on the boundary conditions. The time constant  $T_1$  is usually used as a measure for this process and gives the time after which roughly 37 % ( $1/e$ ) of the magnetisation has left in the excited state.

The value of  $T_1$  is dependent on the local mobility in the sample. The BPP-theory uses this insight to predict it from molecular properties. The general expression for homo-nuclear dipolar coupling is given by equation (4.7) with  $\langle r \rangle$  being the (average) distance between two spins. It also depends on  $\tau_c$  as given by  $J$  (4.5), which is proportional to viscosity and the molecule size. As the frequency of fluctuations considered here is the Larmor frequency, this quantity is only sensitive to motions in the MHz range in the sample. It can also be seen that the double of  $\omega_L$  can induce transitions, these are double quantum processes.

$$\frac{1}{T_1} = \frac{3\gamma^4\hbar^2}{10\langle r \rangle^6} \cdot [J(\omega_L) + 4J(2\omega_L)] \quad (4.7)$$

### Transverse Relaxation

However, not only the part of magnetisation along  $z'$  relaxes, but also the  $y'$ -component  $M_y$  (or  $M_x$  for  $x'$ ) returns to its equilibrium value, that is 0. This process is also called transverse relaxation. The M-component in the  $x'-y'$ -plane is due to the fact that all spins excited by the pulse have the same phase. After the pulse they still rotate with the Larmor frequency around  $z$ , and so does the net-magnetisation vector. This moving magnetic moment induces a voltage in for example the RF-coil of the spectrometer and gives an observable signal [Hahn50, Bovey88].

Yet this signal is only short lived, the spins de-phase over time. The reasons are again the local field perturbations described above: the local magnetic field  $B_0(r)$  experienced by each spin is slightly different due to the perturbations from neighbouring spins and also its own  $\omega_L$ . In the case of homo-nuclear dipolar coupling discussed here, the influence of motions is a function of distance  $\langle r \rangle$  of nuclei. Additionally, the angle  $\theta$  between the direction of  $B_0$  and the vector between the two nuclei is to be considered, as given by eq. (4.8). The dependence on the angle is given by the second Legendre polynomial  $P_2(\cos(\theta))$ . Some precess slightly faster other slower than average, resulting in a fanning out in the rotating frame and a loss of phase coherence. The sum magnetisation along  $y'$  is reduced in the process and the observed signal decays over time giving the free induction decay (FID). Arising from the interaction between spins, this process is also called spin-spin relaxation.

$$\Delta E = 2\mu (B_0 \pm B_{loc}) = 2\mu \left( B_0 \pm \frac{3\mu}{2\langle r \rangle^3} \cdot (3\cos^2 \theta - 1) \right) \quad (4.8)$$

The process can again be described by a relaxation rate and a differential equation (4.9) as introduced by Bloch. The associated time constant is usually given as  $T_2$ . The value of  $T_2$  gives the time in which  $\sim 63\%$  of the phase correlation, that is the transverse magnetisation  $M_y$ , is lost.

$$\frac{dM_x}{dt} = -\frac{M_x}{T_2} \quad \frac{dM_y}{dt} = -\frac{M_y}{T_2} \quad (4.9)$$

The time constant is dependent on the motions in the sample by the same mechanism that was described earlier. The BPP-theory yields an expression to calculate it from sample characteristics (4.10). Here the same values of  $J$  play a role as was the case for  $T_1$  but, additionally, the relaxation process is dependent on motions in the very low frequency range  $J(0)$ . These possess often, given the form of  $J(\omega)$ , more spectral power than at the Larmor frequency. It is a useful tool to probe slow processes in a sample of slower correlations.

$$\frac{1}{T_2} = \frac{3\gamma^4\hbar^2}{40\langle r \rangle^6} \cdot [3J(\Delta\omega) + 5J(\omega_L) + 2J(2\omega_L)] \quad (4.10)$$

However, when using real magnets, especially in LF-NMR, the  $T_2$  relaxation time cannot be computed directly from the FID. Because of the intrinsic inhomogeneities of the  $B_0$ -field, the resonance frequencies differ more than due to motion of the nuclei alone and the apparent  $T_2^*$  from the FID is shortened. Therefore special care has to be taken when measuring  $T_2$  (see section 4.3.3).

$$\frac{1}{T_2^*} = \frac{1}{T_2} + \Delta\omega(B_0) \quad (4.11)$$

## Restricted motion effects

Molecular motions induce the relaxation processes as was shown earlier. However, these motions do not always have to be fast or truly random. Here we will discuss the situation for fixed or partially fixed spin positions.

In this case the autocorrelation function is non-exponential. This leads to interesting points in the relaxation behaviour and yields important information on the sample topology.

The power of the fluctuations, that enable the transverse relaxation process, depend on the angle  $\theta$  which is one important point of eq. (4.8). In a fixed geometry, with discrete values for  $r$  and  $\theta$ , a static dipolar coupling  $D_{\text{stat}}$  is found as the energy levels of the two spins are permanently perturbed by the field of the other nuclei. This results in different local B-fields and therefore resonance frequencies. In the ideal case of solitary pairs of spins, this is reflected in a static Pake-type spectrum, dominated by two distinct lines if all orientations are present [Schmidt-Rohr94]. However, the spin distributions in most solids are more complicated and a lot of interdependent spin-spin interactions are found. This causes a broad range of Larmor frequencies for the spins and a broad peak (of typically Gaussian form) in the spectral domain.<sup>4</sup>

In liquids, a completely different situation is found: because of the fast motions all possible orientations of a molecule are realized during the time in which a FID is recorded. Therefore the effect of dipolar coupling is given by the average of  $P_2(\cos \theta)$ ,<sup>5</sup> the time average of 0. Accordingly no static dipolar coupling is present and no extra line broadening is observed.

In terms of gels, as one example of constrained topologies, the situation is in between the two cases just described. The cross-linked chains can move quite fast on the NMR time-scale ( $\mu\text{s} - \text{ms}$ ), if swollen sufficiently. However, due to the topology not all conformations (values of  $\theta$ ) are accessible. This leads to a "pre-averaging" of  $P_2$  but still yields a small but finite value after averaging and, therefore, a finite interaction named residual dipolar coupling (RDC) described by the constant  $D_{\text{res}}$ . This can be understood as an effect of the autocorrelation function of a polymer chain-segment as

---

<sup>4</sup>The spectral width would be 122 kHz if only proton pairs with a distance between them of 1 Å are considered.

<sup>5</sup>The averaging over all possible conformations of the molecule is required. This can be replaced by the time average, if the motions are fast enough.

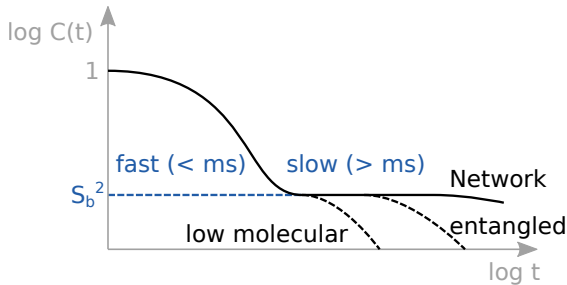


**Figure 4.9.:** Schematic decay of the autocorrelation function  $C(t)$  of a polymer chain-segment. A fast initial a decay is a result of segmental motions, while in constraint systems a plateau (at  $S_b^2$ ) evolves. Figure adapted from [Saalwächter07].

shown in **fig. 4.9**. After an initial decay due to segmental motions the decay to 0 is hampered in longer chains by entanglements and in case of networks does not even occur at very long observation times, as some conformations are not accessible.

The obtained RDC-constants are a direct result of the extent of constraints and therefore are an excellent measure for the topology in the sample. They reflect very slow motions as does  $T_2$  but are only sensitive to those related to the topology. The RDCs can be used to approximate the number of effective repetition units  $N_e$  between two cross-linking points (4.12) [Saalwächter07]. Here  $S_b$  is the plateau value of the autocorrelation function,  $k$  a scaling factor due to pre-averaging and  $r$  the mean squared end-to-end distance of the meshes.

$$S_b = k \frac{D_{\text{res}}}{D_{\text{stat}}} \approx \frac{3r^2}{5N_e} \quad (4.12)$$

### 4.3.2. Longitudinal relaxation measurements

The longitudinal relaxation process is strongly influenced by high frequency motions, about the Larmor frequency of the used spectrometer,<sup>6</sup> in the sample. Therefore, measurements of the  $T_1$  relaxation time constant will give useful information if the sample (or parts of it) show conformational changes or motions on this time scale. If fluctuations with correlation times of  $\tau_c \approx 1/\omega_L$  or  $1/2\omega_L$  are present in the sample a long relaxation time as predicted by the BPP-theory is found [Bloembergen48]. For polymers this is the case only for very high mobilities. Here, hydrogels with different composition were investigated and two distinctly different relaxation process observed. However, the variation of the corresponding time constants was found to be minimal when the same monomer was used and only with changes of the monomer or addition of water a contrast was obtained.

The characteristic time of this process ( $T_1$ ) can be measured by methods with the following approach: the sample is first excited from thermal equilibrium by a pulse, and after an evolution time, the progress of its return is observed by the FID intensity after a second pulse. Two pulse sequences are commonly used for this enterprise: Saturation recovery (SR) and inversion recovery (IR) [Vold68, Freeman71, Anderson72]. Both methods are further explained in the appendix (A.3) together with some comparative results. Both methods were found to yield the same results within the margin of error. The SR-method is employed because it is much faster.<sup>7</sup> After each individual experiment (or scan) no special recycle delay (rd) has to be waited, in contrast to IR where the full relaxation of the sample is required. This latter time is typically  $3 - 5 T_1$  and can easily amount to 20 s in the case of the samples herein.

---

<sup>6</sup>In this work this is 20 MHz for  $^1\text{H}$ .

<sup>7</sup>SR is mostly useful in low-field NMR applications and for polymers or solids less so for low-molecular liquids.

The relaxation time  $T_1$  was measured while systematically varying the samples with regard to several synthetic parameters used in the preparation of hydrogels. The preparation of the samples is detailed in appendix A.1, all were prepared from 10 wt.-% of polymer swollen in  $D_2O$ . A set of four hydrogels was investigated, in which  $Q_{\text{syn}}$  (the amount of water present in the gel at the time of preparation, see sec. 3.1), was changed. The values were 1.5, 2, 4, and 8 g/g, while all other values were held constant. The measured result curves are displayed in **fig. 4.10**. The bimodal relaxation behaviour is easily visible and therefore a double exponential function was adjusted to the data and two time constants were obtained (see appendix p. 233 for details).

The assignment of the shorter of the two time constant, around 36 ms, is to a component of restricted mobility and therefore connected to the polymer component of the sample. It depends on  $Q_{\text{syn}}$  to a small degree only and is shown in **fig. 4.10** on the lower side. It is slightly decreasing with the synthesis parameter. However, the dependence is small and almost within the margin of error, which is given by measuring three samples of the same polymer and using the standard deviation of the mean.

The longer time constant is in the range of 3000 ms, with no systematic change depending on the sample. It is attributed to residual  $HDO$ . This assumption is based on the large value of  $T_1$  usually only found for highly mobile species of low viscosity and low molecular weight. This is supported by a reference sample of only  $HDO$  exhibiting a single exponential decay with a time constant on 9000 ms. This is formed from  $D_2O$  solvent and acidic protons from carboxyl-groups in the polymer while swelling the polymer. The amount of signal, and therefore the amount of protons, is about half for all samples under investigation, so all samples contained considerable amounts of unwanted protons.

The small dependence of the spin-lattice relaxation time of the polymer component holds also for other samples that were investigated. Further data for samples with varying cross-linker concentration (DC) is there-

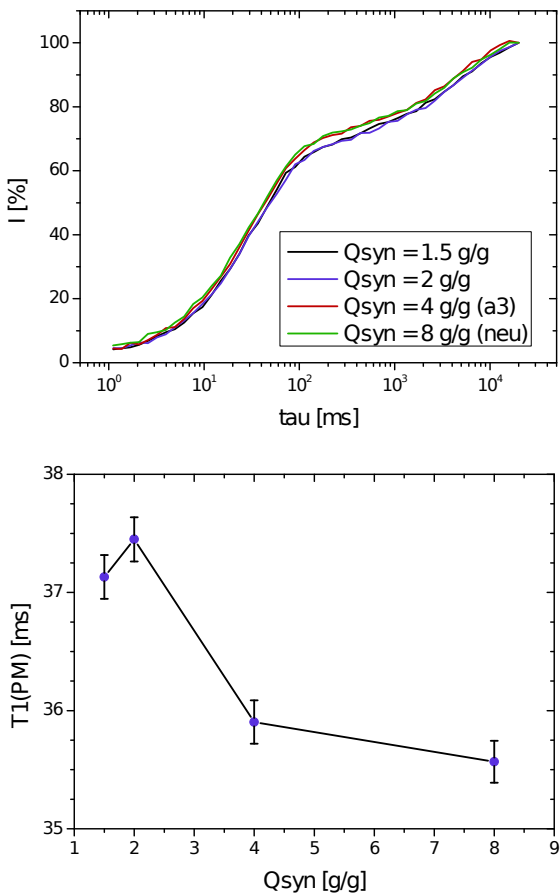


**Figure 4.10.:** Longitudinal relaxation behaviour of samples produced with different water contents in the synthesis mixture ( $Q_{\text{syn}}$ ). The raw data is shown on top. The  $T_1$  time constants are obtained by a fit of bi-exponential functions to the raw data. Only the dependence of the faster component of the fitting function is shown (bottom) which corresponds to the polymer fraction in the sample. For the slower constant, corresponding to  $HDO$ , no systematic variation was found (not shown).

fore not shown. This findings extend to other topologies of the same monomer: commercial samples and non-cross-linked pAAc showed the same behaviour. Only when the monomer is changed to pMAAc, a commercial linear sample is used here (see also p. 115), a clear difference can be seen (**fig. 4.11**). The samples are described further in appendix A.1.

A change in the relaxation behaviour was also found when the composition of sample was changed as displayed in **fig. 4.11**, bottom. Here a higher polymer content leads to faster relaxation of the magnetization, with the exception of 40 wt.-% polymer. In this case it was difficult to obtain a good signal for the polymer component as the signal was very weak, possibly indicating a very fast decay that cannot be resolved with the employed method. The findings of a weak dependence of the *HDO* relaxation time constant on the polymer concentration found by Locke *et al.* could not be supported [Penke98].

The longitudinal relaxation constants  $T_1$  of a set of different hydrogel samples was obtained. It was found to contain two components: a fast one (about 40 ms) arising from the polymer and a slow one (about 3 s) attributed to residual *HDO*. This indicates a low mobility in the polymer component relative to the Larmor frequency (20 MHz). Higher concentrated samples become even more rigid in terms of fast motions. No major dependence of  $T_1$  on the composition of the gels was found, as all time constants were in the range of 34 – 38 ms. Only the switch to another monomer type had a distinct effect. Thus this method is useful for investigating the local unit structure rather than the overall network structure. In contrast, the traverse relaxation process discussed next will enable more insight.

### 4.3.3. Transverse relaxation measurements

The primary effect of introducing constraints in polymeric systems above the  $T_g$ , is a reduction of mobility of the chain segments and an increase of non-isotropy of the motion. Inherently this is reflected in the transverse re-

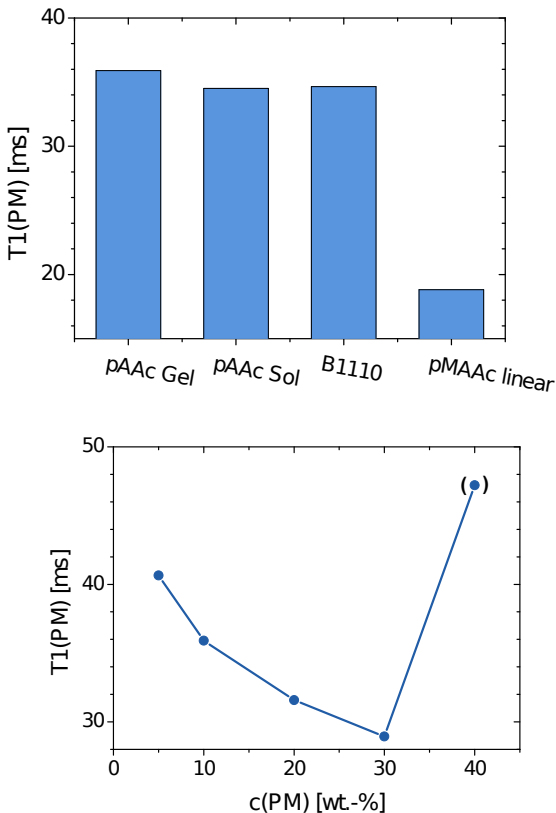


**Figure 4.11.:** Longitudinal relaxation times of samples with different architectures or composition are shown on top. pAAc was synthesised with DC = 1 mol-%,  $Q_{\text{syn}} = 4 \text{ g/g}$ . The gel and gel component of the same sample are shown. B1110 gel and linear pMAAc were of commercial origin. The results of varying the polymer content  $c(\text{PM})$  in the measured sample are given below. The value in brackets at 40 wt.-% is doubtful; see the text for details.

laxation process in NMR, which is especially sensitive to motions with low frequencies. The  $T_2$  relaxation time constant is quite sensitive to all changes in the topology of the network, such as in gels, that are mechanically active [Shapiro11, p. 1226]. It is a good tool to investigate and quantify the effect that chemical changes have on the structure of the resulting gels. However, such measurements are not straight forward to carry out and special care has to be taken to record the full and true relaxation behaviour. The results are complex in nature and yield broad distributions of relaxation processes, which are analysed by different methods to reduce the data. In this work several chemically different hydrogels are investigated, which differ in their reference state (as controlled by e.g.  $Q_{\text{syn}}$ ) and their cross-linking degree (DC). They are compared with their sol extracted counter parts, as well as commercial samples and linear polymers. This yields the possibility to differentiate these samples and gain insight into the underlying structure.

### **Data acquisition and problems thereof**

In the case of the use of LF-NMR equipment, the true transverse relaxation process has to be recovered by echo techniques, as it cannot be measured directly from the FID due to field inhomogeneities (see previous section). The basic concept to produce such an echo is a  $\pi/2$ -pulse that rotates the magnetisation to the  $x'$ - $y'$ -plane, followed by an evolution time and a  $\pi$ -pulse to flip all spins in the plane. After the same time delay an echo forms, which maximum height gives the true loss by transverse relaxation. Descriptions of this process are abundant in the literature [Bovey88, Fukushima81].

The two implementations routinely used for investigating liquid and soft materials to produce the echoes are the Hahn-echo or spin echo and the CPMG-experiment that utilizes a train of echoes to capture large parts of the relaxation curve at once [Hahn50, Carr54, Meiboom58]. These implementations are discussed in more detail in appendix A.3. The decay obtained for a typical hydrogel sample by the two methods is shown on top of

fig. 4.13. Different echo delays  $\tau$  were used to capture larger parts of the relaxation curve. As the same process is investigated the results are expected to coincide on one curve, which however, is not the case. Additionally it was found that early and late stages of the decay process could thus not be measured.

The results do not coincide because of the so called spin-locking effect that is usually used to measure the spin-lattice relaxation in the rotating frame ( $T_{1\rho}$ ) [Fukushima81, 262] [Slichter78, 214] [Kuhn12, Guthausen98]. The very close spacing of the  $\pi$ -pulses with identical phase at short  $\tau$  values in the CPMG-echo train mimic the behaviour of a locking field, as depicted in **fig. 4.12**. In a locking field perpendicular to  $B_0$ , a new relaxation mechanism has to be introduced and the system now decays accordingly. The magnetisation decays in the rotating frame in accordance with  $T_{1\rho}$  which, in the case of the investigated samples, is longer than  $T_2$ . This leads to the relaxation behaviour observed in **fig. 4.13**, top. The influence depends on the strength of the effective lock field, i.e. on the pulse spacing. This effect can be prevented if the  $\pi$ -pulses are not in coherence with each other. This can be achieved by cycling the phases of the  $\pi$ -pulses within the echo train. Advanced phase cycling schemes are known in the literature and were tested: namely XX4 and XY16 which are described in appendixA.3 [Gullion90, Guthausen98]. When using XX4 already an improvement as found, but satisfactory results were only achieved with the XY16 scheme. The relaxation curves obtained with the latter are shown in the lower part of **fig. 4.13**. In this case all measurements do coincide on one curve. The XY16-phase cycle was self implemented into the CPMG-pulse sequence on the instrument in a self written pulse sequence.<sup>8</sup>

This endeavour was undertaken, as the uses  $\pi$ -pulse trains is usually preferred over Hahn echo methods, because it is much faster. By the use of XY16 the dependence on  $T_{1\rho}$  is eliminated. Additionally, pulse spacings

---

<sup>8</sup>The standard CYCLOPS phase cycle is superimposed on the XY16 scheme to compensate for instrument errors.

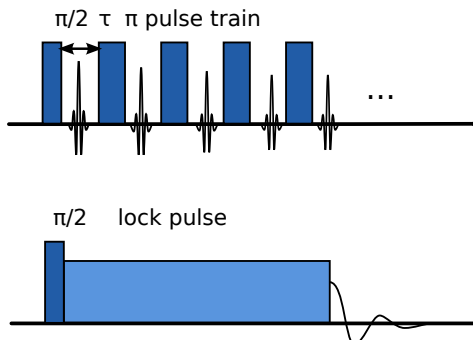


**Figure 4.12.:** Relation between the CPMG-pulse sequence with close pulse spacings (top) and the spin-locking sequence used to measure  $T_{1\rho}$  (bottom), this causes deviations in the transverse relaxation curves as depicted in fig. 4.13.

larger than 10 ms, which would be necessary in Hahn echo experiments to measure long relaxation times, can lead to obfuscation by diffusion of the material. This can be seen in the respective curves in fig. 4.13 as the signal is lost after this threshold.

Several improvements were made to obtain the whole decay curve. The fast decaying signal is obtained by directly measuring the FID at times smaller than 100  $\mu$ s, before field inhomogeneities become dominant. In the case of solid like contributions the dead time of the instrument is a known problem and can be overcome by the use of a solid echo [Powles63]. Here however, the similar but more effective magic sandwich echo (MSE) was used [Maus06]. The result can also be seen in fig. 4.13, below. With these improvements the complete relaxation behaviour of all samples could be acquired and we can turn to the subsequent data treatment and reduction.

## Approaches to data reduction

The obtained relaxation curves are not easy to interpret, because the relaxation behaviour is complex and yields plenty of information. Two different

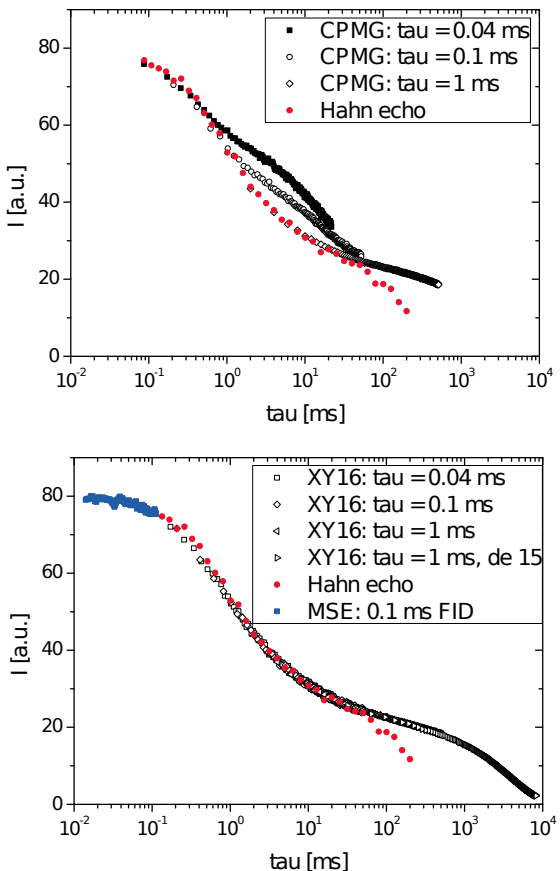


**Figure 4.13.:** Decay of transverse magnetisation in an hydrogel sample as recorded by different implementations of the spin echo method. On top, CPMG-experiments with different evolution times  $\tau$  do not yield a smoothly overlapping curve. This is achieved below by the XY16-phase cycle, with early points measured by the MSE-experiment.

methods for data reduction and improved comparability are employed and discussed hereafter.

The results of different measurements of the same sample are combined to one dataset. Subsequently the component with the longest relaxation time is logarithmically separated from the rest. It is subtracted after fitting with a single exponential function and normalized to 100 % at the maximum; an example and the detailed description of the whole procedure can be found in appendix A.3. The long relaxation constant was always found to be in the range of 2 – 5 s, that is a highly mobile species and therefore attributed to residual *HDO*. Here the same reasons, that were discussed in the section about longitudinal relaxation (p. 96), hold as well.

Thereby, the varying amount of solvent is removed and the signal arising from the polymer component can be compared directly to other samples. The resulting dataset is shown in **fig. 4.14** for the same sample discussed in the previous section. The error of the measurement is again approximated from measuring three samples of the same gel (fig. 4.14). The resulting relaxation curve is one broad decay without distinctive features often found in gel systems [Hong98]. No model will be adopted here a priori, but instead two different options for describing the data will be discussed.

The first approach is a quantitative description of the relaxation dataset by use of an empirical fit function. Several different combinations of exponential and Gauss functions were evaluated. The best case was found to be the combination of an exponential with an Kohlrausch-Williams-Watts-function (KWW, also called stretched exponential) as given by (4.13). The single exponential part is used to describe the earlier behaviour and the KWW-function the later with a notable stretching factor of  $\beta \approx 0.5$ .<sup>9</sup> The relative weight of the two fractions is usually around 1:1, while the time constants vary largely from sample to sample. The fit describes the data well and is almost always within the margin of error. However, this is a purely empirical approach of description and no specific meaning is attached to

---

<sup>9</sup>  $1/\beta$  is approximately the width of the relative time distribution in decades.

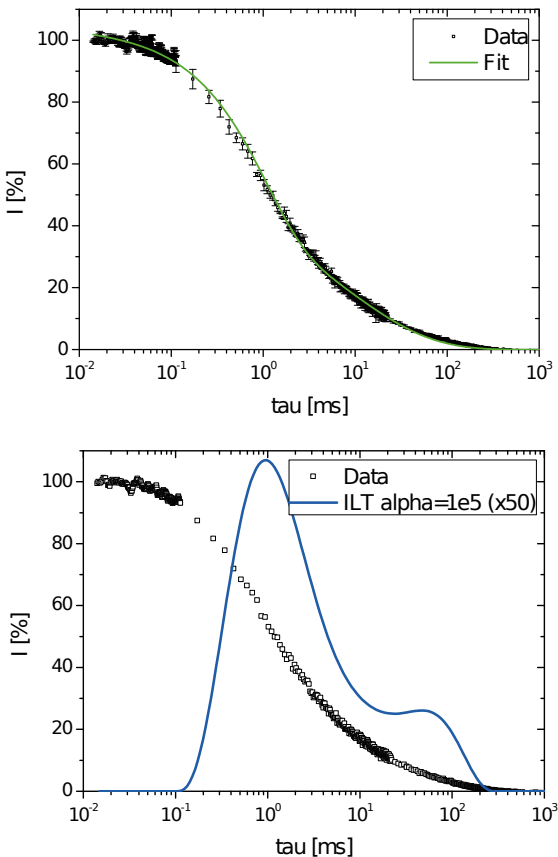


**Figure 4.14.:** Solvent subtracted transverse relaxation data and evaluation results for a typical hydrogel ( $\text{DC} = 1 \text{ mol-}\%$ ,  $Q_{\text{syn}} = 4 \text{ g/g}$ ). A fit to the data as described in the text (green line, top) yields  $T_{2S} = 1.0 \text{ ms}$ ,  $T_{2S} = 7.3 \text{ ms}$  and  $\beta = 0.46$ . The error bars are from comparing three samples of the same gel. Below, the distribution function of relaxation times, obtained by ILT with  $\alpha = 10^5$ , is shown (blue line).

the obtained time constants as the underlying processes are complicated and distributions of relaxation times are expected.

$$I(\tau) = A \cdot \exp\left(-\frac{\tau}{T_{2,S}}\right) + (100 - A - C) \cdot \exp\left(-\left(\frac{\tau}{T_{2,L}}\right)^{\beta}\right) + C \quad (4.13)$$

The fit is a good description in a series of similar gels and the time constants can be compared. However, in systems with large differences, the relaxation curve will differ to a large extend and the time constants will describe a different part of the curve. Consequently the comparability of the values is lost.

Not all features of the relaxation curve can be easily seen and compared. As a second approach, the distribution of relaxation times in the sample is more useful when comparing the data from different samples by eye. The overlay of a set of exponential functions in a signal or decay can be correctly deconvolved using the inverse Laplace transform (ILT) as given by (4.14) [Borgia98]. This path integral can be evaluated for any real value for  $\gamma$  for which the path is completely in the region of convergence of the function.

$$\mathcal{L}^{-1}\{F(t)\} = \frac{1}{2\pi i} \int_{\gamma-i\infty}^{\gamma+i\infty} F(s) \cdot \exp(ts) dt \quad (4.14)$$

Unfortunately, this problem is ill-posed so it can only be solved numerically and with making prior assumptions [Provencher82, Borgia98]. Here, the algorithm proposed by B. Ryland *et al.* is used [Callaghan03a, Callaghan03b] as implemented by the authors in the MATLAB software [Godefroy08]. The main control parameter is the smoothing factor  $\alpha$ ; for more information on the conduct the reader is referred to appendix A.3. Applying the ILT to noisy or incomplete datasets leads to a reduced quality of the evaluation. The present, carefully recorded raw data was found to be good enough to obtain stable results with a small  $\alpha$  parameter of typically  $10^5$ . An example of the result is shown in **fig. 4.14**, below. It should be noted that the intensity scale can only be used for relative comparison as it depends on the

number of points in the inversion curves. This method has been successfully applied to LF-NMR data before [Anferova07], however, other authors noted that this method can be invalid if non-exponential decays are treated [Saalwächter12, p. 9]. With the tools to extract information from the raw data ready, we will now turn to the real samples that are investigated.

### Influence of the gel reference state

The structure of a gel is controlled by several synthetic parameters, as described in sec. 3.1. For a recovery of the influence of these parameters several sample series are investigated. Thereby, one synthetic parameter is changed at a time, while all others were held constant. The above described methods of evaluation were employed.

The first parameter investigated is  $Q_{\text{syn}}$ . Four samples, which contained 1.5, 2, 4, and 8 g water per g monomer at the time of cross-linking were investigated. The DC and DN were held constant at 1.0 and 75 mol-%, respectively. The solvent subtracted datasets obtained are shown in **fig. 4.15**, top. All samples can be clearly distinguished from one another and a trend to slower relaxation behaviour with increasing water content is found. The overall form of the transverse relaxation curve remains the same.

To determine the contribution of the sol component in the gels to the relaxation behaviour, a major part of the sol content was removed from all samples (see section 3.4) and then they were measured again with otherwise same conditions. The results are compared with the non-extracted samples in **fig. 4.15**, below. In all cases, a shift to faster relaxation processes is observed, with the effect being present over most of the time scale, with the effect being most pronounced for  $Q_{\text{syn}} = 8 \text{ g/g}$ .

These trends can be better visualized via the Laplace inverted datasets in **fig. 4.16** on top. The curves show a main peak which is relatively sharp and a broader shoulder at longer relaxation times appears. The main peaks are shifted to faster relaxation times with lower  $Q_{\text{syn}}$  values. The shoulder,

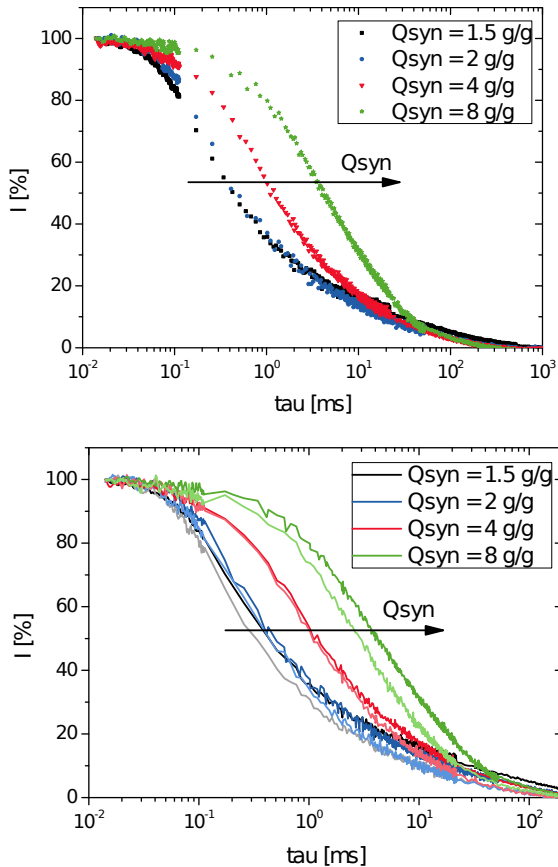


**Figure 4.15.:** Transverse relaxation curves of pAAc hydrogels with different reference states ( $Q_{\text{syn}}$ ) and DC = 1 mol-%. On top, results are shown for the gel samples without being sol extracted. Below, the original data is compared with data acquired on the samples after sol-extraction (in lighter coloured lines).

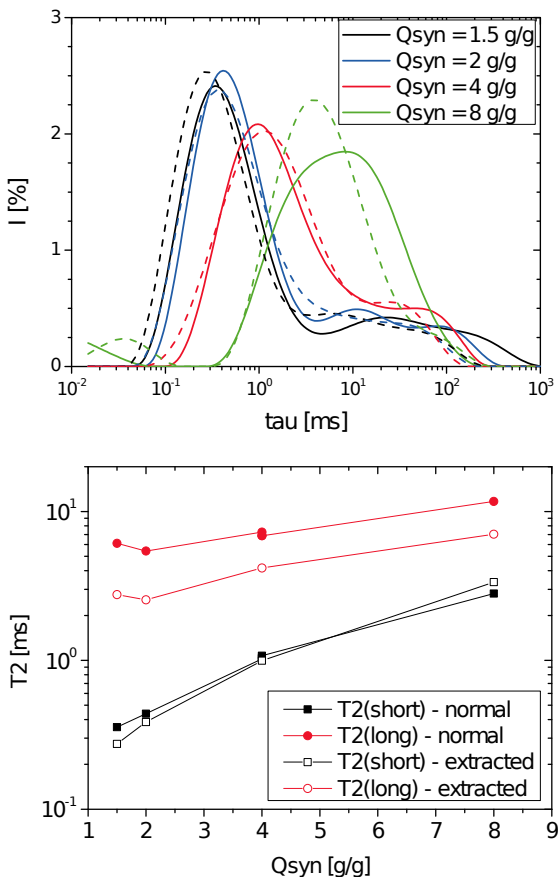


**Figure 4.16.:** On top, Laplace inverted transverse relaxation curves of pAAc hydrogels with different reference states ( $Q_{\text{syn}}$ ) and DC = 1 mol-% are shown. The straight lines represent the samples before and the dashed lines the same samples after sol-extraction. Below, the  $T_2$  time constants obtained by using a fit of the function (4.13) are shown.

however, is becoming more pronounced in the same direction. When comparing with the curves of the extracted samples, a shift of the main peak to fast times is observed while the long-time tail of the shoulders is considerably reduced. The information obtained from the results of the ILT are qualitatively the same for the main peak but the differences at long relaxation times (around 100 ms) are far better observed. For the sample with  $Q_{\text{syn}} = 8 \text{ g/g}$  an almost mono-modal distribution of  $T_2$  relaxation times is found.

The use of a fit function on the original data supports the findings of the ILT. Additionally, the form of the empirical fit function, eq. (4.13), that was proposed in the previous section, is in good agreement with the ILT findings. The obtained fit parameters are visualised in **fig. 4.16**, below. Both relaxation times are found to be almost steadily increasing with  $Q_{\text{syn}}$ . The long relaxation time is always considerably smaller, about a factor of two, for the sol-extracted samples. The shorter one is, within the margin of error, the same for extracted and standard samples. No clear dependence of the stretch parameter  $\beta$  is found — the value is around 0.45 for most samples (for 8 g/g 0.65). This is an indication of a similar dynamic heterogeneity within the samples.

Considering these trends, two major conclusions can be drawn. First, the decrease of water content in the reaction mixture leads to gels with more confined structures. This becomes evident from the overall shortening of the relaxation times. The  $\beta$  parameter obtained from the fits is unchanged so the distribution width found for the samples seems to be unaffected. Secondly, the influence of the sol is clear: it is not a homogeneous component with a single relaxation time that can be directly identified in the primary relaxation curve. It is inhomogeneous, like the gel itself, without only the most rigid parts. This claim is supported by the separate analysis of the extracted sol part (4 g/g sample, shown in the appendix fig. A.6). Here a KWW-function without additional terms was found sufficient as a fit function. A  $\beta$  of 0.51 is found, that is almost similar to the one found in the gel.

The relaxation time of 58 ms is longer but in the same order, while only the initial drop with the short time constant is missing.

### Influence of the cross-linking degree

The main parameter that controls the topology of a gel is the length of a mesh between two cross-linking points, statistically given by the amount of poly-functional monomers added to the reaction mixture, here called cross-linking degree (DC). A series of samples, with otherwise identical composition, was prepared with 0.1, 0.3, 1, and 3 mol-% MBA as cross-linking monomer, while  $Q_{\text{syn}}$  and DN were held constant at 4 g/g and 75 mol-% respectively. The same tests as above were performed, resulting in the solvent-subtracted datasets shown in **fig. 4.17**, top. Here the trend observed in the case of  $Q_{\text{syn}}$  is reversed: A higher cross-link density results in a faster relaxation process. Thus in the network the motions are more restricted. All samples are nicely distinguishable and the result found for the sample with DC = 3 mol-% is remarkable, because a very pronounced initial decay is found. This initial decay is well recorded with the MSE method but could not have been guessed from CPMG/XY16-signals alone. A small increase of the  $T_2$  relaxation time of the HDO component with DC is observed (not shown) which could also be an effect of different amounts of residual  $O_2$ . As comparison with the normal gels, the sol extracted samples were measured as well as shown on the bottom of **fig. 4.17**. Here, the differences between extracted and non-extracted samples are generally less pronounced than in the case of variation of  $Q_{\text{syn}}$ . The main process at shorter relaxation times shows almost no change in the extracted samples while at longer relaxation times differences seem to occur. The Laplace transformed datasets are shown in **fig. 4.18** on top, elucidate these changes further. For DC = 3 and 1 mol-% the shoulders at longer times are reduced due to extraction while in the case of 0.3 the whole form the long time tail is transformed, so no comparison can be made. This suggests that the densely cross-linked

samples are very rigid in their structure and the contained sol is very different in mobility from the gel component.

The fit function (4.13) is adapted to the data (not shown). The obtained relaxation times show a pronounced dependence on DC that is almost linear for the shorter one (**fig. 4.18**, below). The relaxation times as a function of DC follow a power law (fig. 4.18; a fit gives a scaling exponent of  $-0.86$ ). The relaxation time  $T_2(\text{short})$  is a little shorter for the extracted samples than for the non-extracted, while  $T_2(\text{long})$  does not show consistent differences. The latter is unexpected and probably an artefact of errors in the synthesis procedure in the cases of the samples with DC = 0.3 and 3 mol-%. These samples are also considerably more inhomogeneous as the  $\beta$  parameter shows ( $\approx 0.3$  here vs.  $\approx 0.5$  for all other samples).

The effect of cross-linking on the relaxation behaviour is pronounced and the creation of very rigid parts in the highly cross-linked material is evident. The influence of sol content seems to be similar as in the preceding section, however, the argumentation is obscured by two unreliable samples and data treatment.

### Industrial and other samples

In addition to the synthetic variances discussed above, some industrial hydrogel samples were investigated. They offer information on the networks produced in large scale processes and an additional structural feature as also a surface cross-linked sample is investigated. They were employed as a working material for the desalination process described in chapter 6.3. All samples were provided by the BASF and are labelled with Hysorb, 1030 (Luquasorb) and B1110 (Luquasorb), a superabsorbent polymer consisting of particles with additional surface cross-linking. The relaxation curves are shown in **fig. 4.19** in the upper part, together with two self-synthesized gels with DC = 0.3 and 1.0 mol-% ( $Q_{\text{syn}} = 4 \text{ g/g}$ ). The  $T_2$  constants are shown on the lower part of the same figure. The Hysorb and 1030 polymers exhibit

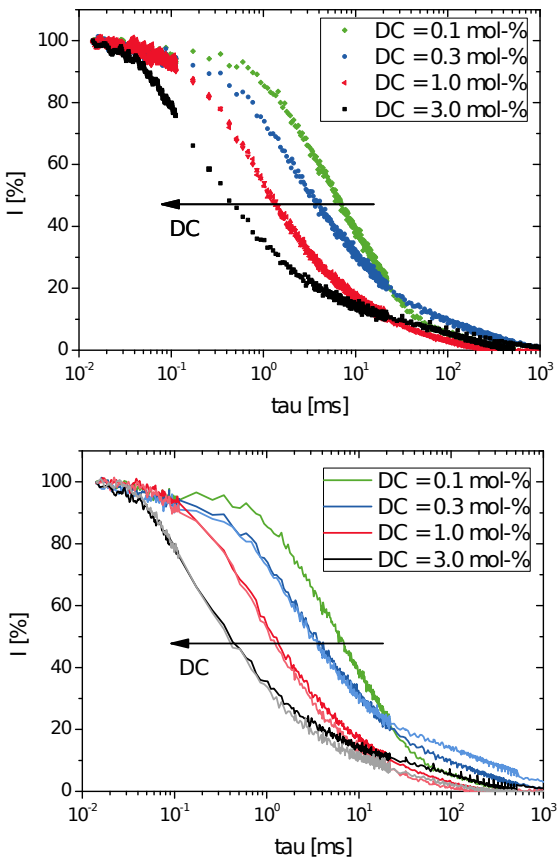


**Figure 4.17.:** Transverse relaxation curves of pAAc hydrogels with different cross-linking degrees (DC) and  $Q_{\text{syn}} = 4 \text{ g/g}$ . On top, results are shown for the gel samples without being sol extracted. Below, the original data is compared with data acquired on the samples after sol-extraction (in lighter coloured lines).

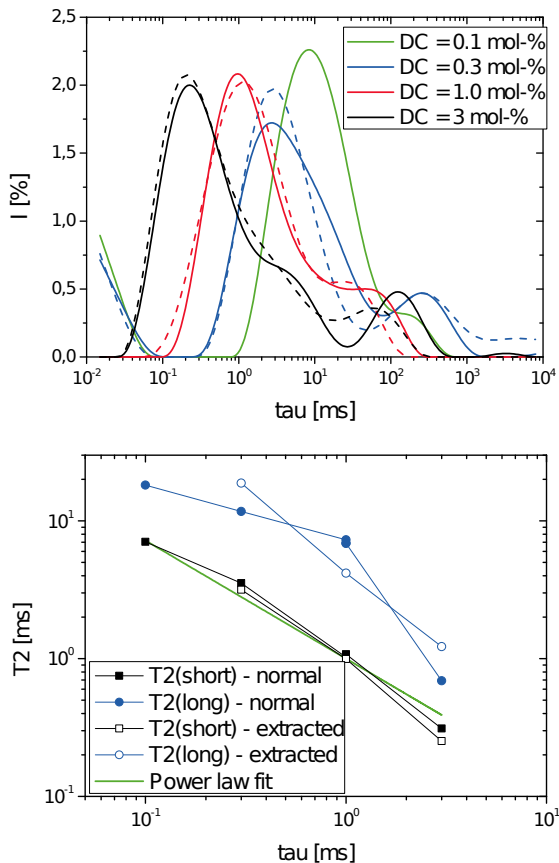


**Figure 4.18.:** On top, Laplace inverted transverse relaxation curves of pAAc hydrogels with different cross-linking degrees (DC) and  $Q_{\text{syn}} = 4 \text{ g/g}$  are shown. The straight lines represent the samples before and the dashed lines the same samples after sol-extraction. Below, the  $T_2$  time constants obtained by using a fit of the function (4.13) are shown. A power law fit to the shorter time constants is given as well (green line).

a similar behaviour. Their DC can be estimated to be a little over 0.3 mol-%, if  $Q_{\text{syn}}$  of all samples is the same. B1110 shows an especially broad relaxation behaviour, if compared with the reference sample (DC = 1 mol-%). The initial decay in B1110 is faster but at long times the relaxation behaviour is similar. This is not reflected in the  $\beta$  parameter (0.44), but rather in the large difference in the two time constants more than one order apart, a spread not encountered in any other sample. The other industrial samples are more homogeneous in terms of  $\beta \approx 0.53$ .

As a last addition in terms of topology, linear counterparts to the cross-linked polymers are investigated. One is a commercial pMAAc with narrow molecular weight distribution (see also p. 98), the other is the sol component extracted from the gel with DC = 1 mol-% and  $Q_{\text{syn}} = 4 \text{ g/g}$ , which was already discussed above. The relaxation curves are presented in appendix A.3 (fig. A.7). Both curves are sufficiently well described with a one component fit (after solvent subtraction). In the case of pMAAc, even a single exponential function offered a good fit with a time constant of 8.9 ms, while for the sol component the use of a KWW-fitting showed significant improvement. The parameters  $T_2 = 56 \text{ ms}$  and  $\beta = 0.51$  are obtained. This means the stretch exponent is quite similar to the gel part, that is quite broad, while the time constant is by a factor of 5 longer and no short decay is observed.

As the last point, the ratio of polymer to water in the NMR samples was varied and its influence recorded by the usual fit function (**fig. 4.20**). It should be noted that this is the ratio at the time of measurement, not at the time of synthesis ( $Q_{\text{syn}}$ ). The relaxation time of pure polymer was found to be very short (0.02 ms). The curve form is Gaussian which is typical for solid state samples. Thus, the relaxation time  $T_2$  is taken to be the half-life (FWHM) of a Gaussian fit of the FID and is only meant as approximate reference. Both relaxation time constants are seen to exhibit a maximum around 30 – 40 wt.-%, which interestingly is the reference state of the gel in which it should be most relaxed (c\*-theorem) [de Gennes79, p. 152].

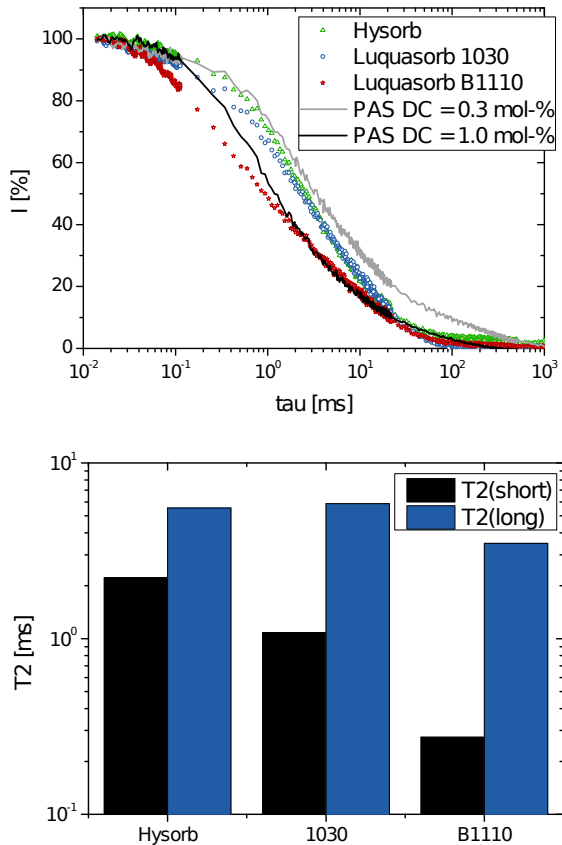


**Figure 4.19.:** Transverse relaxation curves of industrially produced superabsorbers (symbols) and two self-synthesised gels as a reference (lines) are shown on top. The time constants obtained by a least squares fit of eq. (4.13) to the datasets are given in the lower part.

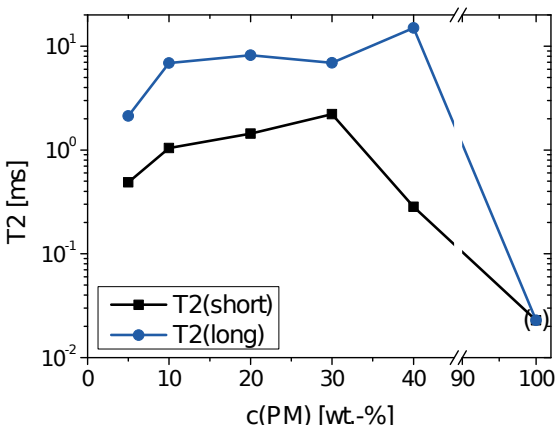


**Figure 4.20.:**  $T_2$  relaxation time constants of hydrogel samples with different polymer content are shown. The time constants were obtained with a pAAc hydrogel with DC = 1.0 mol-% and  $Q_{\text{syn}} = 4 \text{ g/g}$  and a least squares fit of eq. (4.13) to the raw data. The pure polymer shows true solid state behaviour and the time is given by the FWHM of the Gaussian shaped FID. It is therefore not directly comparable.

This means that at a low water content, the solvent works as a plasticizer enabling chain motions. However, at high swelling degrees, the mobility is reduced again, as the chains are stretched and only few conformations of similar length are possible.

The evaluation of the transverse relaxation times gives an impression of the dynamics and its heterogeneity of the polymer forming the gel. The transverse relaxation time constant are always shorter, by a factor of about 4, than the longitudinal counterparts. More interestingly they are very sensitive to changes in the gel topology. This is demonstrated by series varying DC and  $Q_{\text{syn}}$ . A two component fit including a notable stretch exponent (around 0.5) can describe the relaxation data well. The obtained time constants are not attributed to specific "phases" or "inter-phases", in contrast to some work in the literature [Hong98, Shapiro11, Kanekiyo98, Ando02]. However, in recent literature most authors with NMR background acknowl-

edge that this is an unfortunate endeavour. The sol is not a distinguishable part of the primary gel but quite inhomogeneous in itself also at the slower part of the relaxation curve. Industrial samples show a similar behaviour to the self-synthesized polymers, except the surface cross-linked B1110 with an unusual spread in the  $T_2$  time constants.

#### **4.3.4. Residual dipolar coupling measured by double quantum coherences**

The measurement of double quantum (DQ) or higher coherences offers a substantially different way to account for the motional constraints in a gel than does the relaxation time constant  $T_2$ . In the opening section 4.3.1 its is shown, that the extent of residual dipolar coupling (RDC) is directly related to the topology of the gel and offers a measure for its extent. In principle, the effect of RDC can be seen in the early behaviour of the echo signals discussed in the previous section. However, constraints and the resulting RDCs are not the only mechanisms that contribute to the magnetisation decay. They are just one feature in the overall relaxation behaviour. To distinguish them, can, at times, be difficult. The differentiation is possible by using double quantum (or higher order) coherences of spins in the system because their coupling remains constant over time. Other rapidly decaying components do not exhibit these kinds of correlations. So the RDC, quantified as the coupling constant  $D_{\text{res}}$  can be obtained directly. The acquisition pulse sequence for DQ phenomena is explained briefly. In LF-NMR, it is used as a new tool to investigate the same samples that were discussed in the previous sections.

The measurement of DQ-coherences is accomplished by the complex pulse sequence depicted in **fig. 4.21**. The sequence was developed and implemented by K. Saalwächter *et al.* and offered to the author for this project [Saalwächter07, Chasse11]. The pulse sequence was developed for elastomer samples and applied with success [Saalwächter12], however, only

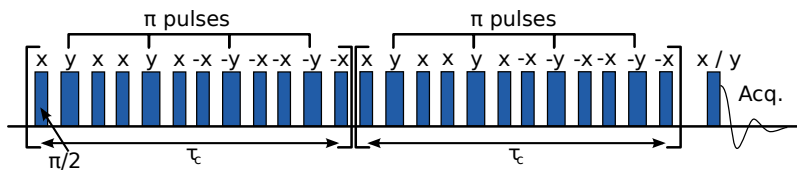


**Figure 4.21.:** Schematic representation of the pulse sequence for measurement of the double quantum coherence build-up. The first part is the stimulation of the coherences and in the second part the coherences are reconverged to form observable magnetisation. By increasing  $\tau_c$  via the pulse spacings, the complete build-up curve can be sampled. The measurement parameters are described in detail in appendix A.3.

one example is known to the author where it was used to investigate hydrogels [Lange11]. Model gels of poly(ethylene glycol) with a defined mesh size were investigated, while here pAAc gels with statistical cross-linking are investigated for the first time.

The sequence is used to stimulate coupling between two spins, in a first part, and afterwards transforms it back to observable magnetisation in the reconvengence part. After the final  $\pi/2$ -pulse, the FID is acquired. The relative phase of this last pulse is used to discriminate between the actual double quantum intensity and all other intensity that has not been transferred to multi quantum coherences. Thus two curves are measured as a function of the sequence length  $t_c$  as shown in fig. 4.21. The measurement parameters are summarised in appendix A.3.

The DQ build-up is unfortunately hampered by apparent transverse relaxation effects ( $T_2^*$ ) and has to be renormalized to its true form. Therefore, two exponentially decaying components are subtracted from the long time part of the signal. An example of the obtained signals as raw data and after renormalisation are shown in **fig. 4.22** for a self-synthesized hydrogel sample (DC = 1 mol-%,  $Q_{\text{syn}} = 4 \text{ g/g}$ ). It should be noted that the DQ signal decays to noise level within about 30 ms which makes the recovery of the build-up curve after this point difficult. This is directly reflected in the renormalized signal which starts to scatter dramatically after this time. The

time is still long enough for the signal to reach a plateau at 0.5, which is the theoretical long time prediction.

The pulse sequence was benchmarked against several types of samples to validate the above claim that it is only sensitive to systems with partially hindered motions. The detailed experimental results are given in the appendix (fig. A.9) but in summary it can be said, that in pure water no DQ-signal is detected at all and in linear polymers only a very weak one, when the same concentration as the gels is used. In solid polymer samples no signal at all could be measured, probably as a result of the fast decay of all magnetisation even within the shortest cycle times. The influence of the polymer concentration in the sample is shown in the appendix as well. At higher polymer contents it takes longer to reach the plateau value.

The RDC constants are obtained from the renormalized data by applying a fit function. Typically a simple Gaussian function is used for this purpose [Chasse11], however, as a quite inhomogeneous network is expected due the statistical preparation process, a distribution of Gaussian functions is assumed. This distribution can either be uni- or bimodal leading to one or two averaged RDC constants,  $D_{\text{res}}(\text{weak})$  and  $D_{\text{res}}(\text{strong})$ , and their respective weight  $w$ . It was found in this work that in all but the softest cases (that is low DC and high  $Q_{\text{syn}}$ ) only the bimodal fit offered a good description of data. Both fits are shown on the example with the respective results in fig. 4.22. The fitting procedure is once more described in the appendix (p. 241).

A comparison of the double quantum build-up and the transverse relaxation behaviour, presented in the previous section, was sought. Therefore the same samples were investigated with both methods. As the first synthetic parameter the gel reference state  $Q_{\text{syn}}$  was investigated; the results are shown in **fig. 4.23**. A clear shift of the build up process to longer times with increasing water content can be seen.  $D_{\text{res}}(\text{strong})$  is decreasing, while the weak coupling is not affected. However, the relative weight of the two constants shifts dramatically from about 15 % of  $D_{\text{res}}(\text{weak})$  at 1.5 g/g to

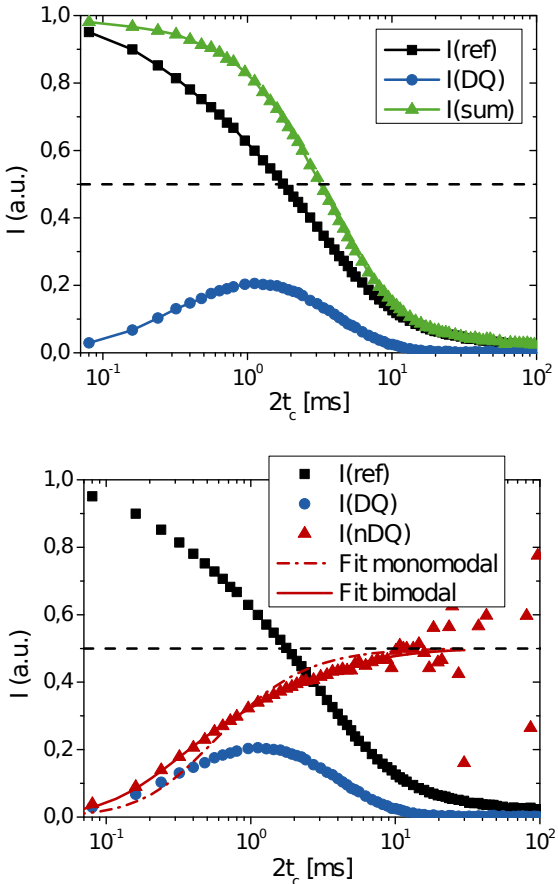


**Figure 4.22.:** Typical result of double quantum experiments, here recorded on a self-synthesised pAAc gel sample ( $\text{DC} = 1 \text{ mol-}\%$ ,  $Q_{\text{syn}} = 4 \text{ g/g}$ ). On top, the raw data  $I_{\text{ref}}$  and  $I_{\text{DQ}}$  and their sum is shown. Below, the renormalised build-up curve  $I_{\text{nDQ}}$  with uni- and bimodal fit models are shown. The unimodal fit yields  $D_{\text{res}} = 0.41 \text{ kHz}$ . The bimodal fit leads to  $D_{\text{res}} = 0.75 \text{ kHz}$  (26 %) and  $D_{\text{res}} = 0.08 \text{ kHz}$  for strong and weak coupling, respectively. The dashed lines give the theoretical upper limit (0.5) for  $I_{\text{DQ}}$  and  $I_{\text{nDQ}}$ .

almost 80 % at 8 g/g. For the sol extracted counterparts the same measurements were conducted. The differences in the fitting parameters are shown in fig. 4.23 as well.  $D_{\text{res}}$ (strong) is slightly higher here, while  $D_{\text{res}}$ (weak) and the relative weight of the two components are unaffected.

The second parameter that was investigated is the cross-linking degree (DC), with the results shown in **fig. 4.24**. For the lowest cross-linking a unimodal distribution was found to be sufficient, but with increasing DC the spread between  $D_{\text{res}}$ (strong) and  $D_{\text{res}}$ (weak) increased dramatically. At the same time the weight of the weak part almost vanished.

By the use of double quantum analysis the differences between types of commercial hydrogels are best observed. In **fig. 4.25** the homogeneously cross-linked sample 1030 is compared with the hydrogel B1110 with additional  $D_{\text{res}}$  constants, obtained by the fit, is seen. The homogeneous gel, in contrast, offers two very similar constants. The values can be seen in the lower part of the same figure. This is in good agreement with the structure of the samples; the difference is very clear being the highest that have been recorded in this work. The results are far clearer than the corresponding differences found in the determination of transverse relaxation behaviour. Further, in the lower part of fig. 4.25 the commercial sample Hysorb and a self-synthesized gel that is closest to the commercial gels are shown.

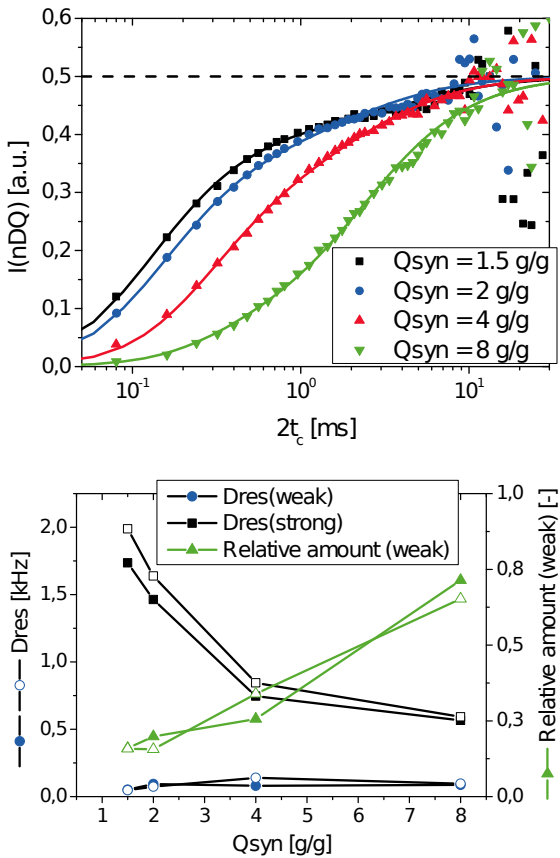


**Figure 4.23.:** Results of double quantum experiments of pAAc gel samples with different  $Q_{\text{syn}}$  values and DC = 1 mol-%. On top, renormalised DQ build-up curves with the corresponding bimodal fits (lines) are shown. The dashed line give the theoretical upper limit (0.5) for  $I_{nDQ}$ . In the lower part, the obtained fit parameters are displayed as a function of  $Q_{\text{syn}}$ . Closed symbols denote the normal gel samples while the open ones the sol-extracted counterparts.

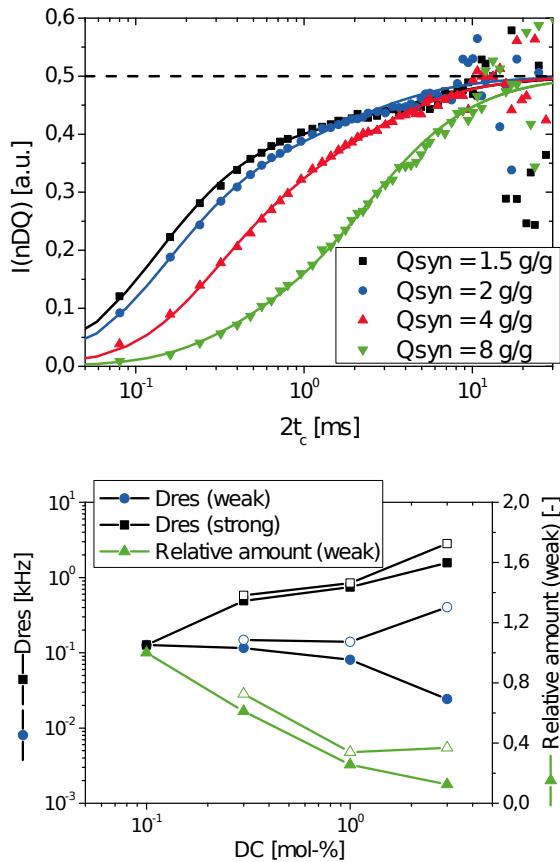


**Figure 4.24.: Results of double quantum experiments for pAAc hydrogel samples of varying DC values and  $Q_{\text{syn}} = 4 \text{ g/g}$ . On top, renormalised DQ build-up curves with the corresponding bimodal fits (lines) are shown. The dashed line give the theoretical upper limit (0.5) for  $I_{\text{nDQ}}$ . In the lower part, the obtained fit parameters are displayed as a function of DC. Closed symbols denote the normal gel samples while the open ones the sol-extracted counterparts.**

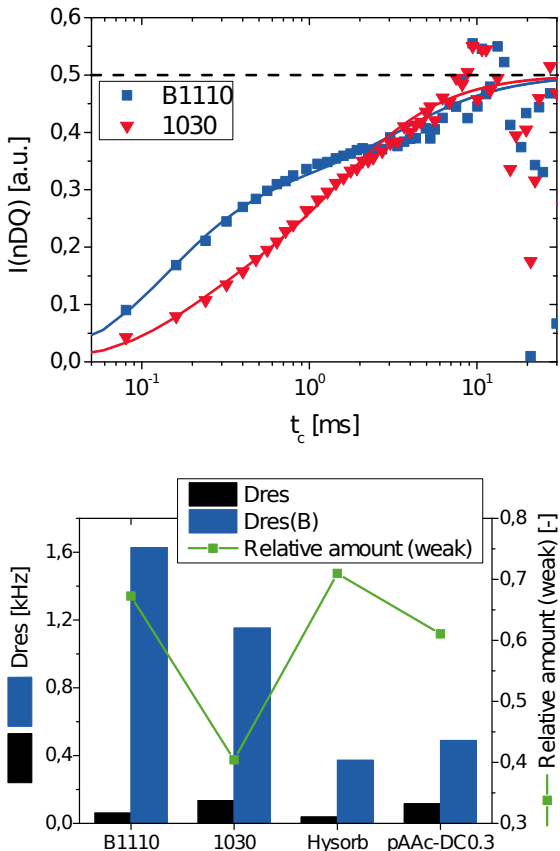


**Figure 4.25.:** Results of double quantum experiments of commercial samples are shown. On top, renormalised DQ build-up curves with the corresponding bimodal fits (lines) are given. The dashed line give the theoretical upper limit (0,5) for  $I_{nDQ}$ . Below, the obtained fit parameters are added. Closed symbols denote the normal gel samples while the open ones reflect the sol-extracted counterparts.

## Conclusion

The heterogeneity in hydrogels can be recorded and quantified by the presented methods. The topological heterogeneity in terms of the pore size distribution (PSD) can be assessed directly by the solute exclusion technique. The heterogeneity of dynamic processes is the domain of the NMR relaxometry which is also connected to the length of the meshes. Both allow an insight in the broad distribution of polymeric structures in hydrogels and the variation of this structures with the chemical parameters during the synthesis, especially the degree of cross-linking (DC).

The technique of solute exclusion has, to the best of the authors knowledge, not been applied to pAAc hydrogels before. This method is able to probe the complete distribution function of probe sizes and given an estimate of the sizes present in the gel. It was found, that the uptake was considerably lower for probes with a higher hydrodynamic radius. Also the rejection was stronger when a higher cross-linked gel was used which have smaller pores in the equilibrium swelling state. These are only first results, but the direction is promising.

Investigations by HF-NMR methods were found to be difficult and did not yield substantial information. The spectral resolution of the method is hampered by the nature of the hydrogel samples. These problems could not be recovered. The application of  $^1\text{H}$  two-dimensional NMR methods failed due to the fast spin-spin relaxation of the samples. The investigation of  $^{13}\text{C}$  nuclei was not attempted due to the low sensitivity.

NMR relaxometry allows insight into the local dynamics of hydrogel networks. However, this is only possible on an averaged basis over several particles. The constraints in the network structure are easily identified in  $T_2$  and  $D_{\text{res}}$  constants obtained in this chapter. The slow or even inhibited motions they probe are largely affected by the amount of constraints in the gel samples. In contrast,  $T_1$  measurements did not show distinct differences of the samples, indicating that motions at  $\omega_L$  are not much affected by changes

in the gel structure. The changes in the synthesis parameters DC and  $Q_{\text{syn}}$  reflect as expected: An increase in cross-link density reduces mobility and therefore shortens  $T_2$  and increases the residual dipolar coupling (RDC) as detected by DQ experiments. In the same way, a decrease in the water content of the synthesis mixture leads to a denser packed network and similar NMR results. It becomes evident, that the gels incorporate domains with large differences in dynamics. The  $T_2$  relaxation behaviour spans several orders of magnitude in time and very mobile components are found even at the highest DC samples investigated. The strong RDC coupling constant is increasing with increasing DC. The beta parameter used in the KWW-fitting function of transverse relaxation data is found to be in the order of 0.5 in all cases. This indicates an inhomogeneous dynamic behaviour. The relaxation time distributions from Laplace inversion clearly show a broad distribution of relaxation times as well. The gel part is affected on almost the complete scale of mobilities while the sol part is similar to the gel part, only some rigid parts are missing. This means at the same time, that the sol content cannot directly be estimated from the raw sample by any sort of multi-component fit. Commercial samples can be evaluated nicely, where DQ experiments give the best contrast between surface cross-linked and normal gels. The dynamic heterogeneity found in the gels is likely to be connected with a topological heterogeneity but the relation between the two is not easily found. With the gel samples characterised in all important macroscopic and microscopic features they can now be employed in the desalination process.



## **5. Construction of a test setup for the desalination process**

Desalination by the use of hydrogels is possible [Höpfner10]. The process described in the introduction (chapter 1) can be used to reduce the salt content in part of a sodium chloride solution by using mechanical force. The three necessary steps are: mixing the polymer with the brine to from the gel, removal of the supernatant solution phase, and forcing the water from the gel by squeezing it. The last step needs energy and a specially constructed setup to separate gel and water under pressure. This setup was first realised in the authors diploma thesis in a simple setup and the proof of principle for the desalination process was established [Höpfner09]. However, this setup had some disadvantages, which are discussed here and resolved in a new design of the setup. Further, the design aspects and construction of the setup are discussed. It is equipped with several sensors which produce raw data, that has to be converted to quantities of interest and analysed by suitable techniques. At last, the setup must be benchmarked to assert the capabilities and the accuracy of the setup. Any data is only valuable when its error is known.

### **5.1. Design and construction of the test setup**

#### **Analysis of first setup**

A first working model for the squeezing step was build during the authors diploma project [Höpfner09]. It consists of an inset, **fig. 5.1**, that can be placed in a hydraulic press which is used to generate the force. In the middle of the setup, the polymer is placed in a water tight sample chamber.

The chamber is confined from above with a piston and below with a sieve and its holder. The only way water can escape to the drainage is through the sieve and the bores in the holder below. Polymer beads are held back by the sieve and remain in the chamber. Released water or eluate is collected in fractions outside the setup. The pressure was adjusted by a reading on the press hydraulics and the volume of the eluate was obtained by weighting the fractions of the eluate. The salt concentration was acquired by the conductivity of the individual fractions. A detailed account of the construction and operation of this setup has been published [Höpfner10].

Despite this setup being fully functional, several points were unsatisfactory in terms of data acquisition and handling, as well as sample size and the drainage construction. These points are summarised in the following:

1. The produced eluate volume and flux are measured by weighing the individual fractions. They can only be measured once for each fraction, being the average over the whole time it took to collect it. This gives a low resolution in time and the overall volume is measured by summing up all fractions, adding up their errors.
2. The concentration can also only be measured once for each fraction giving sparse data, especially in late stage of experiments where the flux is low. Yet, here the concentration changes rapidly.
3. This setup had a duty volume of maximal 92 mL, which, at a typical discharge of 50 % of water in the system, produced only 15 fractions (of 3 mL size). Therefore, only 15 pts of data could be acquired for concentration and volume data, giving precarious resolution in the interesting late stages of the experiments.

4. The pressure can only be read manually off an analogue gauge in the hydraulics of the press with an accuracy of around  $\pm 6$  bar. This limits the number of points that can be recorded. The pressure in the hydraulics is not necessarily the same as the one inside the chamber, as a drop should be observed at the seals and interfaces.

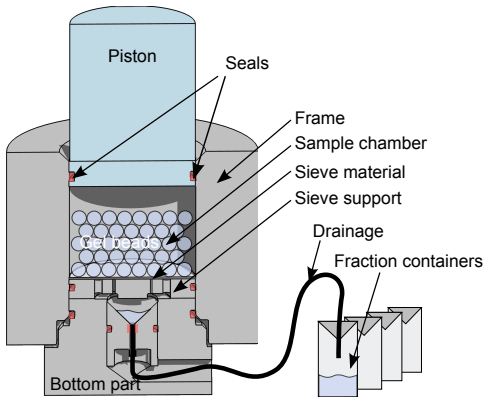


**Figure 5.1.:** Schematic vertical section and photo of the parts of the first press setup for the desalination experiments. The gel is placed in the chamber and squeezed from the top. The water is discharged through the sieve and drainage at the bottom. Fractions are collected while the polymer remains in the chamber.

5. All data is sampled manually and can therefore not be recorded instantaneous. This adds a considerable error to the time coordinate used to align the different types of data.
6. The diameter of the sieve is 50 mm, with only one drainage at the bottom. This means, all eluate has to escape through this outlet which has a sample height of up to 4.7 cm above it. This is quite high and facilitates non-equilibrium effects in the experiment.
7. The drainage is connected over a simple plug connection, that was found to be leaking at times. Also the dead volume in the holder was left to be optimised.

### Desired changes and new design

A remodelling of the setup was sought to improve the previously identified weaknesses [Höpfner11, Höpfner13]. All major conceptual changes are summarised in **tab. 5.1**. The overall concept of the setup was, however, kept the same with the gel compressed in a chamber by the hydraulic press (see **fig. 5.2**). The main change to the setup was an increase of the inner volume of the setup to about 0.5 L by increasing the inner diameter to 12 cm.<sup>1</sup> Thereby, more than 100 fractions can now be sampled in one experiment giving a much improved resolution. A drainage is now installed at the top and bottom and can be evaluated in a combination or separated. This yields, together with the increased diameter, a higher sieve area of two times 113 cm<sup>2</sup>. At full loading, the sample height over one sieve is half as high than in the old setup or when loaded with the old setup's capacity is only 1/12.

For the data acquisition several sensors were installed to automate the process. The data channels distance, pressure, and concentration are measured

---

<sup>1</sup>The height could not be changed, as the clearance of the hydraulic press used was already covered by the old setup.

by sensors. The measurements are remotely time triggered and the data is directly recorded at a computer for later evaluation. With a trigger all three sensor values are aligned over time with respect to each other. The point density can easily chosen to be high (e.g. 1 Hz) for all three channels. The pressure in the sample compartment is measured by an axial flat-top sensor in the range up to 100 bar, giving the real pressure in the sample without loss at the interfaces. The volume flux is measured indirectly by the distance of the two sieve units. The sensor is mounted coaxial to the pressure axis but shifted laterally. The concentration and temperature are measured continuously by the conductivity of the eluate in a flow cell or in fractions. The exact acquisition and treatment of the raw data is discussed in the next section. All tubings and fittings are high pressure chromatography equipment. These parts are easily obtained, hold pressures up to 10 bar, and offer a wide variety of setup combinations.

The new setup consists of nine parts, all made from stainless steel (ANSI 304). The parts and their assembly is illustrated in fig. 5.2. For a detailed description and technical drawings of the parts the reader is referred to appendix A.4. The setup is assembled in the way, that the sample chamber for the gel is given by the round frame element and the two sieve units above and below it. Both units can be moved trough the whole frame for assembly or disassembly. The lower sieve unit is resting, during an experiment, on the base element while the upper one is moved by the piston to compress the gel. The piston is held in place on the upper unit by a recess. The base and the piston are connecting the setup to the hydraulic press surrounding it. The pressure sensor is screwed into the frame in an axial bore and is sealed with a PTFE ring. The distance sensor is mounted on the side of the frame and the piston movement is transferred to it by a cantilever, which is fixed on the piston with a nut. Both, the piston and the base, have bores through which the drainage can enter the setup; it is connected by screw fittings to the sieve units. The flow cell is placed outside the setup.

## 5. Construction of a test setup for the desalination process

---

**Table 5.1.:** Comparison of the features of the old and new press setup.

Feature	Old setup	New setup
duty volume	92 mL	550 mL
drainage	bottom only	top and bottom
sieve area	20 cm <sup>2</sup>	2 × 113 cm <sup>2</sup>
data acquisition	manual only	completely automated and remotely triggered
volume flux by	mass of fractions	continuous by sample height (and fractions)
pressure sensor	external (on press ± 6 bar)	internal (sensor ± 0.01 bar)
salt content	fractions (3 mL)	flow cell (0.1 mL) or fractions
pressure profile fittings	undefined plug connection	controlled high pressure chromatography fittings

The sieve units are composed of three parts: sieve support, sieve material, and sieve holder. At the bottom, the support has a grooved structure to allow the eluate to pass to the middle where the drainage is mounted on the outside. The sieve materials are flat sheets pressed on the support by the holder — a large nut that is screwed on. Axially, a groove is left between the two, which is filled with an O-ring, that is compressed when screwing on the holder to seal the sample compartment. The thread has to be covered in PTFE-ribbon to keep it sealed.

The sieve material can be chosen from different materials to achieve a good mechanical strength and filter performance. By direct experimentation a three layer structure was found to give the best results. The top layer is a cellulose filter paper (3 – 5 µm pores) for separation of liquid and polymer. It is supported by two layers of wire mesh of 25 µm (middle) and 100 µm mesh size (bottom). For more information of the used materials see appendix A.4. After discussing the parts and operational capabilities of the new setup, the data treatment and analysis are given in detail.

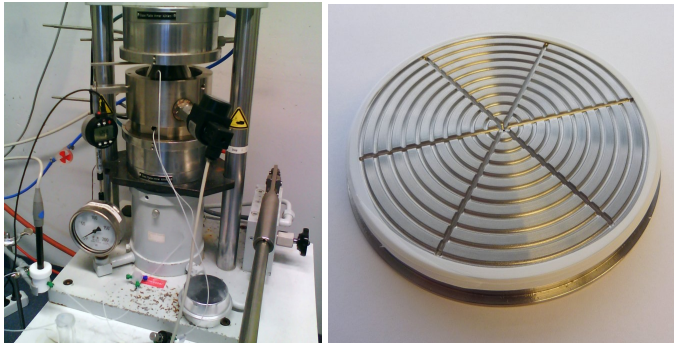
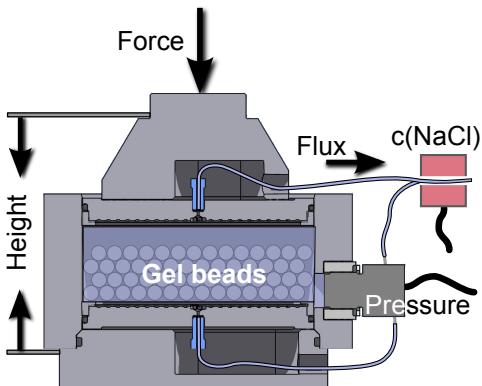


**Figure 5.2.:** Schematic vertical section and photos of the new test setup to separate gel from water in a desalination experiment. The sensors for pressure, distance, and concentration and the general modus operandi are shown in the top part. In the lower left, the complete setup is shown in operation and, on the right, the filter holder used to collect the eluate is depicted.

## 5.2. Experimental procedure and data analysis

A new, unique setup requires a new way to look at the obtained data. In this press inset raw data is generated by three sensors during an experiment. The standard procedure for such an experiment is described here. The raw data has to be processed and transformed to quantities of interest for each channel and the separate channels have to be correlated to obtain a complete picture of the underlying processes. This treatment gives a measure of what can be achieved with the present setup.

### 5.2.1. Experimental procedure

The desalination experiments in the press setup are carried out by a standard experimental procedure to test the influence of the gel structure or process parameters. Any alteration is mentioned in the respective evaluation. The working material for each experiment is dried, ground polymer with a dry bead size of  $350 - 650 \mu\text{m}$ . It is mixed with a model salt solution (brine with e.g.  $c(\text{NaCl}) = 10 \text{ g/L}$ ) by a ratio  $Q$  as defined by (5.1). It is usually beneficial to write  $Q$  with respect to the swelling capacity of the gel  $Q_{\text{eq}}$  as a relative swelling  $Q_{\text{rel}}$ . Typically, a value of  $Q_{\text{rel}} = 2$  is used.<sup>2</sup> The mixture is stirred for a time  $t_Q$  at RT to obtain a gel. This time is usually long enough for complete equilibration of the sample e.g. 12 h as was discussed in section 3.2. After the mixing, in some experiments, part of the supernatant phase, with the volume  $V_S$ , is taken directly from the sample to measure the conductivity.

---

<sup>2</sup>This corresponds to two times the maximum capacity of the gel, meaning half the brine is in the polymer and half is left as supernatant phase. See section 3.2 for the determination of  $Q_{\text{eq}}$ .

$$Q = \frac{m(\text{brine})}{m(\text{polymer})} \quad (5.1)$$

$$Q_{\text{rel}} = \frac{Q}{Q_{\text{eq}}} \quad (5.2)$$

Before the sample is filled into the press, the distance sensor offset is chosen as such at  $d = 0$  mm the two sieve units are in contact. Then, the pressure measurement is started to acquire the voltage baseline signal  $U_0$  with zero pressure. Next, the sample is filled into the chamber, the press is closed with upper sieve unit and the distance measurement started. The upper unit is lowered slowly by the piston to remove trapped air in the setup. The distance  $d_0$  is noted, when the first solution is discharged from the setup. Then, if the flow cell is used, the acquisition of the conductivity (and the temperature) is started. In any case, the eluate is collected in fractions and when switching to the next one, the distance data point  $d_i$  is taken for later alignment.

The pressure is controlled by lowering the piston. First, only 0.5 bar are applied to the sample to remove the supernatant solution until the flux is decreasing considerably (within about 20 min). Next, the desired pressure profile is started by raising the pressure in 1 bar steps as measured via the internal pressure transducer. The time between the pressure steps is given by the desired pressure profile (e.g. every 5 min for 12 bar/h). The experiment is carried out by controlling the pressure accordingly and collecting fractions and data until the endpoint is reached. This can either be reached by the maximal pressure (typically 50 bar), complete lowering of the upper sieve unit ( $d = 0$  mm), or failure of the setup. After the experiment, the obtained fractions are weighed ( $m_i$ ) and their conductivity  $\sigma_i$  and temperature  $T_i$  are measured if no flow cell was used.

The raw data is acquired on three channels with a time trigger. These channels are the distance of the sieve units  $d(t)$ , the voltage of the pressure

sensor  $U(t)$ , and the conductivity of the eluate  $\sigma(t)$  (together with the temperature  $T(t)$ ). The time  $t$  is read from the system clock of the computer to trigger the acquisition of data points after the interval  $t_{\text{step}}$ . The time coordinate of a data point is given by the point number and the interval by  $t_n = n \cdot t_{\text{step}}$ . The acquisition of the channels is started at different times so an alignment in time is necessary. This is discussed further on p. 146.

### 5.2.2. Volume and flux data

The distance of the sieve units  $d(t)$  is measured in mm by the program MarCom (version 2.0, Mahr GmbH, Göttingen, Germany). Usually, the smallest possible interval  $t_{\text{step}} = 1$  s is used. From the distance data, the cumulated eluate volume  $V_e$  is computed by eq. (5.3);<sup>3</sup> an example for the data is shown in **fig. 5.3**. The relation makes use of the starting point of the eluate discharge  $d_0$  and the press cross-section  $A = 11309.7$  mm<sup>2</sup>.

$$V_e(t) = \sum_n V_n(t) = \frac{(d_0 - d(t)) \cdot A}{1000} + V_{\text{Offset}} \quad [V_e] = \text{mL} \quad (5.3)$$

The volume discharge has to be corrected for two effects, however. First, an offset is added, that is equal to the inner volume of the drainage and the earlier removed solution, thus  $V_{\text{Offset}} = V_{\text{Dead}} + V_S$ . The drainage is filled before any solvent leaves the setup. The offset needs to be known to compare the volume produced in different experiments where it might vary. The second effect is the influence of air bubbles trapped in setup at the beginning of the experiment. When the pressure is raised, these bubbles are eventually released with the eluate in the range up to 10 bar. This causes a decrease in distance but no volume discharge. Hence, the recorded discharge from distance data is too large. The true value can be estimated by the mass sum of

---

<sup>3</sup>This is only true in the case that the sample and sieve material are incompressible in the investigated pressure range and the piston is lowered in parallel.

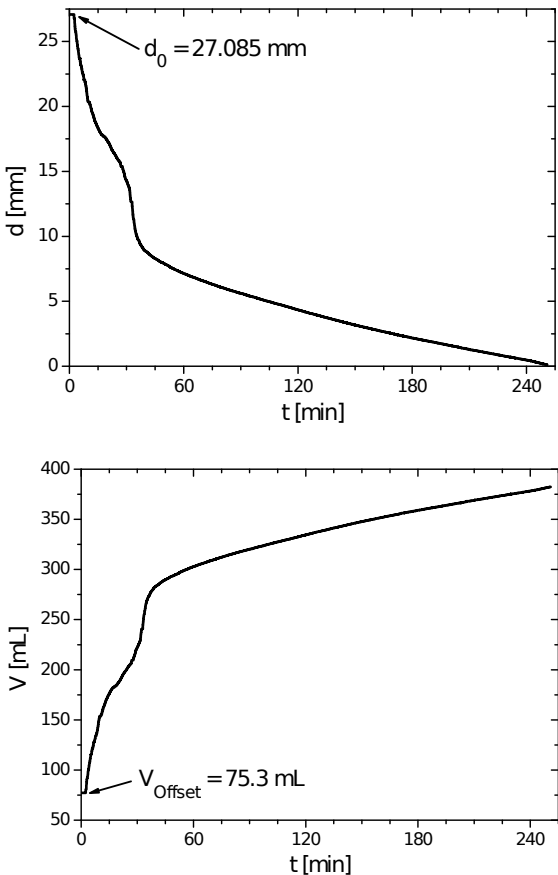


**Figure 5.3.:** Typical distance data obtained in a desalination experiment is shown. On top, raw data recorded with  $1 \mu\text{m}$  accuracy and a  $t_{\text{step}} = 1 \text{ s}$  time interval is shown and, below, the cumulative volume as calculated by (5.3) is shown. The volume offset is needed to compare the volume data from different experiments.

the fractions as given by (5.4) with  $V_i$  as their volume and the eluate density  $\rho_E$ . The difference in the two eluate curves is shown in **fig. 5.4**.

$$V_i(t) = \sum_i^n \frac{m_i}{\rho_E} \quad [V_i] = \text{mL} \quad (5.4)$$

Yet, the fraction data has a much reduced point density compared to the distance data. Here, the following approach for correction is proposed: the high time resolution of the volume by distance measurement and the true volume values by the mass sum are combined. The latter dataset has about a 1000 times less points, which are unequally spaced. The time coordinates of the fraction dataset are used to extract the corresponding volume values from the distance data, giving a new data set with the same number of points. The resulting dataset and the fraction dataset are both used for a smooth polynomial interpolation.<sup>4</sup>. The resulting interpolates  $V_{e,\text{smooth}}(t)$  and  $V_{i,\text{smooth}}(t)$  are computed to have the point density (one per s) of the distance data. The difference of the two is calculated and subtracted from original volume dataset of the distance measurement, as shown by eq. (5.5). The obtained corrected volume is the green line in fig. 5.4. The corrected dataset has on a small time scale the characteristic features of the distance data, but is, on a larger scale, normalised to the true volume values from the fractions.

$$V(t) = V_e(t) - (V_{e,\text{smooth}}(t) - V_{i,\text{smooth}}(t)) \quad (5.5)$$

From the change of the cumulated volume over time the flux can be obtained. In general is this done by the derivative to time or, in the case of discrete values, by the local slope between two points (5.6). However, the values of  $d(t)$  are measured with a certain noise in the experiment and accordingly are not monotonically decreasing. An example for these fluctuations is given in **fig. 5.5** on top. A direct derivative is therefore ill-advised.

---

<sup>4</sup>A cubic polynomial interpolation with the Hermite algorithm as implemented in the SLATEC library is used [Burden01, SLATEC94].

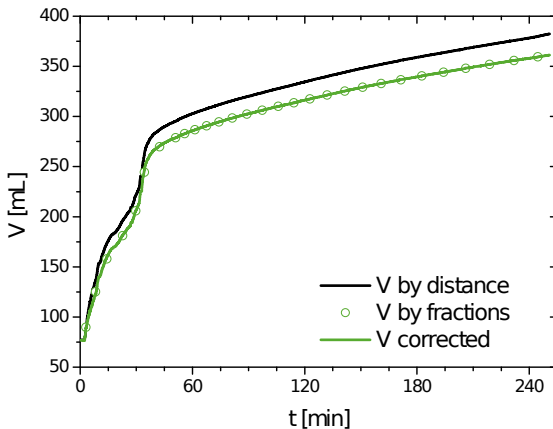


**Figure 5.4.:** Difference of the volume discharged from the press as obtained by the methods of distance (black line) and fraction mass measurement (dots). The correction of the volume data by means of the fraction information gives the green line by a procedure described in the text.

As a solution the distance data is smoothed to obtain a locally monotonic dataset. The averaging is achieved by a simple moving average (SMA) algorithm with a 13 pt window width (fig. [fig. 5.5](#), bottom) [Skoog07]. However, for inspection with the eye a stronger smoothing over 61 s or 301 s was found beneficial.

$$\dot{V}_n(t) = \frac{dV_n(t)}{dt} \approx \frac{\Delta d(t) \cdot A \cdot 3600}{1000 \cdot t_{\text{step}}} = \frac{(d(t_n) - d(t_{n-1})) \cdot A \cdot 3.6}{t_{\text{step}}} \quad [\dot{V}] = \text{mL/h} \quad (5.6)$$

The obtained flux curves contain a lot of information; they can be reduced to comparable quantities when an empirical fit function is used. The combination of an exponential with a linear function (5.7) was found to be a good description for linearly increasing pressure profiles (see [fig. 5.5](#), bottom).<sup>5</sup>

<sup>5</sup>The Marquardt-Levenberg algorithm as implemented in the *SLATEC* library is used to obtain the fit parameters [SLATEC94]. The fit has converged when  $\epsilon < 10^{-6}$  is met. The data range for the fit starts with a dynamically determined value and ends at the end of the dataset. The starting point is the last point with an flux of higher than 300 mL/h, after SMA

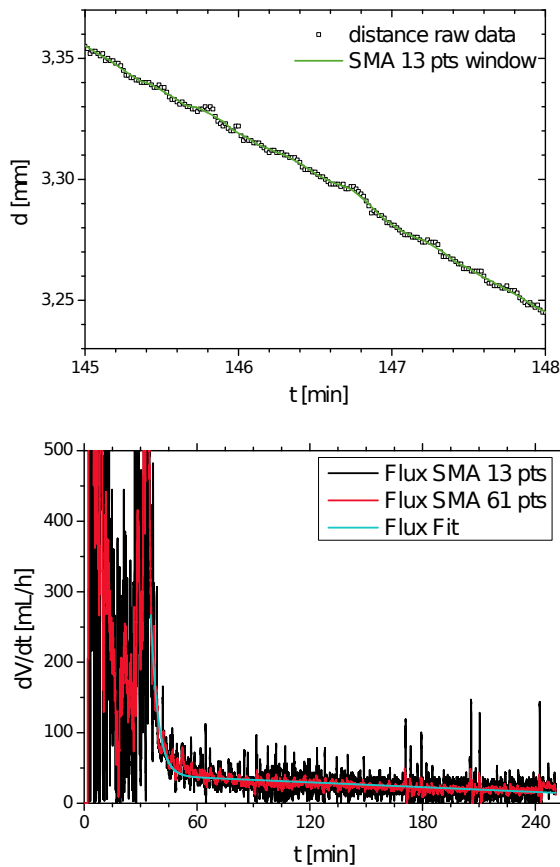


**Figure 5.5.:** Example for the calculation of volume flux data in a desalination experiment. On top, part of the raw distance data from fig. 5.3 is shown in magnification (dots) with a smoothing over a 13 s window by SMA (line). Below, the volume flux is shown. It was calculated from the local slope between the points after SMA with window sizes of 13 and 61 s as well as the fit according to eq. 5.7.

$$\dot{V}(t) = A \cdot \exp\left(-\frac{t - T_0}{T}\right) + B \cdot t + C \quad (5.7)$$

The degree of swelling of the gel at each time can be calculated from the volume data (5.8), if the initial solution in the system  $m(\text{brine})$  and the polymer mass  $m(\text{polymer})$  are known. Here, it is easier to use the relative degree of swelling normalised to the capacity of the gel  $Q_{\text{eq}}$ .<sup>6</sup>

$$Q_{\text{rel}}(t) = \frac{Q(t)}{Q_{\text{eq}}} = \frac{m(\text{brine}) - V(t) \cdot \rho_E}{m(\text{polymer})} \cdot \frac{1}{Q_{\text{eq}}} \quad [Q_{\text{rel}}] = 1 \quad (5.8)$$

### 5.2.3. Pressure data

The second data channel is the voltage  $U(t)$  measured in V, that is obtained from the pressure sensor by a self-made circuit that is explained in appendix A.4. The voltage is linear to the applied pressure and is sampled by an ADC (USB-9215, National Instruments, Austin, USA) and collected on a computer by a self-written LabVIEW-program (version 2010, National Instruments). The sampling rate is typically 1 000 Hz and the measured points are decimated by online oversampling (OS) over 250 pts to 4 Hz [Skoog07, Dusschoten01]. A typical recorded signal is shown in **fig. 5.6**. It is baseline corrected by the initial signal without pressure ( $U_0$ , see sec. 5.2.1) and converted to excess pressure  $p(t)$  by (5.9). The respective proportionality factor  $f$  is 0.0795 V/bar and depends on the circuit used (see appendix A.4).

$$p(t) = \frac{(U(t) - U_0)}{f} \quad [p] = \text{bar} \quad (5.9)$$

---

with a window of 301 s. The  $T_0$  parameter is used only implicitly in the fit by shifting the time axis.

<sup>6</sup>The density of the salt solution is changing with the concentration during the experiment, but this effect is so small it was neglected. In a typical experiment  $c$  is in the range 7 – 13 g/L of NaCl which corresponds to a density change of 0.004 g/cm<sup>3</sup> [Wolf86]. Therefore, the density value for  $c = 10$  g/L is used.

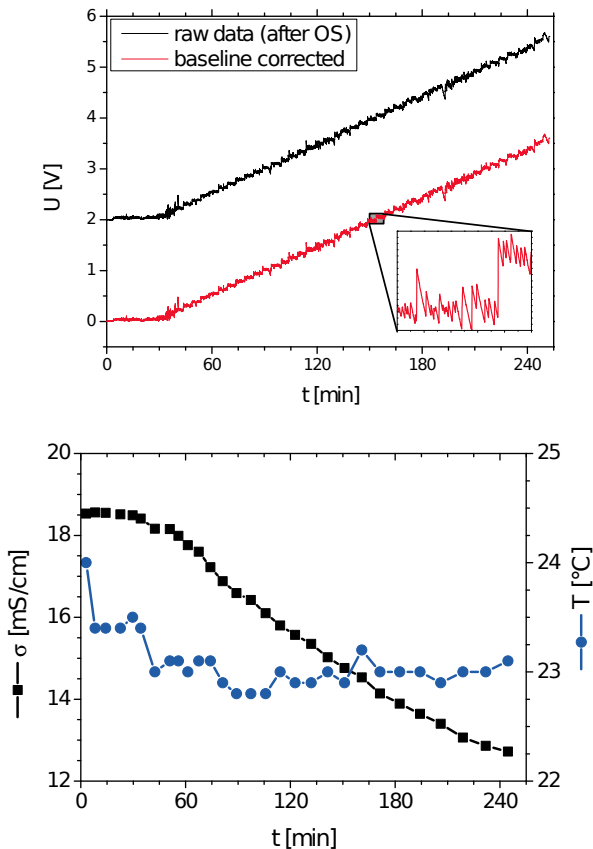


**Figure 5.6.:** Typical data obtained in a desalination experiment: on top, the voltage signal from the pressure sensor is shown before and after baseline correction. Below, the measured conductivity and temperature of fractions are shown. Both are collected by the conductivity meter; the temperature reflects the situation in fraction container not in the press setup.

### 5.2.4. Brine concentration data

The data acquired on the third channel are the conductivity  $\sigma(t)$  in mS/cm and the temperature of the eluate  $T(t)$  in °C. They are measured by a conductivity meter (SevenMulti, Mettler Toledo, Gießen, Germany) and recorded on a computer with the program LabXpress (version 2.1, Mettler Toledo). The acquisition is either done online, with the minimal step width of 3 s, or offline once for each fraction obtained. A typical dataset is shown in the lower part of **fig. 5.6**. The measured temperature does not reflect the situation in the press but the temperature at the time of the conductivity measurement to correct it for thermal effects. The corrected conductance at the reference temperature  $T_{\text{ref}} = 20$  °C is computed by a linear relationship (5.10). The coefficient  $\alpha$  is in the order of 2 %/°C and has to be chosen appropriately for each concentration and temperature range. The values used in this work are compiled in appendix A.4.

$$\sigma(T_{\text{ref}}) = \sigma(T) \cdot \left(1 + \frac{\alpha}{100\%}(T - T_{\text{ref}})\right) \quad [\sigma] = \text{mS/cm} \quad (5.10)$$

From the corrected conductance the equivalent concentration of salt in the solution can be computed, e.g. in g/L. This relationship can be given by Debye-Hückel-Onsager theory, but this is only provides high accuracy for concentrations up to 0.01 mol/L which corresponds to 0.6 g/L NaCl [Hamann07, p. 45]. Therefore, literature data is used as a model and a polynomial of the third degree (5.11) is adjusted to the data to give the desired relation [Wolf86, Höpfner10]. The coefficients  $A$ ,  $B$ ,  $C$ , and  $D$  defined in (5.11) need to be obtained individually for each concentration range and are compiled in appendix A.4.

$$c(\text{NaCl}) = A + B\sigma(T_{\text{ref}}) + C\sigma(T_{\text{ref}})^2 + D\sigma(T_{\text{ref}})^3 \quad [c(\text{NaCl})] = \text{g/L} \quad (5.11)$$

### **5.2.5. Combination of the channels**

The data from the three channels was acquired with different time steps and starting values. They need to be combined to one dataset on a common time axis. The reference time  $t$  is chosen to be zero, when the pressure profile starts (first increase in  $p$  beyond 1 bar). This is achieved by simply shifting the data in time for pressure and distance, as both are acquired directly in contact with the sample. The concentration, however, is measured outside the setup and does not reflect changes within immediately. Rather, an offset is found that is marked by a volume shift. The shift volume corresponds to the way it takes the eluate from the filter to the point where the concentration is measured. It is a constant of the setup geometry, typically  $V_{\text{shift}} = 6.5 \text{ mL}$ . Each concentration corresponds to data, that was measured by  $V_{\text{shift}}$  “earlier”. The shift is thus done by using the time of the concentration data to find a corresponding volume data in the distance channel and subtracting  $V_{\text{shift}}$  from the found value. The result is compared again with the volume data and nearest value gives the true time data of the concentration data point.

When data from different channels is considered together, the differences in point density have to be taken into account. The lowest density is always used in this case (e.g. 30 pts for concentration channel) and the data from the channel with more information is reduced by adjacent averaging.

## **5.3. Error estimation and repeatability**

All measured data is only relevant with an estimation of its error. Here, data is obtained on three separate channels, each with its own error. These three channels and the time data are discussed separately. The errors are combined in the evaluation of a complete measurement in a complex manner. The propagation of errors in this complex process will not be retraced but instead several measurements under the same conditions are performed and compared to estimate the reproducibility.

## Errors of the single channels

The time is obtained from the system clock of the computer which is relatively precise. Only at the time of the program launch a delay can occur, which would mean a systematic error in the starting time. It is assumed to be 3 s at most. The trigger for the data acquisition is used once inside  $t_{\text{step}}$  making the uncertainty at most this interval for each point.

The distance is measured by a dial gauge with an accuracy of  $\pm 1 \mu\text{m}$ .<sup>7</sup> In this measurement, no drift or noise was found. However, a deviation between recorded and true distance (linearity) of up to 6  $\mu\text{m}$  over the whole measurement range of 50 mm was given in the manufacturer's calibration certificate. This error is distributed over the entire measurement span and is as such not to be discovered between adjacent points. Additionally, an error is introduced if the dial gauge is not collinear to the piston. The measurement error in the cumulated volume  $V$  is linearly related to the distance error. An uncertainty of 1  $\mu\text{m}$  in  $d$  corresponds to an error of 11.3  $\mu\text{L}$  in volume or to 0.5 % of the full press capacity (0.5 L). A much stronger effect is given by the air bubbles in the setup, that can cause a systematic error of 15 to 40 mL. This error is corrected in the evaluation by the volume of the collected fractions, as described in the previous section. The uncertainty of mass of each fraction was found to be 0.1 g which would amount at maximum to 4 mL or less than 1 % of the full press capacity for typically 40 fractions. The values of  $Q(t)$  and  $Q_{\text{rel}}$  are directly related to  $V$  and, in the latter case, to  $Q_{\text{eq}}$ . The error of  $Q_{\text{eq}}$  is discussed in section 3.2. The initial masses of polymer and brine are known with a high accuracy of better than 1 %.

The pressure values are calculated from the voltage signal of the corresponding sensor. The conversion of the signal in the ADC is done with a 16 bit resolution in the interval  $-10$  to  $+10$  V which corresponds to a theoretical resolution of  $3.1 \cdot 10^{-4}$  V and, with oversampling over 250 pts,

---

<sup>7</sup>In some early experiments a gauge with only  $\pm 10 \mu\text{m}$  accuracy was used, these cases are indicated where applicable.

this increases to  $1.2 \cdot 10^{-6}$  V. Therefore, when calculating the pressure from the voltage signal the theoretical reading accuracy is  $3.8 \cdot 10^{-5}$  bar. After oversampling no noise could be detected and the drift of the sensor was measured to be below 0.02 bar/h and was therefore not corrected except for the offset. The deviation from linearity is given by the manufacturer as below 0.5 bar for the whole range 0 – 100 bar. A simple test in the interval of 0 – 5 bar supported this claim but no possibility was seen to verify this over the whole range. Furthermore, the pressure cannot be controlled by the hydraulic press with an accuracy of better than  $\pm 0.1$  bar.

The highest error is found for the conductivity measurement. The reading accuracy for  $\sigma$  is 0.01 mS/cm in the interval of 1 – 20 mS/cm and 0.1 for 20 – 200 mS/cm, while it is always 0.1 °C for the temperature  $T$ . Drift and noise are both routinely observed in these quantities, probably as a result of local temperature changes that have a high influence on the conductivity. This effect can be reduced by measuring the fractions in thermal equilibrium. Evaporation is usually not a problem in the time needed for the measurement (below 1 min). The error in  $\sigma$  is dependent on the size of the sample and was found to be about 0.3 % of the measured conductivity for samples above 10 mL and 1.3 % for samples of 3 mL. In the latter case this corresponds to an accuracy of  $\pm 0.2$  mS/cm (0.15 g/L). However, the measurement is also subjected to many systematic errors, arising from the temperature coefficient, the calibration of the electrode, and the fit parameters for the conversion formula making the absolute error possibly larger.

## Reproducibility

The desalination experiment is a complex procedure where the overall error, combined from many points and channels, is difficult to assess. The overall error was not investigated on the basis of the individual errors. As an alternative four experiments were carried out with the same parameters to obtain an estimate on the general reproducibility of a complete experiment.

The experiments are denoted with Test1 to Test4. The main experimental parameters are summarised in **tab. 5.2.** As noted in the previous section, for all experiments the time is set to zero at the point the pressure profile starts to obtain a universal starting point. Test2 was carried only out until 30 bar so no data beyond this point is available.

**Table 5.2.:** Experimental conditions used for assessment of the reproducibility of the desalination results by consecutive runs.

Parameter	Value
polymer	Luquasorb™ B1110
pressure profile	linear, 12 bar/h
sample volume	420 mL
$Q_{\text{rel}}$	2
$c(\text{NaCl})_{\text{Initial}}$	10 g/L
duration	4.2 h (max. 50 bar)

The pressure is the controlled variable in the experiments and is very similar for all runs as can be seen in **fig. 5.7**, top. The increase is, however, a little lower for Test1. The obtained eluent volume, in the same figure on the bottom, is very similar except for Test1 where less eluate was received. The corresponding flux is shown in **fig. 5.8** by the averaged data and the fit functions of equation (5.7) adjusted to the data. The results of Test3 and Test4 are quite similar on the longer time scale and, to a lesser extent, Test2 which is decreasing faster. In the case of Test1 the flux throughout the experiment is much smaller which could be a result of the shallower pressure profile. The salt concentration is given in **fig. 5.9** as a function of time and pressure. The results are quantitatively similar for all runs but with some offset.

Some representative values are taken from the data and are analysed further for a quantitative comparison of the four runs. The main control parameter is the pressure profile given by  $p(t)$ ; a simple line equation is adjusted data and the slopes  $dp/dt$  and their R-values are compared in **tab. 5.3.** The

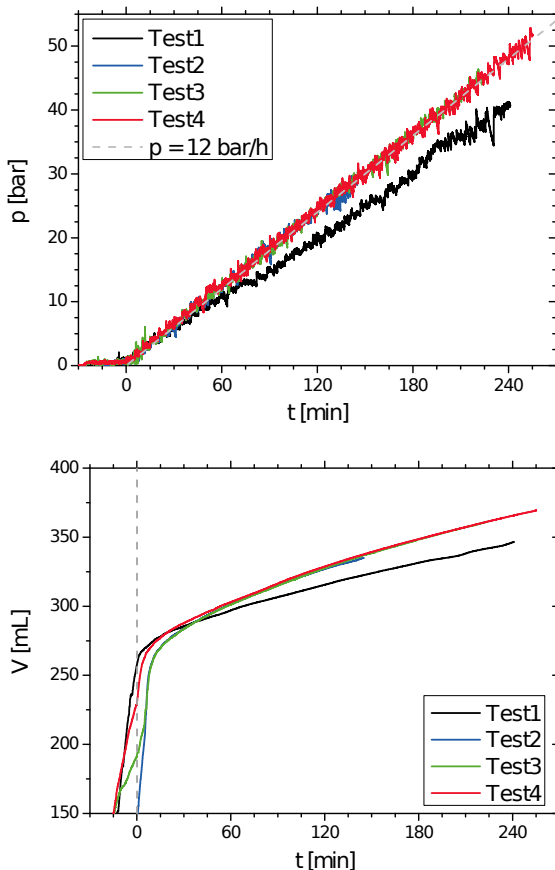


**Figure 5.7.:** Data from reproducibility tests of the desalination experiments (conditions see tab. 5.2): On top, the applied pressure is given. The lines indicate the real pressure while the dashed line gives the ideal profile. In the lower part, the eluate volumes obtained by the squeezing are compared.

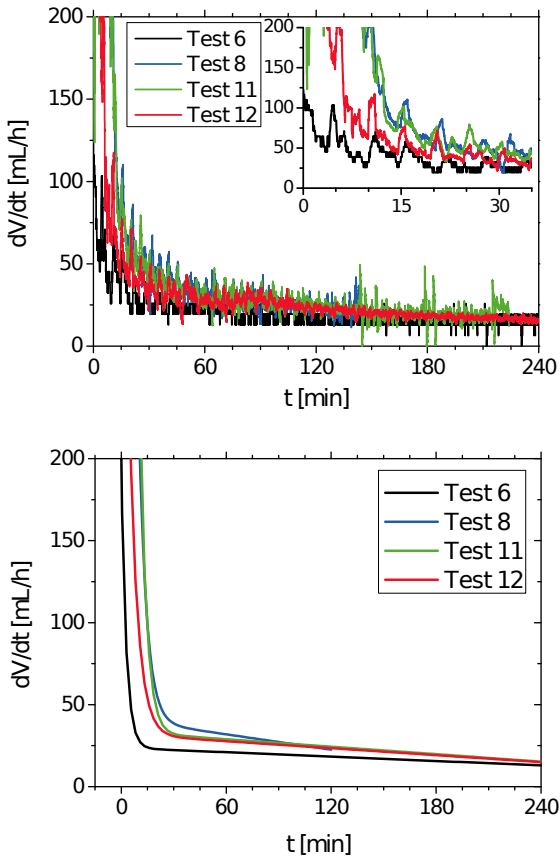


**Figure 5.8.:** Volume flux data from reproducibility tests of the desalination experiments: On top, the smoothed raw data (SMA, 61 pts) is shown with the behaviour at short times magnified in the inset. Below, a fit of a linear exponential function (5.7) to the data is shown for comparison. In the case of Test 1 the data was recorded with a distance accuracy of only 10  $\mu\text{m}$  and a  $t_{\text{step}} = 3$  s (SMA, 21 pts) which leads to a much more discrete result.

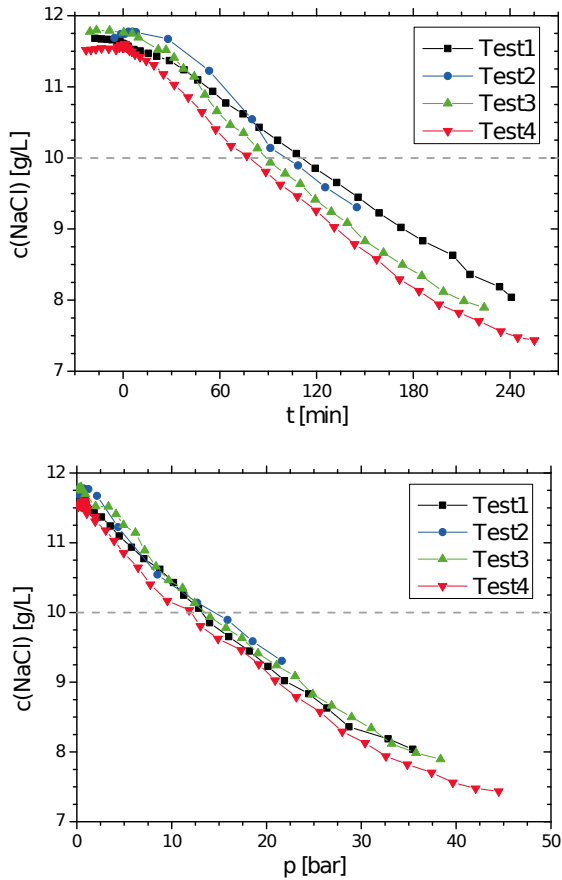


**Figure 5.9.:** Concentration data from reproducibility tests of the desalination experiments: On top, the salt concentration is shown as a function of time and on the bottom of pressure. The dashed line gives the initial concentration of the used brine.

**Table 5.3.:** Parameters describing the pressure data. The maximum pressure reached in each run and the slope with its error obtained by a linear fit are given. The pressure profile has an ideal value of 12 bar/h.

Experiment	$p_{\max}$ [bar]	$dp/dt$ [bar/h]	R-value
Test1	41	9.9	0.9949
Test2	30	11.9	0.9949
Test3	46	12.0	0.9982
Test4	53	11.9	0.9977

desired value of 12 bar/h is well matched for all runs except Test1 where the increase was considerably lower. The eluate volume  $V$  and the salt concentration  $c(NaCl)$  are characterised by their values at 0 (15 in case of  $V$ ), 90 and 210 min, which are shown in **fig. 5.10**. The medium values and the standard deviation are also marked. The standard deviation is small in the beginning of the experiments and increasing for longer times. Especially Test1 is deviating from the results of the others which is probably in part a result of the pressure profile.

The volume flux has to be characterised and compared differently, however. The reason are the large fluctuations at single points that forbid a direct comparison of the values. Instead the adjusted parameter of a fit function (5.7) are compared in **tab. 5.4**. These values describe well the effects already seen in the qualitative plots above. The mean values and their standard deviation show that the differences are considerable, again especially for Test1. The uncertainties can later be used to assess the significance of changes introduced by a variation of the sample type or process parameters.

In addition the concentration change with pressure as given by the slope  $dc/dp$  is evaluated. The value is obtained by a linear fit of the concentration values below the initial concentration. The values are also found in tab. 5.4; they differ to a smaller extent than the flux values and can later be used to investigate the desalination capacity of a material.

**Table 5.4.:** Parameters obtained by a fit of the flux data by the linear exponential function (5.7) and the linear fit of the concentration drop with increasing pressure.

<b>Experiment</b>	<b>Flux fit parameters</b>				<b>dc/dp</b> [ $\times 100$ g / (L bar)]
	A [ml/h]	T [min]	B [h/(mL $\times$ min)]	C [ml/h]	
Test1	176.7	3.23	-0.077	29.2	-8.72
Test2	239.9	3.73	-0.21	46.3	-10.2
Test3	227.5	3.90	-0.11	39.4	-8.82
Test4	208.3	4.41	-0.089	35.1	-8.01
$\emptyset$ Test1–4	$213 \pm 24$	$3.8 \pm 0.4$	$-0.12 \pm 0.05$	$38 \pm 6$	$-8.9 \pm 0.8$

Comparison of all four runs shows qualitatively the same behaviour in all quantities — quantitatively the differences are mostly below 10 %. The first run Test1 shows the highest deviations which might be a result of the slow increase in pressure (only 10 bar/h) in the experiment. In contrast, the runs Test3 and Test4 show very similar results.

## Conclusion

A realisation of the desalination process in a larger scale will probably look somewhat different than the one presented here. This setup was made this way only with the following intentions: make the process well monitorable, use volumes in the scale of a litre, apply up to 100 bar of pressure, and measure all parameters with maximum accuracy and repetition rate. The setup was tailored for this needs and works relatively well in assessing the sample properties. The three data channels yield the pressure in the sample, the eluate volume and flux, and its salt concentration. This gives dynamic information with a good time resolution and low individual errors. The press can be operated well and few experiments fail due to technical

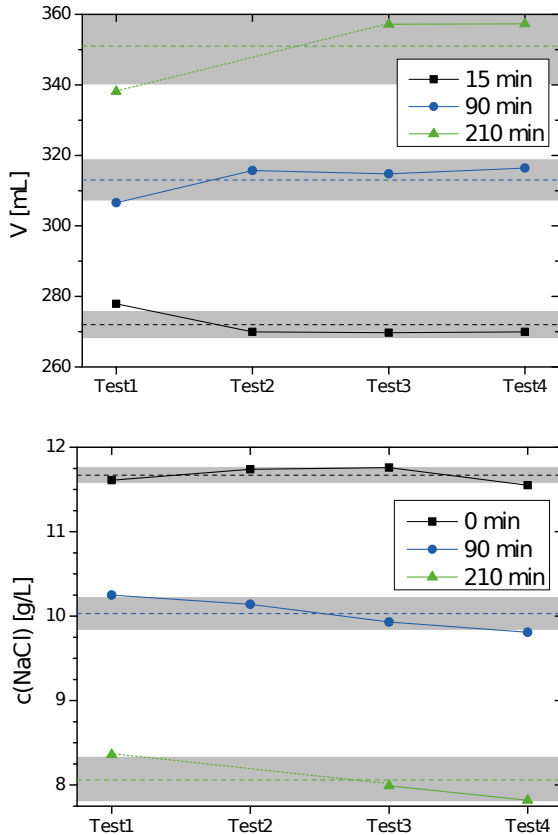


**Figure 5.10.:** Extracted data points from reproducibility tests of the desalination experiments: the corrected eluate volume (top) and the salt concentration (bottom) are sampled at three times. The dashed lines give the mean value and the grey bars the standard deviation at each time.

## 5. Construction of a test setup for the desalination process

---

reasons. The analysis of the raw data is advanced but straight forward due to automation. This is maybe the biggest advance in this setup as the data is automatically generated with many points and can be routinely evaluated. The errors are low enough to obtain characteristic differences between different types of gels which will be discussed next.

## **6. Salt rejection and desalination capacity of hydrogels as a function of the chemical composition**

Tremendous differences in the interaction of hydrogels of different composition with salt solutions were found within this thesis. Some polymeric networks reject salt strongly while others only have a small influence. On the basis of these differences, a preliminary concept of the desalination capacity of a gel shall be defined that uses intuitive parameters: gel has a high desalination capacity when it releases a solution of a low salt concentration at low pressure and with a high flux. Thus, less energy is used for the desalination and a lot of water is regained. Accordingly, one of the main parameters used to optimise the desalination performance is the composition of the hydrogel employed as working material. To open up this field a number of different samples were produced: Networks from acrylic acid are synthesised. They are investigated in terms of the synthetic variables degree of cross-linking (DC), degree of neutralisation (DN), and the reference state of the network during the synthesis ( $Q_{\text{syn}}$ ). These parameters are defined in the appendix A.1. Other monomers are added to the gel to give copolymer networks of various compositions. At last, the use of industrial samples is discussed which also introduce macroscopic structuring of the gel particles. All samples are compared with respect of their desalination capacity and the best gel for the procedure is chosen from a broad range of possible samples.

## 6.1. Influence of the degree of cross-linking, neutralisation, and reference state of poly(acrylic acid) networks

Hydrogels made from poly(acrylic acid) are investigated. The samples were produced by the procedure detailed in appendix A.1. The synthetic parameters were typically set to DC = 1 mol-%, DN to 75 mol-%, and  $Q_{\text{syn}}$  to 4 g/g. Only one of the parameters was changed at a time to keep the number of samples small but get an estimate of the influence of all parameters. Thereby, an independence of the parameters is assumed. The experiments are carried out in accordance with the procedure detailed in section 5.2.1. The main parameters are  $Q_{\text{rel}} = 2$ , a salt solution of 10 g/L (see appendix A.1), and the pressure is increased linearly with  $dp/dt = 12 \text{ bar/h}$  (pressure profile). In the investigation of each synthesis parameter, first, the case of the salt rejection from the gel without pressure is discussed, before the best candidates are subjected to a desalination experiments under pressure.

### Variation of the degree of cross-linking

Four samples with different mesh sizes were investigated. The equilibrium salt rejection, in the case without pressure, is measured by mixing the dry polymer with brine to a ratio  $Q_{\text{rel}}$  (see sec. 5.2.1). The polymer swells and the salt concentration in the supernatant liquid phase is measured via its conductance. This corresponds to the first step of the proposed desalination procedure. The rejection of ions from the gel can be directly measured without the need to squeeze out the gel.

The DC values investigated were 0.1, 0.3, 1.0, and 5.0 mol-% of cross-linking monomer mole fraction.<sup>1</sup> The results are shown in **fig. 6.1** for the different gels. At  $Q_{\text{rel}} = 1$  no supernatant phase would be present and at higher values the amount of supernatant liquid phase is increasing. The ob-

---

<sup>1</sup>The specific samples used were pAAc-DC0.1-DN83-Q4, batch 1, pAAc-DC0.3-DN83-Q4, batch 1, pAAc-DC1-DN75-Q4, batch 3, and pAAc-DC5-DN82-Q4, batch 2. More details on the samples can be found in appendix A.1.

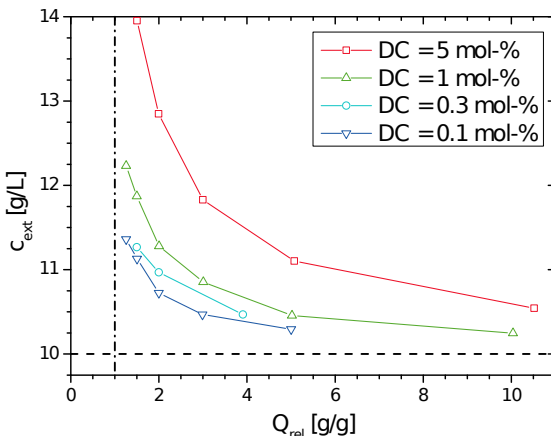


**Figure 6.1.:** Equilibrium salt rejection from a gel in contact with a salt solution phase given for gels with varying degrees of cross-linking (DC). The salt concentration of the supernatant phase is compared to the initial concentration (dashed line) and given as function of the relative volume of the aqueous phase ( $Q_{\text{rel}}$ ).

tained curves are well separated for all samples. The rise in concentration at low  $Q_{\text{rel}}$  is due to the fact that less supernatant solution is available in which the rejected salt is diluted. In first approximation, the rejection effect is the same for all values of  $Q_{\text{rel}}$  but better measurable at low values. Higher  $c_s$  values denote a better salt rejection (up to 40 %) and are better candidates for desalination experiments. Here, the highest DC gel is the most promising candidate.

The desalination experiments with pressure were carried out with a linear pressure increase, as shown in **fig. 6.2**, top. The experiments were conducted until 60 bar, 50 bar, and 34 bar for the samples with 0.1, 1, and 5 mol-% cross-linker, respectively. For the two softer samples the minimum distance was already reached at this pressure values.<sup>2</sup> The obtained

<sup>2</sup>The minimum distance of  $d = 0$  mm is reached, when the upper sieve unit comes in contact with the lower sieve unit while it was moved through the frame while removing eluate. This means, the sample is only left in the gap between the two sieve holders, which can not be pressed out.

## 6. Salt rejection and desalination by hydrogels

---

**Table 6.1.:** List of parameters that describe the desalination performance of gels with different degrees of cross-linking (DC).

DC [mol-%]	T (Time constant) [min]	B (Slope) [h/(mL min)]	C (Offset) [mL/h]	dc/dp [×100 g /(L bar)]
0.1	0.61	-0.35	89.2	-3.71
1.0	7.05	-0.11	47.2	-6.38
5.0	6.64	-0.06	25.0	-9.00

eluate volume is shown in **fig. 6.2**, bottom. For the 0.1 and 1 mol-% samples practically all possible eluate was pressed out ( $V_e \approx 370$  mL), in contrast, much less was recovered for the highest cross-linked sample.

The eluate flux produced by the pressure increase is strongly dependent on DC. In **fig. 6.3**, it is clearly shown that a higher DC lowers the flux considerably. This is expected as a higher DC corresponds to mechanically stronger gels that need a higher pressure to be deformed. However, in the softer gels the flux is decreasing faster. Quantitatively, this can be seen by fitting the volume flux data. The fit parameters are shown in **tab. 6.1**. The offset C is decreasing with DC as is the slope B of the curve.

The resulting salt concentration was measured in fractions and is shown in **fig. 6.4** as function of applied pressure and relative swelling of the gel.<sup>3</sup> In the beginning of the desalination experiment with pressure, the same concentration values are found which were seen in the pressure free case above. As the experiment progresses, the concentration of the eluate is reduced even below the initial concentration. The reduction is stronger for high DC samples than for the low DC samples. The result of DC = 5.0 mol-

---

<sup>3</sup>As was pointed out in the previous chapter, the pressure data was correlated with the concentration data by back extrapolation over the volume offset between the two channels. This is the reason why the last fractions were not collected at the maximum pressure seen in fig. 6.2.

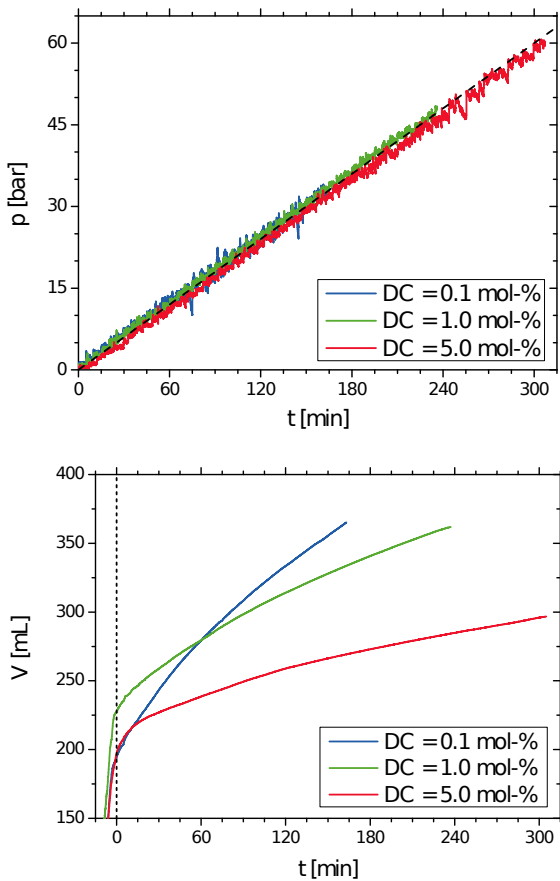


**Figure 6.2.:** Pressure profile (top) and produced eluate volume (bottom) in desalination experiments conducted with samples of varying degree of cross-linking (DC) are shown. The dashed line on top gives the ideal profile and at the bottom the starting point of the experiment.

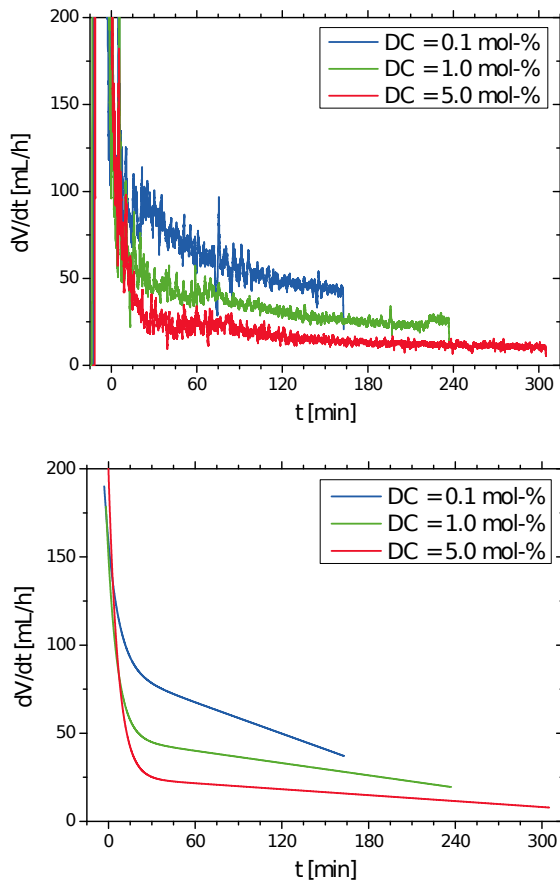


**Figure 6.3.:** The volume flux in desalination experiments conducted with samples of varying degree of cross-linking (DC) is shown. On top, it is given by averaged data (SMA, 61 pts) and, below, represented by a linear exponential fit function (5.7).

% intersects both other curves at 23 and 37 bar, respectively. The reduction can be quantified by the fit of a linear function of the curves below 10 g/L; the slope values ( $dc/dp$ ) are shown in **tab. 6.1**. This leads to the conclusion that the first part of the eluate received is part of the supernatant phase. When the external solution contains a lot of salt the internal solution much be poor in salt, therefore, the reduction should be higher for a larger starting concentration. This point is proven by the data in tab. 6.1.

In dependence on relative degree of swelling, the drop in the concentration only occurs when  $Q_{\text{rel}}$  is smaller than unity.<sup>4</sup> Here, all supernatant solution has been removed. Interestingly, for all experiments 10 g/L in c is passed at the same deswelling ratio ( $\approx 0.7$ ). In general, the more the gel is deswollen, the lower is the concentration of the produced eluate. It can be concluded that a high DC gives the lowest salt concentration in the eluate but the lowest flux, as well.

### Influence of the reference state

The synthesis value  $Q_{\text{syn}}$  controls the “density” of the network and is an important parameter for the desalination capacity. This reference state gives the relaxed state of the network in which no pressure is exerted. A low value should facilitate the deswelling of the network. However, this effect is opposed by the inefficient synthesis at higher  $Q_{\text{syn}}$  values that leads to much softer networks as seen before (sec. 3.3). Three samples were produced with values of  $Q_{\text{syn}}$  of 1.6, 2, and 8 g/g which are compared with the standard case of 4 g/g.<sup>5</sup> This spans roughly the entire synthetically accessible range. At lower values the cross-linker is insoluble and at higher values no continuous network is formed.

---

<sup>4</sup>For best accuracy  $Q_{\text{rel}}$  should be computed using the  $Q_{\text{eq}}$  value at the brine concentration of the supernatant phase after swelling ( $> 10 \text{ g/L}$ ). Here, for simplicity the value at 10 g/L is used.

<sup>5</sup>The additional samples are pAAc-DC1-DN76-Q1.6, batch 1, pAAc-DC1-DN75-Q2, batch 2 and pAAc-DC1-DN75-Q8, batch 1 as described in appendix A.1.

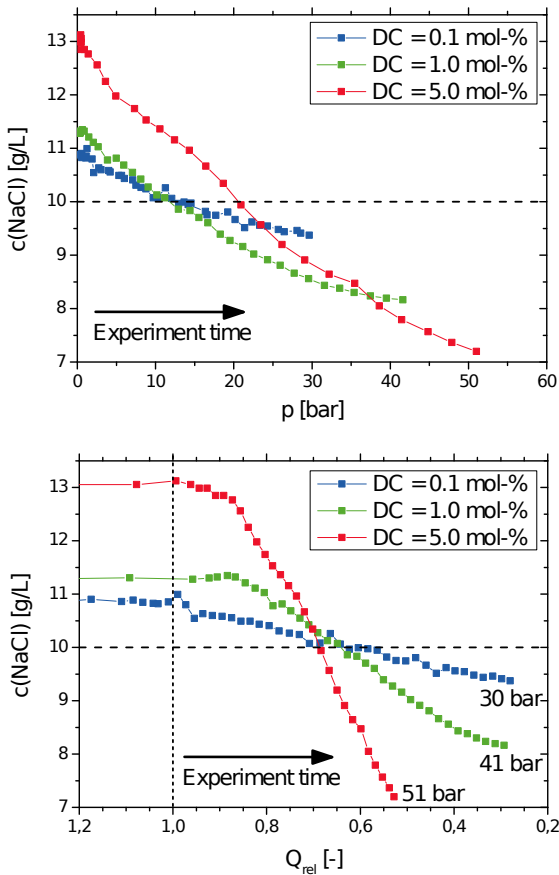


**Figure 6.4.:** Eluate concentration result of desalination experiments conducted with gels of varying degree of cross-linking (DC) are shown. The salt concentration of the produced eluate is shown as a function of applied pressure (top) and relative swelling of the gel (bottom). The vertical dashed line indicates the point where the supernatant solution has been removed completely and the horizontal one gives the initial concentration of the added brine ( $10 \text{ g/L NaCl}$ ) that was also used for the determination of  $Q_{\text{rel}}$ .

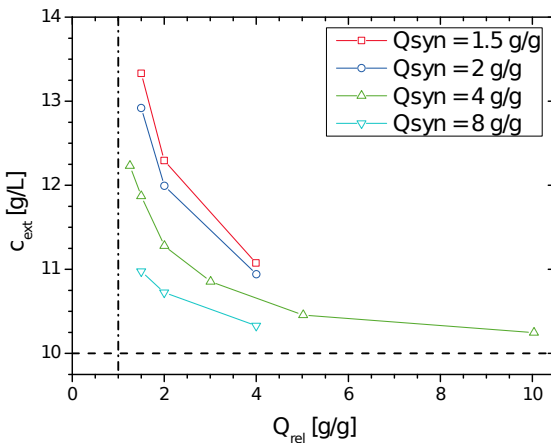


**Figure 6.5.:** Equilibrium salt rejection from a pAAc gel in contact with a salt solution phase given for gels with varying reference states ( $Q_{\text{syn}}$ ). The values of DC = 1 mol-% and DN = 75 mol-% are the same for all samples. The salt concentration of the supernatant phase is compared to the initial concentration (dashed line) and given as function of the volume of the aqueous phase ( $Q_{\text{rel}}$ ).

The static salt distribution, as described above, already gives a good indication of the desalination capacity (**fig. 6.5**). The curves give a clear trend: the lower  $Q_{\text{syn}}$ , the higher is the salt concentration in the supernatant solution. At higher  $Q_{\text{rel}}$  values the effect decreases due to dilution effects as discussed in the previous section. For  $Q_{\text{syn}} = 2 \text{ g/g}$  the salt rejection is 1/3 stronger than for 4 while the difference between 1.6 g/g and 2 g/g is pretty small. Only the best candidate of the samples was chosen to be compared with the standard polymer (4 g/g). This is the sample with  $Q_{\text{syn}} = 2 \text{ g/g}$  because it has almost the same salt rejection but swells better than the one with 1.6 g/g ( $Q_{\text{eq}} = 17 \text{ g/g}$  and  $19 \text{ g/g}$ , respectively).

For the sample  $Q_{\text{syn}} = 2 \text{ g/g}$  the standard experiment was carried out up to a pressure of 59 bar. The results are compared with the previously shown reference sample ( $Q_{\text{syn}} = 4 \text{ g/g}$ ). The eluate volume is shown in **fig. 6.6** in the upper part. It is lower than in the case of the reference sample,

**Table 6.2.:** List of parameters that describe the flux and the desalination performance of pAAc gels with different reference states  $Q_{\text{syn}}$ . The values of DC = 1 mol-% and DN = 75 mol-% are the same for all samples.

$Q_{\text{syn}}$ [g/g]	T (Time constant) [min]	B (Slope) [h/(mL min)]	C (Offset) [mL/h]	dc/dp [ $\times 100$ g /(L bar)]
2.0	1.77	-0.065	33.3	-6.91
4.0	7.05	-0.11	47.2	-6.38

about 50 mL at the maximum pressure. The flux shows the same trend (**fig. 6.6** in the lower part). The coefficient C of the flux fit, given in **tab. 6.2**, is considerably lower (by 30 %). The flux, however, is more sustaining as the slope of the decrease is almost half for  $Q_{\text{syn}} = 2 \text{ g/g}$  as compared to the 4 g/g sample. As a result, the rates are almost similar after 4 h. The salt concentration is decreasing in a qualitatively similar way for both samples as seen in **fig. 6.7** — the extent is different, however. The slope  $dc/dp$  is higher for lower  $Q_{\text{syn}}$  sample but the starting point is about 0.8 g/L higher. As a result, the intersection of the two curves is found late in the experiment around 40 bar. Only here, the desalination performance is better for  $Q_{\text{syn}} = 2 \text{ g/g}$ . In the dependence of  $Q_{\text{rel}}$  is seen that the water coming from the gel contains much less salt at the same degree of deswelling for the lower  $Q_{\text{syn}}$  value proving the higher salt rejection. A sample with a lower  $Q_{\text{syn}}$  possesses a better salt rejection but a reduced flux and the lower salt concentration is only recovered at a high pressure.

### Influence of the degree of neutralisation

The degree of neutralisation (DN) was investigated as the last synthetic parameter. The results of the static salt rejection experiment are shown in **fig. 6.8**. It is easily seen that at the typical value of DN = 75 mol-%

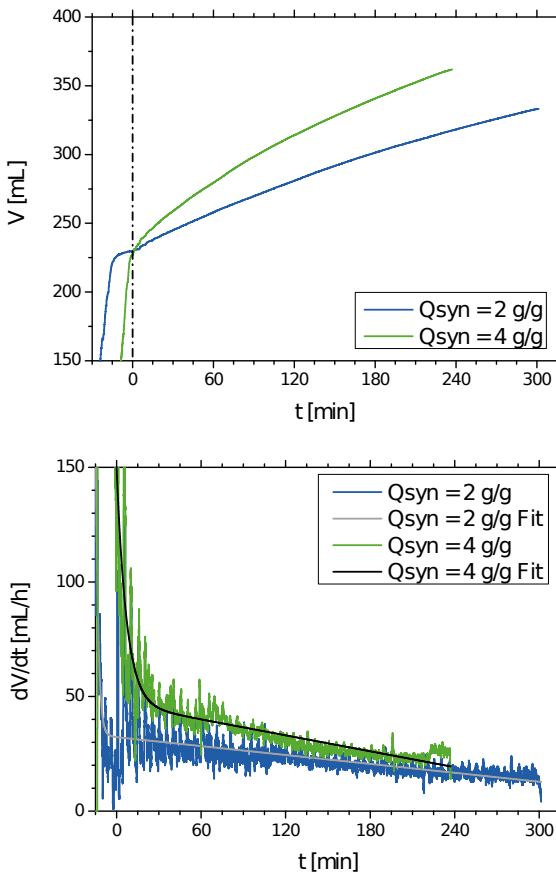


**Figure 6.6.:** Produced eluate volume (top) and volume flux (bottom) in a desalination experiments conducted with samples of varying reference state ( $Q_{\text{syn}}$ ) are shown. The flux is given by averaged data (SMA, 61 pts) and represented by a linear exponential fit function (5.7). The dashed line at the top gives the starting point of the experiment. The fit parameters are given in tab. 6.2.

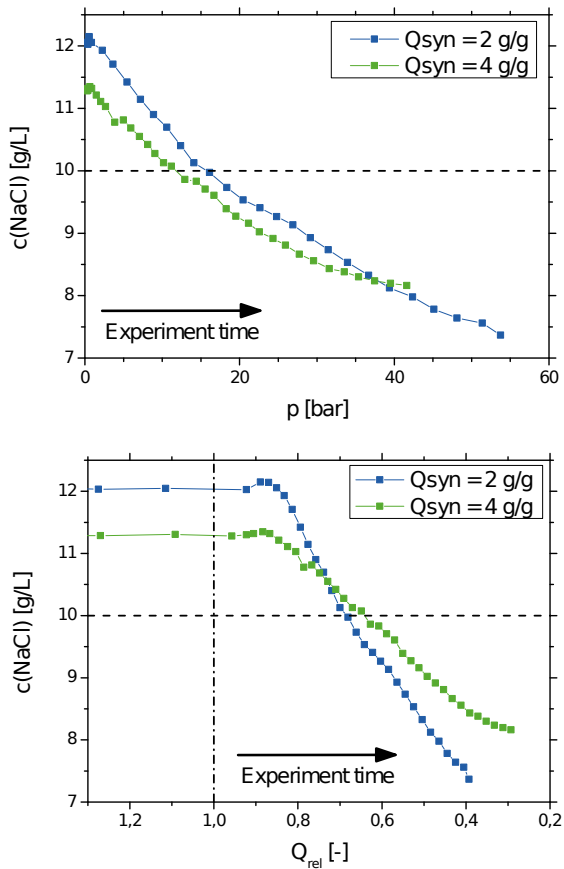


**Figure 6.7.:** Concentration results of desalination experiments conducted with gels of varying reference state ( $Q_{\text{syn}}$ ) are shown. The salt concentration of the produced eluate is shown as a function of applied pressure (top) and relative swelling of the gel (bottom). The vertical dashed line indicates the point where the supernatant solution has been removed completely and the horizontal one gives the initial concentration of the added brine (10 g/L NaCl) that was also used for the determination of  $Q_{\text{rel}}$ .

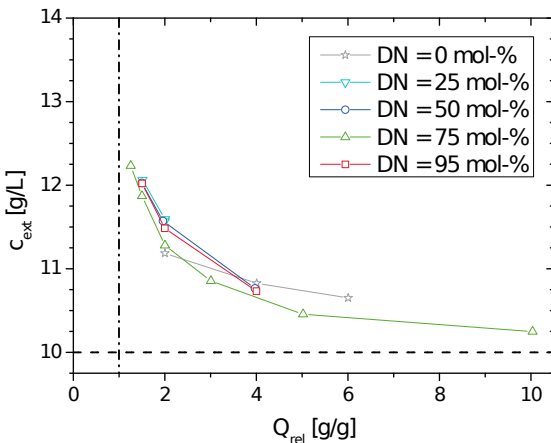


**Figure 6.8.:** Equilibrium salt rejection from a gel in contact with a solution phase given for gels with varying degrees of neutralisation (DN). The salt concentration of the supernatant phase is compared to the initial concentration (dashed line) and given as function of the volume of the aqueous phase ( $Q_{\text{rel}}$ ).

already the highest salt rejection is found and further change is futile as almost no dependence is seen. Furthermore, cross-linking differently ionised monomer solutions at the time of synthesis leads to very different kinetics and network structures. A post-synthesis change of the DN was not attempted in the scope of this work, as it is time consuming and did not promise much improvement. No further experiments under pressure were carried out.

When looking at quantitative differences of the above investigated samples, the parameters  $dc/dp$  for the reduction of salt concentration and the flux fit parameters have proven themselves useful. On this basis, the samples can be compared. The sample with DC = 5 mol-% showed the strongest drop and the lowest values in salt concentration in the end. For a reference state of  $Q_{\text{syn}} = 2 \text{ g/g}$  a lower final sat concentration than for the standard value of  $Q_{\text{syn}} = 4 \text{ g/g}$  is found. Unfortunately, the flux is smaller in both this

cases of higher salt rejection. Both parameters can only be varied in a range given by the solubility of the cross-linker in the reaction mixture. They cannot be optimised further with the system at hand. A change of the synthesis parameter DN did not prove useful. The network can also be modified beyond the just discussed variables by the addition of other monomers, which will be discussed now.

## 6.2. Copolymer networks

The copolymerisation of different monomers is a well used principle in polymer chemistry to alter the properties of neat polymers. A wide variety of monomers is available that can be combined with acrylic acid (AAc) in a random copolymer. The emphasis in this work is on water soluble monomers that have the possibility to be polymerised under the same conditions and initiator system as neat AAc. As comonomers were chosen methacrylic acid (MAAc), (hydroxyethyl)methacrylate (HEMA), acrylamide (AAm), and *N*-isopropylacrylamide (NiPAM). These copolymers were produced by the typical recipe given in appendix A.1. The synthetic parameters of DC = 0.3 mol-%, DN = 75 mol %,  $Q_{\text{syn}} = 4 \text{ g/g}$ , and mostly CO = 50 mol-% were used.<sup>6</sup> The HEMA sample was also produced with a DC of 1 mol-%. This gives a total of five samples to be investigated and compared to the pAAc reference samples. The results of the static rejection of all samples are shown in **fig. 6.9**. Only one of the copolymers showed a better salt rejection behaviour than the corresponding reference sample. This is *p(AAc-co-HEMA)* with a 10 % higher rejection. This is true for the higher and lower DC values. All other samples exhibited in a similar, lower rejection than pAAc. Therefore, only the HEMA containing samples were further investigated as candidates in standard desalination experiments.

---

<sup>6</sup>The samples were prepared by Mr. Dimitri Merger under the supervision of the author. Their shorthands are pMAAc-DC0.3-DN75-Q4, batch 1, *p(AAc-HEMA50)-DC0.3-DN75-Q4*, batch 2, *p(AAc-HEMA50)-DC1-DN75-Q4*, batch 1, *p(AAc-NiPAM50)-DC0.3-DN75-Q4*, batch 1, and *p(AAc-AAm50)-DC0.3-DN75-Q4*, batch 1. The exact composition is detailed in appendix A.1.

Desalination experiments were conducted until 62 bar for the HEMA sample cross-linked with DC = 0.3 mol-% and till 61 bar for the DC = 1.0 mol-%. The eluate volume and the flux form the setup are higher for the pAAc sample than for either of the HEMA containing gels (fig. 6.10). The obtained volume is almost as high for the low cross-linked HEMA sample as for the pAAc sample. However, at the same cross-linking degree 30 mL less eluate was obtained after 4 h. The initial flux value is highest for the pAAc sample, as seen at the bottom of fig. 6.10 and the C fit parameter in tab. 6.3. The drop in flux (B fit parameter) is strongest for the pAAc gel. Considering the concentration in fig. 6.11, the desalination performance of the copolymers is disappointing. The final salt concentration is the same

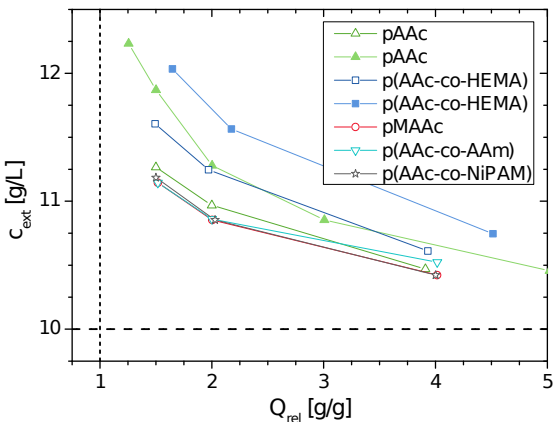


**Figure 6.9.:** Equilibrium salt rejection from a gel in contact with a salt solution phase given for gels with different comonomer and cross-link densities. The salt concentration of the supernatant phase is compared to the initial concentration (dashed line) and given as function of the volume of the aqueous phase ( $Q_{\text{rel}}$ ). The filled symbols denote gels with 1 mol-% cross-linker and the open ones with 0.3 mol-%. The monomer ratio (CO) for the copolymers is 50 mol-% except for pMAAc (100 mol-%).

**Table 6.3.:** List of parameters that describe the desalination performance of hydrogels with different monomer composition.

Polymer	DC [mol-%]	T (Time c.) [min]	B (Slope) [h/(mL × min)]	C (Offset) [mL/h]	dc/dp [×100 g/ (L bar)]
p(AAc-co-HEMA)	0.3	8.98	-0.074	34.1	-4.57
p(AAc-co-HEMA)	1.0	2.21	-0.080	40.2	-5.44
pAAc	1.0	7.05	-0.11	47.2	-6.38

with little over 8 g/L for all samples. However, the pressure necessary to produce this concentration is almost 20 bar lower for the pAAc sample than for the highly cross-linked HEMA sample. The better rejection that was initially measured for this HEMA containing sample, is seen in the dependence on  $Q_{\text{rel}}$  as the concentration coming from particles is decreasing earlier. This observation is maybe too weak to explain the much better rejection. An alternative explanation could be a large content of extractable polymer that was washed into the supernatant phase in the rejection experiment. Considering the final salt concentration and amount of water received from the gel per time, the copolymer samples do not outperform the neat pAAc sample.

### 6.3. Commercial superabsorbent polymers

For comparison and applications in a larger scale, industrially produced hydrogels are well suited. They are produced for commercial applications, mainly for use as superabsorbent polymers (SAP) [Brannon-Peppas90, Buchholz98]. These samples are cheap to obtain (< 2 €/kg), available in large quantities of constant properties and usually optimised for a small sol content, a high absorbency under load (AUL), and the absence of gel

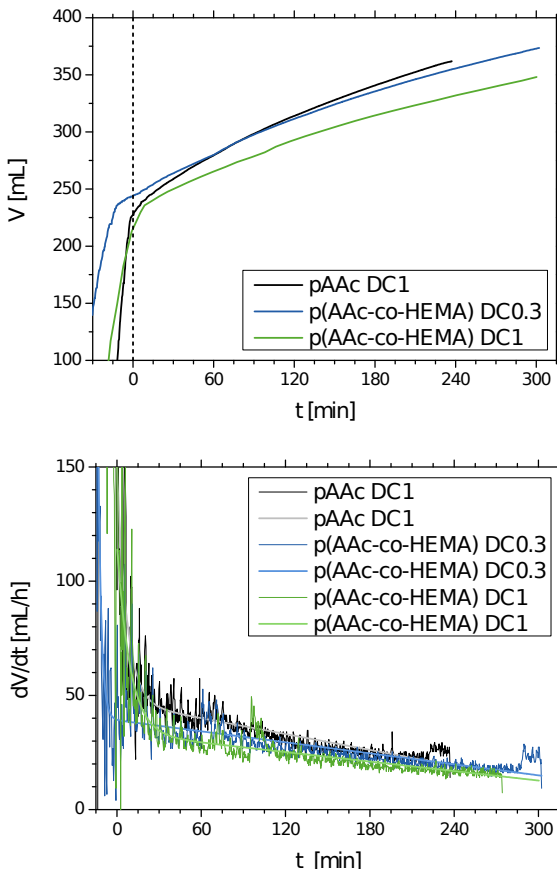


**Figure 6.10.:** The produced eluate in desalination experiments conducted with gels containing HEMA (DC = 0.3 and 1 mol-%) as a comonomer and a neat pAAc (DC = 1 mol-%) reference sample are compared. The obtained eluate volume is shown on top and the volume flux as averaged data (SMA, 61 pts, top) and represented by a linear exponential fit function (5.7) (bottom). The parameters obtained from the fits are given in tab. 6.3.

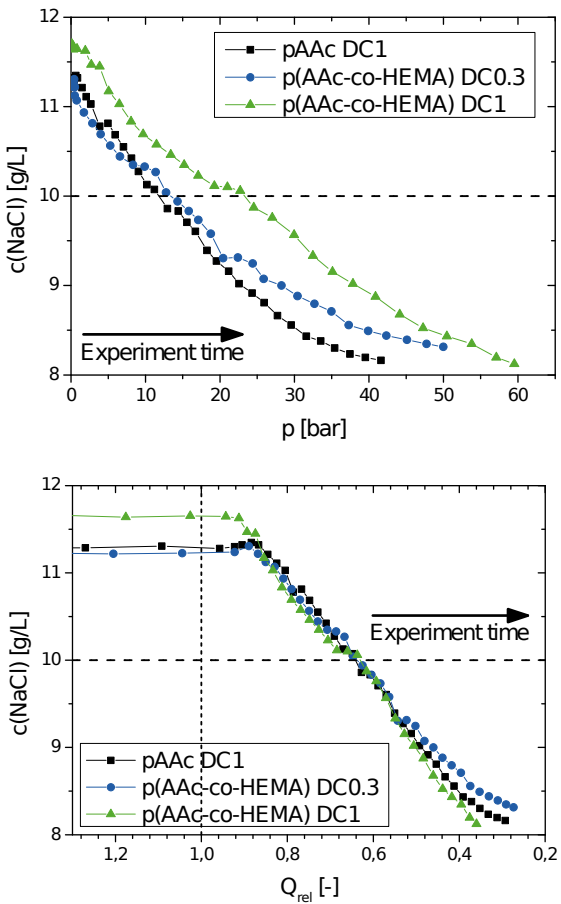


**Figure 6.11.:** The concentration recorded in desalination experiments is shown as a function of pressure (top) and relative swelling of the gel (bottom). Samples containing HEMA as comonomer and a pAAc reference sample ( $\text{DC} = 1 \text{ mol-}\%$ ) are investigated. The vertical dashed line indicates the point where the supernatant solution has been removed completely and the horizontal one gives the initial concentration of the added brine ( $10 \text{ g/L NaCl}$ ) that was also used for the determination of  $Q_{\text{rel}}$ .

blocking. These properties make them interesting for the application in the desalination process described in the previous chapter. A low sol content increases the absorbency per weight and removes a potential health hazard in the produced drinking water. A high AUL is good in terms of high capacity. On the other hand, the high load resistance makes it difficult to squeeze water from the gel. The absence of gel blocking, especially under load, means that the channels between the gel particles stay open even under moderate pressure, in contrast to the collapse of the inter-particle voids in very soft gels. Thus, flux through the gel bed is possible even at moderate pressure and diffusion is only necessary within the particles. These materials deserve therefore a close investigation.

A variety of commercial samples from the BASF are investigated and some are found to be as good as the self-synthesised samples. The results of equilibrium salt distribution are shown in **fig. 6.12** for the Luquasorb<sup>TM</sup> polymers B1110, 1030, 1280 RS, and 1280 RL and the samples VP300 and Hysorb (all from BASF). The information that is known about these samples is summarised in the appendix in tab. 3.1. Here, it is only noted that all are made from AAc, except VP300 that is acrylamide (AAm) based, and B1110 is composed of particles with additional surface cross-linking. As reference, the result of the self-synthesized sample pAAc (DC = 1 mol-%) is reproduced from fig. 6.1. Typical rejection curves are obtained for all samples. The the rejection by VP300, 1030, and Hysorb gels is smaller than in the reference sample, while B1110 and the 1280 polymers show a better performance. For further investigation the samples B1110 and 1030 were selected. The 1280 samples were not considered as their potassium content prevented an easy concentration determination.

Standard desalination experiments show a good performance of the B1110 sample. The obtained volume and flux over time are shown in **fig. 6.13**. The eluate volume obtained after 4 h is almost the same for B1110 and the pAAc sample, but a large volume difference at early experiment times is observed. Accordingly, the flux is higher for the pAAc sample seen from

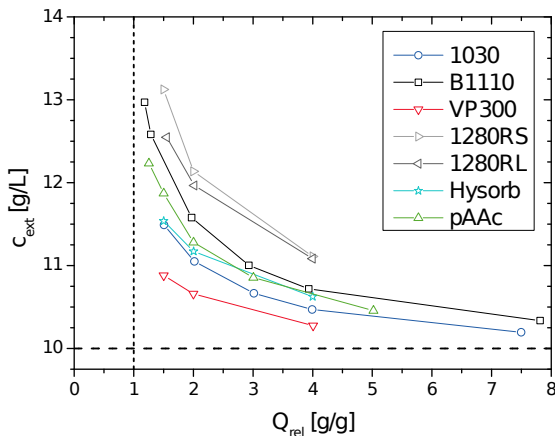


**Figure 6.12.:** Equilibrium salt rejection from a gel in contact with a salt solution phase given for various industrial SAP samples. The salt concentration of the supernatant phase is compared to the initial concentration (dashed line) and given as function of the volume of the aqueous phase ( $Q_{\text{rel}}$ ). The self-synthesised pAAc polymer with DC = 1 mol-% is given as reference sample.

the fit constant with 47 mL/h against 35 for B1110 (**tab. 6.4**). The reduction of the flux (slope of the fit) is rather similar for the two samples. The results suggest that a lot of solution is removed from the B1110 samples by quite low pressure. The related concentration results shown in **fig. 6.14** indicate a concentration decrease only at high values of  $Q_{\text{rel}}$  for B1110. The pressure dependence of the salt concentration is almost identical for all three samples in the beginning. After passing below 10 g/L, they diverge. The reduction is strongest for B1110 reaching about 7.5 g/L; quantitatively this is also shown by the lower  $dc/dp$  values in **tab. 6.4**. Thus the surface cross-linked polymer gives the best desalination performance. The dependence on  $Q_{\text{rel}}$  shows that a large amount of eluate is received from B1110 with almost no change in the salt concentration, afterwards, however, the drop is steep. The industrially produced polymer B1110 is showing a better performance than the reference sample pAAc (DC = 1 mol-%,  $Q_{\text{syn}} = 4$  g/g). It produces

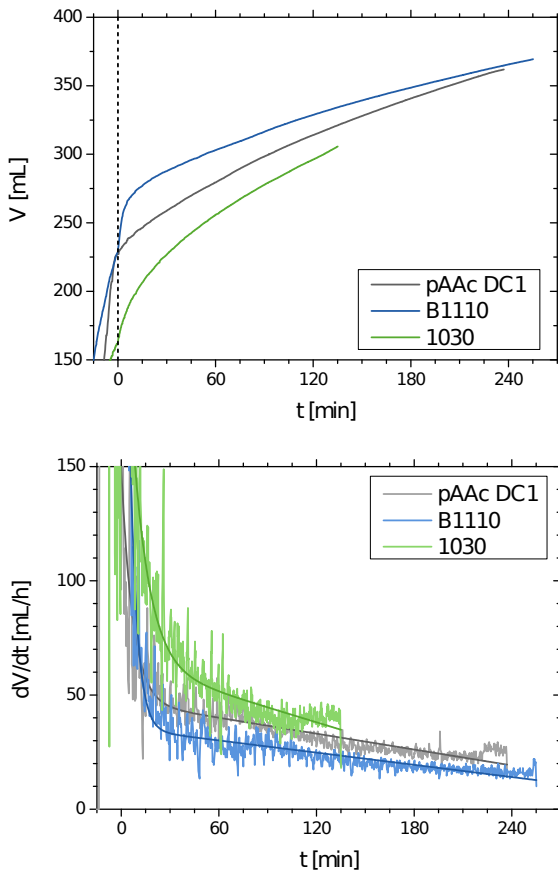


**Figure 6.13.:** Produced eluate in desalination experiments conducted with industrial samples B1110 and 1030 and a pAAc reference sample with a DC of 1 mol-%. The obtained eluate volume is shown on top and the volume flux as averaged data (SMA, 61 pts, top) and represented by a linear exponential fit function (5.7) (bottom). The parameters obtained from the fits are given in tab. 6.4.

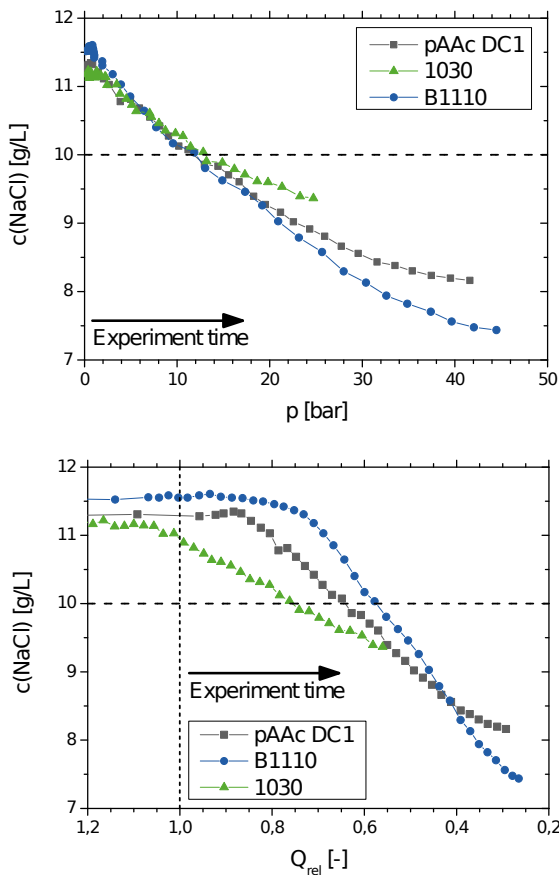


**Figure 6.14:** Concentration results of desalination experiments conducted with industrial samples B1110 and 1030 and a pAAc reference sample with a DC of 1 mol-%. The salt concentration of the produced eluate is shown as a function of applied pressure (top) and relative swelling of the gel (bottom). The vertical dashed line indicates the point where the supernatant solution has been removed completely and the horizontal one gives the initial concentration of the added brine (10 g/L  $\text{NaCl}$ ) that was also used for the determination of  $Q_{\text{rel}}$ .

**Table 6.4.:** List of parameters that describe the desalination performance of industrial polymers and a pAAc reference sample.

Polymer	T (Time constant) [min]	B (Slope) [h/(mL ×min)]	C (Offset) [mL/h]	dc/dp [×100 g /(L bar)]
B1110	4.41	-0.089	35.1	-8.01
1030	10.4	-0.22	63.7	-5.07
pAAc DC1	7.05	-0.11	47.2	-6.38

a lower salt concentration at 40 bar with a comparable eluate volume in the same time. The standard commercial sample 1030 is performing in both respects worse than the other two samples and is therefore not a good choice.

## Conclusion

From the variety of samples investigated in this chapter clear guidelines can be drawn as to what are good choices for the working material of desalination experiments. From the self-synthesised hydrogels it was found that a high DC, e.g. 5 mol-%, is beneficial for salt rejection and in the same line for desalination capacity. A small value of the gel reference state  $Q_{\text{syn}}$  gives better desalination performance but the influence of this synthetic parameter is smaller than for DC. In a desalination experiment the performance of a sample with  $Q_{\text{syn}} = 2 \text{ g/g}$  is only gradually better than the standard value of 4 g/g. However, the flux is reduced when using the former sample. The parameter DN has almost no influence on the salt rejection. Any changes of this variable produced samples inferior to the commonly used standard sample with DN = 75 mol-%. A number of copolymers of acrylic acid with other monomers were investigated. Only the addition of HEMA improves

## 6. Salt rejection and desalination by hydrogels

---

the salt rejection. However, the desalination performance in a standard experiment, at the same DC is not decisively better.

The results of the self-synthesised samples were compared to some industrially produced hydrogels. Especially the hydrogel B1110 with additional surface cross-linking showed a good salt rejection and high eluate flow when compared to a pAAc reference sample. The sample 1030 with regular bead structure was inferior to the reference.

When considering these results in total, they suggest that a high salt rejection and high capacity/flux cannot be achieved with the same values of synthetic parameters. There is always a trade-off to be made. The evaluation of this trade-off will be one of the subjects of the next chapter, where a model is developed to evaluate the samples and explain their behaviour. Here, one possibility for optimisation was discussed: the working material. Other options are provided by the technical parameters of the setup and process. These are investigated in the next chapter.

Due to the relatively good performance of B1110 and the large quantities that are available with the constant properties, this polymer will be used as a model for the evaluation of the technical parameters in the next chapter. Some implications of the structured particles of this polymers are seen in the data that will also be discussed further there.

## **7. Technical aspects of seawater desalination**

The feasibility and optimal condition of the desalination process can be assessed by an in-depth investigation of the experimental results. The technical parameters are equally important as the previously discussed (ch. 6) synthetic parameters of the hydrogel. By the process parameters it is defined whether the proposed desalination process is feasible in a real process and on a larger scale. Also more possibilities for optimisation are offered by these parameters and an understanding of the process and the energy consumption is provided.

In this chapter, several process parameters were identified that influence the desalination result found for a given hydrogel. These are the pressure profile, the swelling time, the water content of the sample, the dependence on salt concentration, and the reusability of the polymer. Of special interest is the influence of the chosen pressure profile, as this could not be evaluated with the first setup under discussion in section 5.1, because no reliable pressure information was available. The information drawn from these experiments and the last chapter are used to propose a model for the microscopic processes in the polymer sample during a desalination experiment. Thereby a qualitative understanding of the form of the desalination results and the trend in the parameters and samples is found. At last, the measured information is used for calculation an estimate of energy consumption of the current process in an application environment. Therefore a simple calculation model is used and the results are compared to reference values.

## 7.1. Relevant process parameters

The proposed method for desalination can only be viable, when the technical parameters meet a number of criteria: the process has to allow a high throughput and make it feasible in the entire range of interest. This requirements and the efficiency are not only controlled by the working material of the process, discussed in the previous chapter 5, but also by the technical parameters which are discussed in this section. Especially the process parameters control whether the requirements can be met. The identified key points are: the throughput should be high, which means a fast process must be developed. Secondly, the operation of the technique must be possible beyond the exemplary brine concentrations of 10 g/L used so far. The operation must be possible in the complete range of interest of salt concentrations e.g. 0.1 – 35 g/L ( $NaCl$ ). The working material should be reusable without considerable performance reductions for a number of times to reduce waste and operating costs. At last, the overall energy efficiency should be increased further.

For the process analysis in this section only the best performing candidates from the previous chapter are used. These are the industrial sample B1110 from the BASF and the self-synthesized polymer pAAc with a high DC of 5 mol-% (DN = 75 mol-% and  $Q_{syn} = 4 \text{ g/g}$ ). The standard procedure described in section 5.2.1 (p. 136) is used.<sup>1</sup>

### Influence of the pressure profile

The pressure profile controls the throughput of the desalination experiment and whether it is carried out in equilibrium conditions (or close to it). The profile is typically linear with a defined and constant slope  $dp/dt$ ; it is the controlled variable in the experiments. In the case of a steep increase a high pressure is reached faster and consequently more eluate is forced from the

---

<sup>1</sup>Here, mostly steeper pressure profiles than the  $dp/dt = 12 \text{ bar/h}$  of the standard procedure were used to speed up the experiments.

**Table 7.1.:** Overview over the investigated pressure profiles.

Experiment	Type	Equation
6bar-h	Linear	$p = t \cdot 6 \text{ bar/h}$
12bar-h	Linear	$p = t \cdot 12 \text{ bar/h}$
20bar-h	Linear	$p = t \cdot 20 \text{ bar/h}$
60bar-h	Linear	$p = t \cdot 60 \text{ bar/h}$
Step50	Step	$p = 50 \text{ bar}$
Square	Square	$p = t^2 \cdot 3,5 \text{ bar/h}^2$

gel and setup per time (higher flux). However, in the case of slow pressure increases the equilibrium of the gel phase with the solution phase is intact. This aspect is discussed further in section 7.2. Here, several experiments with linear and two non-linear pressure profiles were carried out; they are summarized in **tab. 7.1**. Each experiment ended, when the minimal sieve distance was reached, the setup failed, or the maximal pressure was reached (typically 50 bar). Therefore, the final pressure is different for the experiments and is further discussed with the respective evaluations.

The eluate produced by the pressure increase differs in volume and salt concentration depending on the employed pressure profile. The actual input pressure as recorded at the sample is given in **fig. 7.1**, top, for each experiment. It is in good agreement with the desired values. The maximal pressure that was reached is given in **tab. 7.2**. The produced eluate volume is shown in **fig. 7.1** in the lower part. Only the values are shown, that were recorded up to a pressure of 40 bar so the end points can be directly compared. The produced volume is greater, over time, for a steeper pressure profile (e.g. after 30 min were produced 295 mL for 60bar-h and only 278 mL for 6bar-h). Yet, this trend is reversed when the volume produced at the same final pressure of 40 bar (last point of the curves) is compared: 305 mL were produced for 60bar-h but over 370 mL for 6bar-h were produced. This trend also holds for the step experiment, which has the steepest pressure increase. For the Square profile only a very low volume was pro-

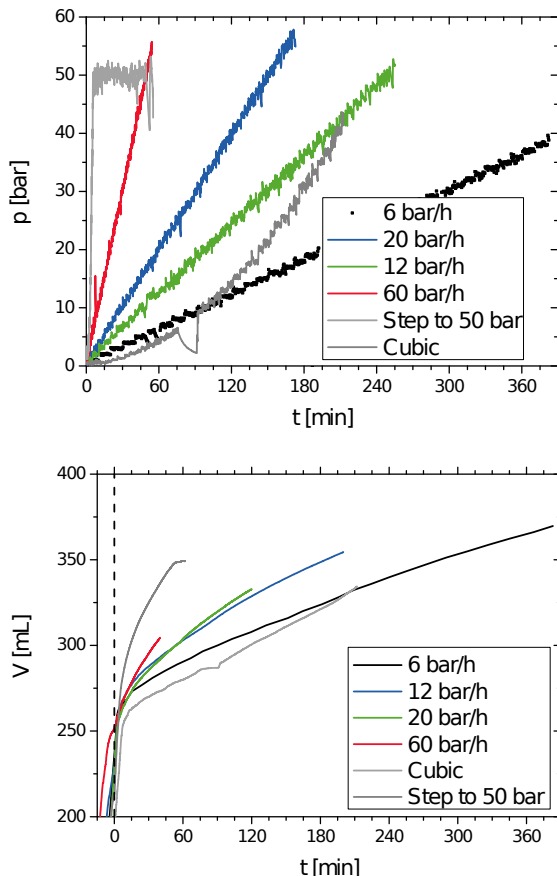


**Figure 7.1.:** The influence of different pressure profiles (top) in desalination experiments on the produced eluate volume (bottom) is shown. The vertical dashed line (top panel) indicates the zero point of the time reference. Linear and non-linear pressure profiles were used to deswell the commercial hydrogel B1110, details are shown in **tab. 7.1**.

duced. The same overall trend can also be seen in **fig. 7.2** on top, where the flux is presented with all available data. The flux is considerably higher in the beginning for steeper pressure profiles but is also decreasing faster. This is quantitatively confirmed by the fit constants given in **tab. 7.2** for the fit function (5.7). A notable exception is the experiment Square where the flux is almost constant over a wide range of time (15 – 200 min).

The pressure profile also effects in the salt concentration of the eluate. The salt concentration is decreasing faster, over time, when a stronger pressure increase is used (**fig. 7.2**, bottom). The concentration value found at the start is always the same, around 11.7 g/L, for all experiments. This caused by the use of the same polymer and  $Q_{\text{rel}}$  ratio. A concentration below 10 g/L (dashed line) is received for much smaller experiment times when a steeper pressure increase is used. Thus, desalinated water is obtained faster e.g. after 25 min for 60bar-h and 182 min for 6bar-h. In the case of the step experiment the concentration drop is almost instantaneous but the decrease levels off to an almost constant value at 8.8 g/L. The Square experiment cuts through 6bar-h and is very steeply decreasing in the end comparable to the 60bar-h experiment.

The representation of salt concentration as a function of pressure shows, that for most experiments the same pressure produces the same salt concentration in the eluate (**fig. 7.3**, top). Only the steepest pressure increase deviates from this behaviour (60bar-h and Step50). The latter shows a completely different form where first almost no decrease in concentration is found with increasing pressure and then the concentration drops at constant pressure. This is obviously an effect of the extremely steep profile by which a strong non-steady state condition is achieved.

The key values from all experiments in this section are summarized in **tab. 7.2**. The slopes  $dc/dp$  are decreasing when a steeper pressure profile is used. In contrast, the flux fits show higher slopes and offsets are found for stronger pressure increases. Taking into account the estimated errors from sec. 5.3 it may clearly be said that all described trends are significant.

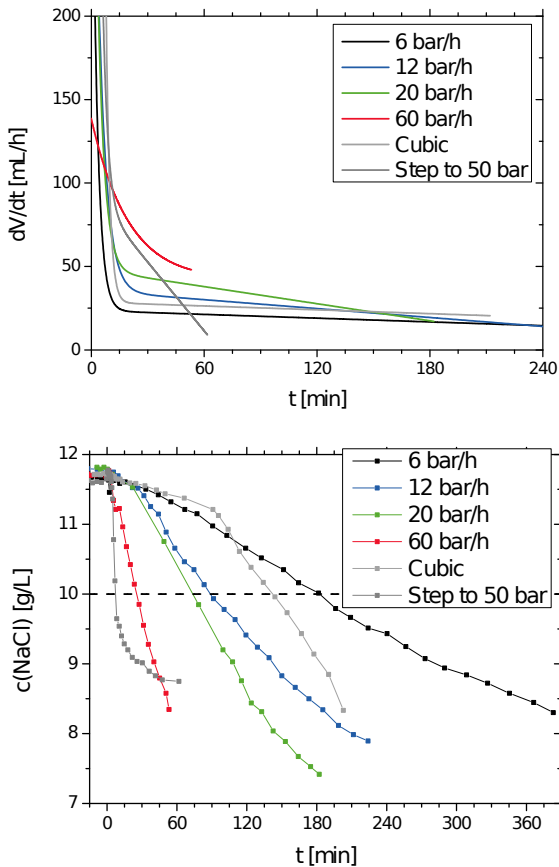


**Figure 7.2.:** The influence of different pressure profiles in desalination experiments on the eluate flux (top) and concentration (bottom) is shown. The volume flux is represented by a linear exponential fit function (5.7) with the coefficients given in **tab. 7.2**. The horizontal dashed line (bottom panel) gives the initial concentration of the added salt solution (10 g/L NaCl).

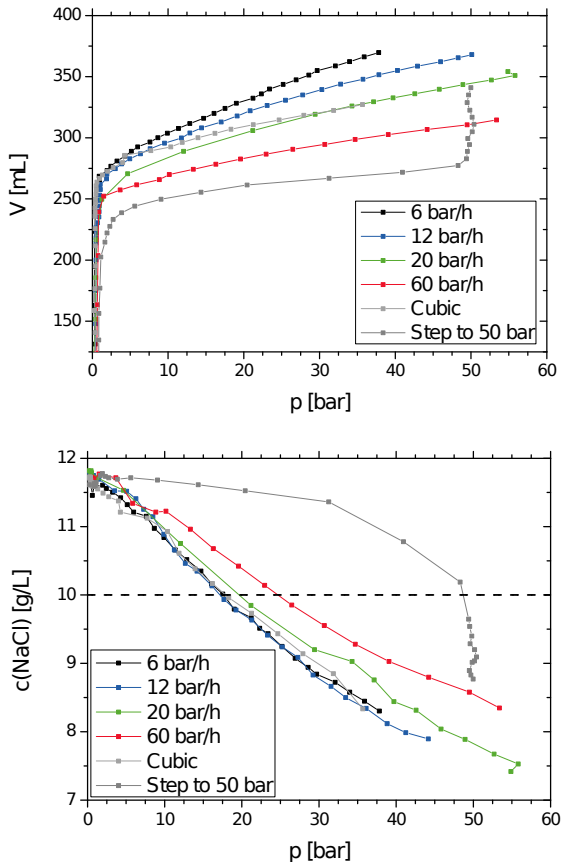


**Figure 7.3.:** The influence of different pressure profiles in desalination experiments on the volume (top) and concentration (bottom) as a function of pressure are shown. The horizontal dashed line (bottom panel) gives the initial concentration of the added brine (10 g/L NaCl).

**Table 7.2.:** List of parameters that describe the desalination performance at different pressure profiles. (\*) The data of Step50 was not linear so no value for  $dc/dp$  was obtained.

Experiment	$p_{\max}$ [bar]	$dc/dp$ [ $\times 100$ g/ (L bar)]	T (Time c.) [min]	B (Slope) [h/(mL $\times$ min)]	C (Offset) [mL/h]
6bar-h	40	-8.05	2.81	-0.038	23.5
12bar-h	53	-8.01	4.41	-0.089	35.1
20bar-h	58	-6.65	3.55	-0.17	47.7
60bar-h	55	-6.11	5.23	-0.76	84.3
Step50	44	(*)	2.65	-1.37	87.0
Square	50	-11.3	2.00	-0.038	28.4

### Influence of swelling time

A high turn over of water is needed for a desalination process. In the case of polymeric material this depends in the process on a fast swelling and deswelling. It has already been established that gels can take up a solution very fast (see sec. 3.2). However, what part of the solution is taken up first and whether the desalination process is immediately possible after very short swelling time remains to be determined. The swelling time is the time that the polymer is in contact with the salt solution before it is subjected to pressure in a desalination experiment.

The influence of the swelling time  $t - Q$  is determined by comparing the standard experiment ( $t - Q = 12$  h) with an experiment carried out with a much shorter swelling time. The reduced time was taken as the time it takes a gel to reach 95 % of its  $Q_{\text{eq}}$ . This time was deducted from the measured swelling kinetics, section 3.2. It was found to be 3 min for the polymer

B1110 and 13 min for pAAc-DC5. This reflects mainly the differences in particle size, not necessarily the polymer characteristics. The threshold was taken to be 95 % for technical relevance, by a trade-off between time and capacity both influencing the turn-over in the process. The results of both experiments are compared for polymer B1110 (**fig. 7.4**). In both cases a pressure increase of 60 bar/h (for about 50 min) was used.

Differences in volume and concentration are seen when the results are compared. The eluate volume is smaller over the whole course of the experiment for the longer swelling time. However, this difference is small, e.g. 5 mL after 45 min and within the margin of error. The flux from the two samples is almost identical as shown by the parameters of the fit function in **tab. 7.3** (first two rows). In contrast, the salt concentration of the eluate as a function of pressure is deviating beyond 25 bar. At 45 bar the concentration is already 0.5 g/L lower for the shorter swelling time, which is an effect above the margin of error. In terms of  $dc/dp$  a clearly steeper decrease is seen for  $t - Q = 3$  min (tab. 7.3). It is not only possible to perform the desalination experiment in a very short time, also the performance is better when the sample is only swollen shortly.

### Influence of brine content of the desalination sample

In the beginning of a desalination experiment an enriched salt solution, compared to the initial concentration  $c_s$ , is received which is counterproductive to desalination. It is beneficial when desalinated water can be received immediately. The first part of the eluate possesses the same concentration as the supernatant phase as was shown by the static experiments in chapter 6. A reduction of the eluate concentration below  $c_s$  often needs 10 – 15 bar pressure for  $c_s = 10$  g/L. In the static experiment, when more solution is added to the same amount of polymer (higher  $Q_{\text{rel}}$  value), the enrichment of salt in the solution phase can be diluted. At a value of  $Q_{\text{rel}} = 12$  the supernatant phase has almost the same concentration as  $c_s$ .

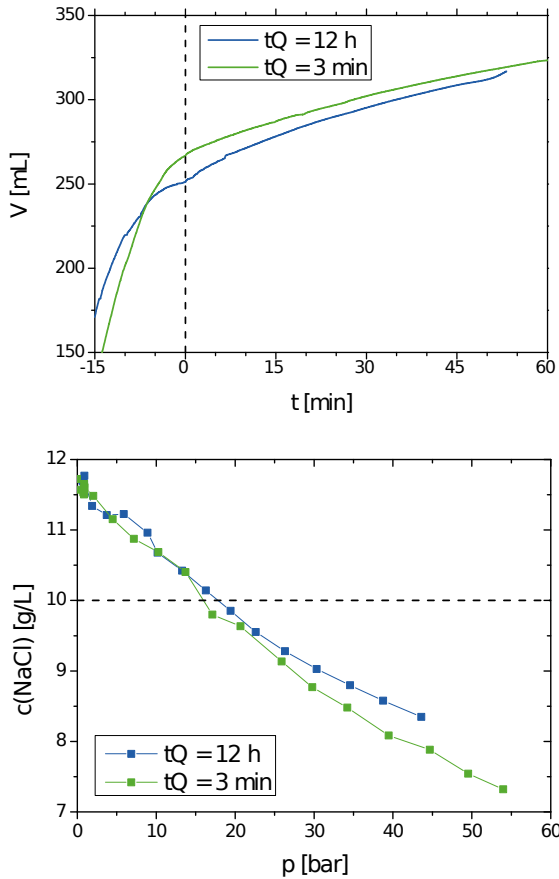


**Figure 7.4.:** Influence of swelling time  $t - Q$  on the produced volume (top) and the desalination performance (bottom) of the industrial B1110 hydrogel is shown. For the shorter swelling time a similar result is found while the concentration of the eluate at a high pressure is even lower. A linear pressure increase of 60 bar/h was used for both experiments. The vertical dashed line (top panel) indicates the zero point of the time reference. The horizontal dashed line (lower panel) gives the initial concentration of the added brine (10 g/L NaCl).

**Table 7.3.:** List of parameters that describe the desalination performance of the commercial hydrogel B1110 for variation of swelling time  $t - Q$  (upper part) and the solution ratio  $Q_{\text{rel}}$  (lower part). The former experiments were carried out with a pressure increase 60 bar/h the latter with 12 bar/h.

$t_Q$ [h]	$Q_{\text{rel}}$ [-]	$p_{\max}$ [bar]	$dc/dp$ [ $\times 100 \text{ g}/(\text{L bar})$ ]	T (Time c.) [min]	B (Slope) [h/(mL $\times$ min)]	C (Offset) [mL/h]
12	2	55	-6.11	5.23	-0.76	84.3
0.05	2	66	-6.88	2.00	-0.78	85.7
12	2	53	-8.01	4.41	-0.09	35.1
12	12	48	-8.88	5.05	-0.13	46.0

This effect can also be used in a desalination experiment under pressure. The dilution effect of the supernatant brine is investigated by two experiments for the polymer B1110. The reference experiment ( $Q_{\text{rel}} = 2$ ) is compared to an experiment with  $Q_{\text{rel}}$  of 12 for an initial salt concentration of 10 g/L.

The change of  $Q_{\text{rel}}$  has an influence on the salt concentration of eluate only but not the volume (**fig. 7.5**). The received volume is larger for  $Q_{\text{rel}} = 2$  in the beginning but the difference vanishes over time. The difference is not large and probably an artefact of the experiment: for the  $Q_{\text{rel}} = 12$  sample a large amount of solution was needed (more than 4 L) and some loss is possible. This effect is also seen in the flux given by the fit parameters in **tab. 7.3** (lower two rows) which are quite similar anyway. A clearer picture is seen for the concentration data. In the beginning the same concentration was received as for the static distribution experiments shown in fig. 6.12 (p. 176) for values of  $Q_{\text{rel}}$  of 2 and 12. Here, the concentration for  $Q_{\text{rel}} = 12$  is always lower than in the standard experiment. The difference is decreasing from 1.4 to 0.9 g/L over the course of the experiment. This results in a

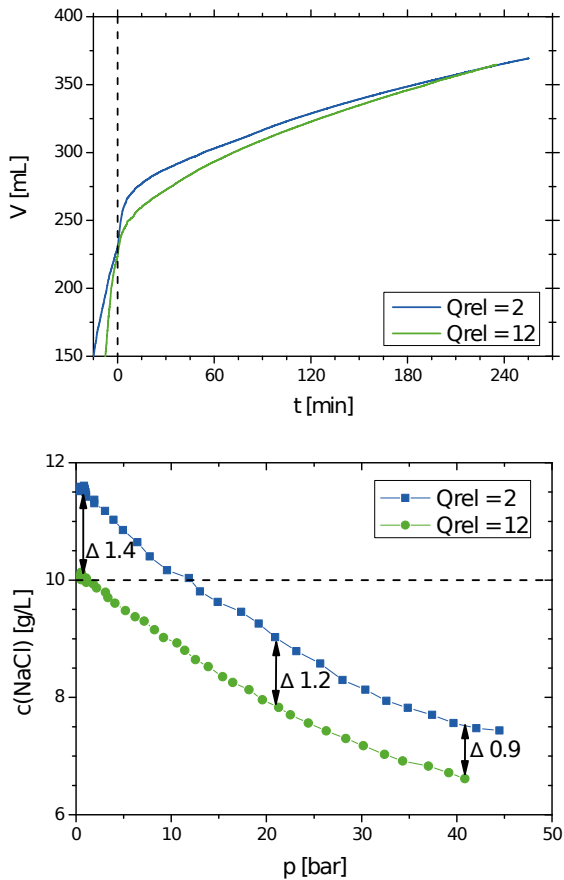


**Figure 7.5.:** Influence of the amount of supernatant phase with respect to the gel ( $Q_{\text{rel}}$ ) on the produced volume (top) and the eluate concentration as a function of pressure (bottom) of the industrial B1110 hydrogel is shown. The desalination capacity is much higher when an excess of brine solution is used. For the experiment  $Q_{\text{rel}} = 12$  only the volume is shown that was filled into the press. The better part of the supernatant solution was discarded beforehand. The vertical dashed line (upper panel) indicates the zero point of the time reference. The horizontal dashed line (lower panel) gives the initial concentration of the added brine (10 g/L NaCl).

higher value for the slope  $dc/dp$  for  $Q_{\text{rel}} = 12$  (in tab. 7.3). The use of a large excess of supernatant solution always fosters a better desalination result. However, large quantities are more difficult to handle and the excess must be available in the process. This is the case for a first step using seawater but maybe not for the subsequent ones.

### Influence of brine concentration

The desalination process using hydrogels is only of importance if it can be used for the better part of the region of interest of salt concentrations. This region is usually  $0.1 - 35 \text{ g/L}$  ( $\text{NaCl}$ ) for seawater desalination or  $1 - 15 \text{ g/L}$  for the treatment of brackish water or other applications [Gerlach94, Khawaji08]. The theoretical treatment of the underlying effect by the Donnan approach (sec. 2.1) shows that the effect is present for any concentrations of ions involved. However, the largest effect is to be expected for highly charged gels in brine solutions of low electrolyte content. With a given gel, the performance should decrease with increasing initial brine concentration  $c_s$ .

The effect is estimated by performing the desalination experiment with three different brines of  $c_s$  of 3, 10, and  $35 \text{ g/L}$   $\text{NaCl}$ . The sample ratio was held constant at  $Q_{\text{rel}} = 2$  but different amounts of polymer are needed to achieve this. This is an effect of smaller  $Q_{\text{eq}}$  in highly concentrated brines. For the polymer B1110 values of  $Q_{\text{eq}}$  of 34.1, 23.1, and 14.0 g/g for 3, 10, and  $35 \text{ g/L}$  were measured, respectively. The polymer amount was adjusted and otherwise the experimental procedure obeyed.

In all experiments the desalination was possible, however, to a different extend. The obtained volume was much smaller for the case of  $35 \text{ g/L}$  (not shown). Also the flux, given by the fit constant C, is lower for higher  $c_s$  (tab. 7.4). This is probably a result of the much higher polymer content of the gel sample. With more polymer per unit volume the sample has higher modulus as was shown in sec. 3.3 and needs a higher force for the same

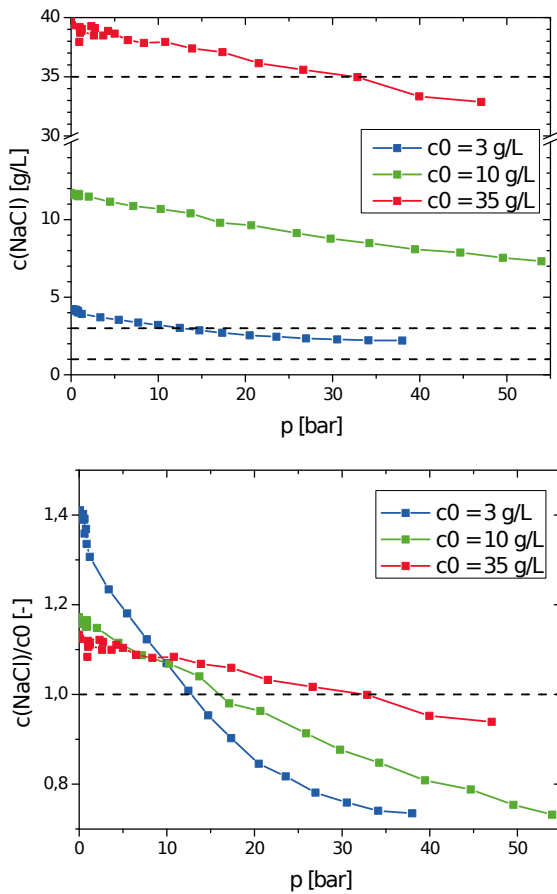


**Figure 7.6.:** Influence of the initial salt concentration  $c_s$  on the eluate concentration as a function of pressure is shown. On top, the nominal concentration is given and at the bottom the relative concentration  $c/c_s$ . A linear pressure increase of 60 bar/h was used. The horizontal dashed lines give the initial concentration of the added brine (3, 10, 35 g/L NaCl) respectively.

**Table 7.4.:** List of parameters that describe the desalination performance of the commercial hydrogel B1110 for different initial brine concentrations. The experiments were carried out with a pressure increase of 60 bar/h and a swelling time of 3 min.

$c_s$ [g/L]	$p_{\max}$ [bar]	$dc/dp$ [ $\times 100$ g/ (L $\times$ bar)]	$\frac{d(c/c_s)}{dp}$ [ $\times 100$ / bar]	T (Time c.) [min]	B (Slope) [h/(mL $\times$ min)]	C (Offset) [mL/h]
3	57	-2.79	-0.93	0.70	-1.4	126
10	66	-6.88	-0.69	2.0	-0.78	85.7
35	70	-13.7	-0.39	3.4	-0.66	63.5

compression. The concentration dependence for the samples is given in **fig. 7.6** in the upper part. A strong reduction in absolute concentration is found for 35 and 10 g/L experiments and a much lower one for 3 g/L. Also the highest slope  $dp/dt$  value is found for 35 g/L (tab. 7.4). This order is reversed when the relative concentration change  $c/c_s$  is considered instead. The strongest decrease is now seen for 3 g/L as shown in fig. 7.6 in the lower part and the corresponding slope in tab. 7.4. The desalination technique works over the whole range of interest. For a high brine concentration the low gel capacity and high modulus decrease both obtained volume and desalination capacity. In absolute terms less salt is removed, the lower the brine concentration is.

A number of process parameters was investigated in this section and none of them is a deal breaker for the process. They rather offer a large potential for optimisation. The desalination capacity of a gel is not reduced when a steeper pressure profile is used. Fast deswelling is possible and this parameter can be adjusted to the needs of the process. The swelling time of the sample can be reduced to the order of minutes, the desalination capacity is then even higher compared to a longer standing sample. Therefore, a high

turn-over of water by fast swelling and deswelling is possible. Here, the constructed press is the limiting factor for the turn-over. The more brine solution is mixed with the polymer, the better is the desalination performance as the salt excess in the supernatant solution is diluted. If the process permits it, this is beneficial. The process does work for all salt concentrations of interest, however, large concentrations introduce several limiting factors. Yet, some experimental factors have not been investigated so far, for example the particle size or size distribution. It is expected, that smaller particles enable a faster process while a broader size distribution would reduce the inter-particle voids. Also the process remains to be evaluated with real seawater. All the collected information can now be used to formulate a model of the processes happening inside the press during an experiment.

## **7.2. Discussion of the separation process by a hydrogel under pressure**

The rich amount of informations collected on the behaviour of hydrogels under pressure is used to understand the processes in the hydrogel sample deswollen under pressure. The information was compiled by investigation of hydrogels of different composition and by external conditions under which desalination was performed. On this basis a model can be developed that explains the qualitative behaviour found in the experiments and also the quantitative trends of the different samples. Within this model the macroscopic process in the sample are explored and used to evaluate the samples at hand.

The sample, when it is filled into the press setup, is compromised of the gel beads and the surrounding aqueous salt solution (brine). The polymer particles are highly swollen and contain more than 90 wt.-% water for experiments reported here ( $Q > 10$ ). The mobile ions (added salt) are distributed between the gel and the solution phase. In the surrounding solution

the concentration of mobile ions is always higher than inside as was shown in section 2.1.

Before the gel phase is introduced to the press setup the surrounding solution cannot be separated completely. By decantation, filtration or even centrifugation only part of it is removed. The part of the solution attached to the surface of gel beads and present in the inter-bead capillaries cannot be removed. The voids between the beads are a result of the packing. Usually, it is not possible to fill all of volume by packing particles. Therefore some 30 vol-% are filled with liquid of the surrounding phase. As a result, in the presented experiments, only the part of the supernatant solution was removed that was easily separated. The major part of the brine is discarded. The rest was filled into the press with the gel. Thus, at the beginning of a desalination experiment under pressure the average salt concentration in the whole of the sample is still close to the initial concentration but with unequal distribution between the phases. Therefore, a change of eluate concentration must be observed when the different phases are probed.

In the beginning of a desalination experiment the applied pressure is low (e.g. 1 bar) and only loosely bound solution is removed. This is part of the supernatant phase (**fig. 7.7 left side**). It is removed with a high flux. The recorded concentration is constant in this region and close to the concentration of the supernatant phase. This was found when probing the sample in a static mixing experiment without pressure (see e.g. sec. 6.1). Therefore, it is assumed, that this first solution to leave the setup is the supernatant phase of the mixture. This region usually lasts until the pressure is increased above 2 bar. In this state the gel is usually still in equilibrium with the surrounding solution as the inter-bead capillaries are still open.

When a loading is applied to the gel the remnants of the supernatant phase are removed and the gel starts to deswell. Not all of the supernatant phase has been removed by the low pressure. The gel is already deswollen by a small pressure as it was in the free equilibrium before. Therefore a mixing of water coming from the both phases is observed (**fig. 7.7 middle**). In

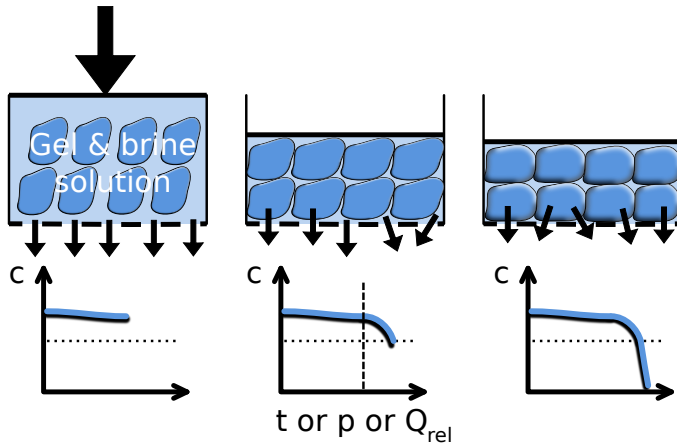


**Figure 7.7.:** Schema of the process of the water release from a gel sample under pressure. The upper row shows the process within the press and in the lower row the resulting change of the concentration of the eluate ( $c$ ). The dashed horizontal line indicates  $c_0$  and the vertical one point where  $Q_{rel}$  is unity.

this region the flux is reduced drastically, as only solution is freed by deforming the gel. The flux is found to obey a linear behaviour thereafter and decreases gradually as by the same pressure increase the gel is deformed less.

The salt concentration is decreasing and passes below the one of the initial brine ( $c_0$ ). The change is gradual over time which is due to a mixing of solution from both phases. The decrease starts only after some time in the experiment at 1 – 5 bar of pressure. When considering the plot of  $c$  against  $Q_{rel}$  (see e.g. fig. 6.4) the decrease in  $c$  should start  $Q_{rel} = 1$ . At this point all of the supernatant phase is removed and desalinated water from the beads is received. Yet, the concentration drop is observed only beyond 0.95 or even 0.9. This is an argument for the mixing in the capillaries. The mixing can also occur in the drainage, especially in the sieve elements and the groves beneath. This dead volume is in the range of 12 mL within our current setup.

When the pressure is raised further the gel is deswollen and the concentration is decreasing. In this region an almost linear decrease of  $c$  against  $t$  and  $p$  is seen which is an analogy to the linear increase of the osmotic pressure of a salt solution with its concentration. Also the employed fit to gain  $dc/dp$  is well justified. In this region water is now released from the gel (see **fig. 7.7** right). The flux is low and follows the same dependency. Thereby an effective desalination of the sample is achieved.

This information can be used to draw conclusions about the salt concentration of the solution leaving a gel bead at a certain time during the experiment. If the gel releases water with the average concentration found inside the beads (e.g. 70 % of  $c_0$ ) it should not show a steady decrease but rather level off to a constant  $c$ -value from a point of e.g.  $Q_{\text{rel}} = 0.7$ . This is not the case rather the constant decrease is seen and suggests that the concentration of the solution released from the gel is also changing gradually. This suggests, that the argumentation given in the first chapter is true. The charge density inside the gel increases when it is compressed (charge density  $\propto \sqrt[3]{V}$ ). If considering this state under pressure to be still in equilibrium, then a higher polymer volume fraction is found and less salt in the gel. The salt rejection curve presented in fig. 2.2 is now probed at a higher value of  $v_2$  and the salt rejection from the gel is stronger. When reducing the swelling in the gel, the system moves along the line to higher  $v_2$ -values and therefore stronger separations.

This argumentation is also supported when considering the desalination experiment after a short swelling time. The salt rejection from such a gel was found to be better. The equilibrium salt concentration in the gel is build up over time when it swells. Therefore a non-equilibrium state of swelling can be beneficial as the salt concentration in the gel is still lower. These findings support the mechanism proposed in the first chapter.

The same line of argumentation can be used to distinguish between the individual samples investigated in chapter 6. As argued in the conclusion of this chapter only the charge density inside the gels controls the rejection

not the specific chemical structure, if no specific interactions are present. Therefore, as a function of the synthetic parameters the plateau value of salt concentration as well as the slope of decrease are influenced. A higher charge density, that is lower swelling, results in a higher plateau but also a stronger decrease. The flux is mainly a function of the capacity of the gel. At a high capacity less polymer is found per unit of gel and less force is needed to deform it.

An interesting feature is found in the concentration data of some samples. The usually linear decrease of the concentration is levelling off to a almost horizontal slope at high pressure. This is especially obvious when the concentration is plotted as a function of pressure (see e.g. fig. 6.7 or fig. 6.11). This effect is rather present in softer samples and for harder samples only at a very high pressure. This leads to the conclusion, that the onset of the collapse of the capillary structure between the gel beads is seen. When the inter-particle voids collapses, the water freed from a gel particle has no immediate path to the outlet. These particles far from the sieve are no longer in equilibrium with the solution phase beyond the sieve. However, a particle close to the sieve still is. In other words the time needed for the eluate to reach the outlet becomes a function of the place in the filter cake. Thereby a back-mixing within the gel filter cake is observed. Water freed at a lower pressure contains more salt but before it reaches the outlet also water at a higher pressure containing less ions is freed. These are mixed giving a higher than expected concentration in the product.

It is thus beneficial for a gel to retain the inter-particle voids at higher pressure. This property is usually the absorbency under load (AUL). Especially particles with additional surface cross-linking show this feature and this is probably the reason for the good desalination performance of the polymer B1110. The flux is high even under load and no upturn in concentration is seen for this sample. B1110 also performs better than pAAc-DC1 which has the same average cross-linking degree as determined by LF-NMR and swelling experiments (see figs. 4.19 and 3.6).

On the basis of the charge density and its change during a desalination experiment can be well understood. The synthetic parameters are chosen optimal when they give a high charge density, chemical characteristics don't matter at first approximation. The process parameters are optimal when the amount of added salt is small (low  $c(NaCl)$ , high  $Q_{rel}$ ) or when the external salt cannot enter the gel kinetically (low  $t_Q$ ). Yet the quantitative behaviour can only predicted on an empirical basis so far and not from the microscopic structure of the gel. To achieve a complete predictability a closer investigation of the Donnan approach might be helpful. However, it is bound to fail when the gel is strongly compressed and the charge density is very high. Another solution would be computer simulations of the system (see conclusion of this chapter p. 206). By placing the hydrogel in contact with an ion reservoir, its salt uptake can be monitored as a function of swelling volume. The nature of salt rejection and distribution could be evaluated on a molecular level.

### 7.3. Estimation of energy consumption

Seawater desalination is an energy intensive technology [Busch04, Shannon08]. The energy costs are a major economic factor and add considerably to the operating costs of a desalination plant. Energy is always needed to separate salt from water as it is an endergonic process. In practice the energy consumption is an important criterion for the economic importance of an individual desalination technology. Therefore, it is prudent to give at least an estimate of the energy demands of the desalination by gels. The new press setup, described in chapter 5, was designed to yield pressure and volume information for this purpose. The energy demand is calculated from the data in two steps, first the consumption for a single experiment is calculated from the known data which is then extrapolated to a comparable

quantity (energy per m<sup>3</sup> freshwater) for the full desalination of water.<sup>2</sup> The obtained values are compared with other existing technologies and the theoretical limit.

In the first step, the energy used in a desalination experiment is calculated from the applied pressure and the produced volume. The energy spend is assumed to be equal to the volume work of moving the eluate volume past the separation layer at a certain pressure. Both, the volume and pressure data were acquired as a function of time as given in section 5.2 for the samples described in this chapter and the previous one. The volume work can be defined as the integral below the *p*-V-curve. An example of this data is given in **fig. 7.8** for the industrial polymer B1110 in an standard experiment (see sec. 6.1). The data of Test4 was replotted for this purpose from p. 177. The plot shows, that most of the volume is produced by a very low pressure and little energy is needed, only when the pressure increases to force water from the gel more energy is required.

The obtained volume work values cannot be compared between experiments done with different samples or conditions. They are neither normalised to the produced volume or the salt concentration found in the eluate. For a judgement on the desalination efficiency by a normalised quantity the amount of energy spend for a certain salt reduction is calculated. The desalination effect is taken to be the amount of salt removed from the eluate during the process (7.1). It is calculated for the desalinated part of the sample only, which are all fractions of volume  $V_n$  and  $c_n$  that were received with a concentration below the initial concentration  $c_0$ .

$$\begin{aligned}\Delta m(\text{NaCl}) &= m(\text{NaCl, initial}) - m(\text{NaCl, fractions}) \\ &= c_0 \cdot \sum_n V_n - \sum_n c_n \cdot V_n\end{aligned}\quad (7.1)$$

---

<sup>2</sup>The evaluation was partly performed by Mr. Julius Albrecht under the supervision of the author.

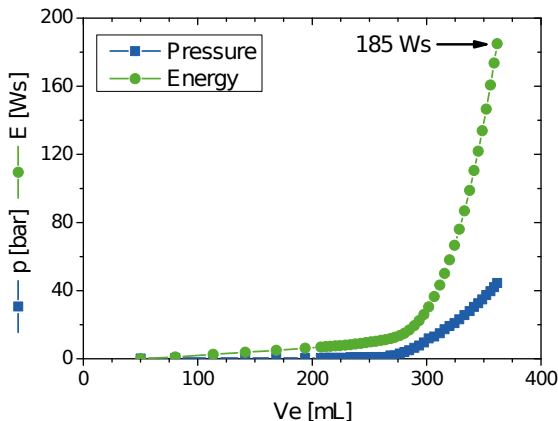


**Figure 7.8.:** The volume work is estimated for a standard experiment of industrial polymer B1110 (data replotted from Test4 p. 177). The blue curve gives the  $p$ - $V$ -data and the green curve the numerical integration of the area under the  $p$ - $V$ -curve up to this point. The energy is obtained on the same scale and given in  $J = Ws$ .

This salt reduction  $\Delta m(\text{NaCl})$  can be normalised to the spend energy in volume work  $E$  by (7.2) to obtain the ratio  $\kappa$  which is the energy needed to remove one gramme salt from a solution. The lower the value the better is the efficiency.

$$\kappa = \frac{E}{\Delta m(\text{NaCl})} \quad (7.2)$$

For the above shown example of polymer B1110, salt removal was calculated to  $\Delta m(\text{NaCl}) = 86 \text{ mg}$  is calculated from the concentration data which converts to  $\kappa = 2.15 \text{ kWs/g}$ . This value can be calculated for all samples under investigation. The results are shown in **tab. 7.5**. However, the maximum pressure for which the last fraction was received was not the same in all experiments. This might reduce the comparability of the results. Most experiments were conducted until an endpoint between 40 – 50 bar.

The lowest  $\kappa$  value is found for the industrially produced gel B1110 with the samples of DC = 1-mol-% being a close second. There is no clear

**Table 7.5.:** Estimated values of energy consumption for seawater desalination for self-synthesised and industrially produced hydrogels. The energy in  $W_s = J$  is the volume work,  $\kappa$  and the energy, in kWh per cubic meter of desalinated water, are calculated according to (7.2) and (7.3), respectively. For all self-synthesised gels a value of  $DN = 75$  mol-% was used.

Sample	$p_{\max}$ [bar]	E [Ws]	$\kappa$ [kWs/g]	$E_{m^3}$ kWh/m <sup>3</sup>
pAAc-DC0.1-Q4	30.0	212.4	8.36	81.3
pAAc-DC1-Q4	41.6	213.3	2.69	26.1
pAAc-DC5-Q4	51.0	156.7	2.93	28.5
pAAc-DC1-Q2	53.7	228.8	2.71	26.4
p(AAc-co-HEMA)-DC0.3-Q4	50.0	253.1	3.33	32.4
p(AAc-co-HEMA)-DC1-Q4	53.3	245.2	4.10	39.9
Luquasorb B1110	44.5	185.0	2.15	20.9
Luquasorb 1030	24.7	127.9	8.52	82.8

trend in the samples with different DC values, as a medium cross-linked sample exhibits the lowest energy consumption. The influence of the reference state ( $Q_{syn}$ ) is found to be small for the two samples investigated. As an overall result the trend upholds: a better performance is found for low swelling capacities and high rejections. Yet, a trade-off is found as the lowest swelling sample with  $DC = 5$  mol-% also needs a high pressure to be deformed while exhibiting the lowest degree of swelling. The B1110 gel seems to profit from the form stability and good AUL discussed in the previous section. It is the best candidate but rather due to kinetic reasons. No experiment conducted in this work reduced the salt concentration from sea-water to fresh water level (e.g. 35 – 0.1 g/L  $NaCl$ ). Therefore, the results gathered in the typical concentration range (12 – 7 g/L) are used for a prediction of the entire range of interest. The  $\kappa$  value is assumed to be valid for the entire range necessary for desalination and for any amount of salt.

The energy consumption of a seawater desalination process is customary given in needed energy per cubic meter of produced fresh water (in units of kWh/m<sup>3</sup>) [Shannon08, Fritzmann07]. This value is calculated under the above assumption by removing 35 kg of salt (from 1 m<sup>3</sup>) with the energy cost of  $\kappa$  by (7.3). In the case of the B1110 experiment discussed before this would amount to 21 kWh/m<sup>3</sup>. For all samples the values are given in tab. 7.5.

$$E_{m^3} = \kappa \cdot \frac{35\,000}{3\,600 \text{ s/h}} \quad (7.3)$$

The theoretical lower limiting value for  $E_{m^3}$  is given by 0.7 kWh/m<sup>3</sup> for any of the standard methods [Shannon08]. Though, in current literature it has been argued that smaller values might be possible in specialised forward osmosis (FO) processes using drawing agents which decompose at low temperatures [McCutcheon05, Cath06].

In practice, however, this value can't be reached but the technologies and types of realisations differ in their consumption. A lower requirement is a proof of quality and marketability for an installation [Busch04]. It is one of the main criteria to rate it. In the literature there is some ambiguity whether some discussion if energy consumption figures should enclose the energy costs for pre- and post-treatment of the water or the direct desalination only. Nevertheless, in practice values between 2 and more than 10 kWh/m<sup>3</sup> are found on an industrial scale [Shannon08, Fritzmann07, Busch04]. The best values are found in modern reverse osmosis plants (RO), while distillation processes are usually more energy intensive. The values found in practice also dependent on the size of the installation as well as the level of sophistication (e.g. energy coverage).

The estimated values for the desalination process via hydrogels of 20 – 80 kWh/m<sup>3</sup> are a very promising result. The best candidates would only use factor of 10 more energy than competitive large scale realisations of RO. Only a factor of two is found when compared to applications on a smaller scale. Considering the very small scale of the current setup and

the short development time this is promising. The level of sophistication of the current implementation is still low and easy changes discussed in the next chapter can increase the efficiency further. Yet, these results need also to be treated with caution as they are based on several approximations. It was shown that the approach via gels is possible over the entire range of salt concentrations but the energy efficiency might be smaller in some parts of this range. Also the requirement to run several consecutive steps might have adverse effects. In this result energy costs for pre- or post-treatment aren't included which might be larger in a hydrogel based approach than for the competing technologies. Also, it should be noted that the pressure data used for the energy calculation is recorded directly at the sample. At last, the pressure actually applied by the press is larger by 10 – 20 % as first investigations showed, probably due to friction at the sealings.

## Conclusion

The proposed desalination process is not met by serious operational limitations and shows a promising energy efficiency. All technical aspects under investigation do not limit the operational range or the possible realisation in a larger scale of the proposed desalination method. By most operational parameters it is possible to increase the desalination capacity of a given gel sample. The pressing speed does only hamper the desalination performance at very high values (above 60 bar/h) which allows for a fast desalination experiment (below 30 min). By the shortening the swelling time and using an excess of brine lower salt concentrations, by 0.5 and 1 g/l, respectively, were received in the experiment. It is not only possible to perform the desalination experiment in a very short time, also the performance is better when the sample is only swollen shortly. The desalination is possible in the entire range of interest of concentration with relative best performance for low brine concentrations.

ch:build

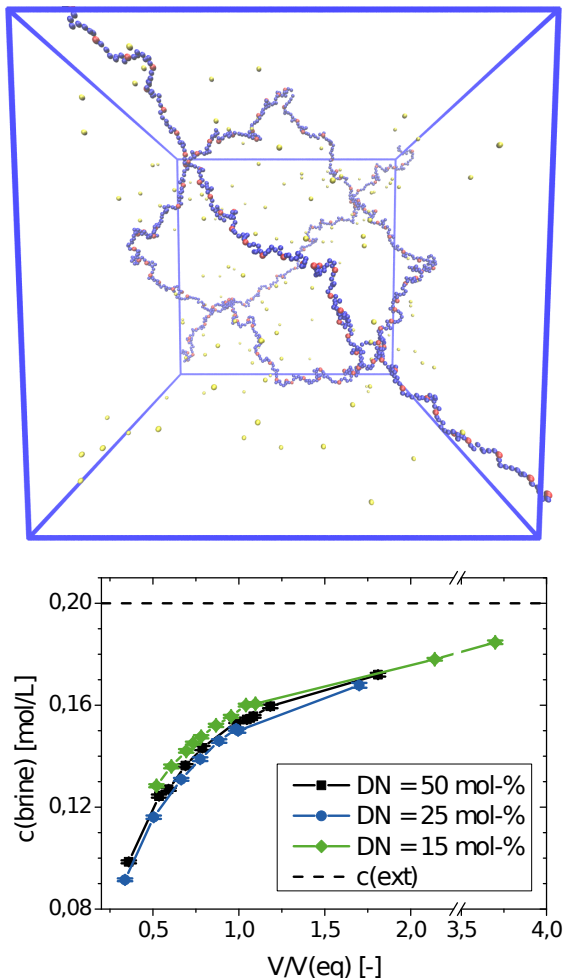


**Figure 7.9.:** Example of a possible coarse-grained simulation using the ESPRESSO package of the ion content in a hydrogel. In this case the hydrogel ( $\text{DC} = 0.17 \text{ mol-}\%$ ) is in contact with an infinite bath of  $0.2 \text{ mol/L}$  electrolyte. On top, a snapshot of the simulation is shown, including four nodes and 16 meshes in a perfect network. The ions are given as well, while the solvent is only implicitly present. Below, the salt content is given inside the gel as a function of swelling relative to the equilibrium swelling  $V_{\text{eq}}$  for different values of the ionisation of the gel.

The true salt concentration inside a hydrogel while deswelling is obtainable by coarse-grained simulations. The simulation of the hydrogel system is just in progress in collaboration with the group of Prof. Holm [Höpfner13]. The simulation is done with the ESPRESSO simulation package [Limbach06]. An example of the obtainable results is given in [fig. 7.9](#). The gel is modelled by a small box which is multiplied using periodic boundary conditions. The gel can shrink and expand due to the conditions present and the equilibrium swelling is obtained ( $V_{eq}$ ) or a specific swelling state is forced upon the gel. Here, it is placed in contact with an external reservoir of salt ions with which it can exchange them. Therefore, the salt concentration in the gel can be monitored as a function of the swelling (box volume  $V$ ) as given in [fig. 7.9](#) in the lower part. This would correspond to fixing the volume by swelling under load in the press experiment. It has to be noted, that the gel can also be forced to a volume beyond its equilibrium value ( $V/V_{eq} > 1$ ) which is not meaningful in practice.

A model was developed that allowed a qualitative understanding of the results obtained in the experiments and which processes in the setup are underlying. The influence of the gel synthesis parameters influence on the desalination capacity can be understood and can serve as a guide for future optimisation. With new setup constructed in the course of this work, it is possible to measure the energy consumption of a desalination experiment (about 200 Ws). With some assumptions it was possible to compute an efficiency value for the case of sea-water desalination (20 – 80 kWh/m<sup>3</sup>) and compare it to established methods (2 – 10 kWh/m<sup>3</sup>). The best samples studied in this work are by a factor of 2 less efficient than established technologies on a pilot plant scale. All informations have been gathered to attempt in a next step a larger realisation of the process, proposition for which are part of the concluding chapter.

## **8. State of research and perspective**

In the present thesis the idea of seawater desalination via hydrogels has been introduced and set the important step forward: from a gedankenexperiment to a real process which has been evaluated. The concept was considered from the theoretical side as well as implemented in a self-designed test setup. This permitted the investigation of the effects arising from using different hydrogels as working material and different process parameters. Many regions in this world experience water stress. Therefore, new fresh water resources need to be developed. As one step in this direction, the development of new methods for seawater desalination is currently of high interest. This interest is shown by the coverage on our newly established process by the public press (Der Standard, Neue Zürcher Zeitung, Bild der Wissenschaft, SWR broadcasting) and specialised press (VAA Nachrichten, Filtrieren und Separieren) alike.

In this chapter, first, the results of the desalination experiments as described in the chapters 5 to 7 are summarised. This information is used to answer the leading questions that were posed in the first chapter about the feasibility and the energy estimate. However, not all parameters that do influence the desalination performance could be assessed in the present thesis. Therefore, in the following, still open points and new questions which did arise, are presented. An educated guess is made as to what measures, open questions, and drawbacks could be tackled in future. Finally, the possibility of a scale-up of the present setup to a larger scale is discussed. This includes the technical realisation, the type of process, and the possible energy consumption.

## Progress made in the present thesis

In the present work, a series of steps were undertaken to answer the leading questions on the new desalination process via hydrogels. First, a set of chemically different hydrogel samples was assembled. They were either self-synthesised or of commercial origin. The materials were consequently characterised to obtain their basic properties relevant for the desalination process. The standard methods in hydrogel analysis were used, namely the determination of equilibrium swelling, mechanical modulus, and sol content. Additionally, the structure was investigated on the microscopic level by more sophisticated methods. The desalination process is implemented by a self-constructed setup tailored to the needs of investigating the deswelling of gels under pressure. The hydrogel samples were used for desalination experiments in the specifically designed setup and the influence of the process parameters was assessed. From the experimental results a model for the desalination process can be established and the energy consumption can be estimated.

A number of hydrogel samples were produced by free radical, cross-linking polymerisation. Different values of the synthetic parameters such as degree of cross-linking, degree of neutralisation, and gel reference state were varied by changing the composition of the synthesis mixture. Additionally, copolymers of acrylic acid with other acrylic monomers were produced. For comparison commercial superabsorbers from the BASF were also investigated.

The use of standard characterisation methods showed large differences in the hydrogel properties. The solvent capacity was found to increase with longer chains and a more diluted reference state, or in terms of synthesis parameters, with a lower degree of cross-linking (e.g. DC = 0.1 mol-%) and with a higher water content of the synthesis mixture (e.g.  $Q_{\text{syn}} = 8 \text{ g}$  water per g monomer), respectively. The number of charges has only an influence at very low neutralisation degrees below 30 mol-%. With an increase of the solvent capacity the amount of extractable polymer in a sample rises

---

as well. Typical values for the sol content are in the order of 10 wt.-%. The speed of solvent uptake is high. When small beads (e.g.  $\varnothing$  200  $\mu\text{m}$ ) are used, the equilibrium swelling is reached within minutes. The modulus was found to follow qualitatively the theoretical prediction (sec. 3.3): it increases with the number of chains, which is proportional to the degree of cross-linking. In contrast, it is reduced when more water is incorporated into the specimen. The modulus values can be used to calculate the real average mesh length in the networks by utilising the statistical theory of networks. Typically, a few 100 monomers are found in one chain. By comparing the mesh length obtained from mechanical measurements with a prediction based on the composition of the reaction mixture it is proven, that the meshes are much longer than predicted. In other words, the cross-linking process offers a quite low efficiency, only around 20 % of possible junctions are elastically active.

Two less used techniques were employed and further developed to gather information about the pore size distribution (PSD) in hydrogels. In a proof of principle experiment, the so-called solute exclusion method was successfully applied to two gels of different cross-linking degrees. It could be shown that in both gels a broad PSD exists. The medium pore size is much larger for a lower degree of cross-linking as implied by simple statistical considerations. As a second method, the low-field NMR-spectroscopy (LF-NMR) was employed. The mobility of the network chains between the junctions is directly related, on the one hand, to their length, and on the other, to the relaxation times and residual dipolar coupling found in LF-NMR. Thereby, it was possible to reproduce the trends found in swelling and mechanical experiments and to add a measure of dynamic heterogeneity to the mean values. This approach works particularly well with the commercial core-shell sample. By additional treatment of the surface a denser shell on a particle is produced. The analysis of residual dipolar coupling (RDC) constants was the only method which able to give an estimate of the PSD in both domains independently and directly.

## 8. State of research and perspective

---

The test of the desalination process needed a press system to separate water from the polymer beads while measuring the parameters controlling the process. This setup was self-designed and was implemented with several key features: a capacity of 0.5 L, two large sieve elements to separate water from the gel beads, and data acquisition with three online, highly accurate sensors. One sensor monitors the pressure in the gel in a range up to 100 bar with  $\pm 0.01$  bar accuracy. The other two record the volume flux from the setup, measurable down to 1 mL/h and the salt concentration in the entire range of interest with an accuracy better than 0.1 g/L.

Conducting desalination experiments with tailored, self-synthesised samples allowed for the assessment of the influence of the most important parameters that define the properties of a hydrogel. The ion rejection and desalination capacity are controlled by the synthesis parameters as discussed above. These parameters are the degree of cross-linking, the degree of ionisation, and the reference state, as well as the copolymerisation with other monomers. It was clearly established that the salt rejection increases with the charge density in the gel as predicted by the Donnan type treatment. The charge density inside the gel can be increased easily by a reduction of solvent capacity. This is done either by an increase of DC or a decrease in  $Q_{\text{syn}}$ . Both predicted trends are also found in the experimental results. A strong increase in desalination capacity is found for higher DC and a weaker one for lower  $Q_{\text{syn}}$ . In contrast, all changes that did not influence the solvent capacity of the resulting gels did not improve the desalination capacity, as shown for the degree of neutralisation or the addition of comonomers beside hydroxyethyl-methacrylate (HEMA). From the set of commercial superabsorbers, the sample with additional surface cross-linking (B1110) did show a good salt rejection and also a high flux under the application of pressure.

The investigation of the technical parameters of the test setup did prove that the new desalination process is feasible. Hydrogels can be used in the

---

whole range of salt concentrations of interest for seawater desalination (35 to 0.1 g/L). The effect was measured and allows up to 40 % removal of salt in one experiment as compared to the initial solution. Therefore, more than one step is necessary, their number being about seven for the current state of development (40 % reduction per step down to 1 g/L). The time it takes to swell the gel is very short and even after a minimum swelling time, 3 min for the industrial sample B1110, the same desalination performance is realised. The speed with which the gel is deswollen, i.e. the increase of pressure in the system, can be high. Even if the deswelling is carried out within 30 min, desalination is possible and the received salt concentration is only slightly different from a slow process (12 h). This leads to the conclusion that a cycle time of half an hour should be possible.

A model of the desalination process based on considerations of charge density was developed. It is able to explain the form of results found in salt distribution and desalination experiments. The trend given by the synthetic parameters is also explained well. The energy consumption of a single desalination experiment is calculated from the measured data and extrapolated to the energy cost of the complete desalination of seawater. In this work, energy consumptions of 20 – 80 kWh per m<sup>3</sup> of fresh water are calculated. When compared to established technologies (2 – 10 kWh/m<sup>3</sup>) this is a promising result considering the early stage of development.

## **Further problems and challenges**

The desalination is possible with the proposed method, however, the efficiency has to be improved further. An even smaller number of necessary desalination steps to remove all salt and a continuous process would be beneficial. This needs a better desalination capacity of the employed working material in each step. Yet, possibilities for further improvement seem limited without greater change in the network architecture. As already mentioned, the difference between charge density inside the gel and

## 8. State of research and perspective

---

outside is important. When the concentration of added salt is high, the rejection from the gel is rather poor in the examples provided in this work. However, the logical consequence to increase the charge density further is met by serious obstacles. A higher charging of the polymer doesn't seem possible. The monomer sodium acrylate already has one chargeable group per three C-atoms and the number of effective ionised groups cannot be increased further. Beyond a degree of neutralisation of 30 mol-% the effective charges are reduced by counter-ion condensation. A further decrease of the gel capacity by increase of DC or decrease of  $Q_{\text{syn}}$  is not possible in the current system due to the limited solubility of the cross-linker. Progress over the samples presented here with the current synthesis method is doubtful. Even worse, a reduction of capacity means, that more polymer is needed and more pressure needs to be applied to deswell it.

Further improvement on the side of the gel is only possible by a change in the network architecture. The introduction of polymeric material that possesses charges but does not add to the elastic response is necessary. This could be done by an increase in sol content which is, however, not advisable due to reasons discussed later. The addition of elastically inactive dangling ends and rings could be one possible avenue which could be explored. Yet, this is difficult to control synthetically. In general, an inhomogeneous network should offer a better performance as the mechanical response is smaller but the same amount of charges can be accommodated. Another possibility is the use of an interpenetrating network where the second network is less densely cross-linked. The first network provides the structure and the degree of swelling while the second network only adds material without increase of modulus or the sol content.

The extractable polymer (sol) can be a hazard to safe drinking water if leaked in the desalination experiment. The sol is produced alongside with the gel and present inside the gel. It can leave the gel when the eluate is pressed out. Being composed of poly(acrylic acid) it is not a strong health hazard in the product water as it is non-reactive and used *in vivo* for e.g.

---

drug delivery but it is unwanted nevertheless. This effect can be reduced by optimising the polymerisation process; something which has been achieved before for industrial samples. Another way is to wash the residual sol from the polymer prior to use or in a few dummy cycles in the start up phase. As the sol is distributed equally in gel and solution phase it can be reduced to trace amounts in the gel in very few cycles with a large solution phase present.

The reuse of the gel samples is not met with adverse effects in the presented experiments. Yet, eventual failure is probable, only the number of cycles before the failure is unknown. Also the growth of bacteria and algae on the material could be a problem, but was not investigated in the scope of this work. Divalent ions, in the case of this work cations, are known to enrich in the gel and reduce its swelling capacity drastically which would impair the material. Yet, the kinetic swelling investigations showed that the adverse effect is only visible after 30 min in which the gel can already be processed. If this accumulates to a bigger problem in the long run remains to be determined.

Theoretically, the proposed desalination mechanism works better the lower the salt concentration is. Indeed, it does work reasonably well with small to intermediate concentrations (0 – 10 g/L) but less for higher ones. This method is therefore proposed rather for the cleaning of brackish or waste water. However, a lower salt content is to be preferred in all desalination methods due to the reduced energy costs.

### **Perspective of a larger scale**

The setup presented in this work was meant as a tool to asses the basic parameters and fundamental questions of the desalination process not as a model for a larger scale realisation. The current volume of 0.5 L does not serve the purpose of direct utilisation; there are parameters which need to be improved. An increase of capacity is needed as well as the possibility to

## 8. State of research and perspective

---

operate it in a continuous process in contrast to the current batch mode and a discussion of the way the gel is pressed out.

In the next implementation of this process, the scale should be raised to a test station with a capacity in the range of 10 to 100 L capacity. Thereby, the problems arising from small quantities will reduce or vanish and the energy estimate is based on more stable data. In the same step, the filter area should be increased and a final design should be found and tested. Only after this intermediate step, the setup size could be raised by e.g. a factor of 100 to a pilot scale plant. The points that need consideration in both stages are the feasibility in that scale, the energy consumption and recovery, as well as the question of how to implement several desalination cycles in one setup. The process would benefit from running continuously or at least in a semi-continuous batch mode where automatically at the end of one batch the next one is inserted. This would facilitate the use of a continuous source without too much storing and also a continuous feed, that is easier to handle. However, in many applications this would not be of the highest priority, as the water usually easily stored.

At last, two possible realisations of the process in a greater scale are presented. Even though they are concepts it is worthwhile to asses their pros and cons as a stimulus for further work. All realisations will have to use several stages of desalination at different stages of salt concentrations.

As a first possibility the current design frame could be maintained with a cartridge of gel that is pressed out over a sieve with a piston. An increase of the filter area could be achieved, by using a sieve basket instead of flat sheets at the top and the bottom. Thereby, the eluate could leave at all sides of the cartridge. Another possibility would be the introduction of active sieve layers into the cartridge in a sandwich type stack. These inlays would have flat sieves at the top and at the bottom and an outlet at the side, reducing the height of gel above the sieve for each inlay. An increase in the diameter of the sieves would also be advantageous as the water can more easily leave and also the gel height above the sieve could be reduced at

---

the same capacity. However, thereby the necessary force would be drastically increased which posses a problem to the employed press. To generate a higher force would drastically increase the acquisition costs of a suitable press. The problem of multiple stages can be solved as well. The use of different presses for all stages would lead to very high setup costs. However, by using several cartridges in a drum type magazine the same press could always be used on different cartridges and the product of one carried over into the next stage. At last, in terms of reducing the energy consumption of the process the exchange of pressure is to be considered. The swelling pressure of a gel in one cartridge could be transferred to another, there used to deswell partly another gel in the process. The pressure at the end of one cycle can be exchanged with the next step to minimise the energy loss.

For separation problems of the type under discussion, solutions are already known which might be applied here. As a second possible realisation, the chamber filter press might be suitable [Marinetti09]. This accordion type setup uses several (20 or more) chambers that are separated by plates and a cloth is clamped between them. When the plates are moved together the filtrate is pressed trough the cloth and the particles form a filter cake on the inside. This cake increases the filtration efficiency. When the maximal amount of filtrate is generated, the press is expanded again and the cloth is removed for cleaning. A filter press is operated in a batch mode and can apply up to 500 bar pressure.

The investigation and development of this desalination process via the constructed model press is a good vehicle to investigate basic questions about how hydrogels behave under these conditions and which features in the underlying structure are responsible. Still, the usage of such a process in a competitive environment will depend on the same criteria as any other process employed today: the feasibility, the total investment costs (space, infrastructure, build-up), and the total operating costs (energy, working material, water treatment), while the actual technology in use is less important. However, new developments may offer an improvement over the status quo.



## A. Appendix

### A.1. Polymer samples and materials

The polymer samples which were used in the investigations in this work are described in detail in this section. Hydrogel samples from sources were used: industrially produced samples obtained from the BASF and self-synthesized hydrogel samples. First the preparation procedure of hydrogels on the basis of acrylic acid is described. Next, the exact compositions of the samples that were prepared for this work are presented. Finally, industrial superabsorbent polymers obtained from the BASF and some linear, commercially available polymers with a narrow size distribution are listed.

### General polymerisation procedure

Hydrogels were produced by free radical polymerisation of acrylic monomers in water. The general considerations and the reaction schema are given in sec. 3.1 and in fig. 3.2. The synthesis is adapted from similar procedures in recent the literature [Oppermann92, Umendra99, Vervoort05]. The cross-linker *N,N'*-methylenebisacrylamide (MBA, 99+ %, Acros, Geel, Belgium) is mixed with deionised water in a three-necked round-bottom flask equipped with a magnetic stirrer and an internal thermometer. Freshly distilled acrylic acid (AAc, 99 %, Sigma-Aldrich, Steinheim, Germany) is introduced to the flask. In some cases other monomers, described below, are added and the flask closed with septa (see sec. 3.1 for details). The mixture is stirred and cooled in an ice bath to  $T \approx 5$  °C. The acidic monomer is neutralised by adding drop-wise aqueous sodium hydroxide solution (33 wt.-%, extra pure, Acros) as such the temperature does not ex-

## A. Appendix

---

ceed 12 °C during this exothermic process. The initiator sodium persulfate (SPS, 98+ %, Acros) is dissolved in 2 mL of water and added to the mixture. The solution is further cooled and purged for 30 min with nitrogen gas to remove residual oxygen. To start the reaction, the accelerator *N,N,N',N'*-tetramethylethylenediamine (TEMED, 99 %, Acros) is added and the ice bath is removed. For rheological tests part of the synthesis mixture was withdrawn with a syringe and transferred to a pre-purged mold to form the specimen. The cross-linking reaction starts when the mixture reaches room temperature, which happens within about 30 min. The reaction was let to proceed for 12 h, before the resulting clear gel was cut, dried in vacuo, and ground to the desired bead size with a mill (cooled to 15°C).

The amounts of substances used in the procedure are described in the next section. All components were used as received, except the liquid acrylic monomers which were purified from inhibitor by distillation prior to the reaction. The distillation was done for AAc at 23 mbar and 43 °C, for (hydroxyethyl)methacrylate (HEMA, 97 %, Acros) at 20 mbar and 95 °C, for methacrylic acid (MAAc, 99.5 %, Acros) at 22 mbar and 67 °C. The solid monomers N-isopropylacrylamide (NiPAM, 98 %, Carl Roth, Karlsruhe, Germany) and acrylamide (AAm, 99+ %, Acros) were used as received.

A typical hydrogel batch consisted of 0.75 mol (1 eq, 54.05 g) AAc and all other components were calculated in this respect. For a DC = 1 mol-% gel 0.01 eq (7.5 mmol, 1.16 g) of MBA are used as a cross-linker. A DN = 75 mol-% is achieved by adding of 0.75 eq (0.56 mol, 22.5 g) of pure NaOH or 50.1 mL of a 33 wt.-% solution. The initiator SPS is added by 0.002 eq (1.5 mmol, 357 mg) and the accelerator TEMED with 0.02 eq (15 mmol, 1.74 g). The amount of water is given by  $Q_{\text{syn}} = 4 \text{ g/g}$  which amounts to 16 eq (12 mol, 217 mL). It has to be noted that water is added in form of the NaOH-solution and additional water to dissolve the solid compounds.

## Overview over the produced samples

The reaction procedure introduced in the previous section offers several parameters (DC, DN,  $Q_{\text{syn}}$ , CO) that can be adjusted to alter the obtained gel. The parameters are defined in sec. 3.1. A batch is described in this work by a shorthand giving the values of all these synthesis parameters. Following the above example it would read pAAc-DC1-DN75-Q4. First the main monomer is given (AAc), next the DC in mol-%, then the DN in mol-% and at the end  $Q_{\text{syn}}$  (in g/g) is written. If a co-monomer is added its type and amount is written after the monomer as in p(AAc-HEMA50)-DC1-DN78-Q4.

A list of all samples that were produced for the tests in this work is given in **tab. A.1**. The parameters are given as the final values that were calculated from the exact additions to the synthesis mixture.

## Commercial samples

Industrially produced samples of superabsorbent polymers (SAP) were obtained from the BASF. The known facts on these samples are summarized in tab. 3.1 in 3.1. The samples were used as received and dried in vacuo at 70 °C before all experiments.

Linear polymer samples with a narrow size distribution where obtained from PSS (Polymer Standards Services, Mainz, Germany). The specifics of the pMAAc (Lot pmakit-06) reference samples were given as  $M_w = 1.3 \text{ kDa}$ ,  $3.2 \text{ kDa}$ ,  $34.9 \text{ kDa}$ ,  $76.8 \text{ kDa}$ ,  $163 \text{ kDa}$ ,  $311 \text{ kDa}$  and  $483 \text{ kDa}$  and a PDI < 1.2 for each. They were used in pore size estimation experiments and the sample with  $M_w = 34.7 \text{ kDa}$  also for LF-NMR measurements. The Dextrans (Lot dxthkit-05) used for pore size estimation were of  $M_w = 1.3 \text{ kDa}$ ,  $24 \text{ kDa}$  and  $273 \text{ kDa}$  and with a PDI of 1.23, 1.3 and 1.66 respectively. The samples were used as received and dried before the usage.

## A. Appendix

---

**Table A.1.:** List of the self-synthesised hydrogel samples: shorthands and synthetic parameters. The samples below the line contain other monomers than AAc.

Shorthand	Batch #	DC [mol-%]	DN [mol-%]	$Q_{\text{syn}}$ [g/g]	CO [mol-%]
pAAc-DC1-DN81-Q2	1	1.00	81.4	1.94	0.0
pAAc-DC1-DN84-Q4	1	1.01	83.5	3.97	0.0
pAAc-DC1-DN65-Q5	1	1.06	64.5	4.95	0.0
pAAc-DC3-DN86-Q4	1	3.11	86.0	4.06	0.0
pAAc-DC5-DN82-Q4	1	4.96	81.9	3.89	0.0
pAAc-DC0.3-DN83-Q4	1	0.30	82.6	3.90	0.0
pAAc-DC0.1-DN83-Q4	1	0.10	82.9	3.92	0.0
pAAc-DC0.05-DN82-Q4	1	0.05	82.1	3.96	0.0
pAAc-DC5-DN82-Q4	2	5.03	82.1	3.99	0.0
pAAc-DC1-DN75-Q4	2	1.04	74.9	3.94	0.0
pAAc-DC0.1-DN76-Q4	2	0.10	76.0	4.04	0.0
pAAc-DC5-DN79-Q4.2	3	5.27	79.1	4.20	0.0
pAAc-DC1-DN75-Q4	3	1.00	75.2	4.00	0.0
pAAc-DC1-DN75-Q2	2	1.00	75.1	2.02	0.0
pAAc-DC1-DN76-Q1.6	1	1.00	75.8	1.57	0.0
pAAc-DC1-DN75-Q8	1	1.00	74.6	7.97	0.0
pAAc-DC1-DN26-Q4	1	1.02	26.0	3.98	0.0
pAAc-DC1-DN50-Q4	1	1.00	50.2	3.95	0.0
pAAc-DC1-DN94-Q4	1	0.99	93.6	4.08	0.0
pAAc-DC1-DN0-Q3.5	1	1.01	0.0	3.55	0.0
pAAc-DC5-DN76-Q4	4	4.87	76.2	3.93	0.0
pAAc-DC0.3-DN75-Q4	2	0.3	78	3.9	0.0
<hr/>					
pMAAc-DC0.3-DN75-Q4	1	0.3	75	4	100
p(AAc-HEMA50)-DC0.3-DN75-Q4	1	0.3	75	4	50
p(AAc-HEMA50)-DC0.3-DN75-Q4	2	0.3	75	4	50
p(AAc-HEMA50)-DC1-DN75-Q4	1	1	75	4	50
p(AAc-NiPAM50)-DC0.3-DN75-Q4	1	0.3	75	4	50
p(AAc-AAm50)-DC0.3-DN75-Q4	1	0.3	75	4	50

## Salt solutions

Salt solutions used to simulate salt water in the desalination and swelling experiments were made from sodium chloride (99.5 %, Acros) with the addition of deionised water to gain a concentration in weight per volume (g/L) at RT. Sodium chloride was always pre-dried at 120 °C. The deionised water always exhibited a conductivity of less than 0.5 µS/cm. For some experiments part of the sodium chloride was replaced by *CaCl<sub>2</sub>* (dehydrated, > 97 %, Fluka, Steinheim, Germany) to simulate divalent cations in seawater.

## A.2. Experimental characterisation procedures

In this section the instruments and procedures are described, that were used in the characterisation of the hydrogel samples detailed in section A.1.

### Swelling measurements

For the determination of the time dependent degree of swelling  $Q(t)$ , polymer is placed in contact with a suitable solvent or solution and the weight gain after swelling for a time  $t$  is recorded. The procedure here has been adapted from previously published work [Buchholz98, Brendel99]. In detail, dried, ground polymer of the mass  $m(\text{dry})$  is placed on a sieve with the mass  $m(\text{sieve})$ . In practice masses from 20 to 100 mg dried polymer proved useful, depending on the degree of swelling. The particles should form a single layer on the sieve and enough polymer should be used, so the measurements can be carried out with good accuracy. The sieve is then placed from above in contact with DI or a brine of a certain concentration  $c$ . Thereby the gel is wetted through the sieve and can absorb the liquid. The solution volume should be in a large excess of the polymer capacity, typically a 20 times excess (with respect to  $Q_{\text{rel}}$ ) was used. The polymer is left to swell for a time  $t$ , usually at RT, and evaporation is prevented by sealing from the surrounding. After  $t$  the sieve is removed and pressed on a sheet of paper towel for 30 s to remove excess solution. It is then weighted to obtain  $m(\text{wet})$ . The swelling degree is calculated as the weight gain of the polymer by

$$Q(t) = \frac{m(\text{H}_2\text{O})(t)}{m(\text{dry})} = \frac{m(\text{wet})(t) - m(\text{sieve}) - m(\text{dry})}{m(\text{dry})} . \quad (\text{A.1})$$

### Sol extraction procedure

The sol content of a hydrogel sample is determined by washing it with an excess of deionised water (DI) and measuring the polymer content in the

extract. About 0.5 g of the dried, ground polymer ( $m(\text{PM})$ ) are mixed with DI ( $m(\text{DI})$ ) in a ratio that is about 5 times the equilibrium swelling capacity of the gel ( $Q_{\text{rel}} = 5$ ). The mixture is sealed and stirred for one week at RT. It is checked that the weight loss of water is below 1 % after this time. Then, the mixture is filtered through 5  $\mu\text{m}$  filter paper and the filtrate is weighted giving  $m(\text{filtrate})$ . It is not necessary to obtain all of the excess water, only the weight has to be determined accurately. The water is removed from the filtrate by evaporation, first in a rotary evaporator then by drying in vacuo at 70 °C and the sol content is measured as the residue mass  $m(\text{sol})$ . Assuming an equipartition of the sol in gel and solution the sol fraction by weight of the sample can be calculated by (A.2). The sol still inside the gel is counted as well with this method. The equipartition assumption is supported by the fact that after reextraction of the same gel the sol content is found to be about 1/5 of the original value.

$$\text{sol content[wt.-\%]} = \frac{m(\text{sol}) \cdot \frac{m(\text{DI})}{m(\text{filtrate})}}{m(\text{PM})} \cdot 100\% \quad (\text{A.2})$$

### Description of mechanical tests and rheometers used

The mechanical characterisation of hydrogel samples was carried out with specimen of a defined cylindrical shape in shear and compression modes. The samples were produced by the general procedure described in section A.2, but were synthesised directly in the final shape [Baselga87]. Specimen of about 30 mm cross-section and 10 mm height were obtained by the use of screw-caped molds (PP material, from Carl Roth, Karlsruhe, Germany).<sup>1</sup> At the time of synthesis the molds were pre-purged with  $N_2$  gas for 5 minutes and about 8 mL of the final reaction mixture were transferred from the reaction vessel to the mold with a syringe. The reaction was allowed to continue for at least 12 h, the same time allowed in the bulk sample. For

---

<sup>1</sup>Molds of different diameters, all close to 30 mm, were used in the course of this work and the geometries and results adapted accordingly.

## A. Appendix

---

each polymer between 4 and 8 specimen were produced. They were only used, if they were clear, transparent, contained no bubbles, and exhibited a smooth homogeneous surface. Until use the specimen were stored in the dark at 6 °C and all were measured in this "as prepared" state.

The shear measurements were carried out on an ARES G2 rotational rheometer (TA Instruments, obtained from Waters GmbH, Eschborn, Germany). Plate-plate disposable geometries made from aluminium with diameter and gap being the same as the specimen were used. The temperature was controlled to  $25 \pm 0.1$  °C by a Peltier element (Advanced Peltier System, TA Instruments). The humidity was not controlled and due to evaporation from the samples the measurements were restricted to short times. The shear modulus in the linear regime was determined from the plateau (usually below  $\gamma_0 = 1\%$ ) in a oscillatory strain sweep (OSS). Typically the result values at  $\gamma_0 = 0.1\%$  were taken to be representative for the plateau. The measurement frequency was  $\omega_1/2\pi = 1$  Hz and a normal force (NF) or normal pressure was applied and held during the experiment to fix the samples. The NF value was individually chosen to deform the samples by about 5 % by compression. For comparing different gel compositions three samples were measured three times each and the average used as the result. The error is given by the standard deviation of this average.

Compression measurements were carried out with an Eplexor 150N (Gabo Qualimeter, Ahlden, Germany). The dynamic mechanical thermal analysis (DMTA) allows testing in continuous and oscillatory deformation modes. Plate-plate geometries (35 mm cross-section) made from aluminium were used. The measurements were carried out at room temperature with no humidity control present. The surface of the specimen was treated to enable reproducible measurements: either one side was coated with Parafilm™ to prevent a tack on the upper geometry or both sides were coated with a silicone oil to allow the sample to slip. The oils were AK grade (Wacker Silicones, obtained from DRAWIN, Riemerling, Germany) with a viscosity chosen to be appropriate for the sample.

In the continuous deformation mode , the sample is steadily compressed with a speed of 0.3 mm/min (4 %/min at a typical sample height of 8 mm) which is the fastest case for which no influence on the modulus is observed. The sample is deformed from  $\lambda = 1$  to 0.8. The modulus  $E$  was determined from the slope of  $\lambda - \lambda^{-2}$  against  $\sigma$  by a linear fit in the range  $\lambda = 0.97$  to 0.80. The contact force was in both cases chosen to be 0.3 N with a tolerance of 0.125 N.

The compression experiments in oscillatory mode were carried out with a frequency of  $f = 1$  Hz. The influence of the frequency is small with the same trends found for the shear experiments (not shown).  $|E^*|$  and  $\tan \delta$  values were recorded for static strains of  $\lambda_s = 2, 10$ , and 20 %. The amplitude of the oscillatory deformation is superimposed on the static compression. The amplitude is given by the dynamic strain  $\varepsilon$  and was varied from 0.1 % to half the value of the respective static strain. The samples were compared by the values obtained at  $\varepsilon = 0.1$  %, which is well inside the linear regime for all investigated samples. The accuracy of the dynamic and the static strain were required to be within 0.05 % and 0.5 %, respectively. The contact force was the same as in continuous deformation experiments. No lubrication was used as it showed no effect.

### **Procedure of pore size estimation by solute exclusion**

For an estimate of the pore size distribution (PSD) in a hydrogel, the migration of linear, low PDI polymers of different sizes into gel is monitored. The polymeric network is put in contact with the solution of reference polymers (probes) and the concentration change in the supernatant phase is monitored over time as the linear polymers migrate into the gel to an extend depending on their size with respect to the pore sizes.

For the experiments pMAAc and Dextrans SEC calibration standard polymers with a narrow size-distribution, described in section A.1, are used. Stock solutions were prepared from the dried standard polymers by weight-

## A. Appendix

---

ing them with high accuracy and dissolving them in DI and stirring over night at RT. These stock solutions are used for the whole experiment including the concentration calibration described below. The two gels pAAc-DC01-DN76-Q4, batch 2 and pAAc-DC1-DN75-Q4, batch 3 were investigated. Fractions with a particle size of 300 – 650 µm were used and two times sol extracted before use to prevent an influence of sol contamination of the solution phase. Two specific approaches were taken that are detailed below.

In the first approach seven different pMAAc standard polymers with different molecular weights were used. They were divided into three mixes in the order 549 kDa, 79.8 kDa (Mix 1); 326 kDa, 34.9 kDa, 1.2 kDa (Mix 2) and 163 kDa, 8.2 kDa (Mix 3). Stock solutions of 10 mL volume were prepared from each mix with polymer concentrations of 0.8 or 0.34 wt.-% for  $M_w$  under and over 50 kDa respectively. 8.2 mL of each test mix is added to 6 g of the gels which were swollen to equilibrium in DI prior to use. The mixes were sealed and stored at RT over two weeks. In an interval of one or two days seven samples of 0.2 mL were taken from the supernatant solutions. All samples and the three stock solutions are investigated by aqueous SEC after taking the last sample. The eluent was water with TRIS buffer (water with 0.15 mol/L  $NaCl$  and 0.01 mol/L  $NaN_3$ ) with a flow rate of 1 mL/min. The setup consisted of a SUPREMA 100 column (8 × 300 mm, 10 µm particle size, 100 Å pore size, PSS, Mainz, Germany), a rheodyne injector with a 100 µL injection loop, and a DRI detector (RI-71, Shodex, Munich, Germany). Data acquisition was performed by the WinGPC-Software (PSS). The recorded elugrams were evaluated in terms of the peak heights for each of the components.

A second series of experiments was carried out with Dextrans as standard polymers. In this case the gels under investigation were used in their dried state and mixed individually with each of three standard solutions of Dextrans. These solutions were prepared from polymers with  $M_w$  of 1 kDa, 24 kDa, and 271 kDa. A final concentration of ≈ 0.5 mg/mL (0.05 wt.-%)

**Table A.2.:** Concentrations of Dextran standards in the supernatant solution above gel sample as a function of time. The dry pAAc gels were mixed with the solution in a ratio of  $Q_{\text{rel}} = 4$ . The data is visualised in fig. 4.3.

Gel DC mol-%	Solution	c [mg/ml]			
		10 min	30 min	100 min	300 min
0.1	Dextran 1 kDa	0.539	0.545	0.553	0.552
0.1	Dextran 24 kDa	0.538	0.549	0.554	0.559
0.1	Dextran 270 kDa	0.554	0.597	0.633	0.608
1.0	Dextran 1 kDa	0.542	0.554	0.558	0.560
1.0	Dextran 24 kDa	0.584	0.639	0.652	0.652
1.0	Dextran 270 kDa	0.589	0.693	0.719	0.729

was prepared by diluting the stock solutions of 1 mg/mL.<sup>2</sup> The ratio of solution to polymer was  $Q_{\text{rel}} = 4$  in a dimension that yields 10 g of gel and 30 g of supernatant solution. In the same way blank test samples with only gel or only dissolved Dextrans were prepared to check for experimental errors. The mixtures were left sealed at RT and test samples were taken from the supernatant solution after 10, 30, 100, and 300 min. The polymer concentrations were determined by the procedure described below. The obtained data is shown in **tab. A.2.**

The concentration of the sample solutions are determined by DRI measurements. First the refractive index increment ( $dn/dc$ ) of the samples in water is determined with a concentration series. The refractive index of the test solution is measured and the concentration computed from the increment value. The analysis was conducted with a DNDC2010 (Brookhaven Instruments, obtained from PSS, Mainz, Germany). The measurements were carried out at 30.0 °C with a 620 nm light source at 80 % intensity. The reference solvent was always neat DI and the solvent signal was subtracted and used for a linear signal drift correction over one measurement

<sup>2</sup>A lower concentration than 1 mg/mL was used as a concentration increase was expected and the results should remain within the RI-detector calibration range.

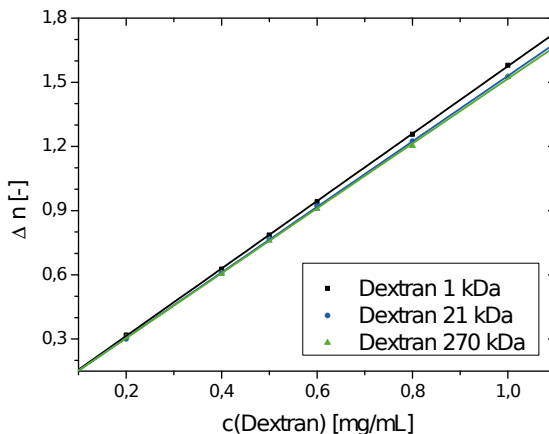


**Figure A.1.:** The refractive index increments for three Dextran solutions are determined by linear fits (lines) to the data of concentration series (points). The slopes of the fits are given in tab. A.3.

session. Samples of 2 mL were used and inserted by syringe through a PVDF (polyvinylidene fluoride) filter with 0.45  $\mu\text{m}$  pore size (Carl Roth, Karlsruhe, Germany). After insertion, sufficient time was given for the signal to stabilize, at least one minute. The calibration is carried out with a concentration series of the standard polymer made from the same stock solution. In the case of Dextran concentrations of 0.2, 0.4, 0.5, 0.6, 0.8, and 1.0 mg/mL were prepared. The calibration results are shown in **tab. A.3** and the fits in **fig. A.1**.

**Table A.3.:** Refractive index increments obtained for various solutions of linear Dextran polymers in water.

Solution	$\frac{\text{dn}}{\text{dc}}$ [mL/g]
Dextran 1 kDa	$0.1554 \pm 0.0007$
Dextran 21 kDa	$0.1523 \pm 0.0007$
Dextran 270 kDa	$0.1527 \pm 0.0012$

### A.3. Low field NMR equipment and measuring schemes

#### The minispec instrument

A simple and convenient way to perform NMR-relaxation experiments is provided by bench-top low-field NMR (LF-NMR) equipment. The instrument used in this work is the minispec mq20 (Bruker, Ettlingen, Germany), depicted in **fig. A.2**. It uses a permanent magnet to create a field of 0.469 T corresponding to a proton resonance frequency of 19.95 MHz. The magnet temperature is adjusted to  $(40 \pm 0.001)$  °C and does not provide a shim. The instrument is a so-called time-domain spectrometer with magnet field homogeneity insufficient for chemical shift resolved experiments. Samples can therefore, only be distinguished in terms of their relaxation or diffusion behaviour. However, the spectrometer works with a variety of preconfigured measurement options and additional pulse sequences can be implemented by the user. The used measurement programs are described with the respective experiments in the following sections.

A variety of samples from the gels used in this work (see appendix A.1) were prepared for the LF-NMR measurements as follows: 60 mg of dried polymer particles and  $D_2O$  were mixed intimately on a glass plate at a ratio of 1:9 and transferred to the bottom of a 10 mm glass tube. The tube was stoppered and sealed with Parafilm™ to prevent evaporation and let to equilibrate for at least 24 h before any measurement. The filling and placing of the sample were adjusted to bring it into the region of the highest homogeneity of the magnet field. Usually the sample height should not be more than 8 mm and the position has to be adjusted correctly. The temperature of the samples can be independently controlled by the BVT (BVT3000 Variable Temperature Unit, Bruker) using a temperature -conditioned air flow. The sample temperature was kept between 30 – 32 °C in this study. For all measurements the receiver gain was adjusted for optimal use of the analogue-to-digital converter (ADC), which corresponds to a maximum intensity of 70 – 90 %. The gain is typically 92 dB for samples used in this

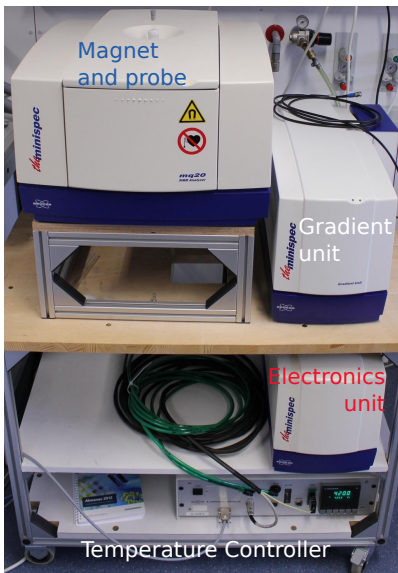


**Figure A.2.:** Photo and description of the parts of the minispec mq20 spectrometer used for LF-NMR measurements.

work. The pulse attenuation is probe specific and was not changed (setting 0 dB). The digital filter was not enabled (setting width to 20 000) and the acquisition mode is set to magnitude unless otherwise noted.

The resonance frequency and the field offset (FOF) of the spectrometer's magnet were adjusted such that the NMR signal was on-resonance. Additionally, the adjustment of the electric circuit of the probe was performed to compensate for the dielectric properties of the sample. With a good adjustment long FID length (half lives of 2 ms or longer) were found.<sup>3</sup>

The experiments were carried out using broad-band  $\pi/2$ - and  $\pi$ -pulses. Their lengths were determined by a nutation experiment. A simple sine function was fitted to the obtained FID amplitudes and the analytical determination of the first maximum and the second zero yielded the length of

---

<sup>3</sup>The programs automatizing this process were kindly provided by Mr. Karl-Friedrich Ratzsch.

the  $\pi/2$ - and  $\pi$ -pulses respectively. The values for the gel samples were usually found to be in the order of 2.7 and 5.0  $\mu\text{s}$ .<sup>4</sup>

### Spin-lattice relaxation measurement schemes ( $T_1$ )

Longitudinal relaxation is typically measured with two standard pulse sequences. These are saturation recovery (SR) and inversion recovery (IR). Both probe, after an excitation, the eventual return of the net-magnetisation to the thermal equilibrium. The return is recorded by means of a variable time delay  $\tau$ .  $M_z$  is obtained by the FID amplitude  $I(\tau)$  after the  $\pi/2$ -pulse. The results of both sequences are quite analogous, however, measurement with the SR-sequence is much faster as a short recycle delay (rd) can be used. This comes at the expense of only half of the dynamic range of the magnetisation. In the following, both sequences and their respective measurement parameters are explained.

A schematic representation of the SR-pulse sequence is depicted in the top of **fig. A.3**. In order to saturate the whole magnetisation in the sample, i.e.  $M_z = 0$ , a sequence of  $\pi/2$ -pulses with non-uniform pulse spacings is applied [Freeman71, Anderson72]. The sum over all pulse spacings is called saturation time. After the end of the saturation cycle, the magnetisation recovery starts. A FID is recorded after the recovery time  $\tau$  and a  $\pi/2$ -pulse is used to convert  $M$  into observable magnetisation  $M_{x,y}$ . The saturation cycle is usually required for gels. Here a 20 pulse saturation cycle was used. This pulse sequence is implemented in the Bruker application `t1_sat_mb.app`. The measurements were performed with a set of standard parameters: 32 scans (ns) to improve the signal-to-noise ratio and 4 dummy scans (ds) to reach a steady state before data acquisition. The time between two scans, the recycle delay (rd), was kept short at 100 ms. The delay time  $\tau$  was varied in an interval from 1 – 20 000 ms with 10 pts per decade. The data acquisition was carried out at 50  $\mu\text{s}$  after the final pulse with a sampling

---

<sup>4</sup>The  $\pi/2$ -pulse is somewhat longer than half of the  $\pi$ -pulse due to the non-negligible rise time of the probe circuit.

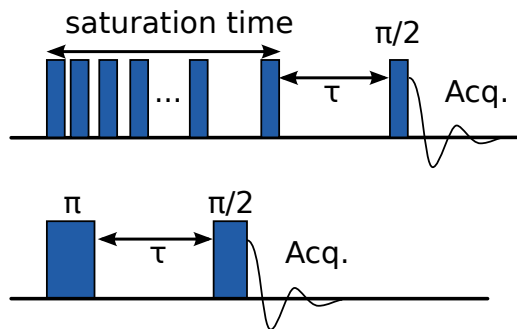


**Figure A.3.:** Schematic representation of the pulse sequences for measurement of spin-lattice relaxation times: Saturation recovery (SR)-sequence above and inversion recovery (IR) below.

window of 20  $\mu\text{s}$ . The saturation time was adjusted by direct experimentation for each sample to reach a minimum intensity for the first point (usually below 2% at 15 ms).

The IR-pulse sequence is similar to the SR one explained above. Here, the inversion is made by  $\pi$ -pulse, the complete sequence is shown in **fig. A.3** bottom. It is implemented in the `t1_ir_mb.app` Bruker application. The standard parameters are the same as above with one notable exception: the recycle delay has to be set long enough. With the  $T_1$  time of the sample still unknown, 20 s are a save value for measurements. In accordance the scans were reduced to 8 to achieve sufficiently short measurement times.

The sample pAAc-DC1-DN75-Q1.5 was measured with both methods and the results are compared in **fig. A.4**. Two logarithmically separated relaxation processes are easily distinguishable. To extract the corresponding time constants a least squares fit of two exponential functions (A.3) is performed. The adjustment to the data is done with the Marquardt-Levenberg algorithm implemented in the software `OriginPro` (version 8.6).

$$I(\tau) = -A \cdot \exp\left(-\frac{\tau}{T_1(\text{Gel})}\right) - B \cdot \exp\left(-\frac{\tau}{T_1(\text{HDO})}\right) + C \quad (\text{A.3})$$

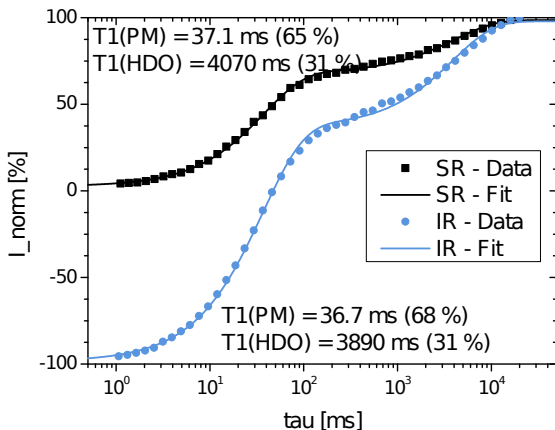


**Figure A.4.:** Determination of the longitudinal relaxation constants of the sample pAAc-DC1-DN75-Q1.5 by the IR and SR pulse sequences. The lines are a fit to the data according to eq. A.3.

### Spin-spin relaxation measurement schemes ( $T_2$ )

The transverse relaxation process can be recovered at least partially by echo techniques as was discussed in the main text 4.3.3. This is done in the case of the Hahn echo by an initial  $\pi/2$ -pulse followed by a variable time delay  $\tau$ . An echo is produced by  $\pi$ -pulse as shown at the top of **fig. A.5**. The maximum of the echo signal  $I(\tau)$  is sampled. By variation of  $\tau$  the decay of the spin system under the spin-spin mechanism is recorded.

The Hahn echo is implemented in the program `t2_se_mb.app` and was used with the following set of parameters:  $ns = 48$  as a trade off between measurement time and signal to noise,  $ds = 4$ ,  $rd = 20 \text{ s}$ ,  $\tau = 0.04 - 100 \text{ ms}$  with 10 pts per decade, shorter times cannot be sampled and longer are obscured by diffusion. The sampling window is automatically adjusted.

The lengthy Hahn echo procedure can be circumvented by using the CPMG-sequence (**fig. A.5** middle), which employs, instead of a single  $\pi$ -pulse, a whole train of equally spaced pulses, that can be used to acquire large parts of the relaxation curve in one shot. The program `t2_cp_mb.app` was used

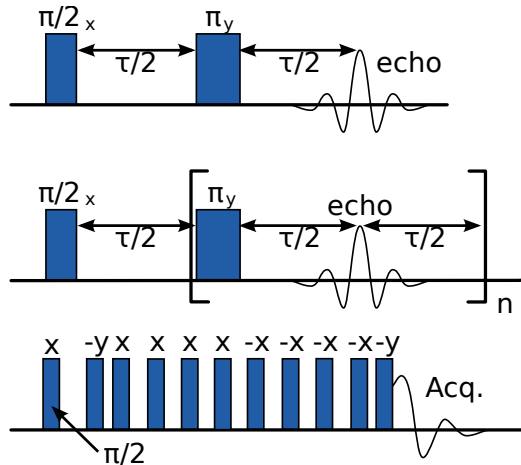


**Figure A.5.:** Schematic representation of the pulse sequences for measurement of spin-spin relaxation times: Hahn echo-sequence at the top, CPMG-sequence in the middle and the solid echo like MSE-sequence at the bottom.

with  $rd = 20$  s,  $ns = 256$ ,  $ds = 4$ ,  $\tau$  was fixed at 0.04, 0.1 and 1 ms for different experiments while  $ne = 256$  consecutive echoes were recorded (dummy echoes ( $de = 0$ )). The sampling window was fixed at 1/10 of  $\tau$ .

The CPMG approach was found, however, to be insufficient because a pronounced spin-locking effect manifested especially at short pulse spacings. This is attributed to all pulses having the same phase. By use of the XX4 and XY16 phase cycling schemes, the phases of subsequent  $\pi$ -pulses are altered with respect to each other as shown in **tab. A.4** [Gullion90, Guthausen98]. In all cases the standard CYCLOPS phase cycling scheme was imposed on subsequent scans. The XY16 phase cycle was implemented into the self-written CPMG-sequence in *xy16\_phasecompr.app*.

The XY16 program is run three times with different parameters as shown in **tab. A.5** to acquire the whole relaxation curve. This could not be achieved by recording more echoes, because due to hardware limitations only a number of echoes ( $ne = 256$ ) can be recorded. Yet, the whole curve can be

Pulse	Standard	XX4	XY16
1	y	y	y
2	REDO	-y	-x
3		-y	y
4		y	-x
5		REDO	-x
6			y
7			-x
8			y
9			-y
10			x
11			-y
12			x
13			x
14			-y
15			x
16			-y
17			REDO

**Table A.4.:**  $\pi$ -Pulse phases for CPMG-type echo trains by different cycling schemes. REDO denotes, that the list is repeated until the total number of echoes is reached.

Parameter	Short	Middle	Long
ns [-]	256	128	128
ds [-]	4	4	4
tau [ms]	0.04	1	1
de [-]	0	0	15
rd [s]	20	20	20
ne [-]	256	256	256

**Table A.5.:** Parameters for different measurements carried out with the program `xy16_phasescompr.app` to acquire the full relaxation curve.

obtained by increasing the pulse spacing to 1 ms and the introduction of dummy echoes (de), for which no data was acquired (15 out of 16 echoes). The relaxation behaviour on the very short time scale is measured by the MSE pulse-sequence, implemented in the `mse.app` program [Maus06].<sup>5</sup> It is depicted in **fig. A.5** at the bottom, and produces an solid-like echo that can be used to overcome the dead time of the instrument (here 14  $\mu$ s). After the dead time, directly 100  $\mu$ s of the FID were recoded with filter set to 1 000, narrow and complex acquisition mode ( $ns = 128$ ,  $ds = 4$ ,  $rd = 20$  s, no supercycle).

The results of the three measurements with XY16 and the initial signal from MSE were combined to one dataset  $I_{\text{raw}}(\tau)$ , the points ordered by their time coordinate and normalized, so the highest intensity value is 100 %.

$$I_{\text{norm}}(\tau) = \frac{I_{\text{raw}}(\tau) \cdot 100\%}{I_{\max}} \quad (\text{A.4})$$

The long-time tail of the dataset is fitted with a single exponential function (**fig. A.6**), which is subtracted from the dataset (A.5) and afterwards normalized again.

$$I(\tau) = I_{\text{norm}}(\tau) - \left[ D \cdot \exp \left( -\frac{\tau}{T_2(\text{HDO})} \right) + E \right] \quad (\text{A.5})$$

The evaluation of the data can be achieved with two techniques described in the main text. First a non-linear least squares fit of the empirical function (A.6), consisting of a single exponential and a KWW-function, is performed as described in the previous section.

$$I(\tau) = A \cdot \exp \left( -\frac{\tau}{T_{2,S}} \right) + (100 - A - C) \cdot \exp \left( -\left( \frac{\tau}{T_{2,L}} \right)^\beta \right) + C \quad (\text{A.6})$$

---

<sup>5</sup>The pulse sequence was implemented from the literature by Mr. Karl-Friedrich Ratzsch.

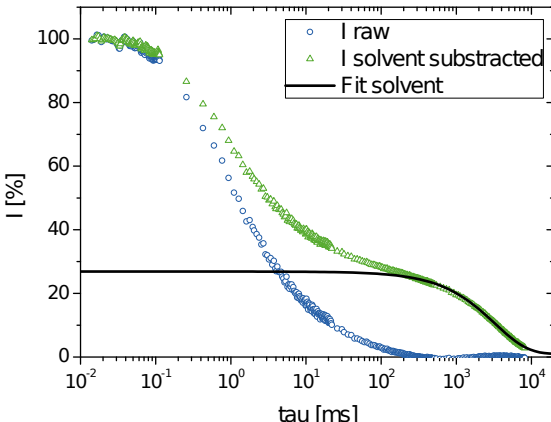


**Figure A.6.:** As an example, the transverse relaxation behaviour of sample pAAC-DC1-DN75-Q4 is shown. The green curve is the normalized data and the black line a fit of a single exponential function to the long-time tail which corresponds to the solvent. The blue symbols represent the solvent-subtracted signal according to eq. (A.5). The grey line is the best fit of eq. (A.6).

As a second method, the Laplace inversion (ILT) is used to obtain the distribution of (exponential) relaxation processes. It is given analytically by the Bromwich-integral (4.14), where  $\tau$  is the input time variable,  $s$  the output time variable and  $\gamma$  the radius of convergence of the function, here  $I$ . The inversion of discrete data is a complicated numerical problem, for which algorithms have been described in the literature. Here the implementation of Ryland *et al.* is used [Callaghan03a, Callaghan03b, Godefroy08]. The program works with an interface to the software MATLAB (version 2011). Important input parameters are the smoothing factor  $\alpha$  (typically  $10^5$ ) as well as the output data range ( $0.015 - 1000$  ms) and point density (200 pts).

### Measuring double quantum coherences

The double quantum (DQ) coherence build-up curves were measured by a complex pulse sequence, shown in fig. 4.21, that was developed and im-

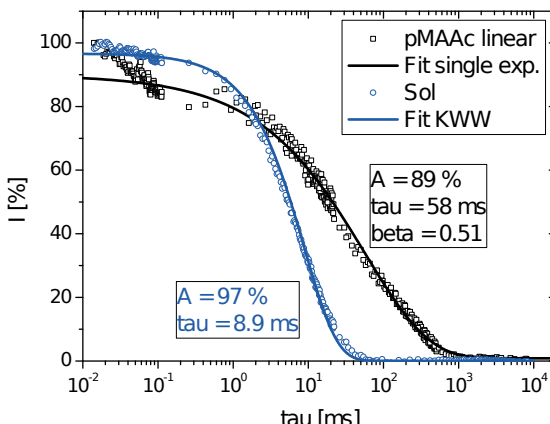


**Figure A.7.:** The transverse relaxation curves of the linear polymer samples pMAAc and the sol component of the pAAc-DC1-DN78-Q4 are shown with the respective empirical fit functions adjusted to the data.

plemented for the minispec in the group of K. Saalwächter [Saalwächter07, Chasse11]. Their program `ksbaum_1di2cfit.app` was used with a minor change, because the pulse spacings were incorrectly computed, causing faulty signals especially at high duty cycles.

The test parameters were optimized to hydrogel samples and read as follows:  $rd = 0.1\text{ s}$ ,  $ns = 1024$ ,  $ds = 16$ ,  $pts = 70$ , cycle time  $\tau_c$  starts from 0 ms, with an increment of 0.04 ms and a double thereof after 10 pts. No supercycle was enabled and acquisition was done in complex mode for the first 0.1 ms of the FID. This results in a fairly long measurement time, around 7 h, which was found necessary to keep the noise level as low as possible for the following analysis.

In the pulse sequence, two different signals can be selected by the relative phase of the final read-pulse. One is the reference signal  $I_{\text{ref}}$  and the other the DQ coherence signal  $I_{\text{DQ}}$ . Both are recorded over the cycle times  $t_c$  to obtain the full build-up curve. The signals are already normalized within the acquisition program to the starting value of  $I_{\text{ref}}$ . The cumulative intensity  $I_{\text{sum}}$  can be calculated by

$$I_{\text{sum}}(t_c) = I_{\text{ref}}(t_c) + I_{\text{DQ}}(t_c) \quad . \quad (\text{A.7})$$

To recover the unhampered build-up curve, a renormalization of  $I_{\text{DQ}}$  is required as it is influenced by decay processes. This done by stepwise fitting the long-time tail of the build-up curve. The thus obtained component is removed from the initial signal by subtraction. Typically, two steps are required as shown in **fig. A.8**. Usually, the components are not easily identified in the tail, so a lin-log representation of the data in fig. A.8 was found beneficial. The subtraction is done by the fit of a simple exponential function (A.8) to the data, which corresponds to a line in the mentioned lin-log representation. The fits yield two fractions and two time constants when substituting A and B for N respectively.

$$I(t_c) = N \cdot \exp\left(-\frac{2t_c}{\tau_N}\right) \quad (\text{A.8})$$

The first fit to the long time tail of  $I_{\text{ref}}$  is performed on the data from 50 ms until the end of the dataset. For the second step, the reduced intensity  $I_{\text{red}}$ , as given by (A.9), is fitted with the second function. Here the data range was usually taken from 10 – 30 ms. The renormalization is finally achieved by subtracting both components from  $I_{\text{sum}}$  in eq. (A.10). This recipe is visualized in fig. A.8. The whole process was automated with a perl-script `evaldq.pl` (version 5.14, PDL numeric package version 2.4.11).

$$I_{\text{red}}(t_c) = I_{\text{ref}}(t_c) - I_{\text{DQ}}(t_c) - A \cdot \exp\left(-\frac{2t_c}{\tau_A}\right) \quad (\text{A.9})$$

$$I_{\text{nDQ}}(t_c) = \frac{I_{\text{DQ}}(t_c)}{I_{\text{ref}}(t_c) + I_{\text{DQ}}(t_c) - A \cdot \exp\left(-\frac{2t_c}{\tau_A}\right) - B \cdot \exp\left(-\frac{2t_c}{\tau_B}\right)} \quad (\text{A.10})$$

The residual dipolar coupling constant  $D_{\text{res}}$  is obtained from the data by use of a fit function. Here a function consisting of a distribution of (half) Gaussian functions is used. The function was developed and provided by K.

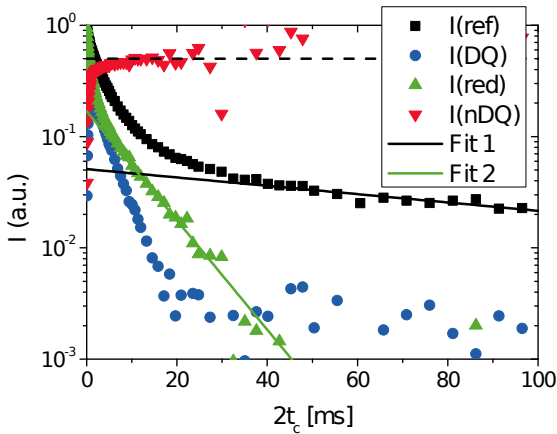


**Figure A.8.:** Evaluation of double quantum build-up data by removal of single exponential tails to compensate for relaxation processes. The tails are removed in two steps: the first fit is made to  $I_{\text{ref}}$  after 40 ms and yields here  $A = 5\%$  and  $\tau_A = 116$  ms. The second fit is on  $I_{\text{red}}$  between 10 – 20 ms and gives  $B = 17\%$  and  $\tau_B = 8.9$  ms. The resulting renormalized DQ build-up is shown with red symbols.

Saalwächter and is described in detail in the literature. The constants were obtained by a least squares fitting procedure with OriginPro. The distribution used was either bimodal yielding two coupling constants  $D_{\text{res}}(\text{weak})$ ,  $D_{\text{res}}(\text{strong})$  and the weight  $w$  of the two or unimodal with only one  $D_{\text{res}}$  constant.

Finally, the DQ pulse sequence was benchmarked with several samples for its validity in constrained samples. In **fig. A.9** the results of pure *HDO*, linear pMAAc-polymer and the gel and the sol fraction of a self-synthesized sample, all dissolved in water, are shown. It is easily seen that a typical DQ signal only develops in the gel sample while all other samples only show noise at various levels. The reference signal is always present but decays only very slowly for water and linear polymer. This is in agreement with the assumptions as only in the gel sample RDC should be present.

In the same figure, the influence of the polymer/water ratio in the sample is

shown. The couplings become much weaker with higher polymer content up to 30 wt.-%. At the highest concentration, however, it was again difficult to obtain any signal at all. Measurements are best carried out at weaker coupling, as more points can be recorded in the region of interest.

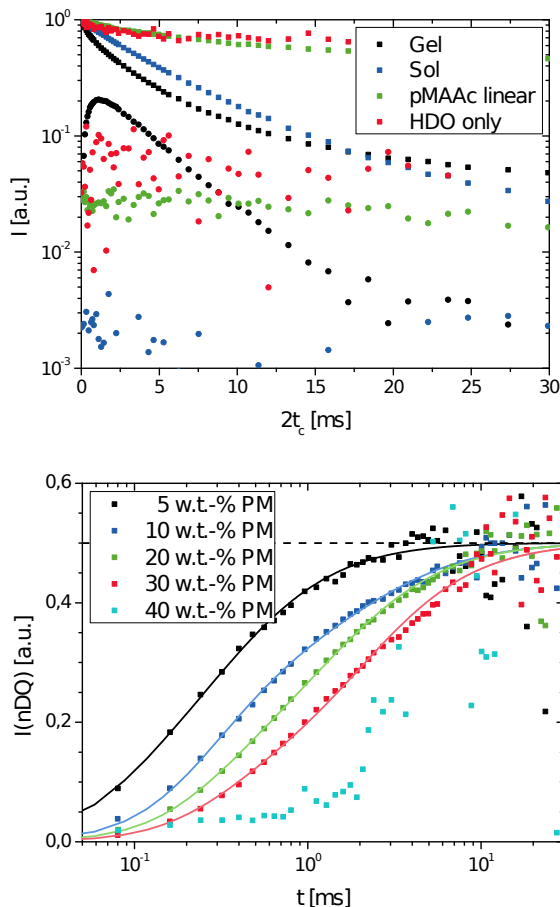


**Figure A.9.:** Results of the DQ build-up on different samples used to benchmark the sequence. On top, only with the cross-linked gel sample a typical DQ signal is observed. Below, the influence of polymer content in the sample shows weakest coupling for 30 wt.-% polymer.

## A.4. Parts and assembly of the press setup

### Determination of salt concentration in aqueous solutions

The concentration of sodium chloride in an aqueous solution is determined by conductivity measurement, either in a flow cell or in the sample/fraction containers. The procedure for data treatment is in both cases the same. First the raw data is corrected to the reference temperature  $T_{\text{ref}} = 20 \text{ }^{\circ}\text{C}$  by a linear relationship, (5.10) on p. 145, that is already implemented in the meter. The coefficient  $\alpha$ , needed here, is dependent on the temperature and concentration of the solution.  $\alpha$  is determined by recording the conductivity change of model salt solutions in a closed vessel with temperature control over a range of temperatures. For this procedure the correction was not used. The relevant coefficients are summarized in **tab. A.6**. Usually, the value at  $24 \text{ }^{\circ}\text{C}$  is used for the whole temperature range as the deviation is small (up to 0.3 %) if done so.

**Table A.6:** Values of the temperature coefficient  $\alpha$  as used in eq. (5.10) to correct the influence of measurement temperature on the conductivity of aqueous sodium chloride solutions.

$c(\text{NaCl})$ [g/L]	$\alpha$ [%/ $^{\circ}\text{C}$ ] at $T$ [ $^{\circ}\text{C}$ ]					
	20	21	22	23	24	25
3	2.28	2.23	2.18	2.13	2.09	2.05
10	2.20	2.15	2.11	2.06	2.02	1.98
50	2.11	2.07	2.03	1.99	1.95	1.91

The corrected conductivity  $\sigma(T_{\text{ref}})$  is transformed to the salt concentration by the use of a third grade polynomial, eq. (5.11) on p. 145, in an empirical approach. The coefficients of the polynomial are only valid in certain concentration ranges as listed in **tab. A.7**. It was found three ranges were sufficient for good accuracy in the conversion in the present study. The coefficients are obtained by fitting the polynomial to literature data [Wolf86, Höpfner10].

## A. Appendix

---

**Table A.7.:** Values for the coefficients of a third degree polynomial (5.11) used for the conversion of conductivity data to concentrations of sodium chloride solutions at 20 °C.

Range of validity		coefficients			
$\sigma$ [mS/cm]	c(NaCl) [g/L]	A [g/L]	B [g × cm/] [L × mS]	C × 10 <sup>-3</sup> [g × cm <sup>2</sup> /] [L × mS <sup>2</sup> ]	D × 10 <sup>-6</sup> [g × cm <sup>3</sup> /] [L × mS <sup>3</sup> ]
1.7 – 29.9	1 – 20	0.0343159	0.579411	3.23002	-5.87361
29.9 – 56.1	20 – 40	-2.25734	0.770430	-1.42087	20.9066
56.1 – 101	40 – 80	2.50918	0.537424	2.50803	-2.12189

### List of parts and components of the press setup

In this section all parts are listed that are necessary for build-up of the desalination setup that is discussed in sec. A.4. First the parts are listed that are self designed and were produced in the workshop of the institute. The technical drawings of those parts are shown in the next section.

1. **Mounting**, 120 mm inner diameter
2. **Two sieve units**, each assembled from a sieve support (a) and sieve holder (b)
3. **Piston**, height 55 mm
4. **Base plate**, height 30 mm
5. **Cantilever**, length 167 mm
6. **Nut** for the cantilever, Ø 60 mm
7. **Mounting** for the distance sensor
8. **Connector** with bore for the pressure sensor
9. **Flow cell** for conductivity measurement with lid

**10. PTFE seal ring** for the pressure sensor

The following parts were obtained commercially:

1. **Universal lab measurement device** SevenMulti with USB-communication module (Mettler Toledo, Gießen, Germany)
2. **Conductivity electrodes** InLab 730, with an operation range of 0.01 – 1000 mS/cm or InLab 751, Ø 4 mm, operation range 0.01 – 100 mS/cm (both Mettler Toledo)
3. **Pressure sensor** SD-40 with flat top membrane, range 0 – 100 bar with max. 0.5 bar deviation from linearity (Suchy Messtechnik, Lichtenau, Germany)
4. **Digital indicator** SA-10 for SD-40 (Suchy)
5. **Power supply** for pressure sensor with 24 V (Volcraft/Conrad, Hirschau, Germany)
6. **ADC** NI 9215 with 16 bit digital resolution in the interval  $\pm 10$  V and a maximal sampling rate of 100 000 Hz (National Instruments, Austin, USA)
7. **Distance gauge** MarCator 1086 with 50 mm measured displacement and 1 or 10  $\mu\text{m}$  accuracy, a USB communication cable is needed for connection to the computer (Mahr, Göttingen, Germany)
8. **Two-way cock** with 0.06" bore and 1/4"-28 connectors (Vici, Schenkon, Switzerland)
9. **T-connector** with 0.06" bore and 1/4"-28 connectors (Vici)
10. **Tubing** from ETFE with 1/16" outer diameter and 0.75 mm inner with 1/4"-28 connectors from PP (Vici)

## A. Appendix

---

11. **Cellulose filter paper** with 3 – 5 µm pore size (Rotilab/Carl Roth, Karlsruhe, Germany)
12. **Metal mesh** from ANSI 304 with 0.025 mm wire diameter and mesh size (Spörl KG, Sigmaringendorf, Germany)
13. **Metal mesh** from ANSI 304 with 0.1 mm wire diameter and 0.13 mm mesh size (Spörl KG)
14. **O-rings** from NBR with outer diameter 114 mm and 3 mm thickness (Simrit/Freudenberg, Weinheim, Germany)

## Technical drawings

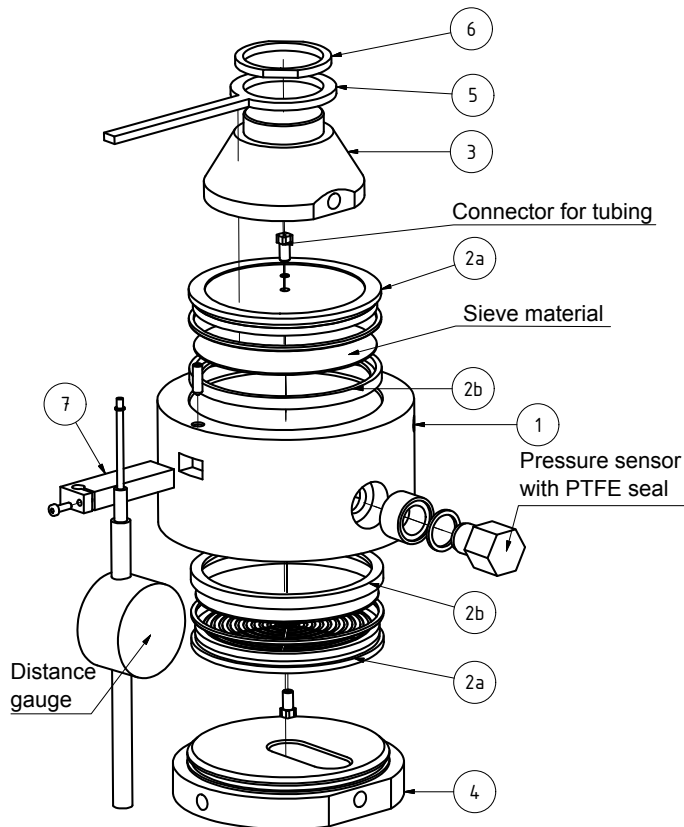


**Figure A.10.:** Exploded view drawing of the complete desalination setup; the numbers are references to the single parts and components shown below.

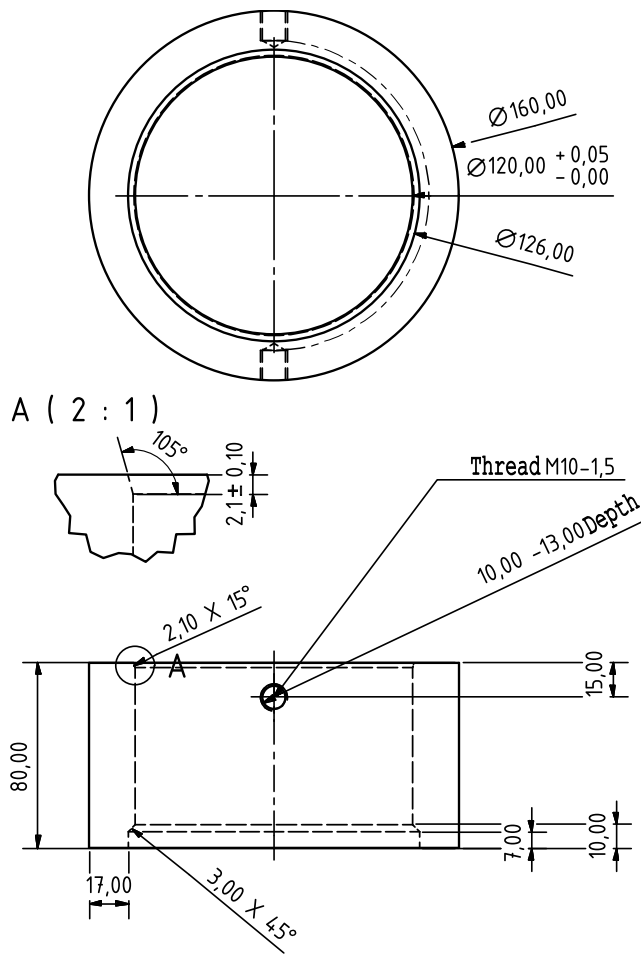


**Figure A.11.: Part 1 – mounting.**

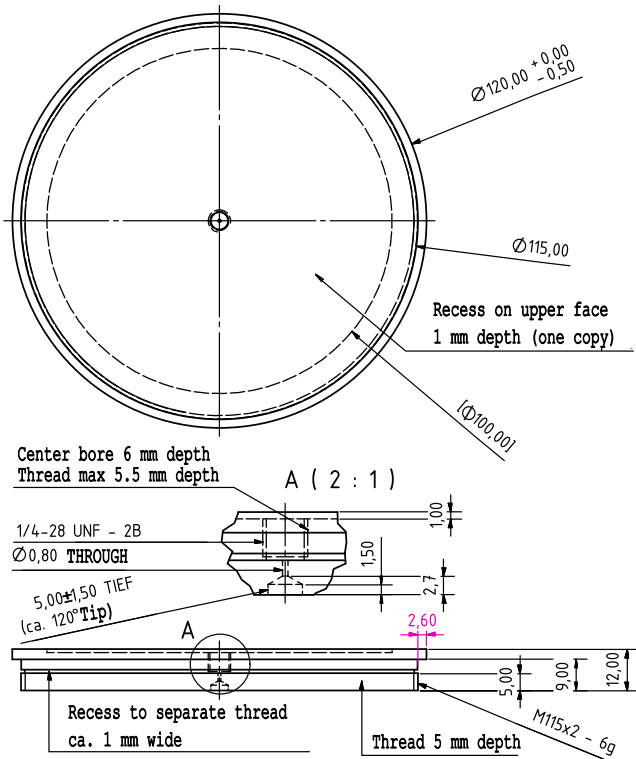


**Figure A.12.:** Part 2a – sieve support, overview.

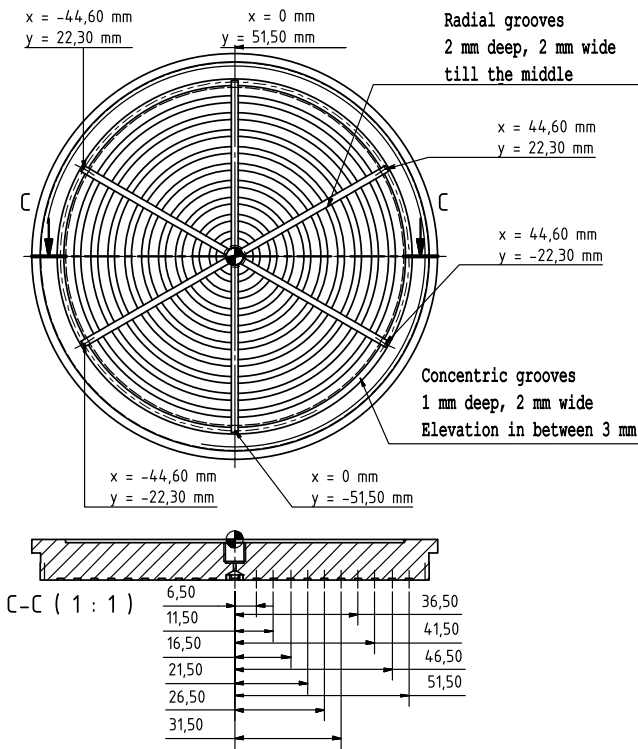


**Figure A.13.: Part 2a – sieve support, detail of channels.**

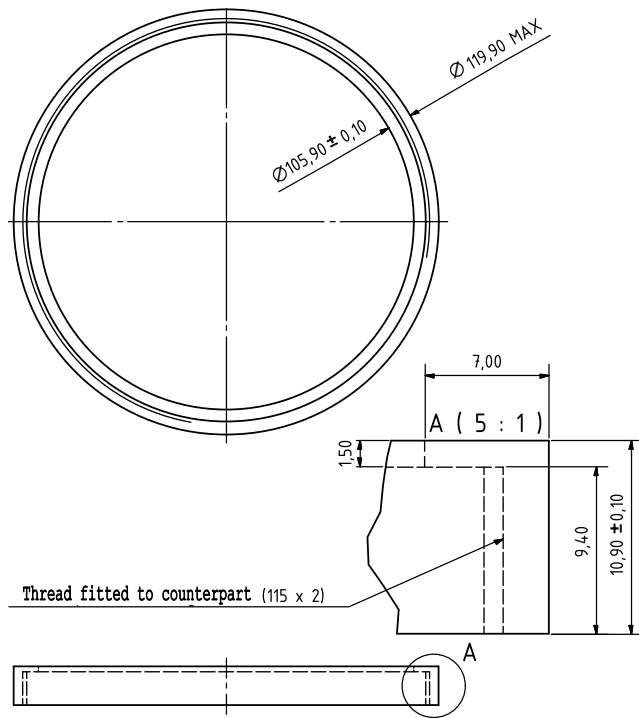


**Figure A.14.: Part 2b – sieve holder.**

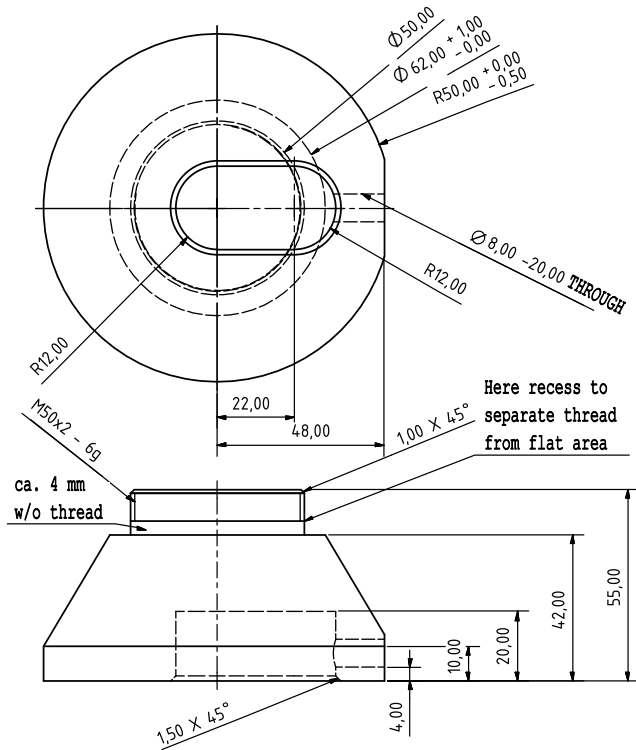


**Figure A.15.:** Part 3 – piston.

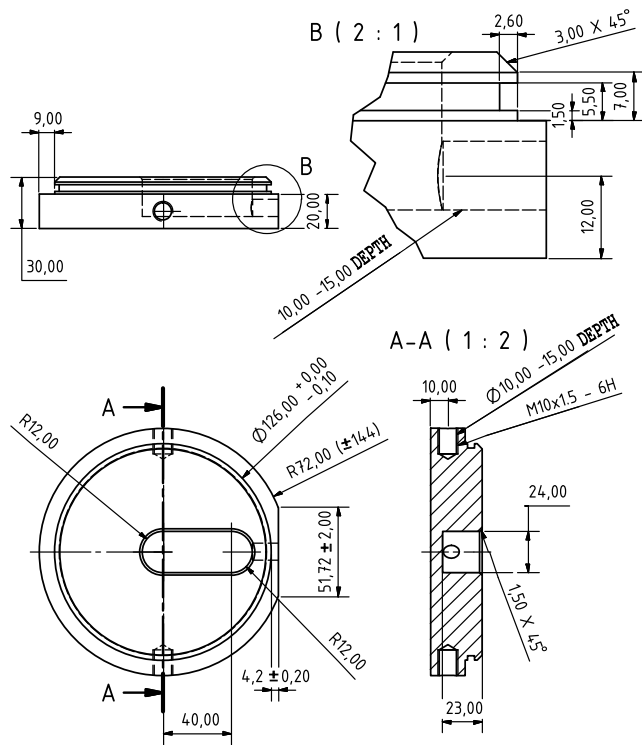


**Figure A.16.:** Part 4 – base plate.

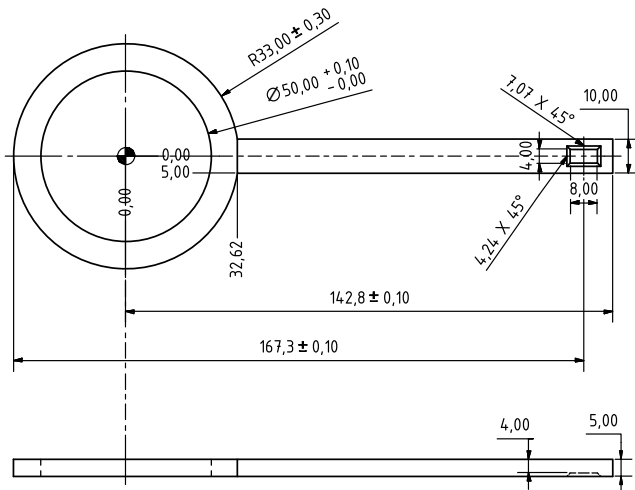


**Figure A.17.:** Part 5 – cantilever.

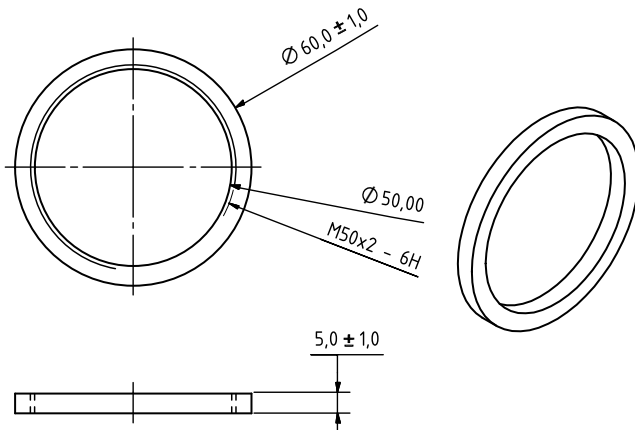


**Figure A.18.:** Part 6 – nut for cantilever.

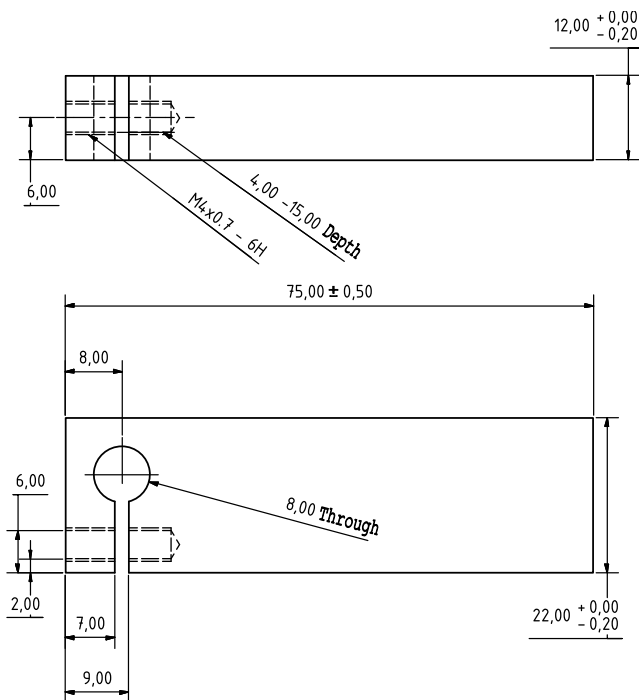


**Figure A.19.:** Part 7 – mounting for distance sensor.



## **B. Lists and tables**

## List of Figures

1.1	Schematic of the separation mechanism of water and dissolved salt by the use of a hydrogel . . . . .	3
1.2	Schematic of the three step process proposed of seawater desalination using hydrogels . . . . .	5
1.3	Synthesis of hydrogels by free radical polymerisation from various monomers . . . . .	6
2.1	Schemata of ideal and regular networks and the calculation of descriptive parameters . . . . .	11
2.2	Sample calculations of Donnan ion distribution between gel and solution phases . . . . .	21
2.3	Schematic drawing of the swelling of a body . . . . .	23
2.4	The different contributions to the chemical potential of the solvent in a swollen hydrogel are calculated for a model sample . . . . .	26
2.5	Schematic drawing of the compression of a body . . . . .	28
3.1	Photograph of swollen hydrogel beads . . . . .	34
3.2	Schema of the free radical polymerisation reaction of acrylic acid to form a hydrogel . . . . .	36
3.3	Comonomers used in the polymerisation with acrylic acid	37
3.4	Equilibrium swelling degree as a function of DC for brine and deionised water . . . . .	41
3.5	Equilibrium swelling degree of pAAc gels as a function of $Q_{\text{syn}}$ and DN in brine and DI . . . . .	43

3.6	Equilibrium swelling degree of home-made copolymers and commercial samples . . . . .	44
3.7	Time dependent swelling behaviour ( $Q(t)$ ) of some hydrogel samples . . . . .	46
3.8	Examples of specimen used for rheological investigations .	48
3.9	Influence of dynamic strain and normal force on the shear response of hydrogels . . . . .	50
3.10	Influence of frequency and water content on the shear modulus of hydrogels . . . . .	52
3.11	Mechanical properties of samples with varying degrees cross-linking . . . . .	53
3.12	Example of the strain-stress curves obtained by the continuous compression of a hydrogel sample . . . . .	55
3.13	Schematic picture of the role of the interface on the deformation type of the sample . . . . .	56
3.14	Young's modulus obtained by continuous compression on different contacts for hydrogel samples with varying degree of cross-linking . . . . .	57
3.15	Typical mechanical behaviour of a hydrogels under oscillatory compression . . . . .	59
3.16	Behaviour of hydrogels with varying degree of cross-linking under oscillatory compression . . . . .	60
3.17	Comparison of moduli of pAAc hydrogels with varying degree of cross-linking (DC) obtained by different mechanical methods . . . . .	63
3.18	Comparison of mesh size in a hydrogel network as given by synthesis and calculated from the modulus . . . . .	64
3.19	Relationship between cross-linking degree from synthesis and as determined from experiments . . . . .	66
3.20	Schematic of the technique to determine the sol content of a gel sample . . . . .	68

3.21 Sol content of neat pAAc gels as a function of DC and $Q_{\text{syn}}$	70
4.1 Schematic of the technique to explore the PSD of a hydrogel with linear probe polymers	75
4.2 Time dependent solute exclusion of pMAAc probes from a hydrogel as investigated by aqueous SEC	77
4.3 Time dependent concentration of Dextran probes over two gel samples with different DC	80
4.4 Example of a routine HF-NMR spectrum recorded on a hydrogel sample	81
4.5 HF-NMR spectra of a hydrogel recorded under MAS conditions with two two spinning frequencies	83
4.6 Spectra of a hydrogel after different Hahn echo delays	84
4.7 Schema of the laboratory frame with a single spin	87
4.8 Examples of the spectral density function $J$	89
4.9 Schematic decay of the autocorrelation function $C(t)$ of a polymer chain-segment	94
4.10 Longitudinal relaxation behaviour of samples with varying $Q_{\text{syn}}$	97
4.11 Longitudinal relaxation times of samples with different architectures or composition	99
4.12 Relation between the CPMG-pulse sequence and the spin-locking sequence	102
4.13 Example for the decay of transverse magnetisation in an hydrogel sample as recorded by different implementations of the spin echo method	103
4.14 Solvent subtracted transverse relaxation data and evaluation results for a typical hydrogel	105
4.15 Transverse relaxation curves of hydrogels with different reference states ( $Q_{\text{syn}}$ )	108

4.16	Transverse relaxation times and Laplace inverted datasets for of hydrogels with different reference states ( $Q_{\text{syn}}$ ) . . . . .	109
4.17	Transverse relaxation curves and Laplace inverted datasets of hydrogels with different cross-linking degrees (DC) . . . . .	113
4.18	Transverse relaxation times for of hydrogels with different cross-linking degrees (DC) . . . . .	114
4.19	Transverse relaxation curves of industrially produced su- perabsorbers . . . . .	116
4.20	Transverse relaxation time constants for hydrogel samples with different polymer content . . . . .	117
4.21	Schematic representation of the pulse sequences for mea- surement of the double quantum coherence build-up . . . . .	119
4.22	Typical result of double quantum experiments recorded on a self-synthesised gel sample . . . . .	121
4.23	Results of double quantum experiments for hydrogel sam- ples with varying $Q_{\text{syn}}$ . . . . .	123
4.24	Results of double quantum experiments for pAAc hydrogel samples with varying DC . . . . .	124
4.25	Results of double quantum experiments for industrially produced hydrogel samples . . . . .	125
5.1	Schematic drawing and photo of the first test setup for sep- arating water and polymer under pressure . . . . .	131
5.2	Schematic and photos of the newly constructed test setup for separating water and polymer under pressure . . . . .	135
5.3	Typical distance and volume data obtained in a desalination experiment . . . . .	139
5.4	Difference of the volume data obtained by distance and fraction measurements . . . . .	141
5.5	Example of calculation of the flux from the volume data by averaging and differentiating . . . . .	142

5.6	Typical data recorded by the pressure and conductivity sensors in a desalination experiment . . . . .	144
5.7	Pressure and eluate volume data of four desalination experiments run under the same conditions to quantify the reproducibility . . . . .	150
5.8	Volume flux of four desalination experiments run under the same conditions to quantify the reproducibility . . . . .	151
5.9	Obtained eluate concentration as function of time and pressure of four desalination experiments run to quantify the reproducibility . . . . .	152
5.10	Key values of obtained brine volume and concentration compared for an estimation of accuracy . . . . .	155
6.1	Equilibrium salt distribution between gel and solution phase for gels with varying degrees of cross-linking (DC) . . . . .	159
6.2	Pressure profile and produced eluate volume in desalination experiments conducted with samples of varying degree of cross-linking (DC) . . . . .	161
6.3	Volume flux in desalination experiments conducted with samples of varying degree of cross-linking (DC) . . . . .	162
6.4	Concentration results of desalination experiments conducted with gels of varying degree of cross-linking (DC) . . . . .	164
6.5	Equilibrium salt distribution between gel and solution phase for gels with varying reference states ( $Q_{\text{syn}}$ ) . . . . .	165
6.6	Produced eluate volume in desalination experiments conducted with samples of varying reference state ( $Q_{\text{syn}}$ ) . . . . .	167
6.7	Concentration results of desalination experiments conducted with gels of varying reference state ( $Q_{\text{syn}}$ ) . . . . .	168
6.8	Equilibrium salt distribution between gel and solution phase for gels with varying degrees of neutralisation (DN) . . . . .	169

6.9	Equilibrium salt distribution between gel and solution phase of gels with different monomer compositions . . . . .	171
6.10	The produced eluate in desalination experiments conducted with samples containing HEMA as co-monomer . . . . .	173
6.11	Concentration results of desalination experiments with sam- ples containing HEMA as comonomer . . . . .	174
6.12	Equilibrium salt distribution between gel and solution phase of various industrial SAP samples . . . . .	176
6.13	Produced eluate in desalination experiments conducted with industrial samples . . . . .	177
6.14	Concentration results of desalination experiments conducted with industrial samples . . . . .	178
7.1	Influence of the pressure profile on desalination experi- ments: pressure and volume data . . . . .	184
7.2	Influence of the pressure profile on desalination experi- ments: flux and concentration data . . . . .	186
7.3	Influence of the pressure profile on desalination experi- ments: derived quantities . . . . .	187
7.4	Influence of swelling time $t - Q$ on desalination perfor- mance of hydrogel B1110 . . . . .	190
7.5	Influence supernatant phase volume on desalination perfor- mance of B1110 . . . . .	192
7.6	Influence of the initial salt concentration on desalination performance of hydrogel B1110 . . . . .	194
7.7	Schema of the process of the water release from a gel sam- ple under pressure . . . . .	198
7.8	$p$ - $V$ -data and integration for hydrogel B1110 to estimate the energy spend . . . . .	203
7.9	Example of simulation results of ion uptake of hydrogels .	207

A.1	Determination of refractive index increments for Dextran solutions in water by means of a concentration series . . . . .	230
A.2	Photo and description of the parts of the LF-NMR instrument	232
A.3	Schematic representation of the pulse sequences for measurement of spin-lattice relaxation times . . . . .	234
A.4	Example of the determination of the longitudinal relaxation constants by two methods . . . . .	235
A.5	Schematic representation of the pulse sequences for measurement of spin-spin relaxation times . . . . .	236
A.6	Example of solvent subtraction and fitting of transverse relaxation data . . . . .	239
A.7	Transverse relaxation curves of linear polymer samples pMAAc and a sol component . . . . .	240
A.8	Evaluation procedure of double quantum build-up data by step-wise removal of relaxation components . . . . .	242
A.9	Benchmarking results of the DQ build-up sequence . . . . .	244
A.10	Exploded view drawing of the complete desalination setup; the numbers are references to the single parts and components shown below . . . . .	249
A.11	Part 1 – mounting . . . . .	250
A.12	Part 2a – sieve support, overview . . . . .	251
A.13	Part 2a – sieve support, detail of channels . . . . .	252
A.14	Part 2b – sieve holder . . . . .	253
A.15	Part 3 – piston . . . . .	254
A.16	Part 4 – base plate . . . . .	255
A.17	Part 5 – cantilever . . . . .	256
A.18	Part 6 – nut for cantilever . . . . .	256
A.19	Part 7 – mounting for distance sensor . . . . .	257

## List of Tables

3.1	Details of the commercial hydrogel samples obtained from the BASF. The Luquasorb 1280 samples were produced with $K^+$ counter-ions to the acrylate groups instead of the $Na^+$ ions normally used . . . . .	39
3.2	Fit parameters obtained by adjusting (3.6) to the time dependent swelling data of hydrogels in various electrolyte solutions shown in fig. 3.7 . . . . .	46
5.1	Comparison of the features of the old and new press setup .	134
5.2	Experimental conditions used for assessment of the reproducibility of the desalination results by consecutive runs .	149
5.3	Parameters describing the pressure data. The maximum pressure reached in each run and the slope with its error obtained by a linear fit are given. The pressure profile has an ideal value of 12 bar/h . . . . .	153
5.4	Parameters obtained by a fit of the flux data by the linear exponential function (5.7) and the linear fit of the concentration drop with increasing pressure . . . . .	154
6.1	List of parameters that describe the desalination performance of gels with different degrees of cross-linking (DC)	160
6.2	List of parameters that describe the flux and the desalination performance of pAAc gels with different reference states $Q_{syn}$ . The values of DC = 1 mol-% and DN = 75 mol-% are the same for all samples . . . . .	166
		267

6.3	List of parameters that describe the desalination performance of hydrogels with different monomer composition . . . . .	172
6.4	List of parameters that describe the desalination performance of industrial polymers and a pAAc reference sample . . . . .	179
7.1	Overview over the investigated pressure profiles . . . . .	183
7.2	List of parameters that describe the desalination performance at different pressure profiles. (*) The data of Step50 was not linear so no value for $dc/dp$ was obtained . . . . .	188
7.3	List of parameters that describe the desalination performance of the commercial hydrogel B1110 for variation of swelling time $t - Q$ (upper part) and the solution ratio $Q_{\text{rel}}$ (lower part). The former experiments were carried out with a pressure increase 60 bar/h the latter with 12 bar/h . . . . .	191
7.4	List of parameters that describe the desalination performance of the commercial hydrogel B1110 for different initial brine concentrations. The experiments were carried out with a pressure increase of 60 bar/h and a swelling time of 3 min . . . . .	195
7.5	Estimated values of energy consumption by seawater desalination for self-synthesised and industrially produced hydrogels . . . . .	204
A.1	List of the self-synthesised hydrogel samples: shorthands and synthetic parameters. The samples below the line contain other monomers than AAc . . . . .	222
A.2	Concentrations of Dextran standards in the supernatant solution above gel sample as a function of time. The dry pAAc gels were mixed with the solution in a ratio of $Q_{\text{rel}} = 4$ . The data is visualised in fig. 4.3 . . . . .	229
A.3	Refractive index increments obtained for various solutions of linear Dextran polymers in water . . . . .	230

A.4	$\pi$ -Pulse phases for CPMG-type echo trains by different cycling schemes. REDO denotes, that the list is repeated until the total number of echoes is reached . . . . .	237
A.5	Parameters for different measurements carried out with the program xy16_phasecompr.app to acquire the full relaxation curve . . . . .	237
A.6	Values of the temperature coefficient $\alpha$ as used in eq. (5.10) to correct the influence of measurement temperature on the conductivity of aqueous sodium chloride solutions . . . . .	245
A.7	Values for the coefficients of a third degree polynomial (5.11) used for the conversion of conductivity data to concentrations of sodium chloride solutions at 20 °C . . . . .	246



## Bibliography

- [Abragam61] A. Abragam, *The principles of nuclear magnetism*, 1st ed., Clarendon Press, Oxford, **1961**.
- [Aggebrandt64] L. G. Aggebrandt, O. Samuelson, *J. Appl. Polym. Sci.* **1964**, 8, 2801.
- [Anderson72] W. A. Anderson, R. Freeman, H. Hill, *Pure Appl. Chem.* **1972**, 32, 27.
- [Ando02] I. Ando, M. Kobayashi, Z. C, S. Matsukawa, S. Kuroki, in *Polymer Gels and Networks* (Eds. Y. Osada, A. R. Khokhlov), 1st ed., chap. Structural and Dynamic Behavior of Polymer Gels as Elucidated by Nuclear Magnetic Resonance Spectroscopy, Marcel Dekker, New York, **2002**, pp. 235–305.
- [Andrady80] A. L. Andrady, M. A. Llorente, J. E. Mark, *J. Chem. Phys.* **1980**, 72, 2282.
- [Anferova07] S. Anferova, V. Anferov, J. Arnold, E. Talnishnikh, M. A. Voda, K. Kupferschläger, P. Blümller, C. Clauser, B. Blümich, *Magn. Reson. Imag.* **2007**, 25, 474.
- [Baker10] B. A. Baker, R. L. Murff, V. T. Milam, *Polymer* **2010**, 51, 2207.

- [Baselga87] J. Baselga, I. Hernandez-Fuentes, I. F. Piérola, M. A. Llorente, *Macromolecules* **1987**, *20*, 3060.
- [Bastide96] J. Bastide, S. J. Candau, in *Physical properties of polymeric gels* (Ed. J. P. C. Addad), 1st ed., John Wiley & Sons, Chichester, **1996**, pp. S. 19–39.
- [Belkebir-Mrani77] A. Belkebir-Mrani, J. E. Herz, P. Rempp, *Makromol. Chem.* **1977**, *178*, 485.
- [Bloch46] F. Bloch, *Phys. Rev.* **1946**, *70*, 460.
- [Bloembergen48] N. Bloembergen, E. M. Purcell, R. V. Pound, *Phys. Rev.* **1948**, *73*, 679.
- [Borgia98] G. Borgia, R. Brown, P. Fantazzini, *J. Magn. Reson.* **1998**, *132*, 65.
- [Bovey88] F. A. Bovey, *Nuclear Magnetic Resonance Spectroscopy*, 2nd ed., Academic Press, San Diego, **1988**.
- [Brannon-Peppas90] L. Brannon-Peppas, R. S. Harland, *Absorbent Polymer Technology*, 1st ed., no. 8 in Studies in polymer Science, Elsevier, Amsterdam, **1990**.
- [Breedveld04] V. Breedveld, A. P. Nowak, J. Sato, T. J. Deming, D. J. Pine, *Macromolecules* **2004**, *37*, 3943.
- [Brendel99] U. Brendel, *Quellungsverhalten und mechanische Eigenschaften von Polyelektrolytnetzwerken und technischen Superabsorbern*, Ph.D. thesis, Johannes Gutenberg-Universität, Mainz, **1999**.
- [Brown06] R. Brown, *Physical Testing of rubber*, 4th ed., Springer Science, New York, **2006**.

- [Buchholz98] F. L. Buchholz, A. T. Graham, *Modern Superabsorbent Polymer Technology*, 1st ed., Wiley-VCH, New York, **1998**.
- [Burden01] R. L. Burden, J. D. Faires, *Numerical analysis*, 7th ed., Brooks/Cole-Thomson Learning, Pacific Grove, **2001**.
- [Busch04] M. Busch, W. Mickols, *Desalination* **2004**, *165*, 299.
- [Callaghan03a] P. Callaghan, S. Godefroy, B. Ryland, *J. Magn. Reson.* **2003**, *162*, 320.
- [Callaghan03b] P. Callaghan, S. Godefroy, B. Ryland, *Magn. Reson. Imag.* **2003**, *21*, 243.
- [Carr54] H. Carr, E. Purcell, *Phys. Rev.* **1954**, *94*, 630.
- [Castignolles09] P. Castignolles, R. Graf, M. Parkinson, M. Wilhelm, M. Gaborieau, *Polymer* **2009**, *50*, 2373.
- [Cath06] T. Y. Cath, A. E. Childress, M. Elimelech, *J. Membr. Sci.* **2006**, *281*, 70.
- [Chasse11] W. Chasse, J. L. Valentin, G. D. Genesky, C. Cohen, K. Saalwächter, *J. Chem. Phys.* **2011**, *134*, 44907.
- [Clark87] A. H. Clark, S. B. Ross-Murphy, in *Advances in Polymer Science 83*, 1st ed., Springer, Berlin and Heidelberg, **1987**, p. 58.
- [Cohen91] A. Cohen, *Rheol. Acta* **1991**, *30*, 270.

## Bibliography

---

- [de Gennes79] P.-G. de Gennes, *Scaling Concepts in Polymer Physics*, 1st ed., Cornell University Press, Ithaca and London, **1979**.
- [de las Heras Alarcon05] C. de las Heras Alarcon, S. Pennadam, C. Alexander, *Chem. Soc. Rev.* **2005**, *34*, 276.
- [Donnan32] F. G. Donnan, E. A. Guggenheim, *Z. physik. Chem.* **1932**, *A162*, 346.
- [Dusschoten01] D. van Dusschoten, M. Wilhelm, *Rheol. Acta* **2001**, *40*, 395.
- [Dušek69] K. Dušek, W. Prins, in *Advances in Polymer Science 6*, vol. 6/1, 1st ed., Springer, Berlin and Heidelberg, **1969**, pp. 1–102–.
- [Erman82] B. Erman, P. J. Flory, *Macromolecules* **1982**, *15*, 806.
- [Ferry80] J. D. Ferry, *Viscoelastic properties of polymers*, 3rd ed., Wiley, New York, **1980**.
- [Flory41] P. J. Flory, *J. Chem. Phys.* **1941**, *9*, 660.
- [Flory43] P. J. Flory, J. Rehner, *J. Chem. Phys.* **1943**, *11*, 512.
- [Flory53] P. J. Flory, *Principles of Polymer Chemistry*, 1st ed., Cornell University Press, Ithaca, New York, **1953**.
- [Flory82] P. J. Flory, B. Erman, *Macromolecules* **1982**, *15*, 800.
- [Franck08] A. Franck, *Appl. Rheol.* **2008**, *18*, 44.

- [Freeman71] R. Freeman, H. D. W. Hill, *J. Chem. Phys.* **1971**, *54*, 3367.
- [Fritzmann07] C. Fritzmann, J. Löwenberg, T. Wintgensand, T. Melin, *Desalination* **2007**, *216*, 1.
- [Fukushima81] E. Fukushima, S. B. W. Roeder, *Experimental Pulse NMR - A Nuts and Bolts Approach*, 1st ed., Addison-Wesley, Reading, **1981**.
- [Ganta08] S. Ganta, H. Devalapally, A. Shahiwala, M. Amiji, *J. Controlled Release* **2008**, *126*, 187.
- [Geissler80] E. Geissler, A. M. Hecht, *Macromolecules* **1980**, *13*, 1276.
- [Geissler82] E. Geissler, A. M. Hecht, R. Duplessix, *J. Polym. Sci. B: Polym. Phys. Ed.* **1982**, *20*, 225.
- [Geissler88] E. Geissler, A. M. Hecht, F. Horkay, M. Zrinyi, *Macromolecules* **1988**, *21*, 2594.
- [Gent70] A. N. Gent, E. A. Meinecke, *Polym. Eng. Sci.* **1970**, *10*, 48.
- [Gerlach94] S. A. Gerlach, *Marine Systeme*, 3rd ed., Springer, Heidelberg, **1994**.
- [Gerlach10] G. Gerlach, K.-F. Arndt (eds.), *Hydrogel Sensors and Actuators - Engineering and Technology*, 1st ed., Springer, Berlin, **2010**.
- [Ghaddum91] V. F. Ghaddum, *Der Kunststoffberater* **1991**, 57.
- [Godefroy08] S. Godefroy, B. Ryland, P. T. Callaghan, *Matlab-program for laplace inversion of nmr relaxation data*, **2008**, version 2.5 (27.11.2008).

## Bibliography

---

- [Graessley08] W. W. Graessley, *Polymeric Liquids and Networks*, 1st ed., Garland Science, London and New York, **2008**.
- [Gullion90] T. Gullion, D. B. Baker, M. Conradi, *J. Magn. Reson.* **1990**, *89*, 479.
- [Gumbrell53] S. M. Gumbrell, L. Mullins, R. S. Rivlin, *Trans. Faraday Soc.* **1953**, *49*, 1495.
- [Gupta83] M. K. Gupta, R. Bansil, *J. Polym. Sci. C: Polym. Lett. Ed.* **1983**, *21*, 969.
- [Guthausen98] A. Guthausen, G. Zimmer, P. Blümller, B. Blümich, *J. Magn. Reson.* **1998**, *130*, 1.
- [Hahn50] E. L. Hahn, *Phys. Rev.* **1950**, *80*, 580.
- [Hamann07] C. H. Hamann, A. Hamnett, W. Vielstich, *Electrochemistry*, 2nd ed., Wiley-VCH, Weinheim, **2007**.
- [Hatada04] K. Hatada, T. Kitayama, *NMR spectroscopy of polymers*, 1st ed., Springer laboratory, Springer, Berlin, **2004**.
- [Hiraoka82] K. Hiraoka, H. Shin, T. Yokoyama, *Polymer Bulletin* **1982**, *8*, 303.
- [Hogari94] K. Hogari, F. Ashiya, in *Superabsorbent Polymers Science and technology* (Eds. F. L. Buchholz, N. A. Peppas), 1st ed., no. 573 in ACS Symposium Series, American Chemical Society, Washington D.C., **1994**, pp. 128 – 140.

- [Hong98] P.-D. Hong, J.-H. Chen, *Polymer* **1998**, *39*, 5809.
- [Hooper90] H. H. Hooper, J. P. Bakerand, H. W. Blanch, J. M. Prausnitz, *Macromolecules* **1990**, *23*, 1096.
- [Horkay00] F. Horkay, I. Tasaki, P. J. Basser, *Biomacromolecules* **2000**, *1*, 84.
- [Horkay07] F. Horkay, G. B. McKenna, in *Physical Properties of Polymers Handbook* (Ed. J. E. Mark), 1st ed., chap. Polymer Networks and Gels, Springer, New York, **2007**, pp. 497 – 523.
- [Horkay10] F. Horkay, J. Magda, M. Alcoutabi, S. Atzet, T. Zarembinski, *Polymer* **2010**, *51*, 4424.
- [Hu10] Y. Hu, X. Zhao, J. J. Vlassak, Z. Suo, *Appl. Phys. Lett.* **2010**, *96*, 121904.
- [Huggins41] M. L. Huggins, *J. Chem. Phys.* **1941**, *9*, 440.
- [Hyun11] K. Hyun, M. Wilhelm, C. O. Klein, K. S. Cho, J. G. Nam, K. H. Ahn, S. J. Lee, R. H. Ewoldt, G. H. McKinley, *Prog. Polym. Sci.* **2011**, *36*, 1697.
- [Höpfner09] J. Höpfner, *Auswirkungen von mechanischen Feldern und Drücken auf gequollene Polymernetzwerke*, Diploma thesis, Karlsruhe Institute of Technology, Karlsruhe, **2009**, mine!
- [Höpfner10] J. Höpfner, C. Klein, M. Wilhelm, *Macromol. Rapid Commun.* **2010**, *31*, 1337.

## Bibliography

---

- [Höpfner11] J. Höpfner, M. Wilhelm, in *Tagungsband 7. Thüringer Grenz- und Oberflächentage*, INNOVENT e.V., Jena, **2011**, p. 87, ISBN 978-3-00-035347-5.
- [Höpfner13] J. Höpfner, T. Richter, P. Košovan, C. Holm, M. Wilhelm, *submitted to Progr. Colloid. Polym. Sci.* **2013**.
- [James43] H. M. James, E. Guth, *J. Chem. Phys.* **1943**, *11*, 455.
- [James47] H. M. James, E. Guth, *J. Chem. Phys.* **1947**, *15*, 669.
- [JMP10] W. JMP, *Progress on Sanitation and Drinking-water: 2010 Update*, 1st ed., WHO and UNICEF, Geneva, **2010**.
- [Joanny96] J. F. Joanny, in *Physical properties of polymeric gels* (Ed. J. P. C. Addad), 1st ed., John Wiley & Sons, Chichester, **1996**, pp. S. 1–18.
- [Jones00] C. D. Jones, L. A. Lyon, *Macromolecules* **2000**, *33*, 8301.
- [Kanekiyo98] M. Kanekiyo, M. Kobayashi, I. Ando, H. Kurosu, T. Ishii, S. Amiya, *J. Mol. Struct.* **1998**, *447*, 49.
- [Katchalsky49] A. Katchalsky, *Experientia* **1949**, *5*, 319.
- [Katchalsky55] A. Katchalsky, I. Michaeli, *J. Polym. Sci.* **1955**, *15*, 69.

- [Kazanskii92] K. Kazanskii, S. Dubrovskii, *Adv. Polym. Sci.* **1992**, 98, 98.
- [Khawaji08] A. D. Khawaji, I. K. Kutubkhanah, J.-M. Wie, *Desalination* **2008**, 221, 47.
- [Kuga81] S. Kuga, *J. Chromatogr. A* **1981**, 206, 449.
- [Kuhn49] W. Kuhn, *Experientia* **1949**, 5, 318.
- [Kuhn50] W. Kuhn, B. Hargitay, A. Katchalsky, H. Eisenberg, *Nature* **1950**, 165, 514.
- [Kuhn12] A. Kuhn, M. Kunze, P. Sreeraj, H.-D. Wiemhöfer, V. Thangadurai, M. Wilkening, P. Heitjans, *Solid State Nucl. Magn. Reson.* **2012**, 42, 2.
- [Kwon10] G. H. Kwon, Y. Y. Choi, J. Y. Park, D. H. Woo, K. B. Lee, J. H. Kim, S.-H. Lee, *Lab Chip* **2010**, 10, 1604.
- [Lange11] F. Lange, K. Schwenke, M. Kurakazu, Y. Akagi, U.-i. Chung, M. Lang, J.-U. Sommer, T. Sakai, K. Saalwaechter, *Macromolecules* **2011**, 44, 9666.
- [Larson99] R. G. Larson, *The structure and rheology of complex fluids*, 1st ed., Topics in chemical engineering, Oxford University Press, New York, **1999**.
- [Lechner03] M. D. Lechner, K. Gehrke, E. H. Nordmeier, *Makromolekulare Chemie*, 3rd ed., Birkhäuser Verlag, Basel, **2003**.

## Bibliography

---

- [Limbach06] H. J. Limbach, A. Arnold, B. A. Mann, C. Holm, *Comp. Phys. Comm.* **2006**, *174*, 704.
- [Lionetto05] F. Lionetto, A. Sannino, A. Maffezzoli, *Polymer* **2005**, *46*, 1796.
- [Macosko94] C. W. Macosko, *Rheology Principles, measurements and applications*, 1st ed., VCH Interscience, New York, **1994**.
- [Marinetti09] M. Marinetti, F. Malpei, L. Bonomo, *J. Environ. Eng.* **2009**, *135*, 1380.
- [Mark88] J. E. Mark, B. Erman, *Rubberlike elasticity*, 1st ed., Wiley-Interscience, New York, **1988**.
- [Masuda94] F. Masuda, in *Superabsorbent Polymers Science and technology* (Eds. F. L. Buchholz, N. A. Pepas), 1st ed., no. 573 in ACS Symposium Series, American Chemical Society, Washington D.C., **1994**, pp. 88 – 98.
- [Maus06] A. Maus, C. Hertlein, K. Saalwächter, *Macromol. Chem. Phys.* **2006**, *207*, 1150.
- [McCutcheon05] J. R. McCutcheon, R. L. McGinnis, M. Elimlech, *Desalination* **2005**, *174*, 1.
- [Meiboom58] S. Meiboom, D. Gill, *Rev. Sci. Instrum.* **1958**, *29*, 688.
- [Mirau05] P. A. Mirau, *A practical guide to understanding the NMR of polymers*, 1st ed., Wiley-Interscience, Hoboken, New York, **2005**.
- [Mooney40] M. Mooney, *J. Appl. Phys.* **1940**, *11*, 582.

- [Mudiyanselage08] T. K. Mudiyanselage, D. C. Neckers, *J. Polym. Sci. A Polym. Chem.* **2008**, *46*, 1357.
- [Odian04] G. Odian, *Principles of polymerisation*, 4th ed., Wiley Interscience, New Jersey, **2004**.
- [Ohmine82] I. Ohmine, T. Tanaka, *J. Chem. Phys.* **1982**, *77*, 5725.
- [Oppermann85] W. Oppermann, S. Rose, G. Rehage, *Br. Polym. J.* **1985**, *17*, 175.
- [Oppermann92] W. Oppermann, in *Polyelectrolyte Gels - Properties, Preparation, and Applications* (Eds. R. S. Harland, R. K. Prud'homme), 1st ed., chap. Swelling Behavior and Elastic Properties of Ionic Hydrogels, American Chemical Society, Washington DC, **1992**, p. 159.
- [Osada92] Y. Osada, H. Okuzaki, H. Hori, *Nature* **1992**, *355*, 242.
- [Osada01] Y. Osada, K. Kajiwara, *Gels Handbook – The Fundamentals*, chap. 7.4 Application of superabsorbent polymers gels to oil-water separation, 1st ed., Academic Press, San Diego and London, **2001**, pp. 381 – 392.
- [Penke98] B. Penke, S. Kinsey, S. J. Gibbs, T. S. Moerland, B. R. Locke, *J. Magn. Reson.* **1998**, *132*, 240.
- [Powles63] J. G. Powles, J. H. Strange, *Proc. Phys. Soc. London* **1963**, *82*, 6.
- [Prange89] M. M. Prange, H. H. Hooper, J. M. Prausnitz, *AIChE J.* **1989**, *35*, 803.

## Bibliography

---

- [Provencher82] S. W. Provencher, *Comput. Phys. Commun.* **1982**, *27*, 229.
- [Queslel85] J. P. Queslel, J. E. Mark, *J. Chem. Phys.* **1985**, *82*, 3449.
- [Rangaraj97] A. Rangaraj, V. Vangani, A. K. Rakshit, *J. Appl. Polym. Sci.* **1997**, *66*, 45.
- [Reinheimer11] K. Reinheimer, M. Gross, M. Wilhelm, *J. Colloid Interface Sci.* **2011**, *360*, 818.
- [Rivlin48] R. S. Rivlin, *Philos. Trans. Roy. Soc. London A* **1948**, *241*, 379.
- [Saalwächter07] K. Saalwächter, *Prog. Nucl. Mag. Res. Spectr.* **2007**, *51*, 1.
- [Saalwächter12] K. Saalwächter, *Rubber Chem. Technol.* **2012**, *85*, 350.
- [Schmaljohann06] D. Schmaljohann, *Adv. Drug Delivery Rev.* **2006**, *58*, 1655.
- [Schmidt-Rohr94] K. Schmidt-Rohr, H. W. Spiess, *Multidimensional Solid-State NMR and Polymers*, 1st ed., Academic Press, London, **1994**.
- [Schröder96] U. P. Schröder, W. Oppermann, in *Physical properties of polyelectrolyte gels* (Ed. J. P. C. Addad), 1st ed., John Wiley & Sons, Chichester, **1996**, pp. S. 19–39.
- [Shannon08] M. A. Shannon, P. W. Bohn, M. Elimelech, J. G. Georgiadis, B. J. Marinas, A. M. Mayes, *Nature* **2008**, *452*, 301.

- [Shapiro11] Y. E. Shapiro, *Prog. Polym. Sci.* **2011**, *36*, 1184.
- [Skolnick77] J. Skolnick, M. Fixman, *Macromolecules* **1977**, *10*, 944.
- [Skoog07] D. A. Skoog, F. J. Holler, S. R. Crouch, *Principles of Instrumental Analysis*, 6th ed., Thomson, Belmont, **2007**.
- [SLATEC94] SLATEC, *Slatec common mathematical library v4.1*, www.netlib.org/slatec, **1994**.
- [Slichter78] C. P. Slichter, *Principles of Magnetic Resonance*, 2nd ed., Springer-Verlag, New York, **1978**.
- [Snowden96] M. J. Snowden, B. Z. Chowdhry, B. Vincent, G. E. Morris, *J. Chem. Soc., Faraday Trans.* **1996**, *92*, 5013.
- [Stone69] J. E. Stone, E. Treiher, B. Abrahamson, *Tappi J.* **1969**, *52*, 108.
- [Tanaka79] T. Tanaka, D. J. Fillmore, *J. Chem. Phys.* **1979**, *70*, 1214.
- [Tieke05] B. Tieke, *Makromolekulare Chemie Eine Einführung*, 2nd ed., Wiley-VCH, Weinheim, New York, u.a., **2005**.
- [Treloar44] L. R. G. Treloar, *Trans. Faraday Soc.* **1944**, *40*, 59.
- [Treloar75] L. R. G. Treloar, *The physics of rubber elasticity*, 3rd ed., Clarendon Press, Oxford, **1975**.

## Bibliography

---

- [Ulijn07] R. V. Ulijn, N. Bibi, V. Jayawarna, P. D. Thornton, S. J. Todd, R. J. Mart, A. M. Smith, J. E. Gough, *Materials Today* **2007**, *10*, 40.
- [Umendra99] D. Umendra, S. K. Metha, M. S. Choudhary, R. Jain, *Rev. Macromol. Chem. Phys.* **1999**, *C39*, 507.
- [Vervoort05] S. Vervoort, S. Patlazhan, J. Weyts, T. Budtova, *Polymer* **2005**, *46*, 121.
- [Victorov06a] A. Victorov, C. Radke, J. Prausnitz, *Phys. Chem. Chem. Phys.* **2006**, *8*, 264.
- [Victorov06b] A. I. Victorov, *Fluid Phase Equilib.* **2006**, *241*, 334.
- [Vold68] R. L. Vold, J. S. Waugh, M. P. Klein, D. E. Phelps, *J. Chem. Phys.* **1968**, *48*, 3831.
- [Wall42] F. T. Wall, *J. Chem. Phys.* **1942**, *10*, 485.
- [Walther94] D. H. Walther, G. H. Sin, H. W. Blanch, J. M. Prausnitz, *J. Macromol. Sci. B* **1994**, *33*, 267.
- [Weiss79] N. Weiss, T. Van Vliet, A. Silberberg, *J. Polym. Sci. B: Polym. Phys. Ed.* **1979**, *17*, 2229.
- [Weiss81] N. Weiss, T. van Vliet, A. Silberberg, *J. Polym. Sci. B: Polym. Phys. Ed.* **1981**, *19*, 1505.
- [Wiertz11] P. Wiertz, *Sustainability report*, 3rd ed., EDANA, Brussels, **2011**.
- [Wolf86] A. V. Wolf, M. G. Brown, P. G. Prentiss, in *CRC Handbook of Chemistry and Physics* (Ed. R. C.

- Weast), 67th ed., CRC Press, Boca Raton, **1986**, pp. D–253.
- [WWAP12] W. WWAP, *Managing Water under Uncertainty and Risk - The UN World Water Development Report*, 4th ed., UNESCO, Paris, **2012**.
- [Yarimkaya07a] S. Yarimkaya, H. Basan, *J. Macromol. Sci. A* **2007**, *44*, 939.
- [Yarimkaya07b] S. Yarimkaya, H. Basan, *J. Macromol. Sci. A* **2007**, *44*, 699.
- [Yin92] Y.-L. Yin, R. K. Prud'homme, F. Stanley, in *Polyelectrolyte Gels - Properties, Preparation, and Applications* (Eds. R. S. Harland, R. K. Prud'homme), 1st ed., chap. Relationship Between Poly(acrylic acid) Gel Structure and Synthesis, American Chemical Society, Washington DC, **1992**, p. 91.
- [Zhao09] Y.-L. Zhao, J. F. Stoddart, *Langmuir* **2009**, *25*, 8442.



## C. Curriculum vitae



### Personal information

Name	<u>Johannes Höpfner</u>
Address (Work)	ITCP, Engesserstr. 18, 76131 Karlsruhe, Germany
Phone (Work)	+49 (0) 721 608 48501
E-Mail	<a href="mailto:Johannes.Hoepfner@kit.edu">Johannes.Hoepfner@kit.edu</a>

### Education and training

Since July 2009	Postgraduate studies at Karlsruhe Institute of Technology (KIT), Institute of Chemical Technology and Polymer Chemistry under the supervision of Prof. M. Wilhelm. Including a three month research stay at Ben Gurion University, Beer Scheva, Israel
October 2004 – June 2009	Studies of pure chemistry at Karlsruhe University (TH), emphasis on polymer and physical chemistry
1994 – 2003	Secondary school attendance at the Humboldt Gymnasium in Vaihingen, Certificate of secondary education (Abitur)

### Professional experience

Since July 2009	Scientific assistant Karlsruhe Institute of Technology (KIT), Institute of Chemical Technology and Polymer Chemistry, project work with in- dustrial partners on mechanical characteri- sation of hydrogels
October 2007 – July 2008	Tutor for the lecture "Mathematical concepts in physical chemistry", Karlsruhe University (TH), Chair for Theoretical Chemistry
July 2007 – August 2007	Assistant to the departmental manager
April 2008 – August 2008	of Chemical and Bio Sciences, tasks in- cluded administrative work and evalua- tion of new students, Karlsruhe University (TH)
May 2006 – August 2006	Guide to the exhibition "History of the chemical laboratory", Carl Bosch Museum gGmbH, Heidelberg
August 2003 – May 2004	Civil service at the GSD Retirement Home in Vaterstet- ten, care for the residents and administra- tive tasks

## Awards and Scholarships

- 2008                    Award of the Chancellor of Karlsruhe Technical University for outstanding student commitment
- 2009                    Award of the Deutsche Kautschuk Gesellschaft (DKG) for an outstanding diploma thesis in polymer sciences
- 2010 – 2012            Stipend for postgraduate studies of the Heinrich-Böll Foundation
- 2012                    LANXESS Talent Award, participant of the final round
- 2012                    Neo innovation price of the Technologieregion Karlsruhe, participant of the final round

## Publications

J. Höpfner, C. Klein, M. Wilhelm, A Novel Approach for the Desalination of Seawater by Means of Reusable Poly(acrylic acid) Hydrogels and Mechanical Force, *Macromol. Rapid Commun.* **2010**, *31*, 1337.

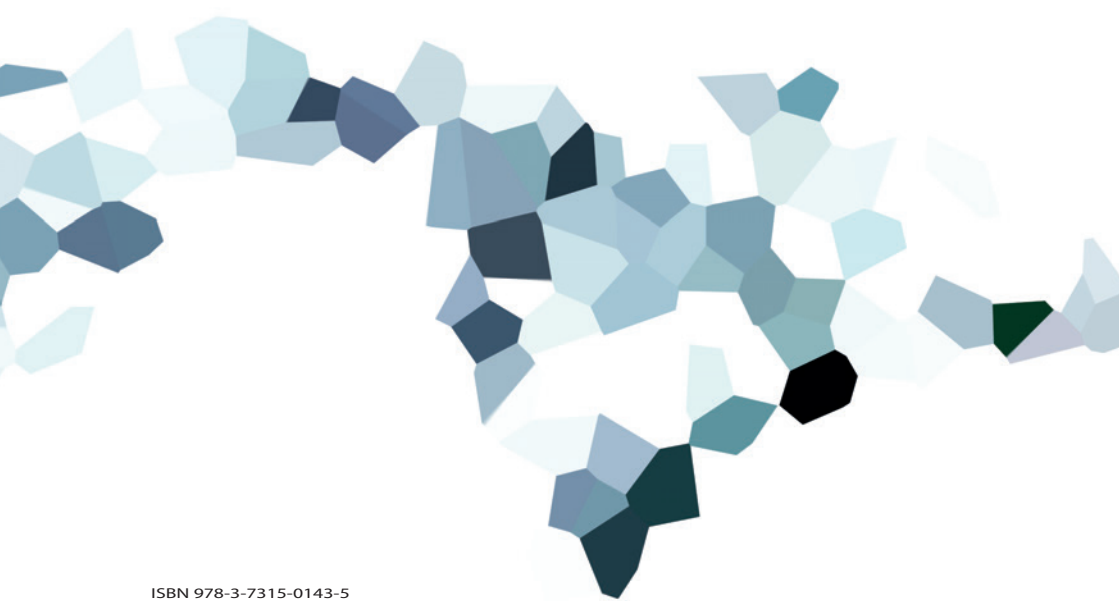
J. Höpfner, M. Wilhelm, Neuartige Meerwasserentsalzung mit Hilfe von polymeren Hydrogelen in Tagungsband 7. Thüringer Grenz- und Oberflächentage, Innovent e.V., Jena, **2011**, S. 87 – 91 (ISBN: 978-3-00-035347-5).

J. Höpfner, T. Richter, P. Košovan, C. Holm, M. Wilhelm, Seawater desalination via hydrogels: Coarse grained simulations and practical realisation, accepted in *Progr. Colloid. Polym. Sci.* **2014**.

C. Merle, G. Kummerlöwe, J. C. Freudenberger, F. Halbach, W. Stöwer, C. L. v. Gostomski, J. Höpfner, T. Beskers, M. Wilhelm, B. Luy, Crosslinked Poly(ethylene oxide) as a Versatile Alignment Medium for the Measurement of Residual Anisotropic NMR Parameters, *Angew. Chem. Int. Ed.* **2013**, *52*, 10309.



The scarcity of potable water is one the great challenges of the 21st century. It may be partially resolved by the desalination of seawater. In this work, the possibilities of a new desalination technique using polymeric hydrogels as a separation medium for water and salt is explored. The bound charges in such a polymeric network prevent salt from entering it – under subsequent pressure the desalinated water is released from the gel. It is demonstrated that this approach is viable and the influence of various process parameters investigated. The employed acrylic hydrogels are characterised by novel methods.



ISBN 978-3-7315-0143-5

A standard linear barcode representing the ISBN number 978-3-7315-0143-5.

9 783731 501435 >